



National Library  
of Canada

Bibliothèque nationale  
du Canada

Canadian Theses Service    Service des thèses canadiennes

Ottawa, Canada  
K1A 0N4

1

## NOTICE

The quality of this microform is heavily dependent upon the quality of the original thesis submitted for microfilming. Every effort has been made to ensure the highest quality of reproduction possible.

If pages are missing, contact the university which granted the degree.

Some pages may have indistinct print especially if the original pages were typed with a poor typewriter ribbon or if the university sent us an inferior photocopy.

Reproduction in full or in part of this microform is governed by the Canadian Copyright Act, R.S.C. 1970, c. C-30, and subsequent amendments.

## AVIS

La qualité de cette microforme dépend grandement de la qualité de la thèse soumise au microfilmage. Nous avons tout fait pour assurer une qualité supérieure de reproduction.

S'il manque des pages, veuillez communiquer avec l'université qui a conféré le grade.

La qualité d'impression de certaines pages peut laisser à désirer, surtout si les pages originales ont été dactylographiées à l'aide d'un ruban usé ou si l'université nous a fait parvenir une photocopie de qualité inférieure.

La reproduction, même partielle, de cette microforme est soumise à la Loi canadienne sur le droit d'auteur, SRC 1970, c. C-30, et ses amendements subséquents.

UNIVERSITY OF ALBERTA

TURBULENT JET DISCHARGES IN RIVERS

BY

JOHN EDMUND HODGSON

A THESIS

SUBMITTED TO THE FACULTY OF GRADUATE STUDIES AND RESEARCH

IN PARTIAL FULFILMENT OF THE REQUIREMENTS FOR THE DEGREE

OF

DOCTOR OF PHILOSOPHY



IN

WATER RESOURCES ENGINEERING  
DEPARTMENT OF CIVIL ENGINEERING

EDMONTON, ALBERTA

SPRING 1991



National Library  
of Canada

Bibliothèque nationale  
du Canada

Canadian Theses Service    Service des thèses canadiennes

Ottawa, Canada  
K1A 0N4

The author has granted an irrevocable non-exclusive licence allowing the National Library of Canada to reproduce, loan, distribute or sell copies of his/her thesis by any means and in any form or format, making this thesis available to interested persons.

The author retains ownership of the copyright in his/her thesis. Neither the thesis nor substantial extracts from it may be printed or otherwise reproduced without his/her permission.

L'auteur a accordé une licence irrévocable et non exclusive permettant à la Bibliothèque nationale du Canada de reproduire, prêter, distribuer ou vendre des copies de sa thèse de quelque manière et sous quelque forme que ce soit pour mettre des exemplaires de cette thèse à la disposition des personnes intéressées.

L'auteur conserve la propriété du droit d'auteur qui protège sa thèse. Ni la thèse ni des extraits substantiels de celle-ci ne doivent être imprimés ou autrement reproduits sans son autorisation.

ISBN 0-315-66720-6

UNIVERSITY OF ALBERTA

RELEASE FORM

NAME OF AUTHOR: John Edmund Hodgson

TITLE OF THESIS: Turbulent Jet Discharges in Rivers

DEGREE: Doctor of Philosophy

YEAR THIS DEGREE GRANTED: 1991

Permission is hereby granted to THE UNIVERSITY OF ALBERTA LIBRARY to reproduce single copies of this thesis and to lend or sell such copies for private, scholarly or scientific research purposes only.

The author reserves other publication rights, and neither the thesis nor extensive extracts from it may be printed or otherwise reproduced without the author's written permission.

  
\_\_\_\_\_  
John Edmund Hodgson

23 Glen Meadow Crescent  
ST. ALBERT, Alberta  
T8N 3A2

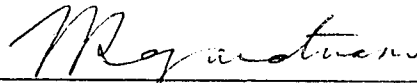
Date: 17 March 1991



THE UNIVERSITY OF ALBERTA

FACULTY OF GRADUATE STUDIES AND RESEARCH

The undersigned certify that they have read, and recommend to the Faculty of Graduate Studies and Research for acceptance, a thesis entitled "Turbulent Jet Discharges in Rivers" submitted by John Edmund Hodgson in partial fulfilment of the requirements for the degree of Doctor of Philosophy in Water Resources Engineering.



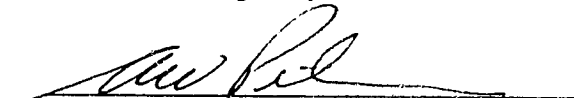
N. Rajaratnam  
Supervisor



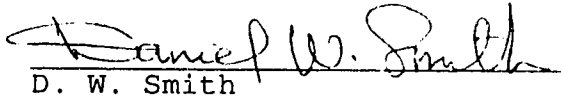
P. Steffler



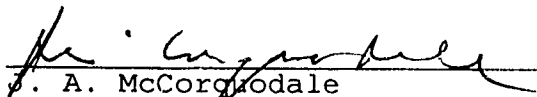
K. C. Cheng



A. W. Peterson



D. W. Smith



P. A. McCorquodale  
External Examiner

Date: 19 December 1990

## ABSTRACT

Downstream of an effluent discharge to a river there may be a region (called the limited use zone) where concentrations for various water quality parameters meet effluent discharge standards but do not meet receiving water quality guidelines. There is interest in maximizing the dilution in the region near the outfall (the near field) so that the extent of the river which exceeds receiving water quality guidelines is minimized. Jet discharges normal to the direction of flow are a simple and effective means to maximize this dilution. In addition to shortening the length of the limited use zone, jet discharges also provide the benefit of a more reliable design for dealing with buoyant or non-buoyant effluents.

The overall objective of this dissertation is to provide a basis for designing effluent diffusers in rivers. The work focusses on turbulent jet discharges in crossflows. Available literature is reviewed to provide a description of the phenomena and a starting point for this work. Laboratory work by others has been examined and utilized where possible. A photographic investigation has been carried out to indicate the location, width and thickness of jet discharges in deep and shallow crossflows. A field study has been carried out to measure the dilution of various jet discharges in a real river. The field work has been augmented by a laboratory investigation which covers a wider range of discharge

conditions. Based on this work, relationships have been developed for the dilution of jet discharges in crossflow. The results of the field work have been used to verify the wide applicability of the laboratory work.

In addition to the near field mixing phenomena, mixing in the far field has been investigated. The two dimensional dispersion equations have been examined in a manner which provide a quantification of the extent of the limited use zone for line source outfalls. Finally, a case history is presented as an example of the application of the findings of this work. This application is particularly relevant to Alberta due to the recent construction in this province of four new pulp mills over the past three years.

## ACKNOWLEDGEMENTS

I am indebted to many people and organizations who provided support for this undertaking. Dr. N. Rajaratnam should be the first to be acknowledged. His unfailing enthusiasm for the subject matter helped steel my resolve throughout the entire period of study.

I am thankful to those involved in the photographic study of jets in crossflow of finite depth. The work was carried out in the T. Blench Hydraulics Laboratory at the University of Alberta in Edmonton, Alberta. Sheldon Lovell constructed the apparatus and Doug Tovell assisted in the data collection and reduction effort. The study was supported through scholarships from the Alberta Research Council and North American Life Assurance Company through the Canadian Council of Professional Engineers.

I would like to thank those who assisted in making the Lesser Slave River field program a success. Sheldon Lovell and Sid Lodewyk fabricated the experimental apparatus and assisted in conducting the field work. Arbind Manali assisted in the preparation of the graphic material for the work. Funding for the study was provided through a research grant from the Alberta Environmental Research Trust.

The laboratory dilution study was carried out in the T. Blench Hydraulics Laboratory. Martin Jasek assisted in the photography.

Stanley Associates Engineering Ltd. should also be thanked for their tolerance of my general absence and use of their resources over the past five years. The impact of my years with the company should be evident in the pragmatic approach to this work.

Finally, my greatest appreciation is extended to my wife Patti, for her support, and my children (Daniel, Megan and Julie) for their tolerance of my protracted absences over the past five years. If they understand that the pursuit of knowledge is noble, then our sacrifices have been worthwhile.

## TABLE OF CONTENTS

	<u>page</u>
ABSTRACT.....	iv
ACKNOWLEDGEMENTS.....	vi
TABLE OF CONTENTS.....	viii
LIST OF TABLES.....	xi
LIST OF FIGURES.....	xiii
LIST OF PLATES.....	xvii
LIST OF SYMBOLS.....	xviii
 <b>Chapter</b>	
1 INTRODUCTION.....	1
1.1 General Discussion.....	1
1.2 Guidelines and Standards for Stream Protection.....	3
1.3 Mixing Phenomena.....	7
1.3.1 The Near Field Mixing Zone.....	8
1.3.2 The Far Field Mixing Zone.....	10
1.3.3 The Subsequent Dilution Zone.....	11
1.4 Study Objectives.....	12
2 A REVIEW OF LITERATURE ON JETS IN CROSSFLOW.....	18
2.1 General.....	18
2.2 Experimental Investigations.....	19
2.3 Description of Jet Discharges.....	26
2.3.1 Jet Discharges into a Quiescent Ambient.....	26
2.3.2 Jet Discharges in Crossflow.....	28
2.4 Length Scales for Buoyant Jet Discharges .....	32
2.5 Analytical and Computational Investigations.....	35
2.5.1 Empirical Methods.....	35
2.5.2 Analytical Methods.....	37
2.5.3 Turbulence Modelling.....	39
3 A PHOTOGRAPHIC ASSESSMENT OF CIRCULAR JET DISCHARGES IN CROSSFLOWS OF FINITE DEPTH.....	55
3.1 General.....	55
3.2 Previous Investigations.....	57
3.2.1 Profile Equations.....	57
3.2.2 Width and Thickness Equations.....	65
3.3 Effects of a Finite Free Stream Depth.....	66
3.3.1 General.....	66
3.3.2 Dimensional Considerations.....	67
3.3.3 Flow Fields for Jets Discharging into Crossflows of Finite Depth.....	69
3.4 Experimental Setting.....	72
3.4.1 Facilities.....	72
3.4.2 Photographic Analysis.....	73
3.4.3 Experimental Error and Variance.....	75
3.5 Results and Analysis.....	76
3.5.1 Conditions Investigated.....	76

3.5.2	Jet Strength and the Onset of Surface Effects.....	77
3.5.3	Comparison of Deep Water Jet Profiles With Previous Study Results.....	78
3.5.4	Centreline Profiles - Jet Penetration.....	80
3.5.5	Centreline Profiles - Momentum Dominated Near Field.....	81
3.5.6	Centreline Profiles - Momentum Dominated Far Field.....	82
3.5.7	Centreline Profiles - Surface Dominated Field.....	82
3.5.8	Terminal Levels.....	84
3.5.9	Terminal Level Distance.....	86
3.5.10	Flow Field Boundaries.....	86
3.5.11	Jet Widths.....	88
3.5.12	Jet Thickness.....	92
3.6	Conclusions.....	95
4	A FIELD STUDY OF JET DILUTION IN A RIVER.....	140
4.1	General.....	140
4.2	Jet Discharges in a Quiescent Ambient.....	141
4.3	Buoyant Jet Discharges in a Quiescent Ambient.....	144
4.4	Jet Discharges in Crossflow.....	146
4.5	Experimental Arrangement.....	152
4.5.1	River Conditions.....	152
4.5.2	Equipment.....	154
4.5.3	Sampling Procedures.....	156
4.5.4	Experimental Error and Variance.....	158
4.6	Results and Analysis.....	159
4.6.1	Conditions Investigated.....	159
4.6.2	Maximum Concentration Along Jet Axis.....	160
4.7	Conclusions.....	163
5	A LABORATORY STUDY OF JET DILUTION IN CROSSFLOWS.....	182
5.1	General.....	182
5.2	Experimental Arrangement.....	183
5.2.1	Flume Conditions.....	183
5.2.2	Sampling Procedures.....	184
5.2.3	Experimental Error and Variance.....	188
5.3	Results and Analysis.....	188
5.3.1	Conditions Investigated.....	188
5.3.2	Maximum Concentrations.....	189
5.3.3	Centreline Profiles.....	193
5.3.4	Jet Widths.....	194
5.3.5	Jet Thicknesses.....	195
5.4	Conclusions.....	197
6	FAR FIELD CONSIDERATIONS.....	229
6.1	General.....	229
6.2	Transverse Mixing Equations.....	231
6.2.1	The Governing Equation.....	231
6.2.2	General Dispersion Equations.....	235
6.2.3	Dispersion Downstream of Point Source Outfalls.....	237

6.2.4 Dispersion Downstream of Line Source	
Outfalls.....	238
6.3 Mixing Lengths.....	239
6.3.1 Point Source Discharges.....	240
6.3.2 Line Source Discharges.....	243
6.4 Crossing Lengths.....	245
6.4.1 Point Source Discharges.....	245
6.4.2 Line Source Discharges.....	246
6.5 Limited Use Zone Concepts.....	247
6.5.1 Definitions.....	247
6.5.2 LUZ Boundary (Critical Point) Constraints...	248
6.5.3 Shoreline Concentration Constraints.....	251
6.5.4 Determining Allowable Effluent	
Concentration.....	253
6.6 Conclusions.....	254
7 THE DESIGN OF JET DIFFUSER DISCHARGES IN RIVERS .....	261
7.1 General.....	261
7.2 Constraint Considerations.....	262
7.2.1 Cavitation.....	264
7.2.2 Jet Nozzle Size.....	266
7.2.3 Jet Spacing.....	268
7.2.4 Other Considerations.....	269
7.3 Application of Design Principles - A Case History.	270
7.4 Conclusions.....	275
8 CONCLUSIONS.....	280
8.1 General.....	280
8.2 Findings.....	281
8.3 Further Investigation.....	286
REFERENCES.....	289
APPENDIX A - Data Summary for Photographic Study.....	301
APPENDIX B - Summary of Regression Analyses.....	313
APPENDIX C - Summary of Concentration Measurements	
- Lesser Slave River Field Trip.....	319
APPENDIX D - Data Summary for Laboratory Dilution Study...	332
APPENDIX E - Application of Reichardt's Hypothesis to the	
Concentration Field of Multiple Jet Discharges	
in a Quiescent Ambient.....	343
APPENDIX F - Glossary.....	380



## LIST OF TABLES

<b>Table</b>	<b>page</b>
1.1 Theoretical mixing zone lengths for selected Alberta rivers.....	15
2.1 Summary of experimental work on jet discharges in crossflow.....	42
2.2 Solution procedures for jet discharges in crossflow...	45
2.3 Trajectory and dilution relationships from Wright (1977a and 1977b).....	48
3.1 Range of parameters used in various photographic studies of jets in crossflow.....	101
3.2 Measurement precision and experimental error - photographic investigation.....	102
3.3 Range of conditions investigated.....	103
3.4 Reynolds number data.....	104
3.5 Maximum terminal levels and minimum jet strengths....	105
4.1 Characteristics of jet discharges in crossflows.....	165
4.2 Parameters from selected studies of jet discharges in quiescent ambients.....	166
4.3 Parameters from selected studies of buoyant jet discharges in quiescent ambients.....	167
4.4 Parameters from selected studies of jet discharges in crossflows.....	168
4.5 Measurement precision and experimental error - field dilution study.....	169
4.6 Jet discharge conditions in the Lesser Slave River field program.....	170
5.1 Measurement precision and experimental error - laboratory dilution study.....	200
5.2 Conditions investigated in laboratory dilution study.	201
6.1 Dimensionless mixing lengths ( $\phi_m$ ) for point source outfalls.....	256

6.2	Dimensionless mixing lengths ( $\phi_m$ ) for line source outfalls.....	256
6.3	Dimensionless crossing lengths ( $\phi_c$ ) for point source outfalls.....	257
6.4	Dimensionless crossing lengths ( $\phi_c$ ) for line source outfalls.....	257

## LIST OF FIGURES

<b>Figure</b>	<b>page</b>
1.1 Receiving stream regions.....	16
1.2 Coordinate system for jet in crossflow.....	17
2.1 Jet discharge into a quiescent ambient.....	49
2.2 Jet discharge into a crossflow.....	50
2.3 Length of potential core.....	51
2.4 Axial velocities and potential core length.....	52
2.5 Velocity centreline data from selected studies velocity ratios: 3.9 to 4.3.....	53
2.6 Velocity centreline data from selected studies velocity ratios: 7.7 to 8.8.....	54
3.1 Wright's data for momentum dominated near field coefficient $C_1$ .....	106
3.2 Wright's data for momentum dominated far field coefficient $C_2$ .....	107
3.3 Boundary between near and far fields from Wright's momentum dominated equations.....	108
3.4 Wright's data for concentration centreline location..	109
3.5 Boundary data for Run 1232 ( $\alpha d/D = 0.18$ ).....	110
3.6 Boundary data for Run 1136 ( $\alpha d/D = 0.46$ ).....	111
3.7 Width data for runs 1232 and 1136.....	112
3.8 Variance and confidence interval of photographic measurements for inner boundary terminal level region of Run 1232.....	113
3.9 Inner boundary location for deep water jets.....	114
3.10 Outer boundary location for deep water jets.....	115
3.11 Jet centreline profile for deep water jets.....	116
3.12 Jet centreline penetration distance....	117

3.13 Momentum dominated near field coefficients.....	118
3.14 Momentum dominated far field coefficients.....	119
3.15 Surface dominated field coefficients.....	120
3.16 Surface dominated field exponents versus $\frac{\alpha d}{D}$ .....	121
3.17 Surface dominated field exponents versus $\frac{\alpha^2 d}{D}$ .....	122
3.18 Jet terminal levels versus $\frac{\alpha d}{D}$ .....	123
3.19 Jet terminal levels versus $\frac{\alpha^2 d}{D}$ .....	124
3.20 Terminal level distances versus $\frac{\alpha d}{D}$ .....	125
3.21 Terminal level distances versus $\frac{\alpha^2 d}{D}$ .....	126
3.22 Shallow water jet discharges - flow fields for $D/d = 15$ .....	127
3.23 Shallow water jet discharges - flow fields for $D/d = 25$ .....	128
3.24 Jet widths for deep water jets.....	129
3.25 Jet width ( $\frac{\alpha^2 d}{D} < 2$ ) .....	130
3.26 Jet width ( $\frac{\alpha^2 d}{D} > 2$ ) .....	131
3.27 Jet width equations and coefficients.....	132
3.28 Jet thickness for deep water jets versus $\frac{x}{\alpha d}$ .....	133
3.29 Jet thickness for deep water jets versus $\frac{\xi}{\alpha d}$ .....	134
3.30 Thickness equation coefficients for deep water jets..	135

3.31	Thickness equation exponents for deep water jets.....	136
3.32	Jet thicknesses for selected deep water and shallow water jets.....	137
4.1	Dilution ratios for jet discharges into quiescent ambients.....	171
4.2	Dilution ratios for buoyant jet discharges into quiescent ambients.....	172
4.3	Published data for jet dilution versus downstream distance.....	173
4.4	Lesser Slave River location plan.....	174
4.5	Field program equipment schematic.....	175
4.6	Fluorometer calibration - field study.....	176
4.7	Dilution ratios for discharges with low velocity ratios.....	177
4.8	Dilution equation parameters - coefficient a.....	178
4.9	Dilution equation parameters - exponent b.....	179
4.10	Comparison of dilution equations.....	180
5.1	Boundary layer velocity distribution for 200 and 300 series runs.....	202
5.2	Boundary layer velocity distribution for 100 series runs.....	203
5.3	Fluorometer calibration - laboratory study.....	204
5.4	Concentration distribution for Run 300 - $x/d = 94$ ....	205
5.5	Concentration distribution for Run 301 - $x/d = 95$ ....	206
5.6	Concentration distribution for Run 302 - $x/d = 95$ ....	207
5.7	Concentration distribution for Run 303 - $x/d = 95$ ....	208
5.8	Concentration distribution for Run 101 - $x/d = 95$ ....	209
5.9	Concentration distribution for Run 102 - $x/d = 50$ ....	210
5.10	Concentration distribution for Run 103 - $x/d = 30$ ....	211
5.11	Concentration distribution for Run 104 - $x/d = 15$ ....	212

5.12	Centreline dilution ratios along curvilinear axis - 300 series runs.....	213
5.13	Centreline dilution ratios along curvilinear axis - 200 series runs.....	214
5.14	Centreline dilution ratios along curvilinear axis - 100 series runs.....	215
5.15	Centreline dilution ratios for 300 series runs.....	216
5.16	Centreline dilution ratios for 200 series runs.....	217
5.17	Centreline dilution ratios for 100 series runs.....	218
5.18	Centreline dilution ratios - all runs.....	219
5.19	Comparison of field and laboratory dilution data....	220
5.20	Concentration centreline locations.....	221
5.21	Jet width data for 50% concentration location.....	222
5.22	Jet width along curvilinear axis.....	223
5.23	Jet thickness data for 50% concentration location....	224
5.24	Jet thickness along curvilinear axis.....	225
6.1	Characteristics of the mixing zone .....	258
6.2	Dimensionless mixing and crossing lengths.....	259
6.3	Limited use zone and critical point.....	260
7.1	Maximum permissible velocities for jet discharges....	276
7.2	River cross-section at Peace River outfall.....	277
7.3	Jet dilution for Peace River outfall.....	278

## LIST OF PLATES

Plate	page
3.1 Typical side view photograph for Run 1232 ( $\alpha d/D = 0.18$ ); minimal surface effects are present.....	138
3.2 Typical side view photograph for Run 1136 ( $\alpha d/D = 0.46$ ); surface effects are significant.....	138
3.3 Typical plan view photograph for Run 1232 ( $\alpha d/D = 0.18$ ); minimal surface effects are present.....	139
3.4 Typical plan view photograph for Run 1136 ( $\alpha d/D = 0.46$ ); surface effects are significant.....	139
4.1 Jet discharge equipment.....	181
4.2 Sampling equipment.....	181
5.1 Side view of Run 101 (exposure time = 1/30 s).....	226
5.2 Side view of Run 104 (exposure time = 1/30 s).....	226
5.3 Plan view of Run 102 (exposure time = 1/15 s).....	227
5.4 Plan view of Run 102 (exposure time = 15 s).....	227
5.5 Plan view of Run 104 (exposure time = 1/15 s).....	228
5.6 Plan view of Run 104 (exposure time = 15 s).....	228
7.1 Jet diffuser outfall on shore prior to launch.....	279
7.2 Structure being pulled into place along downstream berm.....	279

## LIST OF SYMBOLS

Symbol	Units	Description
a		coefficient in dilution equation
A		thermal expansion coefficient ratio $A = (\alpha_{\infty}/\alpha_0)^{1/3}$
b	L	exponent in dilution equation also: jet half-width
B	$L^4/T^3$	specific buoyancy of a discharge
C or c	$M/L^3$	concentration of effluent parameter
$C_a$	$M/L^3$	increase in mixed concentration due to effluent $(C_a = \frac{C_a Q_e}{Q + Q_e})$
$C_b$	$M/L^3$	background concentration
$C_e$	$M/L^3$	effluent concentration
$C_{ea}$	$M/L^3$	allowable effluent concentration
$C_l$	$M/L^3$	critical concentration
$C_m$ or $c_m$	$M/L^3$	concentration maximum at a given section also: concentration downstream of mixing zone
$C_o$	$M/L^3$	concentration at discharge nozzle
$C_s$	$M/L^3$	receiving stream guideline
$C_1$		coefficient for Wright's centreline equation in MDNF
$C_2$		coefficient for Wright's centreline equation in MDFF
$C_3$		coefficient for Wright's dilution equation in MDNF
$C_4$		coefficient for Wright's dilution equation in MDFF



C1		centreline equation coefficient - MDNF
C2		centreline equation coefficient - MDFF
C3		centreline equation coefficient - SDF
C4		width equation coefficient - DWJ
C5		width equation coefficient - SWJ
C6		thickness equation exponent
d	L	jet nozzle or orifice diameter (corrected for vena contracta)
D	L	depth of crossflow
D <sub>m</sub>	L <sup>2</sup> /T	molecular diffusion coefficient
D <sub>z</sub>	L <sup>5</sup> /T <sup>2</sup>	constant of diffusion
e <sub>y</sub>	L <sup>2</sup> /T	vertical dispersion coefficient
e <sub>z</sub>	L <sup>2</sup> /T	transverse dispersion coefficient
E <sub>z</sub>	L <sup>2</sup> /T	transverse mixing coefficient
F <sub>o</sub>		densimetric Froude number: $F_o = \frac{U_o}{\sqrt{g \frac{\rho - \rho_o}{\rho_o} d}}$
g	L/T <sup>2</sup>	gravitational acceleration
g'	L/T <sup>2</sup>	apparent gravitational acceleration
h	L	local river depth
H	L	hydraulic depth (section or reach) also: depth above jet nozzle
k		number of terms in dispersion equations also: dispersion constant also: diffusion coefficient ratio
K	L <sup>5</sup> /T <sup>2</sup>	diffusion factor
l <sub>b</sub>	L	buoyancy length scale for jet/plume in crossflow (l <sub>b</sub> = B/U <sup>3</sup> )

$l_c$	L	length of potential core
$l_m$	L	momentum length scale for a jet in crossflow ( $l_m = M^{1/2}/U = \sqrt{\pi/4} \alpha d$ )
$l_M$	L	characteristic length scale for jet/plume ( $l_M = M^{3/4}/B^{1/2}$ )
$l_Q$	L	characteristic length scale for a jet ( $l_Q = Q_o/M^{1/2} = \sqrt{\pi/4} d$ )
$m$	M/T	mass flux at a given section; also: exponent in SDF centreline equation
$m_o$	M/T	mass flux at jet nozzle
$m_x$		metric coefficient (stream curvature ratio)
$M$	$L^4/T^2$	specific momentum flux of the discharge $M = Q_o U_o$
$n$		width equation exponent - SWJ also: number of reflections in mixing equations
$p$		inverse of velocity ratio ( $p = 1/\alpha$ ) also: location in cross section ( $p=q/Q$ ) also: exponent in jet thickness equation
$p_l$		permissible width of limited use zone
$p_o$	$M/L/T^2$	ambient pressure at jet nozzle ( $p_o = \rho_o g H$ )
$p_s$		location of point source outfall
$p_v$	$M/L/T^2$	vapor pressure of fluid
$P$	L	piezometric pressure
$q$	$L^3/T$	distance (in terms of flow) from stream bank to point in cross section
$q_l$	$L^3/T$	permissible width of limited use zone
$Q$	$L^3/T$	volumetric flux of river or jet at a given section
$Q_e$	$L^3/T$	effluent discharge rate

$Q_0$	$L^3/T$	volumetric flux of jet at nozzle
$Q_r$	$L^3/T$	river discharge
$r$	$L$	radius of curvature for a river bend
$R$	$L$	hydraulic radius of river
$R_d$		jet/crossflow Reynold's number ( $R_d = U d/v$ )
$R_D$		crossflow Reynold's number ( $R_D = U D/v$ )
$R_j$		jet Reynold's Number ( $R_j = U_0 d/v$ )
$R_0$		Richardson Number
$s$		slope of river
$S_0$		dilution ratio ( $S_0 = C_0/C_m$ )
$t$	$T$	time
$T$	$^{\circ}C$	fluid temperature
$T'$	$^{\circ}C$	deviation from mean fluid temperature
$u$	$L/T$	local depth-averaged velocity also: local instantaneous velocity also: local time-averaged velocity
$u_m$	$L/T$	maximum velocity at section
$u'$	$L/T$	deviation from mean velocity (x direction)
$U$	$L/T$	velocity of crossflow or river
$U_0$	$L/T$	velocity at discharge nozzle
$U_*$	$L/T$	shear velocity ( $U_* = \sqrt{gRs}$ )
$v$	$L/T$	local velocity in the y direction
$v'$	$L/T$	deviation from mean velocity (y direction)
$w$	- $L/T$	width of line source outfall also: local velocity in the z direction

$w'$	L/T	deviation from mean velocity (z direction)
$W$	L	width of river
$W_y$	L	thickness of jet (as seen from the side)
$W_z$	L	width of jet (as seen from above)
$x$	L	distance downstream of jet nozzle (along jet axis for quiescent ambient; along ambient flow direction for crossflows) distance downstream of effluent outfall
$X_c$	L	distance to centreline terminal level
$X_l$	L	critical length of limited use zone
$X_m$	L	mixing zone length
$X_p$	L	maximum permissible length of LUZ
$X_s$	L	length of limited use zone
$X_v$	L	vertical mixing zone length
$y$	L	distance above bed
$y_i$	L	inner boundary location, jet in crossflow
$y_c$	L	centreline location, jet in crossflow
$y_o$	L	outer boundary location, jet in crossflow
$Y_c$	L	jet centreline terminal level
$Y_i$	L	jet inner boundary terminal level
$Y_o$	L	jet outer boundary terminal level
$Y_p$	L	jet centreline penetration distance
$z$	L	distance from nozzle across free stream
$\alpha$		velocity ratio for jet in a crossflow $\alpha = U_o/U$
$\alpha_e$		entrainment rate coefficient

$\alpha_0$	$^{\circ}\text{C}^{-1}$	thermal expansion coefficient - discharge
$\alpha_{\infty}$	$^{\circ}\text{C}^{-1}$	thermal expansion coefficient - ambient
$\beta$		empirical factor-jet centreline equation also: outfall/LUZ width factor
$\Gamma$	$\text{L}^2/\text{T}$	vorticity
$\delta$		criteria for mixing and crossing lengths
$\epsilon_x, \epsilon_y, \epsilon_z$	$\text{L}^2/\text{T}$	turbulent diffusion coefficients
$\overline{\epsilon_z}$	$\text{L}^2/\text{T}$	reach-averaged diffusion coefficient
$\theta$		angle between crossflow and jet centreline
$\nu$	$\text{L}/\text{T}$	kinematic viscosity
$\xi$	mm	distance along curvilinear jet axis also: dimensionless distance downstream of outfall
$\rho$	$\text{M}/\text{L}^3$	fluid or ambient density
$\rho_0$	$\text{M}/\text{L}^3$	density of discharge
$\Delta\rho$	$\text{M}/\text{L}^3$	density difference ( $\Delta\rho = \rho_0 - \rho$ )
$\sigma$		cavitation index
$\phi$		dimensionless distance downstream of outfall
$\phi_c$		dimensionless crossing length
$\phi_m$		dimensionless mixing length
$\psi$		shape velocity factor

## CHAPTER 1

### INTRODUCTION

#### 1.1 General Discussion

Rivers have long been used by mankind for the disposal of wastes. This practice recognizes and takes advantage of the assimilative capacity of the natural environment. The wastes of civilization enter river systems as both diffuse and point source loadings. The extent of these loadings has grown in North America over the past century in conjunction with the increases in urbanization and industrialization. Some of the consequences of these developmental activities include an increase in the pollutant loadings on the major river systems and the introduction of significant loadings to many other smaller streams. As a result of this pollution potential, and the growing concern about it, more effort is needed in developing and implementing advanced wastewater treatment and discharge facilities.

In recent years, the number of contaminants in the environment and the concern about the health risk have increased dramatically. There are now over 30,000 chemicals in use in Canada (Environment Canada, 1988a). This widescale use and disposal of potentially hazardous materials poses new problems in the evaluation of a receiving stream's assimilative capacity. In addition to the consideration of the physical condition (e.g. temperature, suspended solids

and turbidity) and biological processes (e.g. biochemical oxygen demand and dissolved oxygen), the more subtle effects of toxic and carcinogenic chemicals must also be considered. Experiences in Canada and Alberta to date indicated that our rivers have been able to assimilate the wastes from municipal and industrial activities with varying degrees of success. However, public opinion is clearly moving to favour higher levels of protection.

Out of concern for the risks to the environment, the provincial and federal governments in Canada have environmental departments whose mandates are to ensure the protection of the environment. To achieve this objective for rivers, environmental department responsibilities include:

- a) setting effluent standards for municipal and industrial water uses,
- b) monitoring and setting monitoring requirements for existing effluent discharges,
- c) reviewing and approving effluent discharges proposed by municipalities and the various industries,
- d) setting receiving stream guidelines, and
- e) investigating watercourses to determine their condition and assimilative capacities.

In assessing the assimilative capacity of a receiving stream, there are many processes that can occur. These include:

- a) mixing,
- b) dilution,

- c) sedimentation,
- d) adsorption/ desorption,
- e) absorption,
- f) organism die-off,
- g) chemical reactions,
- h) biological processes (assimilation, biodegradation and bioaccumulation), and
- i) heat loss processes (evaporation and radiation).

In this dissertation, it is the mixing phenomena which are of interest.

## **1.2 Guidelines and Standards for Stream Protection**

The development and application of sound receiving stream guidelines are fraught with difficulty. Strachan (1986) indicated that the development of guidelines seems to be a never ending process. Many reasons for this can be given:

- a) the number of chemicals found in the environment is growing,
- b) there are sometimes a number of states for a given chemical or slightly different chemical compounds in the same family (having varying characteristics) to be considered,
- c) the knowledge on the effects of these chemicals on the environment is not complete,
- d) each receiving stream has a wide range of aquatic species at various life stages and experiences a wide range of flow conditions,



- e) the ability to detect many of the chemicals of concern in the environment is constantly improving; however, these detection limits sometime fail to identify levels in the receiving stream at which there may be some subtle effect,
- f) synergistic or antagonistic effects of more than one chemical in the discharge are difficult to quantify, and
- g) background levels for some chemicals in the receiving stream sometime exceed the receiving stream guidelines (which raises the questions: is the impairment too subtle to notice; or, is the guideline too conservative).

It is important to note that there are several terms used in water quality studies when dealing with limits on effluent discharges or chemicals in the environment:

**criteria:** scientific data evaluated to derive the recommended limits for water uses;

**water quality guideline:** numerical concentration or narrative statement recommended to support and maintain a designated water use;

**water quality objective:** a numerical concentration or narrative statement which has been established to support and protect the designated uses of water at a specified site;

**water quality standard:** an objective that is recognized in enforceable environmental control laws of a level of government.

These definitions were used by the Canadian Council of Resource and Environmental Ministers (CCREM, 1987) in their efforts to develop a set of water quality guidelines for

Canada. These guidelines are intended to be applied to receiving streams based on knowledge of the chemical, physical and biological characteristics of the water body and the behaviour of the substance once it has been discharged. The objectives set are usually based on the most critical use of the affected reaches. In addition to the Canadian guidelines, a number of provinces have their own receiving water guidelines (Alberta Environment, 1977; Northwest Territories Water Board, 1981; and Saskatchewan Environment and Public Safety, 1988).

The limits on concentrations in the receiving stream are usually called objectives or guidelines as they are general requirements. Setting standards for the receiving environment is not common as it is difficult to monitor (with dilution, the chemicals become harder to detect) and difficult to enforce (non-compliance may be temporary or the result of several dischargers). Fortunately, standards on the effluent discharge from a municipality or a particular industrial facility can be monitored and enforced more effectively.

Effluent discharge standards are often based on the principles of **Best Practical Technology** (the most commonly used and economical in-plant environmental control practices and effluent treatment technologies). Increased concern for the environment has resulted in new industrial facilities being pressured to make use of **Best Available Technology**

(the most sophisticated and effective protection and treatment technologies). Reasons for this would include:

- a) concern about the cumulative effects of loadings on receiving streams by multiple dischargers,
- b) concern about the more subtle effects of certain chemicals, and
- c) desire for a greater level of protection.

Environmental protection can be achieved with effluent standards based on technologies provided that the standards are also evaluated considering the entire river system, all flow conditions, all water users and all effluent dischargers. These considerations and the concerns of the public have manifested themselves in Alberta by the recent recommendation not to proceed with Alberta-Pacific Ltd.'s proposed bleach kraft pulp mill on the Athabasca River (Alberta-Pacific Environmental Impact Assessment Review Board, 1990).

Effluent discharge standards are usually less stringent than receiving stream guidelines as the effluent discharge has not received the benefit of the major assimilative process in a river system (i.e. dilution). Inherently, the philosophy of effluent discharge standards and receiving stream guidelines allows the discharge of chemicals at concentrations which could potentially be hazardous. As the complete mixing of an effluent discharge in a receiving stream takes a considerable distance to occur, there is a possibility for undesirable conditions within the **mixing**

**zone** extending for some distance downstream of the outfall. Further knowledge on the concentrations within the mixing zone is needed to deal with this concern. As a result of this concern, the International Joint Commission (1981) has indicated a need for more knowledge of mixing processes and standards relative to conditions within the mixing zone.

### 1.3 Mixing Phenomena

Many effluents do not meet all receiving stream guidelines at the point of discharge. Dilution occurs within mixing zone and the concentrations of a particular parameter will decrease as the flow progresses downstream. With appropriately set effluent standards, the concentrations downstream of some point in the river will satisfy the receiving stream guidelines. This concept implies that there may be a region within the mixing zone, termed the **limited use zone** by Gowda (1980 and 1984), where the receiving stream guidelines are not met. As a result, it is important that the extent of this adversely affected region be known. Similar to the regions described by Yotsukura and Sayre (1976), three different zones of mixing exist downstream of an outfall (Figure 1.1):

- a) the near field mixing zone,
- b) the far field mixing zone, and
- c) the subsequent dilution zone.

These zones are described in the following.

### 1.3.1 The Near Field Mixing Zone

Near field mixing is of importance for many effluent discharges. It is in the **near field mixing zone** that vertical mixing is achieved. In the case of **passive plume** discharges (i.e. where the discharge velocity is low and the buoyancy is essentially the same as that in the receiving stream), vertical mixing is established within a distance of 50 to 100 times the river depth (Yotsukura and Sayre, 1976). For an effluent whose density is significantly different from the density of the river, this distance can be much greater.

Conditions in the near field mixing zone are important as this region is relatively short and concentrations rapidly decrease. Some or all of the near field mixing zone has been termed the **initial dilution zone** by A. A. Aquatics Research Limited (1987). The provision of some minimum degree of dilution in the vicinity of the outfall (i.e. the initial dilution zone) is now necessary to satisfy some of the new provincial water quality guidelines.

For a neutrally buoyant effluent discharged with negligible momentum from the river bottom, the mixing process is first dominated by the turbulence of the river in the vertical direction. The average vertical dispersion coefficient ( $e_y$ ) can be quantified according to Jobson and Sayre (1970) by:

$$e_y = 0.067 U_* h \quad (1.1)$$

where  $U_*$  is the shear velocity of the flow, and  $h$  is the local depth of flow.

For a bottom discharge, the vertical mixing length ( $X_v$ ) can be determined from Fischer et al (1979):

$$X_v = 0.4 u h^2 / e_y \quad (1.2)$$

where  $u$  is the local depth-averaged velocity of flow.

Based on equations (1.1) and (1.2), rivers in Alberta have vertical mixing lengths in the order of 20 m to 200 m at mean annual flow conditions (Table 1.1). These lengths are in the order of 35 to 100 times the river depth, which is in keeping with that suggested by Yotsukura and Sayre (1976).

This vertical mixing condition may not occur for all effluent discharges as the neutral substance assumption is not satisfied by all effluents. This would be particularly important for effluents of high density being discharged from the bottom of the river. Here, the effluent would tend to stratify on the river bottom.

A high velocity jet discharge can be used to overcome this density related problem (Figure 1.2). If the effluent is discharged through one or more high velocity ports, vertical mixing can be achieved more quickly than with passive plume discharges in spite of any density difference. As a result, improved mixing in the near field can be achieved.

A jet discharge can also shorten the length of the vertical mixing zone and, hence, the initial dilution zone. For a jet discharge, it is the turbulence generated by the effluent discharge that dominates the mixing. This is an important consideration in designing an outfall as it is the

jet turbulence (not that of the river) which is under the control of the designer. Mixing occurs in a jet discharge as it entrains the fluid from the surrounding environment. This mixing phenomenon is effective when the jet discharge velocity is greater than several times the receiving stream velocity. The effects of a well designed jet discharge can extend downstream for a distance of 20 to 40 times the diameter of the jet. In this region, initial dilutions in the order of 20:1 can often be accomplished.

### **1.3.2 The Far Field Mixing Zone**

The **far field mixing zone** extends downstream from the section where vertical mixing has been established. For a discharge source which does not occupy the entire width of the river (i.e. a point source outfall or an effluent diffuser across part of the river) the mixing becomes two dimensional. The effluent is gradually mixed with the river until, at some point, all concentrations across the width of the river are approximately equal. The variation of concentrations within the far field mixing zone can be estimated by analytical methods outlined by Yotsukura and Cobb (1972) and others.

In the far field, mixing processes are dominated by the turbulence of the river. Mixing in this region is controlled by the transverse dispersion coefficient ( $e_z$ ). The transverse dispersion coefficient can be quantified according

to Fischer et al (1979) as a function of the shear velocity and the hydraulic depth of the river cross-section (H):

$$e_z = k U_* H \quad (1.3)$$

Fischer et al (1979) indicated that the dispersion constant (k) has a typical value of about 0.6. Studies by Beltaos (1978a, 1979, and 1980) indicate that the dispersion constant for Alberta rivers is usually in the range of 0.3 to 1.0.

Similar to equation (1.2), Fischer et al (1979) indicated that the theoretical mixing length ( $X_m$ ) for a bank discharge can be estimated by:

$$X_m = 0.4 U W^2 / e_z \quad (1.4)$$

where U is the average velocity of flow, and W is the average river width.

For rivers in Alberta, the theoretical mixing zone lengths are in the order of 30 km to 425 km (Table 1.1). These theoretical lengths are in the order of 400 to 1400 times the river width. In actual fact, the presence of bends, mid-channel islands and other channel irregularities will shorten these lengths considerably. Notwithstanding, the information in Table 1.1 indicates that the length of the mixing zone is about three orders of magnitude greater than the length of the initial dilution zone.

### 1.3.3 The Subsequent Dilution Zone

The **subsequent dilution zone** extends downstream of the mixing zone for as far as the effluent concentrations are detectable. In this zone, further mixing occurs as the



streamflow increases due to tributary inflows and diffuse lateral inflows.

#### **1.4 Study Objectives**

The present body of knowledge for far field mixing in rivers is quite large. Elhadi et al (1984) provide a review of mixing processes which includes 80 references on the subject. Gowda (1980 and 1984) presents procedures to assess the limited use zone for bank outfalls based on the analytical equations for transverse mixing in the far field.

Although the understanding of far field mixing is not yet complete, there is presently a greater need to know more about the initial dilution zone. This is important in the river environment as a significant degree of mixing can be achieved within a distance that is in the order of 1/1000 of the mixing zone length. In recognizing this potential, the Northwest Territories Water Board (1981) limit the extent of this zone to 100 m downstream of the outfall and no more than 1/3 of the river width. The control of the length of the initial dilution zone to occupy only a fraction of the mixing zone requires more knowledge of mixing processes in the near field. ***The overall objective of this dissertation is to provide a means to quantify conditions within an initial dilution zone established using a jet diffuser outfall.***

Jet discharges into crossflows have been studied previously in the context of V/STOL (vertical/short takeoff

and landing) aircraft, atmospheric emissions and ocean outfalls. These studies have examined velocity fields, turbulence and, to a lesser extent, concentrations in a variety of discharge conditions. They all have been carried out in free streams of great depth. In evaluating jet discharges into river systems, it is necessary to know the effect that the depth of flow has on mixing efficiency. In this regard, a number of specific research objectives were established:

- a) to quantify the centreline position and boundary locations for deep and shallow water jet discharges,
- b) to quantify the dilution achieved by jet discharges,
- c) to verify the dilution relations by means of field and laboratory work, and
- d) to develop procedures for application in the design of jet diffuser outfalls.

In this dissertation, available literature on simple jets and jets in crossflow are first reviewed to provide a description of jet mixing phenomena and a starting point for this work. Laboratory work by others is examined and is utilized where possible. A photographic investigation has been carried out to indicate the location, width and thickness of jet discharges in deep and shallow crossflows. A field study has been carried out to measure the dilution of various jet discharges in a real river. The dilution data from this work are compared with laboratory studies of jet dilution to determine coefficients for simple dilution

equations. This field work has been augmented by a comprehensive laboratory investigation of jet dilution in crossflows which identifies a more general dilution equation and indicates the effects of shallow flows.

In addition to this treatment of the near field mixing phenomena, work has been carried out on mixing in the far field. The two dimensional dispersion equations have been examined in a manner which will provide a quantification of the extent of the limited use zone for line source outfalls.

Finally, a case history is presented to give an example of the application of the findings of this work. This knowledge was applied to an outfall built for Daishowa Canada Ltd.'s Peace River pulp mill on the Peace River in 1988. This application is particularly relevant to Alberta as it is one of four new pulp mills constructed over the past three years in this province. Prior to 1988, there were only two pulp mills in Alberta.

Table 1.1 Theoretical mixing zone lengths for selected Alberta rivers

River	Conditions at Mean Flow <sup>1</sup>						Vertical			Transverse			
	Q <sub>r</sub> (m <sup>3</sup> /s)	s	U (m/s)	H (m)	W (m)	U* (m/s)	e <sub>y</sub> (m <sup>2</sup> /s)	X <sub>v</sub> (m)	X <sub>v</sub> /H	e <sub>z</sub> (m <sup>2</sup> /s)	X <sub>m</sub> (km)	X <sub>m</sub> /W	X <sub>m</sub> /X <sub>v</sub>
Oldman River @ Brocket	31	0.00160	0.61	0.70	73	0.105	0.005	24	35	0.044	30	404	1250
Red Deer River @ Red Deer	51	0.00120	0.67	0.82	89	0.098	0.005	33	41	0.049	44	493	1333
Bow River @ Calgary	93	0.00180	0.98	0.94	101	0.129	0.008	43	45	0.073	55	539	1279
South Saskatchewan River @ Medicine Hat	212	0.00041	0.76	1.58	178	0.080	0.008	90	57	0.076	128	716	1422
North Saskatchewan River @ Edmonton	220	0.00035	1.16	1.40	136	0.069	0.007	140	100	0.058	147	1081	1050
Athabasca River @ Athabasca	432	0.00029	0.88	1.71	283	0.070	0.008	129	76	0.071	398	1404	3085
Peace River @ Peace River	1804	0.00035	1.10	3.47	469	0.109	0.025	208	60	0.228	425	905	2043

Notes: 1. River data taken from Kellerhals et al (1972).  
 2. Dispersion constant assumed for e<sub>z</sub> is k ≈ 0.6.

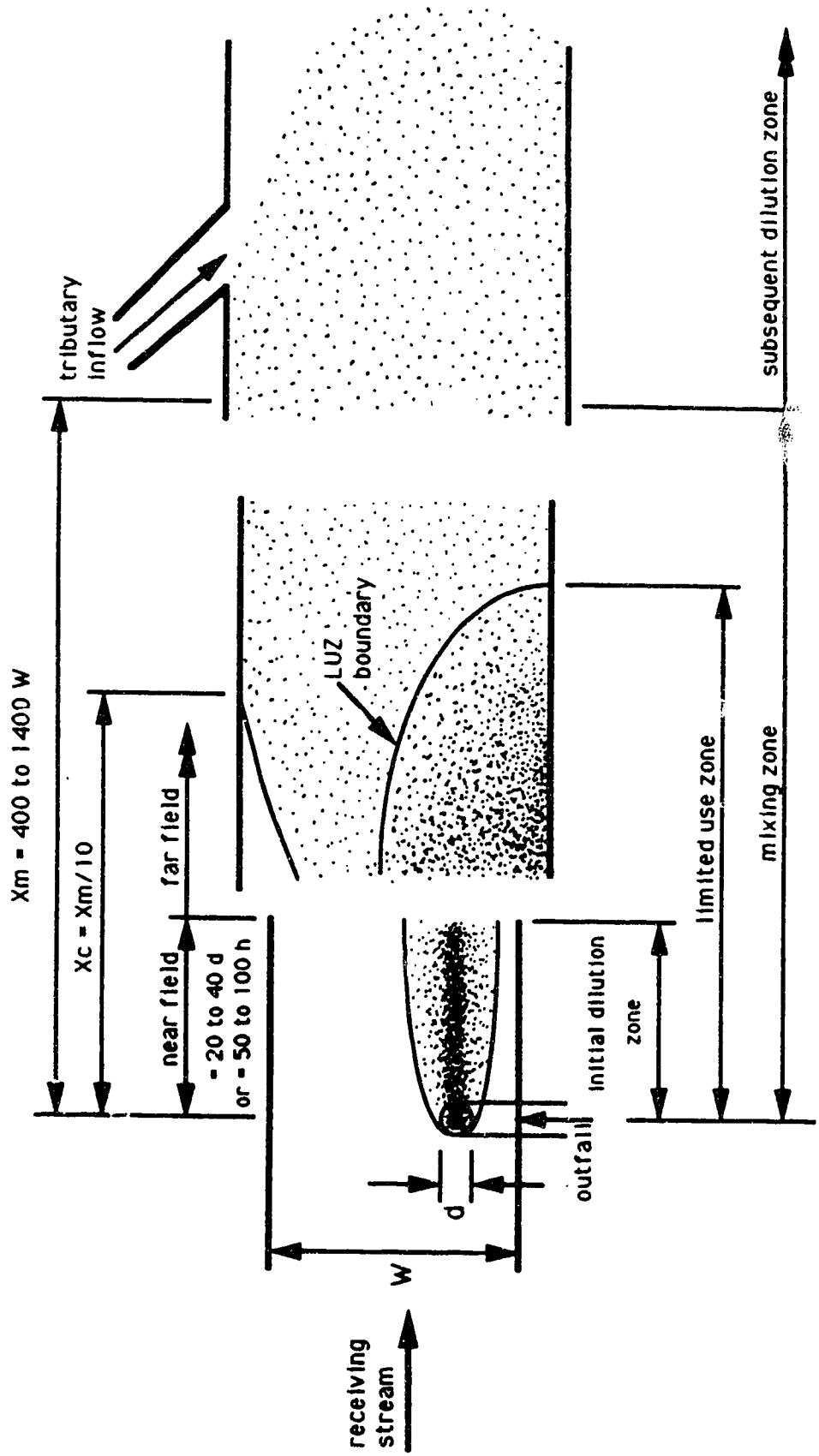


Figure 1.1 Receiving stream regions

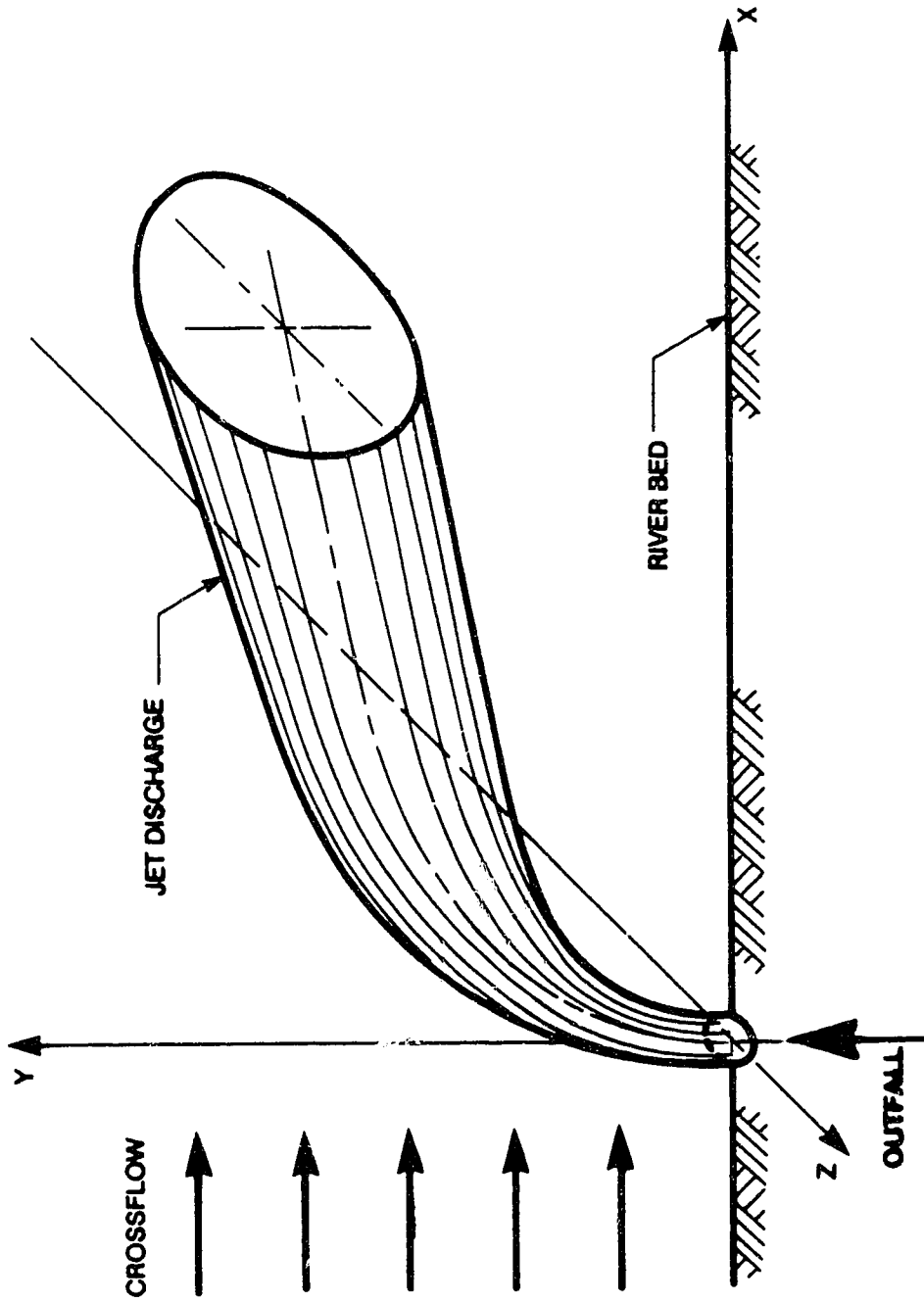


Figure 1.2 Coordinate System for Jet in Crossflow

## Chapter 2

### A REVIEW OF LITERATURE ON JETS IN CROSSFLOW

#### 2.1 General

Society's interest in jets and buoyant jets is mainly related to the aviation industry (e.g. jet engines, turbines, V/STOL aircraft) and the environment (e.g. discharges to the atmosphere and the ocean). According to List (1982), in his review of the mechanics of jets and plumes, the earliest published work on the subject was by Young (1800) who indicated that the included angle of a turbulent jet was independent of the jet velocity. List's review indicated that a considerable research effort has been spent examining the characteristics of jets and plumes in the region near (i.e. within a distance of a few diameters downstream) of the nozzle. He also laments that little effort has been expended on examining the characteristics of the distant regions of these discharges. Examining List's review further indicates that, of his 154 references, fewer than 20 deal with jets or buoyant jets in crossflow.

Sherif and Pletcher (1989) indicated that most of the literature on jets and buoyant jet discharges in crossflow can be classified as experimental, analytical or computational. In this chapter, previous experimental investigations of these discharges will be described. The basic components of jet flow will be examined and, although

the focus will be on jets in crossflow, the nature of simple jets will also be described. In addition, information on buoyant jet discharges will be provided to allow the discrimination between momentum dominated and buoyancy dominated discharges. Although it is expected that well designed effluent discharges in rivers will be momentum dominated due to the shallow nature of rivers, criteria for determining when a discharge is dominated by momentum or buoyancy are necessary. Finally, various analytical and computational investigations of jet discharges in crossflow will be identified to indicate the direction of this area of research.

## **2.2 Experimental Investigations**

Almost all of the relevant literature for jets in crossflow has been published since 1950. This coincides with the initial interest in V/STOL (vertical/short takeoff and landing) aircraft. Most of the initial studies were conducted using pitot and static tubes to measure the total and dynamic pressure heads in the jet discharges (Table 2.1). Many of these investigations have been carried out in wind tunnels. Ruggeri et al (1949) examined the penetration (outer boundary) of jet discharges in a wind tunnel for various orifice shapes. They found that the penetration data could be best explained when the orifice diameter was corrected, to account for the vena contracta, using the flow coefficient. Jordinson (1956) measured total head



distributions for three jet discharges in crossflow and indicated the jet centreline location by the points of maximum pressure. Fearn and Weston (1974 and 1979) conducted several investigations of jets in crossflow at the Langley V/STOL wind tunnel. Their work examined the velocity and pressure distributions in jet discharges having velocity ratios ( $\alpha = U_0/U$ , where  $U_0$  is the velocity of the jet discharge and  $U$  is the crossflow velocity) of 4 and 8. The primary focus of their work was the examination of the vortex properties of the jet discharges.

Experimental work using water as the medium has also been conducted using pitot or Prandtl probes to measure the pressure and velocity distributions in the flow. Gordier (1959) measured the total pressure distribution of jet discharges in a water duct and found them to be similar to those found in previous studies for air jets. Rajaratnam and Gangadhariah (1980) measured the velocity and piezometric pressure distributions for a series of four jet discharges in a water flume. Measurements were made for distances along the curvilinear axis of  $0.25 < \xi/d < 58$ . From these data, they identified relationships for the centreline profile, the shape of the deflected jet, the velocity distribution and the mass and momentum fluxes of the discharges.

Measurements by hot-wire anemometry during the 1960's added new information on jet discharges. The hot-wire experiments allowed the velocity profiles, the location of the jet centreline, the turbulence structure, the vortex

structure, and the temperature distributions in the flow to be measured. Keffer and Baines (1963) examined the velocity and turbulence characteristics of several air jet discharges in crossflow. Their data provided information on the jet centreline location and on the turbulence characteristics of these discharges. Moussa et al (1977) examined the near field of a jet discharge into a crossflow in detail, describing the vorticity ( $\Gamma$ ) of the jet and its wake, the jet boundaries and the velocity distributions within. The jet, which had a velocity ratio of 3.5, was examined for a distance downstream of one nozzle diameter ( $d$ ) and vertically for up to 4.5  $d$ . Andreopoulos and Rodi (1984) examined three jet discharges with low (0.5, 1 and 2) velocity ratios. Their work gave information on the three mean velocity components, the three turbulent shear stresses and the turbulent kinetic energy profiles. Measurements were made as far as 10  $d$  downstream.

The availability of laser Doppler anemometry (LDA) in the mid 1970's allowed a new wave of investigations to be carried out, taking advantage of the new system's capabilities of non-intrusive measurement. Experiments using LDA could provide all of the same measurements as hot-wire anemometry except for temperature. Kotsovinos (1975) conducted one of the earlier investigations on velocity and turbulence distributions in plane jet discharges in water. Crabb et al (1981) were the first to use LDA to investigate the turbulence characteristics of jet discharges in

crossflow. They also used helium tracer techniques to provide some limited concentration data. One notable finding of their work was that the motion of the two vortices could be detected even in the two weak jets ( $\alpha = 1.15$  and  $2.3$ ) examined.

Numerous photographic studies have been carried out to assist in the understanding of jet discharges. Photographic analysis allows the observation of the structure of jet discharges as well as the quantification of jet boundary and jet centreline locations. Photographic analysis formed a large part of the work by Gordier (1959) to quantify the jet outer boundary locations and the widths of jet discharges into crossflows in a water flume. Pratte and Baines (1967) conducted a notable investigation using an oil aerosol to determine the centreline location, the width and thickness of air jet discharges in a crossflow. Margason (1968) did similar work using water vapour for the flow visualization. Crowe and Riesebieter (1967) used smoke to identify the centreline position and spreading rate of air jet discharges in crossflow. Wright (1977a) photographed dye discharges in a water flume. Abdelwahed and Chu (1978) used photographic methods to investigate the characteristics of bifurcating jets and buoyant jet discharge in crossflows.

Sherif and Pletcher (1989) indicated that studies investigating the mean temperature and concentration fields are not as numerous as those examining the velocity field. A number of studies using temperature and other tracers have

been carried out to provide knowledge on the dilution of jet and buoyant jet discharges in quiescent ambients (these are described in Chapter 4). Of the 33 experimental studies of jet discharges in crossflow identified in Table 2.1, only 8 provide significant analyses of temperature or concentration distributions.

Patrick (1967) provided a thorough investigation of both the velocity and concentration distributions of jet discharges in crossflows. He used nitrous oxide ( $\text{NO}_2$ ) as a tracer and presented relations for the dilution of the axial centreline concentration. The dilution was found to be a function of the dimensionless distance along the jet centreline ( $\xi/d$ ). Patrick's work covered distances downstream as far as  $\xi/d = 50$  and dilutions as high as 100:1.

Fan (1967) investigated the dilution of buoyant jet discharges in crossflow. He used a conductivity meter to determine the concentrations within the flow field resulting from the injection of a salt solution through an orifice towed along a stationary flume. Fan examined discharges having velocity ratios of  $4 < \alpha < 16$  and densimetric Froude numbers of  $10 < F_o < 80$ . He found that the jet mixing was dominated by self-generated turbulence for distances of up to  $x = 250 d$ .

Ramsey and Goldstein (1971) examined the temperature distribution for air jet discharges with low velocity ratios ( $\alpha = 0.1, 0.5, 1.0$  and  $2.0$ ). They measured the temperature profiles over a distance of  $x = 10 d$  and found that the two

weaker jets remained attached to the wall. The strongest jet had clearly separated from the wall.

Kamotani and Greber (1972a) examined two heated air jet discharges at higher velocity ratios than were investigated by Ramsey and Goldstein. Kamotani and Greber found that the vortex structure of the weaker jet discharge ( $\alpha = 3.9$ ) did not become established. The stronger jet discharge ( $\alpha = 7.7$ ) exhibited the twin vortex structure typical of jet discharges in crossflow. The centreline temperature was found to decrease as a function of  $\xi/d$ . The decrease was faster for the weaker jet initially but, as the discharge approached  $\xi/d = 70$ , the two jets had about the same dilution.

Chu and Goldberg (1974) conducted an investigation on the location and dilution of buoyant jet discharges in crossflow. They used photographic analysis and salinity measurements to evaluate the results of their theoretical analysis. The analysis indicated that the jet dilution component could be related to the distance downstream by a two-thirds power law. Although the dilution of purely momentum jets were not analysed, their data tended to support this relation in the momentum dominated region.

In addition to conducting photographic work to determine jet centreline location, Wright (1977a) measured the dilution of jet and buoyant jet discharges in crossflows, some of which were stratified. Wright used Rhodamine B Extra dye and fluorometric analysis equipment to measure the concentrations for various discharge conditions. He also developed a light

probe (making use of a laser light generator, a photo detector and a logarithmic amplifier) as another means to measure concentration. The results of Wright's work include:

- a) relationships for the jet centreline location ( $y_c$ ) as a function of the distance downstream from the jet nozzle ( $x$ ),
- b) relationships for jet and buoyant jet dilution as a function of the vertical position above the bed.

Andreopoulous (1983) investigated the temperature, velocity and turbulence characteristics for two weak jet discharges. Their work indicated that jet dilution was proportional to the square root of the distance downstream (i.e.  $C_o/C_m \propto (x/d)^{-1/2}$ ) and was independent of the velocity ratio.

Abdel-Gawad and McCorquodale (1985) conducted a laboratory examination of wall and surface jets discharging perpendicularly into a half-trapezoidal channel. They measured the velocity, concentration and temperature distributions for several discharge configurations. They found that the dilutions for the horizontal outfalls were about one-half that determined by Rajaratnam and Gangadhariah (1980) for vertical jet discharges into crossflows. Although the dilutions achieved with the horizontal outfalls were less than those for the vertical jet discharges, they were about twice that for simple jet discharges into quiescent ambients.

## 2.3 Description of Jet Discharges

### 2.3.1 Jet Discharges into a Quiescent Ambient

A jet discharging into a quiescent ambient has two distinct zones of flow (Figure 2.1). The first is the **potential core**. As the discharge exits from a well designed nozzle, it will have a nearly uniform velocity over the entire exit area. There will be little turbulence in this essentially potential flow. As the flow enters the receiving water, tremendous shear occurs at the interface. Turbulence is generated and increases in magnitude and extent as the flow advances into the ambient. At some point, all evidence of potential flow disappears at the tip of the potential core. This region has also been called the **zone of flow establishment** (ZFE) by others (Albertson et al, 1950; Abraham, 1960; Hirst, 1972). The length of this region has been indicated to be about  $6d$  by Albertson et al (1950), Abraham (1960), Rajaratnam (1976), and others.

Beyond the potential core is the second region of flow, termed the **zone of established flow** (ZEF). The velocity and concentration along the centreline decrease linearly with distance (Rajaratnam, 1983):

$$\frac{u_m}{U_o} = 6.13 \frac{d}{x} \quad (2.1)$$

$$\frac{C_m}{C_o} = 5.34 \frac{d}{x} \quad (2.2)$$

where:  $U_0$  is the jet velocity at the nozzle,  
 $u_m$  is the centreline velocity at a section,  
 $x$  is the distance from the nozzle to the section,  
 $d$  is the jet nozzle diameter,  
 $C_0$  is the concentration at the jet nozzle, and  
 $c_m$  is the centreline concentration at a section.

The radial distributions of longitudinal velocity and concentration for a jet are self-similar in the ZEF:

$$\frac{u}{u_m} = \exp \left\{ -\ln 2 \left( \frac{r}{b} \right) \right\} \quad (2.3)$$

$$\frac{c}{c_m} = \exp \left\{ -\ln 2 \left( \frac{r}{k b} \right) \right\} \quad (2.4)$$

where:  $u_m$  is the maximum velocity at the section,  
 $u$  is the velocity at a point,  
 $r$  is the radial distance to the point,  
 $b$  is the jet half-width at the section,  
 $c_m$  is the maximum concentration at the section,  
 $c$  is the concentration at a point, and  
 $k$  is the diffusion coefficient ratio.

For a circular turbulent jet discharge in a quiescent ambient, the **jet half-width** (the distance from the centreline to the point where the velocity is one half the centreline value) grows in proportion to the distance from the nozzle (as was qualitatively observed by Young in 1800):

$$b = 0.096 x \quad (2.5)$$



The jet half-width for concentration also grows in a linear fashion but at a faster rate proportional to the diffusion coefficient ratio (i.e.  $b = 0.096 k x$ ).

The diffusion coefficient ratio has been determined to have a constant value over the length of the jet of about 1.17 (Hinze and van der Hegge Zijnen, 1949; Forstall and Gaylord, 1955; Rajaratnam, 1983). Work by Shaughnessy and Morton (1977) indicates that the diffusion coefficient ratio may vary, being lower near the jet outlet and increasing slightly as the discharge progresses into the ambient.

Equations (2.1) through (2.5) have been developed based on experimental and analytical procedures. These equations indicate that, as the flow progresses along the ZEF, the magnitude of the velocities and concentrations decrease and the discharge is dispersed into the ambient. They are appropriate for circular turbulent jet discharges. Fischer et al (1979) indicated that most jets, depending on the initial velocity profile, will be turbulent when the jet Reynolds number ( $R_j = \frac{U_o d}{\nu}$  - where  $\nu$  is the kinematic viscosity) has a value of 2000. All jet discharges will be turbulent for  $R_j > 4000$ .

### **2.3.2 Jet Discharges in Crossflow**

A circular jet discharge into a crossflow of infinite depth begins in a similar fashion to the simple jet but experiences three zones of flow (Figure 2.2):

### Potential Core

The potential core begins similarly to that described previously for jet discharges in quiescent ambients. However, due to the increased shear that the crossflow exerts on the jet, the length of this region is less. A number of investigators have examined the length of the potential core of jets in crossflow (Pratte and Baines, 1967; Keffer and Baines, 1971; Hirst, 1972; Stoy and Ben-Haim, 1973; Rajaratnam and Gangadhariah, 1980). Their measurements indicate that the potential core length ( $l_c$ ) varies with the velocity ratio, being in the order of 1 to 4 times the jet diameter when  $\alpha < 10$  (Figure 2.3). Stoy and Ben-Haim presented an equation for the potential core length:

$$\frac{l_c}{d} = 5 \exp \left\{ \frac{-1.93}{\alpha} \right\} \quad (2.6)$$

Hirst (1972) developed a method for predicting the length of the zone of flow establishment for discharges to quiescent, moving and stratified ambients. Hirst also presented an empirical equation which correlated well with the results of his analysis and the experimental work of others:

$$\frac{l_c}{d} = 6.2 \exp \left\{ \frac{-3.4}{\alpha} \right\} \quad (2.7)$$

It would be difficult to accurately determine a relation for  $l_c$  based on these data as the potential core lengths have not been consistently determined. Many have been determined based on extending the centreline velocity profile back to

the point where ( $u_m/U_o = 1$ ) on a log-log plot (Figure 2.4). This method tends to overestimate  $l_c$  as the velocity profile varies in a non-linear fashion near the potential core.

Another interesting feature of the potential core is that it can be displaced downstream by the crossflow. This is due to the difference in pressure that occurs between the upstream and downstream sides of the jet as the free stream flows past the quasi-solid cylindrical jet near the nozzle. For jets in weak (i.e.  $\alpha < 2$ ) crossflows, this effect is significant (Platten and Keffer, 1971). This phenomenon can also be observed in the velocity profile measurements of Kamotani and Greber (1972a). Rajaratnam (1976) indicates that the potential core remains aligned with the jet axis for  $\alpha > 4$ .

#### ***Zone of Maximum Deflection***

The zone of maximum deflection is the transition between the potential core (which is oriented along the jet axis) and the vortex zone (when the jet discharge is almost parallel with the crossflow). In the zone of maximum deflection, the jet is deformed from its original circular shape to a kidney shaped cross section. This is because the upstream outer layers of the jet lose their velocity through the entrainment of free stream fluid. The deformed jet comprises a pair of attached counter-rotating vortices. Fearn and Weston (1974) indicated that the magnitude of vorticity (and, hence, the extent of the kidney shape) generated is a function of the jet's diameter and initial velocity. Moussa et al (1977)

indicated that the interactions at the interface of the jet and the crossflow also generate vortices which shed and flow in the wake downstream of the jet.

As the jet progresses through the zone of maximum deflection, it grows due to further entrainment of the free stream fluid. During the progression, the total flow rate of the jet increases while the maximum velocity and concentration decrease. This zone extends along the curvilinear jet axis for a dimensionless distance ( $\xi/d$ ) of 15 to 20. This zone is important when considering the location, the velocity distribution and the concentration distribution within the jet discharge.

#### **Vortex Zone**

In the vortex zone, the jet direction and the jet velocities are similar to those of the free stream. The jet maintains its two distinct vortices in this zone. Pratte and Baines (1967) and Fearn and Weston (1979) indicated that the vortices begin to dominate the discharge starting about  $x = 10 d$  downstream of the discharge nozzle. They indicated that these vortices have been observed as far as  $1000 d$  downstream of the jet nozzle. Abdelwahed and Chu (1978) indicated that the vorticity is not preserved in the vortex zone flow but decreases as the discharge progresses downstream. This has also been indicated by Fearn and Weston (1974 and 1978).

The dilution of the discharge is dominated by vortex entrainment in this region. Examination of the entrainment

velocity and dilution curves for the jet region and vortex zone in the work of Kamotani and Greber (1972a) indicates that the dilution in the vortex zone will be less than the initial region of the jet discharge.

#### **2.4 Length Scales for Buoyant Jet Discharges**

The quantification of the nature of jet or buoyant jet discharges in crossflow begins with the determination of a number of basic length scales. These have been identified by Wright (1977a), Fischer et al (1979) and List (1982):

$$\text{volume length scale: } l_Q = \frac{Q}{M^{1/2}} = \sqrt{A} = \sqrt{\frac{\pi}{4}} d \quad (2.6)$$

$$\text{buoyancy length scale: } l_M = \frac{M^{3/4}}{B^{1/2}} = \frac{U_o A^{1/4}}{\sqrt{g'}} = \sqrt[4]{\frac{\pi}{4}} F_o d \quad (2.7)$$

$$\text{momentum length scale: } l_m = \frac{M^{1/2}}{U} = \sqrt{\frac{\pi}{4}} \alpha d \quad (2.8)$$

$$\text{buoyant jet length scale: } l_b = \frac{B}{U^3} = \frac{g' U_o A}{U^3} = \frac{\pi \alpha^3}{F_o^2} d \quad (2.9)$$

where:  $Q = \frac{\pi d^2}{4} U_o$  is the initial volume flux,

$M = U_o Q$  is the initial momentum flux,

$B = g' Q$  is the initial buoyancy flux,

$g' = g \frac{\rho - \rho_o}{\rho_o}$  is the apparent gravitational constant,

$g$  is the gravitational constant,

$\rho$  is the density of the ambient,

$\rho_o$  is the density of the discharge, and

$F_o = \frac{U_o}{\sqrt{g' d}}$  is the densimetric Froude number.

The first two length scales relate to buoyant jet discharges in a quiescent ambient. They indicate when a discharge is jet-like or plume-like (the two extreme cases):

$l_Q \gg l_M$  - the flow is momentum dominated (jet-like),

$l_Q \ll l_M$  - the flow is buoyancy dominated (plume-like).

Most discharges are affected to some extent by both momentum and buoyancy (i.e. buoyant jets). In the initial region of any discharge (i.e.  $y < 10 l_Q$ ) the flow characteristics will be influenced mainly by the geometry of the outlet. In the subsequent region, buoyant jet discharges will be affected by both momentum and buoyancy (initially behaving first like a jet, then like a plume). Based on work by Kotsovinos (1978) it can be determined that a buoyant jet discharge will be equally affected by momentum and buoyancy effects at a section located  $x/d = 2 F_0$  from the outlet.

The latter two length scales ( $l_m$  and  $l_b$ ) can be used to identify the various zones of flow for jet and buoyant jet discharges in crossflow:

$l_m \gg l_b$  - jet effects dominate the discharge; then:

$y < l_c$  - flow partially develops (potential core),

$y < l_m$  - flow is dominated by the jet, and

$y > l_m$  - flow is dominated by the crossflow.

$l_b \gg l_m$  - buoyancy effects dominate the discharge; then:

$y < l_Q$  - flow develops (nozzle effects govern),

$y < l_m$  - flow is dominated by the jet,

$y < l_b$  - flow is buoyancy dominated (rising), and

$y > l_b$  - the flow is dominated by the crossflow.

The length scales have been used in dimensional analysis to develop fundamental profile, velocity, and concentration relationships (Wright, 1977a). They also can be used to determine which processes govern for a given discharge. As an example, consider a high temperature effluent being discharged to a northern river in winter:

effluent temperature: 30 °C

discharge velocity: 3 m/s

nozzle diameter: 0.15 m

river temperature: 0 °C

river depth: 3 m

river velocity: 0.5 m/s

The densimetric Froude number and the length scales for this discharge condition are:

$$F_o = 38.1$$

$$l_o = 0.13 \text{ m}$$

$$l_c \approx 0.53 \text{ m}$$

$$l_M = 5.38 \text{ m}$$

$$l_m = 0.80 \text{ m}$$

$$l_b = 0.07 \text{ m}$$

The discharge is momentum dominated since the momentum length scale is much greater than the buoyant jet length scale (i.e.  $l_m \gg l_b$ ). The discharge is developing in the initial region ( $y < l_c = 0.53 \text{ m}$ ). Jet effects next govern for  $y < 0.80 \text{ m}$ , then the crossflow begins to dominate the discharge for  $y > l_m$ . The discharge is not significantly affected by

buoyancy since the depth of the river is less than the buoyancy length scale (i.e.  $l_M > D$ ).

From these considerations, it can be seen that most effluent discharges to rivers can be designed, using jet diffusers, to eliminate any undesirable effects of density stratification.

## **2.5 Analytical and Computational Investigations**

Many attempts have been made to provide a quantitative description of jet and buoyant jet discharges in crossflow. These have taken the form of empirical relations (based on dimensional analysis and experimental investigation), analytical approaches (which yield either closed form solutions or require numerical methods) and turbulence models.

Rajaratnam (1976) presents seven empirical relations which have been developed by others and describes four analytical methods used to quantify jets in crossflow. Wright (1977a) presents a review of dimensional analysis and the results of 16 analytical approaches to the problem.

### **2.5.1 Empirical Methods**

Empirical approaches have usually involved dimensional analysis in conjunction with experimental measurements. Many of the early investigations focussed primarily on the location of the jet centreline ( $y_c$ ). They usually presented the results of their work in a dimensionless form:



$$\frac{y_c}{d} = c \alpha^a \left(\frac{x}{d}\right)^b \quad (2.10)$$

where  $a$ ,  $b$  and  $c$  are constants.

Many of the investigations have attempted to determine the most appropriate dimensionless form for data presentation. The work of Pratte and Baines (1967) appears to be the first to use the form:

$$\frac{y_c}{\alpha d} = c \left(\frac{x}{\alpha d}\right)^b \quad (2.11)$$

This form of relation provides the most universal explanation of the location of jets in crossflow. Figures 2.5 and 2.6 present data from selected experimental investigations to indicate the nature of the information they provide. The computed velocity centreline locations, using the equation from Rajaratnam and Gangadhariah (1981a), are also shown to indicate the type of predictions achievable. The equation, presented in Table 2.2, has been modified by the writer to include a simpler function for the empirical factor ( $\beta$ ) in order to facilitate its application.

Wright (1977a) provides one of the more detailed investigations of jet and buoyant jet discharges in crossflow. He used dimensional arguments to identify two regions of flow for jet discharges in crossflow - the momentum dominated near field (MDNF) and the momentum dominated far field (MDFF). He also developed relationships for the dilution ratio ( $S_o = C_o/C_m$ ) for these two flow fields (Table 2.3). The exponents in his relationships are fixed,

due to the results of his dimensional arguments, leaving only one coefficient to be determined for each relation. Wright similarly presented relationships for the two flow fields for buoyant jet discharges in crossflow (i.e. BDNF and BDFE).

Wright's experimental work focussed on providing values for the coefficients. In some cases the coefficients were found to vary slowly as a function of one of the scaling parameters (e.g. in the case of the jet centreline location,  $C_1$  and  $C_2$  are slowly increasing functions of  $\alpha$ ). Careful examination of figures 2.5 and 2.6 support this - the trend line for the latter would have higher values.

### **2.5.2 Analytical Methods**

Analytical methods to determine the path of a discharge in a crossflow have been developed in a number of different ways:

#### **Kinematic Methods**

Kinematic methods involve some method of geometric superposition of the two interacting flows. These methods have been put forth in the earlier works of Abramovich and others. Abramovich indicated that several attempts were made in the 1930's at this type of solution. However, the conclusions of Abramovich (1963) and of Vizek and Mostinskii (1964) are that these solutions are only appropriate for ideal fluids and show poor agreement with experimental values.

### **Dynamic Methods**

Dynamic methods are based on the analysis of the forces exerted on the jet by the free stream. These methods equate the normal component of the drag force to the centrifugal force of the jet (based on the jet's radius of curvature). They also usually assume that the momentum of the jet in the vertical direction is preserved. Many analyses have been developed based on these premises (Table 2.2). The list in Table 2.2 is only partially complete as it does not include many of the solution procedures for buoyant jet discharges. Wright (1977a) has a more complete compilation of these.

Dynamic methods usually result in closed form solutions. One of the main difficulties with the dynamic solutions is that the drag coefficients required to establish the force balance must be unrealistically high in order to properly predict the jet trajectory in the zone of maximum deflection. The problems often continue in that, after the drag coefficients have been defined for this zone, the procedures do not perform well in the far region where the curvature is much less.

### **Integral Methods**

Integral methods involve specifying the equations for the conservation of mass, momentum, energy and pollutant. These equations are integrated across a section normal to the jet trajectory under the assumption that all turbulent transport vanishes at the jet boundary (Wright, 1977a). This method was proposed by Morton, Taylor and Turner (1956) for

buoyant jet discharges to a quiescent stratified ambient. It has also been used later in the analysis of buoyant jets in crossflow.

All integral analyses make use of an entrainment function to provide the source of free stream fluid for the buoyant jet's growth as the discharge progresses into the flow. Most make the assumption of a hydrostatic pressure distribution throughout the flow field. As a result, they do not include the pressure drag considerations which are fundamental to the dynamic solutions. Fan's (1967) analysis and that by Chan et al (1976) are integral procedures which also include drag forces.

### **2.5.3 Turbulence Modelling**

The discharge of jets or buoyant jets into receiving waters are slender shear flows. These are complex free turbulent flows. The governing equations for turbulent flow are called the Navier-Stokes equations. Rodi (1980) indicated that there are numerical procedures available to solve these equations but the storage and computational requirements for solution are too great for such methods to be of interest. As a result, simpler models of turbulent flow have been sought.

One of the most frequently used simplifications to the Navier-Stokes equations is the statistical approach of time-averaging the equations and assuming that the fluctuations are small relative to the mean values. The subsequent

equations are called the Reynolds equations and describe the mean characteristics of the flow (i.e. velocity, pressure, temperature and concentration). These simplifications also require certain assumptions on the turbulent transport of mass and pollutant. The simplifications have been found to be reasonable for many aspects of slender flows. Part of this success is due to the relative transport of material; List (1982) indicates that the mean flow is responsible for about 85% of both the momentum flux and the pollutant flux for jet discharges into a quiescent ambient.

As the nature of a turbulent flow gets more complex (e.g. a jet in a crossflow), the flow gets more difficult to quantify with the simpler analytical methods discussed in Section 2.5.2. Analytical methods are also of limited use if the main interest is in the turbulence characteristics of the flow. In such circumstances, the investigation can proceed in one of two directions: experimental work and/or turbulence modelling.

Turbulence models require the specification of a mathematical model of the turbulent transport processes so that the related terms can be computed at all parts of the flow. Rodi and Svrivatsa (1979) developed a procedure for analysing a jet in a ducted crossflow which greatly reduced the computational requirements. Their model was fully three-dimensional in the vicinity of the jet discharge nozzle, but was two-dimensional downstream. In an intermediate region,

the equations were three-dimensional for pressure but were two dimensional for all other parameters.

Rodi (1980) identified several other turbulence models which could be considered. He indicated that two-equation k- $\epsilon$  model was much superior to the simpler turbulence models and required only marginally more computational resources. Hossain and Rodi (1982) presented even more complex turbulence models (two forms of the k- $\epsilon$  model and an algebraic stress/flux model) and applied them with good success to jet and buoyant jet discharges in a quiescent ambient.

As the interests for most environmental problems (particularly for effluent discharges to rivers) are in the characteristics of the mean field, turbulence modelling has not yet found wide acceptance. However, the interest in turbulence modelling will grow in the years to come. There will be interest from other areas of environmental science (such as atmospheric emissions - this area would have a greater need for knowledge on the nature of the fluctuating flow). The anticipated increase in computer capabilities will facilitate the more sophisticated numerical analyses, making their application more pragmatic. Finally, the continued public pressure for more knowledge on environmental issues will demand more sophisticated solutions.

Table 2.1 Summary of experimental work on jet discharges in crossflow

Experiment	medium	equipment	outlet	$\alpha$ (#runs)	maximum	
					x/d	results
Ruggeri et al (1949)	air	pitot/TC	various	(several)	n/a	$y_0, P, T$
Shandorov (1955)	air	pitot	n/a	2.2-4.0 (2)	<4	$Y_c$
Jordinson (1956)	air	pitot	orifice	4.3-8.1 (3)	17	$Y_c, u, P$
Ivanov (1959)	air	pitot	n/a	3.5-20 (3)	30	$Y_c$
Gordier (1959)	water	pitot/photo	nozzle	4.0-8.0 (3)	17	$Y_c, Y_0, u, W_z, P$
Keffer and Baines (1963)	air	HWA	orifice	2.0-10 (5)	4	$Y_c, u, u', W_z, m, \alpha_e$
Crowe & Riesebieter (1967)	air	photo	tube	2.8-7.4 (3)	<2	$Y_c, W_z$
Pratte & Baines (1967)	air	photo	orifice	5-35 (4)	1200	$Y_c, Y_i, Y_0, W_z, W_y$
Patrick (1967)	air	pitot/photo	nozzle	8.5-54 (23)	44	$Y_c, u, C(NO_2)$
Fan (1967)	water	photo/CP	orifice	4.0-16 (10)	232	$Y_c, C$
Margason (1968)	air	photo	nozzle*	1.2-10 (23)	22	$Y_c$
McMahon and Mosher (1969)	air	pitot	various	8.0-12 (3)	10	$Y_c, P$
Platten and Keffer (1971)	air	HWA	pipe*	4.0-8.3 (3)	8	$Y_c$

Table 2.1 Summary of experimental work on jet discharges in crossflow (continued)

Experiment	medium	equipment	outlet	$\alpha$ (#runs)	maximum	
					x/d	results
Ramsey and Goldstein (1971)	air	HWA/TC	tube*	0.1-2.0 (4)	10	$u, u', T$
Kamotani and Greber (1972a,b)	air	HWA/TC	nozzle	3.9-7.7 (2)	15	$Y_c, u, u', W_z, P, \alpha_e, T$
Campbell and Schetz (1973)	water	pitot	orifice*	9.0-29 (2)	15	$Y_c$
Stoy and Ben-Haim (1973)	air	pitot/photo	nozzle	2.5-6.8 (3)	<2	$Y_c, l_c$
Fearn and Weston (1974)	air	pitot	nozzle	3-10 (7)	45	$Y_c, u, v, \Gamma$
Chu and Goldberg (1974)	water	photo/CP	tube	6.3-44 (8)	60	$Y_c, C$
Chaissang et al (1976)	air	pitot/HWA	tube	2.4-6.4 (3)	12	$Y_c, u, W_z, W_y$
Chan et al (1976)	air	pitot/HWA	nozzle	4.2-8.8 (3)	<3	$Y_c, u, W_z, P, \alpha_e$
Moussa et al (1977)	air	HWA	pipe	3.48 (1)	1	$u, v, w, \Gamma$
Wright (1977a)	water	photo/dye	orifice	0.8-116 (184)	113	$Y_c, C$
Abdelwahed and Chu (1978)	water	photo	nozzle	2-40 (64)	460	$Y_c, W_z, W_y$
Fearn and Weston (1979)	air	pitot	nozzle*	4-8 (2)	20	$Y_c, u, v$
Steffler (1980)	water	pitot	nozzle	4.1-13 (6)	38	$Y_c, u$



Table 2.1 Summary of experimental work on jet discharges in crossflow (continued)

Experiment	medium	equipment	outlet	$\alpha$ (#runs)	maximum	
					x/d	results
Rajaratnam & Gangadhariah (1980)	water	pitot	nozzle	2.7-23 (4)	29	$Y_c, u, W_z, W_y, P$
Crabb et al (1981)	air	LDA/HWA	tube	1.15-2.3 (2)	20	$u, v, w, u', v', w'$ $uv, uw, C(He)$
Andreopoulos (1983)	air	HWA/TC	tube	0.25-2.0 (4)	10	$u, v, u', v', T,$ $T', uT, vT$
Andreopoulos and Rodi (1984)	air	HWA	tube	0.5-2.0 (3)	10	$u, v, w, u'$
Chu (1985)	water	photo	tube*	2.0-10 (5)	40	$Y_c, W_z, W_y$
Abdel-Gawad & McCorquodale (1985)	water	dye/TC/pitot	tube	2.0-5.2 (16)	24	$Y_c, u, C, T$
Sherif and Pletcher (1989)	water	HFA	tube*	4.0-6 (2)	13	$u, v, w, u',$ $v', w'$

Notes: n/a indicates that the information was not available from the literature.

\* denotes work where the angle of the jet discharge was varied from 90°.

CP - conductivity probe (salinity measurements)

HFA - hot-film anemometer

HWA - hot-wire anemometer

LDA - laser Doppler anemometer

TC - thermocouple

Table 2.2 Solution procedures for jet discharges in crossflow

Investigators	Method	Equation	Remarks
Gordier (1959)	empirical	$\frac{Y_c}{\alpha d} = 1.31 \alpha^{0.11} \left(\frac{x}{\alpha d}\right)^{0.37}$	pressure
Pratte and Bains (1967)	empirical	$\frac{Y_c}{\alpha d} = 1.76 \left(\frac{x}{\alpha d}\right)^{0.28}$	photos
Patrick (1967)	empirical	$\frac{Y_c}{\alpha d} = \alpha^{0.23} \left(\frac{x}{\alpha d}\right)^{0.38}$	velocity
Patrick (1967)	empirical	$\frac{Y_c}{\alpha d} = \alpha^{0.19} \left(\frac{x}{\alpha d}\right)^{0.34}$	tracer
Margason (1968)	empirical	$\frac{Y_c}{\alpha d} = 1.59 \left(\frac{x}{\alpha d}\right)^{1/3}$	photos
Ziegler and Wooler (1971)	integral	forces and entrainment	iterative
Kamotani and Greber (1972a)	empirical	$\frac{Y_c}{\alpha d} = 0.89 \alpha^{0.30} \left(\frac{x}{\alpha d}\right)^{0.36}$	velocity
Kamotani and Greber (1972a)	empirical	$\frac{Y_c}{\alpha d} = 0.73 \alpha^{0.33} \left(\frac{x}{\alpha d}\right)^{0.29}$	temperature

Table 2.2 Solution procedures for jet discharges in crossflow (continued)

Investigators	Method	Equation	Remarks
Campbell and Schetz (1973)	integral	forces and entrainment	iterative
Stoy and Ben-Haim (1973)	integral	entrainment	iterative
Chaissang et al (1974)	empirical	$\frac{Y_c}{\alpha d} = \left( 0.61 \alpha^{0.385} + \frac{1}{\alpha^{0.615}} \right) \left( \frac{x}{\alpha d} \right)^{0.385}$	velocity
Fearn and Weston (1974)	empirical	$\frac{Y_c}{\alpha d} = 0.98 \alpha^{0.25} \left( \frac{x}{\alpha d} \right)^{1/3}$	velocity
Fearn and Weston (1974)	empirical	$\frac{Y_c}{\alpha d} = 0.35 \alpha^{0.56} \left( \frac{x}{\alpha d} \right)^{0.43}$	vortex
Fearn and Weston (1974)	dynamic	filament & diffuse vortex	iterative
Chu and Goldberg (1974)	integral	$\frac{Y_c}{\alpha d} = 1.44 \left( \frac{x}{\alpha d} \right)^{1/3}$	photos
Chien and Schetz (1975)	Navier-Stokes	finite difference	iterative
Chan et al (1976)	integral	forces and entrainment	closed form
Sucec and Bowley (1976)	dynamic	forces (finite difference)	iterative

Table 2.2 Solution procedures for jet discharges in crossflow (continued)

Investigators	Method	Equation	Remarks
Adler and Baron (1979)	integral	forces and entrainment	iterative
Srivatsa and Rodi (1979)	turbulence	locally elliptical; 3-d & 2-d	
Rajaratnam and Gangadhariah (1981a)	dynamic	$\frac{x}{d} = \frac{C_d}{\pi} \left( \frac{y_c}{\alpha d} \right)^2 \left( \frac{\beta y_c}{3 d} + 1 \right)$	$C_d=1.5$ ; $\beta=\frac{12}{\alpha}$
Rodi (1980)	turbulence	k-ε	
Hossain and Rodi (1982)	turbulence	k-ε and algebraic stress/flux	
Chu (1985)	integral	forces and entrainment	closed form
Steffler and Rajaratnam (1985)	integral	$\frac{y_c}{\alpha d} = 2.47 \left( \frac{x}{\alpha d} \right)^{1/2}$	moment of momentum

Note: Several of the equations have been rearranged to provide consistency in presentation.

Table 2.3 Trajectory and dilution relationships from Wright (1977a and 1977b)

Flow Regime	Trajectory relation	Dilution relation
Momentum dominated near field (MDNF)	$\frac{y_c}{l_m} = C_1 \left( \frac{x}{l_m} \right)^{1/2}$	$\frac{S_0 Q}{U l_m^2} = C_3 \left( \frac{y_c}{l_m} \right)$
Momentum dominated far field (MDF)	$\frac{y_c}{l_m} = C_2 \left( \frac{x}{l_m} \right)^{1/3}$	$\frac{S_0 Q}{U l_m^2} = C_4 \left( \frac{y_c}{l_m} \right)^2$
Buoyancy dominated near field (BDNF)	$\frac{y_c}{l_b} = C_5 \left( \frac{x}{l_b} \right)^{3/4}$	$\frac{S_0 Q}{U l_b^2} = C_7 \left( \frac{y_c}{l_b} \right)^{5/3}$
Buoyancy dominated far field (BDF)	$\frac{y_c}{l_b} = C_6 \left( \frac{x}{l_b} \right)^{2/3}$	$\frac{S_0 Q}{U l_b^2} = C_8 \left( \frac{y_c}{l_b} \right)^2$

Notes:

- Coefficients: C<sub>1</sub> - photos: 0.8 to 2.0 (varies with  $\alpha$ ); concentration:  $\approx 2.35$   
 C<sub>2</sub> - photos: 0.9 to 1.9; concentration:  $\approx 2.1$  (both vary with  $\alpha$ )  
 C<sub>3</sub> -  $\approx 0.35$   
 C<sub>4</sub> -  $\approx 0.14$   
 C<sub>5</sub> - photos:  $\approx 1.35$ ; concentration:  $\approx 1.8$  (both vary with  $l_c/l_b$ )  
 C<sub>6</sub> - photos:  $\approx 0.85$  ( $l_m/l_b$ )<sup>1/6</sup>; concentration:  $\approx 1.4$  ( $l_m/l_b$ )<sup>1/6</sup>  
 C<sub>7</sub> -  $\approx 0.20$   
 C<sub>8</sub> -  $\approx 0.41$

$y_c$  values used in dilution relations are from concentration profiles.

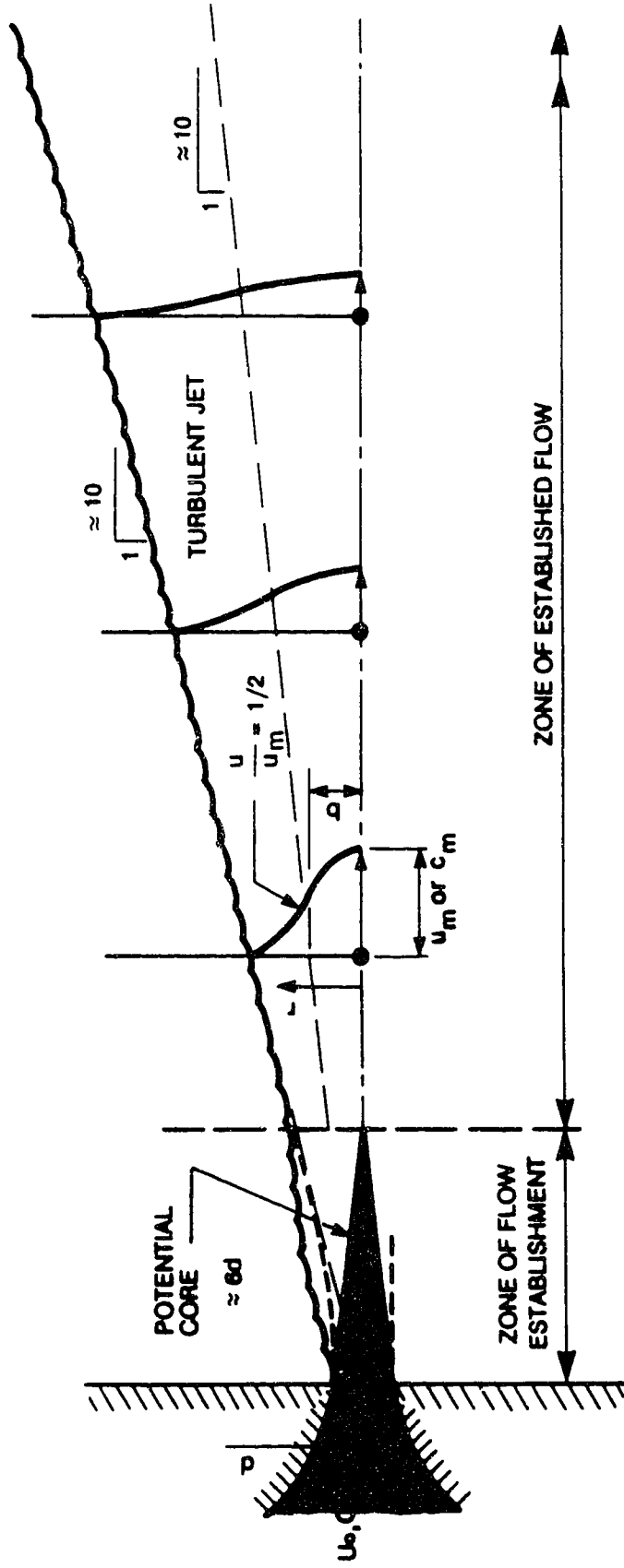


Figure 2.1 Jet Discharge into a Quiescent Ambient

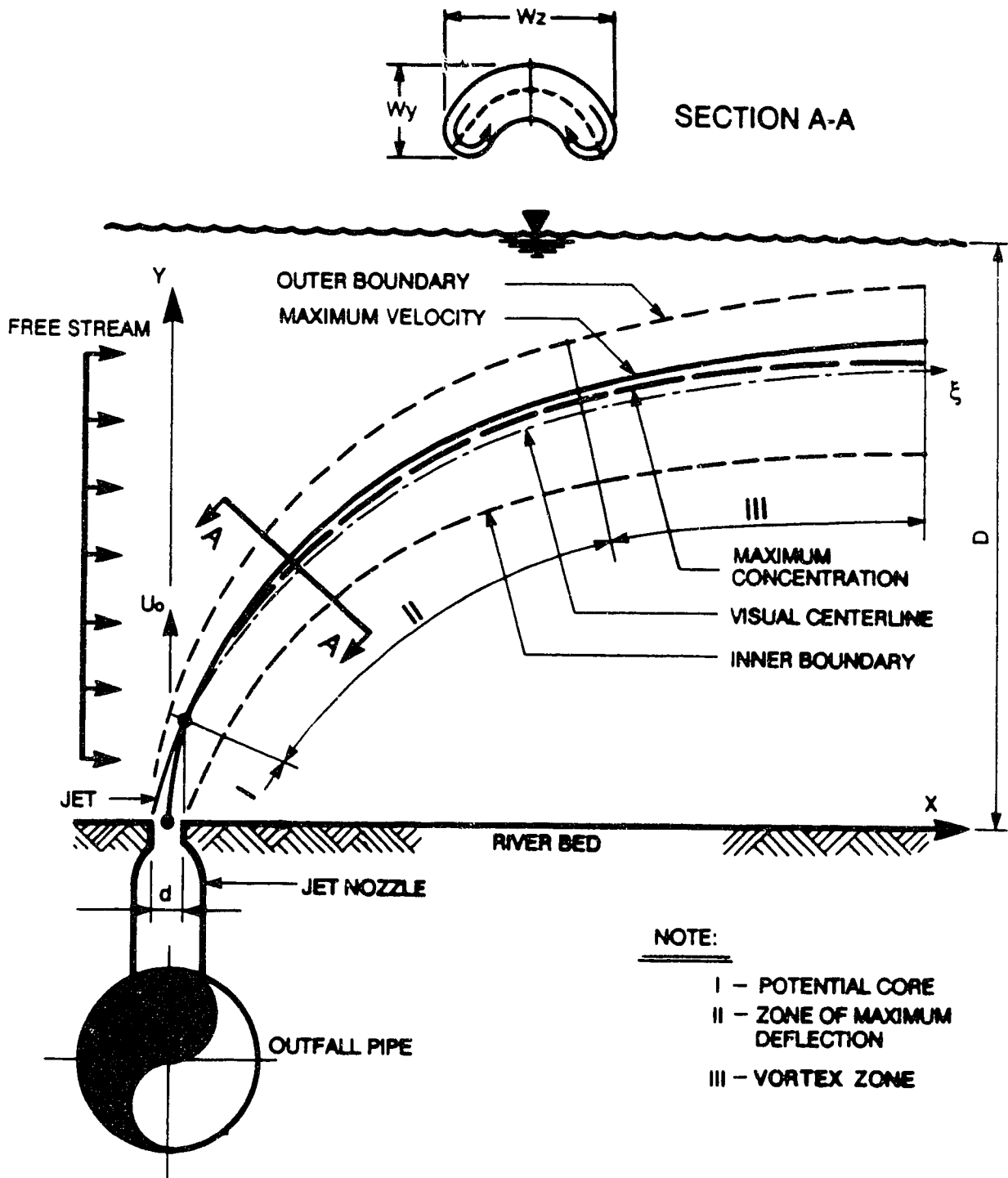


Figure 2.2 Jet Discharge into a Crossflow

Figure 2.3 Length of potential core

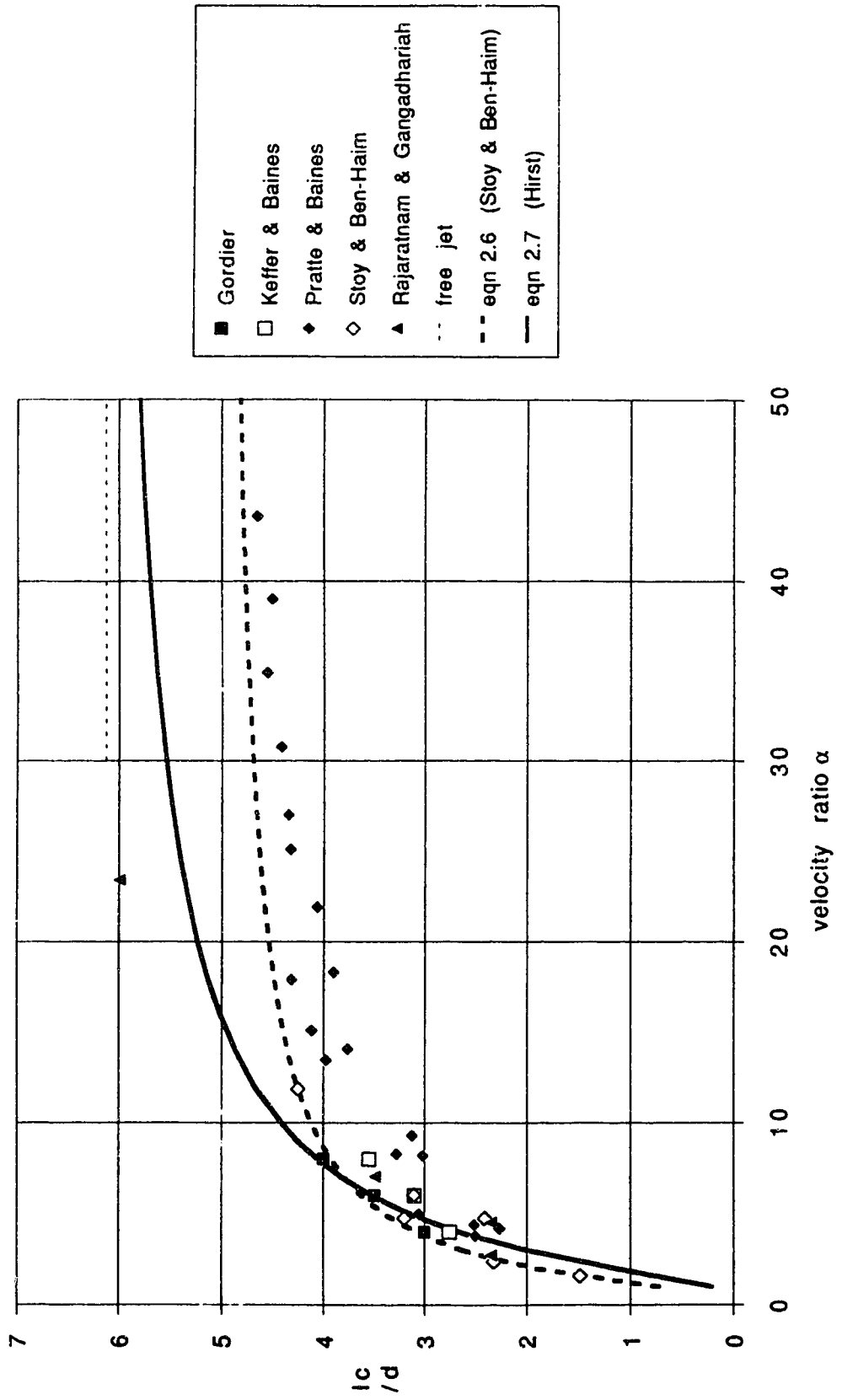




Figure 2.4 Axial velocities and potential core length

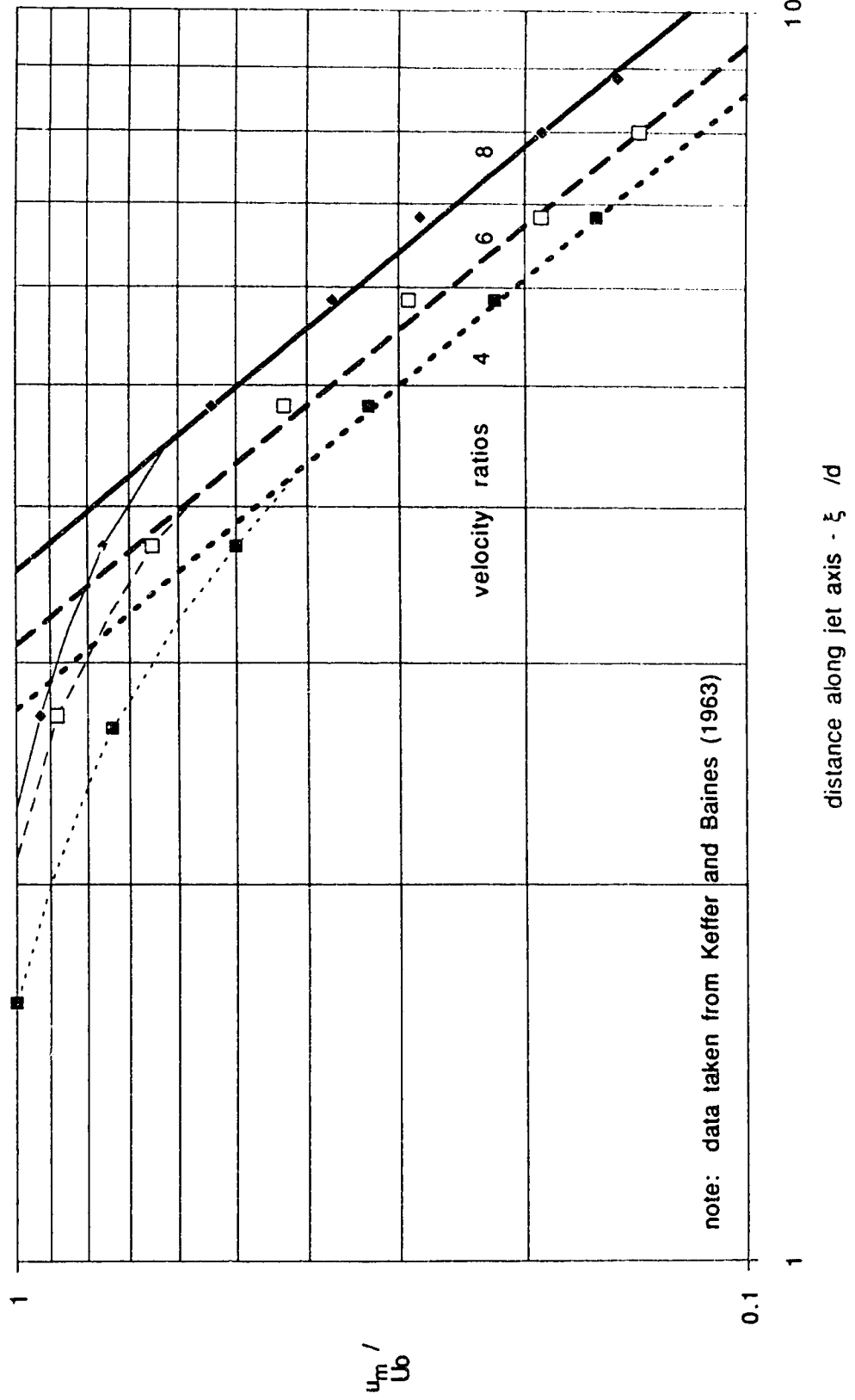


Figure 2.5 Velocity centreline data from selected studies  
velocity ratios: 3.9 to 4.3

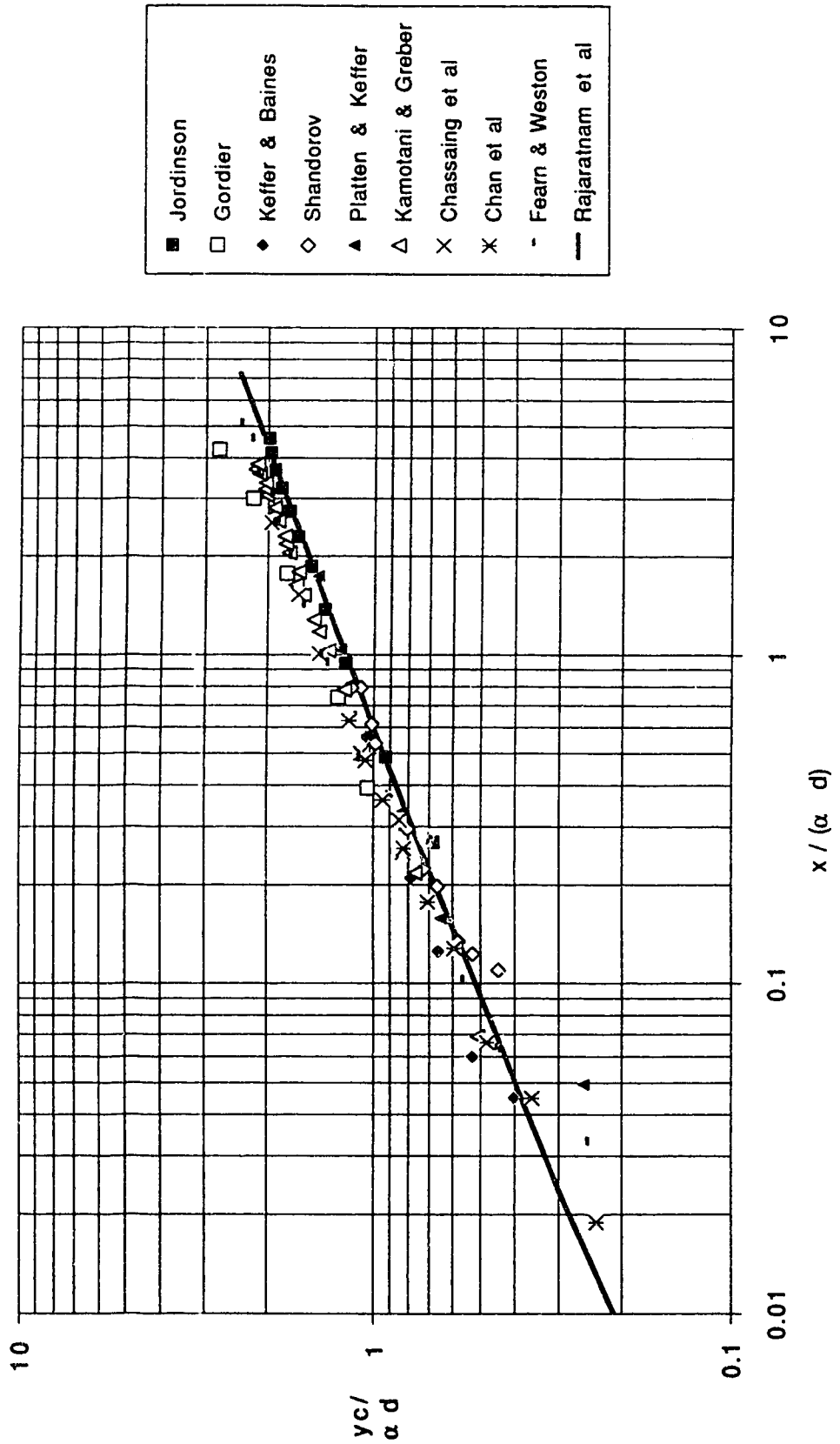
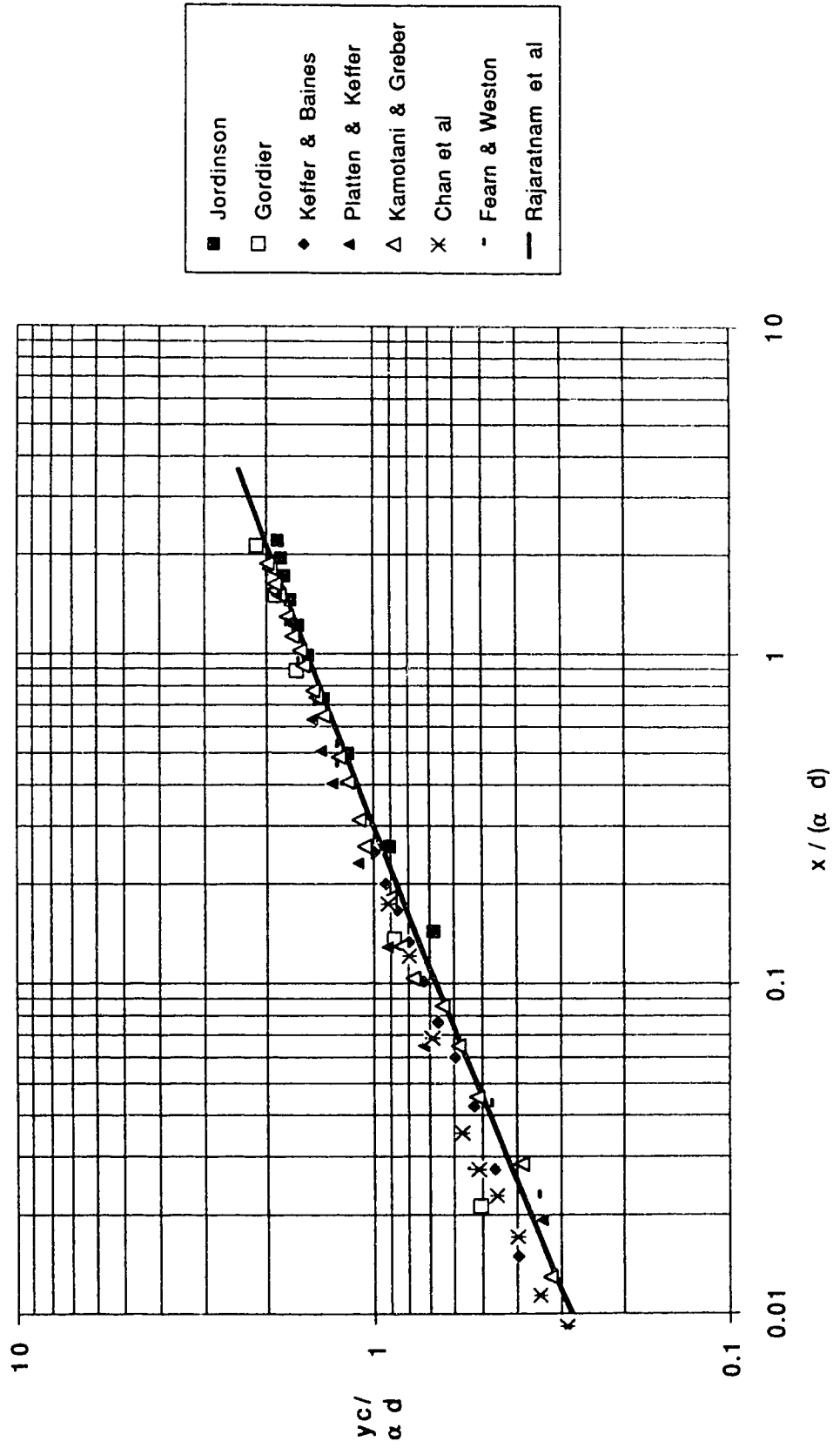


Figure 2.6 Velocity centreline data from selected studies  
velocity ratios: 7.7 to 8.8



## CHAPTER 3

A PHOTOGRAPHIC ASSESSMENT OF CIRCULAR JET DISCHARGES  
IN CROSSFLOWS OF FINITE DEPTH**3.1 General**

Many investigations have been carried out identifying the location of circular jet discharges in crossflows of infinite depth. Most of these investigations have concerned themselves with the location of the points of maximum velocity and have defined the jet centreline by these. Some of the more notable studies of this kind have been discussed in Section 2.

The jet centreline can be identified by several criteria (Figure 2.2):

- a) the points of maximum velocity,
- b) the points of maximum concentration, and
- c) the midpoint between the inner and outer boundaries.

These centrelines are not necessarily coincident. Patrick (1967) compared jet centrelines determined from the location of maximum concentrations with centrelines determined from photographic analysis. He found that the maximum concentration centreline was higher than that determined by visual methods. Also, the relations Patrick presented for the jet centreline indicate that the velocity centreline is higher than the concentration centreline (Table 2.2). Kamotani and Greber (1972a and 1972b) measured velocity and

temperature (the latter being analogous to concentration) profiles for two heated jet discharges. They found that the velocity centreline was located higher than the temperature centreline.

Velocity measurement investigations provide useful information on the dynamic structure of the jet but, for environmental purposes, they do not provide as much useful information as photographic analysis or concentration measurements would. Photographic analysis allows the boundaries of the jet to be clearly defined whereas velocity measurements must define the boundaries by the locations of points where the velocities are a small fraction of the maximum velocity (ignoring the fact that the diffusion of a tracer is greater than the diffusion of momentum). Photographic analysis can also be conducted for a greater distance downstream of the jet discharge. The studies on jet centreline location by velocity measurements have been conducted for distances of up to  $x = 45 d$  (Table 2.1). Pratte and Baines (1967) conducted a photographic study investigating jet centreline locations for distances of up to  $x = 1200 d$  and three others photographically examined buoyant jets in crossflow for distances exceeding  $100 d$ .

The review of the literature indicated that no equations exist to describe the bulk properties of vertical jet discharges in crossflows of finite depth. A quantification of these attributes is of importance for most natural rivers as their depths are relatively small. Depth becomes an

important factor for the spreading and mixing of high momentum jet discharges.

This chapter describes a photographic study which was carried out to determine the characteristics of jets discharging in crossflows of finite depth. The configuration examined is representative of a single port on a diffuser outfall structure discharging upward into the river from the bed. A comprehensive photographic analysis of thirteen jet discharge conditions allowed relations to be developed describing the jet penetration distance, the jet centreline profile and the terminal levels of the jet boundaries. The data have also been used to develop equations for the plan view width and the thickness of the jet. The results are evaluated in light of earlier photographic works, the most significant of which are studies by Wright (1977a), Pratte and Baines (1967) and Gordier (1959).

### **3.2 Previous Investigations**

#### **3.2.1 Profile Equations**

There are many equations reported in the literature describing the location of circular jet discharges into crossflows of infinite depth. Rajaratnam (1976) described seven different closed form equations that have been reported. Wright (1977a) identified sixteen solution procedures, presented in the literature, for buoyant and non-buoyant jet discharges into a crossflow. Most of these

analyses have considered the jet centreline as being defined by the points of maximum velocity at successive sections. These studies have often also involved the measurement of velocities throughout the jet; most have used air as the fluid.

Photographic studies have also been used to identify the location of deflected jets (Table 3.1). In these, the inner and the outer boundaries are found by measurement and the **visual jet centreline** is determined by the midpoint between these boundaries. Such a study was carried out by Pratte and Baines (1967) for jets of an oil aerosol discharging into a wind tunnel. They found that the location of the inner and outer boundaries ( $y_i$  and  $y_o$ ) and of the jet centreline ( $y_c$ ), which was defined to be halfway between, can be expressed by the equations:

$$\frac{y_i}{\alpha d} = 1.15 \left( \frac{x}{\alpha d} \right)^{0.28} \quad (3.1)$$

$$\frac{y_c}{\alpha d} = 1.76 \left( \frac{x}{\alpha d} \right)^{0.28} \quad (3.2)$$

$$\frac{y_o}{\alpha d} = 2.35 \left( \frac{x}{\alpha d} \right)^{0.28} \quad (3.3)$$

where:  $d$  is the jet nozzle diameter,

$x$  is the distance downstream from the jet nozzle,

$\alpha$  is the velocity ratio ( $\alpha = U_o/U$ ),

$U_o$  is the jet discharge velocity, and

$U$  is the crossflow velocity.

These relations were developed from data where  $\alpha$  had a range of 5 to 35 and where  $\frac{x}{\alpha d}$  had a range of 0.1 to 300.

Wright (1977a) conducted photographic experiments for both buoyant and non-buoyant jets discharging into uniform and stratified crossflows. Wright determined the jet boundaries by drawing the most representative curve through the inner and outer boundaries of a single photograph for each run. The jet centreline was determined by the midpoint between the two. The effects of parallax and refraction were eliminated by scaling the distances relative to registration marks on the front and back of the flume walls. Wright did this analysis for 60 discharges into unstratified crossflows where buoyancy had varying degrees of influence. Forty-two of these runs indicated some influence by the momentum of the jet discharge. His data covered values of  $\alpha$  from 0.8 to 116 and values of  $\frac{x}{\alpha d}$  from 0.04 to 22.

Based on dimensional arguments, Wright indicated that non-buoyant jets discharging into a uniform crossflow exhibit two distinct regions of flow: the **momentum dominated near field** (MDNF) and the **momentum dominated far field** (MDF). These are not to be confused with the near field and the far field of the mixing zone described earlier in Section 2 and by Yotsukura and Sayre (1976). Wright's MDNF and MDF relate to the region dominated by the jet discharge and would be the initial portion of what Yotsukura and Sayre called the near field.



For a jet discharging into a uniform crossflow of infinite depth, Wright argued that the jet centreline in the MDNF would be a function of the distance downstream and the momentum length scale ( $l_m = \sqrt{\pi/4} \alpha d$ ):

$$\frac{y_c}{l_m} = C_1 \left( \frac{x}{l_m} \right)^{1/2} \quad (3.4)$$

Wright presented values of the coefficient  $C_1$ , determined from the analysis of his photographic data, on a plot of  $C_1$  versus  $l_0/l_m$  (where  $l_0 = \sqrt{\pi/4} d$ , and is called the initial volume flux length scale - it should be noted that  $l_m/l_0 = \alpha$ ). From Wright's data, it can be seen that the coefficient  $C_1$  is dependent on  $\alpha$ ; Wright's data can be fitted by the equation (Figure 3.1):

$$C_1 = 2.0 - \frac{2.2}{\alpha^{2/3}} \quad (3.5)$$

Changing the form of equation (3.4) to:

$$\frac{y_c}{\alpha d} = C_1 \left( \frac{x}{\alpha d} \right)^{1/2} \quad (3.6)$$

results in a new coefficient ( $C_1$ ):

$$C_1 = 1.88 - \frac{2.07}{\alpha^{2/3}} \quad (3.7)$$

Wright also argued that the equation form for the jet centreline location in the MDFF would be:

$$\frac{y_c}{l_m} = C_2 \left( \frac{x}{l_m} \right)^{1/3} \quad (3.8)$$

Wright presented values of the coefficient  $C_2$ , determined from the analysis of his photographic data, on a plot of  $C_2$  versus  $l_0/l_m$ . Again, a dependency on  $\alpha$  could be found; Wright's data can be fitted by the equation (Figure 3.2):

$$C_2 = 0.89 \alpha^{1/6} \quad (3.9)$$

Changing the form of equation (3.8) to:

$$\frac{y_c}{\alpha d} = C_2 \left( \frac{x}{\alpha d} \right)^{1/3} \quad (3.10)$$

results in a new coefficient ( $C_2$ ):

$$C_2 = 0.82 \alpha^{1/6} \quad (3.11)$$

In order to determine the jet centreline location using the latter equation forms, the appropriate centreline equation (3.6) or (3.10) is used in conjunction with corresponding coefficient equation. Since the flow passes through the MDNF first, the appropriate centreline equation is the one which gives the lower value of  $\frac{y_c}{\alpha d}$ .

The point at which the transition between the MDNF and MDFF occurs can be determined by equating equations (3.6) and (3.10):

$$C_1 \left( \frac{x}{\alpha d} \right)^{1/2} = C_2 \left( \frac{x}{\alpha d} \right)^{1/3} \quad (3.12)$$

which gives:

$$\frac{x}{\alpha d} = \left( \frac{C2}{C1} \right)^6 \quad (3.13)$$

Substituting equations (3.7) and (3.11) for C1 and C2 gives:

$$\frac{x}{\alpha d} = \left( \frac{0.44 \alpha^{5/6}}{\alpha^{2/3} - 1.10} \right)^6 \quad (3.14)$$

Values computed from equation (3.14) for the boundary between the MDNF and the MDFF for deep water jet discharges are shown on Figure 3.3. For jets discharging into design flow conditions in most receiving streams (where  $\alpha$  would be between 3 and 10) it can be seen that the MDNF occupies a small portion of the flow field.

Wright also made concentration measurements on a series of 20 non-buoyant jet discharges into unstratified crossflows (Figure 3.4). Almost all of these discharge conditions were limited to the MDNF. The velocity ratios for these runs were in the range of 20 to 35. These data indicate that the concentration centreline is located about 20% higher than that predicted by his visual centreline equations.

Gordier (1959) measured the jet penetration (i.e. the outer boundary) for jets discharging into a crossflow from the bottom of a water tunnel. The jets were discharged through nozzles mounted flush with the channel bottom. The outer boundary was identified by either injecting dye into the jet (in the nozzle supply line) or into the crossflow upstream of the jet nozzle. Gordier's data were presented on a plot of the outer visual boundary  $\left( \frac{y_0}{d} \right)$ , based on the average

of 4 photographs) versus the distance downstream from the upstream edge of the jet nozzle ( $\alpha \sqrt{x/d}$ ). For low velocity ratios ( $\alpha \leq 6$ ), the functional relation indicated by the plot is:

$$\frac{y_0}{\alpha d} = 1.70 \left( \frac{x}{\alpha d} \right)^{1/3} \quad (3.15)$$

Gordier's data appears to have identified only the MDFP in that the exponent for the outer boundary profile equation is  $1/3$ . His data also indicate that the jet profile coefficient in equation (3.10) has a dependency on  $\alpha$ . For  $\alpha = 8$ , Gordier's data indicate that the coefficient has a value of 1.82 and, for  $\alpha = 13.2$ , the coefficient has a value of 1.92.

Margason (1968) took photographs of jets discharging into a wind tunnel at various angles to the crossflow. He presented photographs of 23 jets discharging at  $90^\circ$  to the crossflow. Margason introduced water vapour into the jet discharge to allow the visualization of the jet boundaries.

Margason indicated that the jet centreline for his jet discharges could be represented by the equation:

$$\frac{y_c}{\alpha d} = 1.59 \left( \frac{x}{\alpha d} \right)^{1/3} \quad (3.16)$$

In examining Margason's photographs (and by his own discussion of his work), the relation is only generally representative. For several of the photographs, the visual centreline appears to be significantly different from the predicted location. Thus, although the form of equation

(3.16) and the earlier equations can be seen to be generally applicable to jets over a wide range of crossflow conditions, the coefficient and the exponent cannot be considered to be fixed quantities. Clearly, other factors are providing secondary effects on the profile and boundary locations of jet discharges into crossflows.

Crowe and Riesebieter (1967) developed a model for a jet discharge into a crossflow based on momentum considerations. They also conducted experimental work in a 250 mm wide by 700 mm high wind tunnel using smoke as a tracer to identify the jet centreline and jet boundaries. They introduced smoke through a small tube to the centre of the jet at the nozzle exit in order to identify the jet centreline. They introduced smoke through a second tube at a lateral distance from the nozzle centreline of  $z/d = 0.35$  as a means to approximate the jet width. Photographs from the side and from above were used to determine the coordinates of the centreline profile and the width of the jet based on these smoke traces. Although this procedure allowed Crowe and Riesebieter to develop relations for jet width to incorporate into their model and centreline profile data to verify their model, the range of their photographic data was limited to the potential core region and not much beyond.

Chu has been involved in three investigations which have made use of photographic analysis (Chu and Goldberg, 1974; Abdelwahed and Chu, 1978; Chu, 1985). In all of these works, the jet boundaries were determined from the mean position

indicated by four photographs. In his 1974 work, Chu verified the 1/3 power for the MDFF. The coefficient C2 was found to have a value of 1.44. His 1985 work focussed on oblique jet discharges (i.e. not at 90° to the flow). In this work, Chu found C2 = 1.81. The 1978 work was interesting in that it dealt with buoyant jet discharges which were severely affected by the water surface (i.e. bifurcating buoyant jets).

### 3.2.2 Width and Thickness Equations

The cross-section of a circular jet discharging into a crossflow differs from that for a simple jet in that it has a major axis and a minor axis due to the kidney shape that develops (Figure 2.2). The widths of a jet in each of these directions ( $W_z$  for the plan view width, and  $W_y$  for the side view width or jet thickness) were determined by Pratte and Baines (1967) to be functions of the distance downstream from the jet nozzle:

$$\frac{W_z}{\alpha d} = 1.54 \left( \frac{x}{\alpha d} \right)^{0.4} \quad (3.17)$$

$$\frac{W_y}{\alpha d} = 1.24 \left( \frac{x}{\alpha d} \right)^{0.4} \quad (3.18)$$

Pratte and Baines also presented the jet width as a function of the distance ( $\xi$ ) along the jet's visual centreline axis:

$$\frac{W_z}{\alpha d} = 1.45 \left( \frac{\xi}{\alpha d} \right)^{0.333} \quad (3.19)$$

$$\frac{W_y}{\alpha d} = 1.11 \left( \frac{\xi}{\alpha d} \right)^{0.333} \quad (3.20)$$

This equation form allows for a better comparison with simple jet discharges (assuming the equivalency of  $\xi$  and  $x$ ).

Gordier (1959) measured the maximum plan view jet width for jet discharge conditions of  $\alpha = 4, 6$  and  $8$ . The relationship he determined can be expressed as:

$$\frac{W_z}{\alpha d} = 1.2 \alpha^{0.04} \left( \frac{x}{\alpha d} \right)^{0.39} \quad (3.21)$$

For  $\alpha = 8$ , the term  $1.2 \alpha^{0.04}$  becomes  $1.30$ . Equation (3.21) can then be seen to be similar in form to equation (3.17) from Pratte and Baines. It should be noted however, that even though Gordier measured the maximum jet width (while Pratte and Baines measured the average width), Gordier's relation gives widths which are about 15% smaller.

### **3.3 Effects of a Finite Free Stream Depth**

#### **3.3.1 General**

The work discussed previously did not address the effects that a finite depth of the free stream might have on the jet. The ratios of the free stream depth to the jet diameter ( $D/d$ ) for the work of both Pratte and Baines (1967) and Wright (1977a) were large. Values of  $D/d$  for jet

discharges that would be typical of rivers at design low flow conditions are in the order of 15 to 30. Only the work of Gordier (1959) had values near this range (Table 3.1).

As the jet discharge approaches the water surface, the jet would feel a force due to a portion of its own weight as water flowing over the jet's outer extremity tries to advance above the water surface. This force would limit the vertical growth of the jet. The outer boundary of the jet would be limited to a maximum value determined by the depth of the free stream. The inner boundary and the jet centreline would be limited to values which are somewhat less than the outer boundary.

The width of a jet may also be affected by the effects of a finite free stream depth. With the restriction on the vertical growth of the jet, there would be a tendency for the jet to grow faster in the lateral direction than if the free stream were deeper.

### **3.3.2 Dimensional Considerations**

This analysis considers circular non-buoyant jets discharging vertically from the bed into a horizontal crossflow of uniform density. The jet flow is assumed to be fully turbulent so that the effects of viscosity can be ignored. In addition, the turbulence of the crossflow is assumed to be small relative to that of the jet (i.e. jet turbulence dominates in the region that is being analysed).



The parameters of interest for jets discharging into crossflows of finite depth are the jet velocity at the nozzle ( $U_0$ ), the jet nozzle diameter ( $d$ ), the free stream velocity ( $U$ ) and the depth of the free stream ( $D$ ). Wright (1977a) indicated that it is advantageous to use the kinematic fluxes of mass ( $Q_0 = \frac{\pi d^2 U_0}{4}$ ) and momentum ( $M = U_0 Q_0$ ) as the variables for characterizing a non-buoyant jet. Thus, a general dependent variable (such as the centreline location, the inner or outer boundary locations, the width or the thickness of the jet) can be found to be a function of the following independent variables:

$$\phi = f(Q_0, M, U, D) \quad (3.22)$$

These independent variables have units as follows:

$$\begin{array}{ll} Q_0 & L^3 T^{-1} \\ M & L^4 T^{-2} \\ U & L T^{-1} \\ D & L \end{array}$$

As the four variables have units of length and time only, the Buckingham  $\pi$  theorem indicates that there will be  $4 - 2 = 2$  dimensionless groups of the four variables. If the mass flux is disregarded as a minor influence (except near the source) the first relevant length scale is the momentum length scale:

$$l_m = \frac{M^{1/2}}{U} = \sqrt{\pi/4} \alpha d \quad (3.23)$$

For  $\frac{y}{l_m} \ll 1$  (where  $y$  is the vertical distance above the jet nozzle), the jet will rise almost vertically as the jet momentum dominates the flow. For  $\frac{y}{l_m} \gg 1$ , the momentum of the crossflow dominates and the jet will move nearly horizontally. These are the limiting conditions typical of jets discharging into crossflows of infinite depth.

The depth of the flow can be combined with the momentum length scale to form the dimensionless group:

$$\frac{l_m}{D} = \frac{\sqrt{\pi/4} \alpha d}{D} \quad (3.24)$$

This **relative jet strength parameter** (or, alternatively,  $\frac{\alpha d}{D}$ ) characterizes the jet flow condition by comparing the jet strength to the depth of flow.

A similar case could be made for the dimensionless group  $\frac{\alpha^2 d}{D}$  as being the measure of relative jet strength. This parameter can be developed by taking the ratio of the jet momentum flux to the momentum flux of the crossflow (for a cross-section of dimensions  $d$  by  $D$ ).

### 3.3.3 Flow Fields for Jets Discharging into Crossflows of Finite Depth

Examination of the data from the experiments conducted at the University of Alberta laboratory and intuitive arguments can be used to indicate that there are five zones of flow for jets discharging into crossflows of finite depth

(as opposed to the three zones discussed earlier for jets discharging into crossflows of infinite depth):

#### **Potential Core**

The nature of this region is the same as that for crossflows of infinite depth as the length scale of the potential core is significantly less than the depth of the crossflow. This can be inferred considering the work of Pratte and Baines (1967) and others (discussed in Section 2) where the length of the potential core is less than  $4d$  for velocity ratios of less than 10. Thus,  $y < 4d < 15d < D$  and, therefore,  $y \ll D$ .

#### **Momentum Dominated Near Field**

This region is the same as Wright's MDNF, where the jet centreline can be represented by either of equations (3.4) or (3.6). In this region, the jet flow experiences the effects of the crossflow but still does not feel any surface effects.

#### **Momentum Dominated Far Field**

This region is the same as Wright's MDFF, where the jet centreline profile can be represented by either of equations (3.8) or (3.10). The MDNF and the MDFF, when considered together, are analogous to the zone of maximum deflection discussed in Section 2. In the MDFF, the jet again does not feel any surface effects.

#### **Surface Dominated Field**

The surface dominated field (SDF) is the transition between the MDFF and the jet terminal level region. The surface of the crossflow is felt by the jet in this zone even

though the outer extremity of the jet may not have reached the surface; entrainment is inhibited due to the limited amount of flow above the jet. As a result, the growth of the jet is at a slower rate than the 1/3 power indicated in equations (3.8) and (3.10). The equation for the surface dominated field is:

$$\frac{Y_c}{\alpha d} = C_3 \left( \frac{x}{\alpha d} \right)^m \quad (3.25)$$

The coefficient (C3) and the exponent (m) for the SDF are expected to be functions of the relative jet strength.

#### **Terminal Level Region**

Experimental observations at the University of Alberta laboratory indicated that, after the jet discharge is deflected by the free stream and is flowing nearly parallel with the free stream, the jet reaches a relatively stable position in the flow. The jet maintains this **terminal level** for some distance downstream until it is gradually dispersed by the turbulence of the free stream. This terminal level concept does not follow from momentum considerations or the observations of jets discharging into crossflows of infinite depth. However, by considering the jet momentum and the weight of some portion of the water above the jet as it tries to advance above the water surface, a force balance could be achieved. With a finite depth, the water surface is an obvious limitation to the advance of the jet across the crossflow. Like the centreline location in

the SDF, the terminal levels are also expected to be a function of the relative jet strength parameters.

### **3.4 Experimental Setting**

#### **3.4.1 Facilities**

The experiments were conducted in a rectangular water channel at the University of Alberta's T. Blench Hydraulics Laboratory. The channel has a length of 17.6 m, a depth of 0.60 m and a width of 1.22 m. The flow was supplied to the channel from a head tank, through screens and a rounded channel entrance which evenly distributed the flow in the channel. The jet nozzle was located in the channel floor, midway across the channel, and about 7.8 m downstream of the entrance. The depth of the flow could be controlled by a tailgate at the downstream end of the channel and the flow rate by a throttling valve and a bypass valve on the recirculating pump's discharge. The free stream flow was measured by a 200 mm diameter Foxboro magnetic flow meter in the pump discharge line. Flow rates of up to 83 L/s could be achieved in the channel.

The jet flows were produced by a small pump which took water from the channel's head tank and pumped it into a smaller head tank which was elevated about 4 m above the channel. The flow from the jet head tank to the jet nozzle was controlled by a Brooks (model 1114-10H4A1A) rotameter which could measure flows from 4.0 L/min to 40.0 L/min. The

pump capacity limited the jet flow rate to a maximum of 13.5 L/min. For smaller jet flows, the excess flow was returned to the channel's head tank by means of an overflow from the jet head tank.

The jet flow was conveyed from the jet head tank to the jet nozzle through 25 mm diameter plastic and copper piping. Specially designed and fabricated converging jet nozzles were inserted into this piping at the outlet. As a result, the jet diameter needed no correction factor applied to account for the vena contracta. The outlets of the jet nozzles were made flush with the channel floor.

The jet was coloured by the introduction of Cochineal food colour into the plastic piping between the jet head tank and the rotameter by gravity (the dye tank was elevated above the jet head tank). This dye has a specific gravity of 1.020 at a temperature of 16.5°C. As the dye was significantly diluted before being discharged into the free stream, density effects could be considered negligible.

#### **3.4.2 Photographic Analysis**

At least six photographs were taken of each jet discharge condition both from the side and from above. Typical photographs for the jet viewed from the side are shown on plates 3.1 and 3.2. The dimensions of the side view photos were scaled by calipers relative to a 20 mm square mesh grid which was photographed when located in the water along the jet centreline prior to the experiment. This

procedure eliminated the need to calculate parallax and refraction corrections for these measurements. Measurements of the outer and inner jet boundaries were taken every 17 mm for the first 50 mm and then every 25 mm to a total distance of 450 mm downstream of the jet nozzle. The profile data for the runs illustrated on plates 3.1 and 3.2 are shown on figures 3.5 and 3.6. The jet centreline location was determined as the midpoint between the inner and outer jet boundaries at each station.

The widths of the jet, as seen in plan view, were measured relative to a 50 mm square grid painted on the floor of the channel. Typical photographs for the jet, viewed from above, are shown on plates 3.3 and 3.4. Measurements were taken from six photographs of each run. Knowing the camera location, the depth of flow and the jet centreline location, the jet width readings were corrected for parallax and refraction. Corrections were also made for parallax and refraction to determine the exact station of each width reading. The total width data for the runs illustrated on plates 3.3 and 3.4 are shown on figure 3.7.

The measurements were input to a micro-computer spreadsheet program for processing, checking and summarizing. The 90% confidence interval limits for each determination of the jet boundary position were computed. Generally, the averages of the six readings were sufficient to keep the 90% confidence interval within +/- 10% of the computed average.

Most of this variation is due to turbulence and not due to measuring error.

### 3.4.3 Experimental Error and Variance

There were a number of sources of error to be considered in the laboratory analysis (Table 3.2). In the table, the measuring precision is indicated along with the range of values measured during the course of the experiment and the estimated probable error.

The probable errors were considered to be greater than suggested by the measurement precision. The depth of flow and the jet positions were always scaled to the nearest mm but the estimated accuracy is  $\pm 2$  mm. This results in large error potential for the inner jet boundaries of the weaker jets. This error was much less than the variability of the jet position due to turbulence (see figures 3.5, 3.6 and 3.7). The six photograph averages reduce the measuring error and variation due to turbulence considerably.

An indication as to the significance of the number of photographic measurements has been presented on Figure 3.8. This has been carried out assessing the inner boundary of Run 1232 in the terminal level region. Although only six photographs had been taken of each run, the photographs between  $x = 302$  mm and  $x = 452$  mm have been assumed to be independent measurements of the same mean value. Accepting this, the mean, standard deviation and 95% confidence interval has been computed for the addition of each



successive photograph from  $n = 2$  (at  $x = 452$  mm) to  $n = 42$  (at  $x = 302$  mm).

From Figure 3.8 and the earlier photographs it can be seen that six photographs are sufficient to approximate the mean position at a station. The appropriate number to accurately identify the mean position would initially appear to be about 20. However, considering that much of the variance is due to turbulence, a lesser number would suffice. This work is concerned with the variation of the boundary location, the width and the thickness as functions of the distance downstream and not at a specific distance. As a result, regression analysis was used to develop the relations, significantly improving the accuracy. In this manner, photographic data can be used to provide a valuable quantitative analysis of jet flow.

### **3.5 Results and Analysis**

#### **3.5.1 Conditions Investigated**

Jet profiles and widths were measured at two flow depths (174 mm and 298 mm) and for two jet nozzle diameters (11.0 mm and 12.7 mm). The depth to diameter ratios ( $D/d$ ) examined were 15.8 and 23.5 (tables 3.3 and 3.4). The free stream flow rates were 50 L/s at 174 mm depth and 47 L/s, 80 L/s and 83 L/s at 298 mm depth. The jet flow rates were varied to obtain a range of 2.32 to 13.05 for the jet velocity ratio ( $\alpha$ ). A total of 13 different flow conditions

were examined (Table 3.3). The profile and width data (corrected for parallax and refraction where necessary) are summarized in Appendix A.

### 3.5.2 Jet Strength and the Onset of Surface Effects

Experimental observations at the University of Alberta indicated that, for  $\frac{1_m}{D} < 0.38$  (or  $\frac{\alpha d}{D} < 0.34$ ), the outer boundary of the jet does not reach the surface of the free stream and the major portion of the jet is unaffected by the finite depth of flow. Jets where  $\frac{\alpha d}{D} < 0.34$  will be termed **deep water jets** in this dissertation.

For  $\frac{\alpha d}{D} > 0.34$ , the outer boundary of the jet approaches and contacts the surface of the free stream and the effects of the finite depth are significant. Jets where  $\frac{\alpha d}{D} > 0.34$  will be termed **shallow water jets** in this dissertation.

With respect to the second relative jet strength parameter, the experimental observations at the University of Alberta indicated that surface effects were dominant when  $\frac{\alpha^2 d}{D} > 2.5$ .

The jet discharge conditions analysed by Wright (1977a) were examined to shed further light on these relative strength parameters. Wright made 42 runs for jet discharges which were significantly affected by the jet momentum. In the case of the parameter  $\frac{\alpha d}{D}$ , only one run would be

classified as a shallow water jet discharge. In the case of the parameter  $\frac{\alpha^2 d}{D}$ , 14 of the 42 runs would be classified as shallow water jet discharges. As Wright would have made adjustments to avoid having one third of his runs extending the full depth of flow, it seems likely that the jets did not do so. As a result, a case for the parameter  $\frac{\alpha d}{D}$  can be made indirectly. However, the selection of the appropriate relative jet strength parameter should be more directly determined. In the following assessment, both parameters are examined as the means to characterize the discharges.

### **3.5.3 Comparison of Deep Water Jet Profiles With Previous Study Results**

The boundary and profile data for the deep water jets were plotted for comparison with the results of previous photographic studies (figures 3.9, 3.10 and 3.11). The location and downstream distances were made non-dimensional by dividing by  $\alpha d$ . This comparison is made to put the data observations into context with the previous work prior to more detailed examination of the jet centreline in the various flow fields.

#### **Inner Boundary Location**

Profiles of the inner boundary indicate that bottom effects were present in the weaker jet discharges (Figure 3.9). The three runs (1236, 1231 and 2111) with velocity ratios less than 3.8 had lower profiles than the other four

runs which had velocity ratios greater than 4.1. This may be the result of reduced entrainment on the underside of the jet in the vortex region as the floor restricts the supply of water from the free stream. Another interesting feature of the inner boundary of the weaker jets was the tendency of the jet profile to dip toward the channel bottom over the reach where  $\frac{x}{\alpha d}$  was between 8 and 12. No reason for these observations could be found.

The profiles of the stronger jets did tend toward a single line. However, the equations developed by Pratte and Baines (1967) predicted higher values than were observed.

#### **Outer Boundary Location**

The outer boundary profiles for all seven of the deep water jet discharges tended to conform to a single trend line (Figure 3.10). The outer boundary equation by Pratte and Baines (1967) resulted in predictions which were again higher than indicated by these data. The outer boundary relation presented by Gordier (1959) better represents the data.

#### **Centreline Profiles**

The centreline profiles for all seven of the deep water jets tended to conform to individual straight lines on the dimensionless log-log plot (Figure 3.11). The locations predicted by the centreline equations of Pratte and Baines (1967) and Margason (1968) were once again higher than the observations. The data also indicate that there is a tendency to higher profiles for jets with higher velocity

ratios (e.g. compare the profiles of runs 1236 and 1234 on the figure). This observation supports the trend for the coefficient values ( $C_1$  and  $C_2$ ) in Wright's MDNF and MDFF equations being increasing functions of  $\alpha$ .

#### 3.5.4 Centreline Profiles - Jet Penetration

For a jet discharging into a crossflow, the jet penetrates vertically into the flow before deflecting downstream. In studies using velocity measurements to identify the jet location, this penetration distance is usually represented by the maximum extent of the potential core. However, for a photographic study, a broader definition is necessary as the potential core cannot be identified quantitatively from photographs. The jet penetration is the maximum distance ( $y$ ) measured at the centreline of the jet nozzle (i.e.  $x = 0$ ). One half of this distance would approximate how far the jet centreline penetrates the flow at  $x = 0$ . A strong correlation was found to exist between the **jet centreline penetration distance** ( $Y_p$ ) and the relative jet strength (Figure 3.12). The data were fitted by the equation:

$$\frac{Y_p}{D} = 0.53 \frac{\alpha d}{D} \quad (3.26)$$

Examination of equation (3.26) indicates that jet penetration is actually independent of the flow depth in the

range of discharges investigated ( $\frac{\alpha d}{D} < 0.6$ ) and a simpler relation exists:

$$Y_p = 0.53 \alpha d \quad (3.27)$$

It should be noted that the regression analyses were carried out to establish all of the relations determined from the photographic data. Coefficients of determination and tests for significance are documented in Appendix B.

### 3.5.5 Centreline Profiles - Momentum Dominated

#### Near Field

Values for the coefficient  $C_1$  in equation (3.6) for the MDNF were determined from the photographic data (Figure 3.13). The data were fitted by the equation:

$$C_1 = 0.72 \alpha^{0.52} \quad (3.28)$$

The values indicated by equation (3.28) are larger than those determined by equation (3.7) using Wright's data. They are about 33% higher for the runs where a reasonable amount of data have been used to establish a value for  $C_1$  ( $2 < \alpha < 4$ ) and about 75% higher for the runs where there is a paucity of data ( $10 < \alpha < 13$ ).

The reason for the larger values for the coefficient  $C_1$  could be the velocity distribution in the vertical dimension. In Wright's experiments, the crossflow velocities were uniform as he towed the jet nozzle along a channel to establish his crossflow. In this study, a distinct velocity

distribution (low near the bed and maximum at the surface) existed due to the boundary layer in the flume. The flume conditions for this study would allow the jet to penetrate farther, resulting in the higher values for C1.

### **3.5.6 Centreline Profiles - Momentum Dominated**

#### **Far Field**

Values for the coefficient C2 in equation (3.10) for the WDF were determined from the photographic data (Figure 3.14). The data were fitted by the equation:

$$C2 = 1.01 \alpha^{0.22} \quad (3.29)$$

Correlations to the relative jet strength parameters ( $\frac{\alpha d}{D}$  and  $\frac{\alpha^2 d}{D}$ ) were also tried but the dependency on  $\alpha$  was greater.

The values for C2 indicated by equation (3.29) are larger than the values indicated by equation (3.11) based on Wright's data. They are about 30% higher throughout the range investigated herein. This again could be attributed to the different velocity distributions for the crossflow.

### **3.5.7 Centreline Profiles - Surface Dominated Field**

A coefficient (C3) and an exponent (m) are needed when using equation (3.25) to determine the location of the jet centreline in the SDF. The relations between these and the relative jet strength parameters are illustrated on figures 3.15, 3.16 and 3.17.

The coefficient (C3) appears to be independent of all parameters when the jet strength is high (i.e. the shallow water jet condition). However, some dependency on the velocity ratio was noted for the weaker flow conditions; the coefficient for these conditions was found to be given by:

$$C3 = 0.86 \alpha^{0.28} \quad (3.30)$$

This dependency was not as strong as those observed for the other coefficients. Examination of equation (3.30) indicates that it is applicable for velocity ratios as high as  $\alpha = 6.3$ . Above this value, the constant value of  $C3 = 1.44$  applies.

The profile exponent (m) was found to be strongly dependent on both relative jet strength parameters (figures 3.16 and 3.17). The data indicated two distinct regions that had to be evaluated separately. The first region is for what are termed **transition zone jets**. For jets in this region, the surface effects are not felt as strongly; the values of the exponent for the weaker jets (i.e. ones that approach deep water jet conditions) are near 1/3 (as indicated by Wright). For the transition zone jets, the profile exponent gradually decreases with increasing relative jet strength. The data for the exponent in this region were fitted by the equations:

$$m = 0.34 \left( 1 - \frac{1.2 \alpha d}{D} \right) \quad (3.31)$$

$$m = 0.29 - \left( \frac{\alpha^2 d / D}{27} \right) \quad (3.32)$$



These equations are valid until the point where the relative jet strength is sufficient for the outer boundary of the jet to reach the water surface. These equations indicate that this point occurs at about  $\frac{\alpha d}{D} \approx 0.35$  and  $\frac{\alpha^2 d}{D} = 2.7$  (which are similar to the observed values of 0.34 and 2.5, respectively).

As the relative jet strength continues to increase (i.e. going into the shallow water jet region), the exponent decreases rapidly. The data for the exponent in this region were fitted by the equations:

$$m = 0.03 \left( \frac{\alpha d}{D} \right)^{-1.8} \quad (3.33)$$

$$m = 0.51 \left( \frac{\alpha^2 d}{D} \right)^{-1.0} \quad (3.34)$$

### 3.5.8 Terminal Levels

After the jet discharge was deflected by the free stream, and flowing essentially parallel with the free stream, the jet would reach a relatively stable position in the flow. The jet would maintain this position for some distance downstream until it was gradually dispersed by the turbulence of the free stream. The heights of the outer and inner jet boundaries in this equilibrium condition were measured for each run (Figure 3.18). It was found that the equilibrium position (expressed in dimensionless form as  $Y/D$ ) was a function of the relative jet strength.

Examination of the data indicates that the terminal levels for the inner boundary ( $Y_i$ ), the centreline ( $Y_c$ ) and the outer boundary ( $Y_o$ ) increase with the relative jet strength. Considering the first relative jet strength parameter, the terminal level data were fitted by the equations:

$$\frac{Y_i}{D} = 1.55 \left( \frac{\alpha d}{D} \right)^{1.30} \quad (3.35)$$

$$\frac{Y_c}{D} = 1.06 \left( \frac{\alpha d}{D} \right)^{0.83} \quad (3.36)$$

$$\frac{Y_o}{D} = 2.18 \left( \frac{\alpha d}{D} \right)^{0.73} \quad (3.37)$$

The terminal level data were fitted equally well using relations based on the second relative jet strength parameter (Figure 3.19):

$$\frac{Y_i}{D} = 0.22 \left( \frac{\alpha^2 d}{D} \right)^{0.74} \quad (3.38)$$

$$\frac{Y_c}{D} = 0.47 \left( \frac{\alpha^2 d}{D} \right)^{0.46} \quad (3.39)$$

$$\frac{Y_o}{D} = 0.71 \left( \frac{\alpha^2 d}{D} \right)^{0.37} \quad (3.40)$$

At some degree of relative jet strength, the jet encountered the surface of the free stream and could not advance further (this study is not concerned with jets which break through the water surface as they are of no interest for effluent discharges into rivers). As the jet strength

increased further, the centreline and the inner boundary also reached their maximum values. These **maximum terminal levels**, and the minimum jet strength at which they occurred, are outlined in Table 3.5.

### 3.5.9 Terminal Level Distance

It is desirable to know the distance downstream of the jet nozzle to the point where the terminal level has been reached. As the jet is bent and approaches the terminal level asymptotically, this location was not easy to accurately identify. Relations for the jet centreline terminal level distance ( $X_c$ ) as a function of the relative jet strength parameters were sought (figures 3.20 and 3.21). The relationships determined were:

$$\frac{X_c}{\alpha d} = 0.85 \left( \frac{\alpha d}{D} \right)^{-1.41} \quad (3.41)$$

$$\frac{X_c}{\alpha d} = 7.38 \left( \frac{\alpha^2 d}{D} \right)^{-0.77} \quad (3.42)$$

These relations should be used for approximation purposes only. The profile and terminal level equations discussed earlier should be used to more precisely determine the jet location.

### 3.5.10 Flow Field Boundaries

The equations that have been presented in the previous paragraphs can be manipulated to identify the boundaries

between the various flow fields. Plots similar to that developed earlier for Wright's deep water jets (Figure 3.3) can be developed for transition zone and shallow water jets.

The first boundary to consider is between the MDNF and the MDFF. The location of this boundary can be determined by using equations (3.6) and (3.10) to obtain equation (3.13). Substituting equation (3.28) for C1 and equation (3.29) for C2 gives:

$$\frac{x}{\alpha d} = \left( \frac{1.01 \alpha^{0.22}}{0.72 \alpha^{0.52}} \right)^6 = \frac{7.62}{\alpha^{1.8}} \quad (3.43)$$

The second boundary to consider is between the MDFF and the SDF. The location of this boundary can be determined by using equations (3.10) and (3.25) to obtain:

$$C2 \left( \frac{x}{\alpha d} \right)^{1/3} = C3 \left( \frac{x}{\alpha d} \right)^m \quad (3.44)$$

which gives:

$$\frac{x}{\alpha d} = \left( \frac{C3}{C2} \right)^{1/(1/3-m)} \quad (3.45)$$

Using equation (3.29) for C2 and equation (3.30) for C3 (up to a maximum value of C3 = 1.44), the boundary between these two zones is given by:

$$\begin{aligned} \frac{x}{\alpha d} &= \left( \frac{0.86 \alpha^{0.28}}{1.01 \alpha^{0.22}} \right)^{1/(1/3-m)} \\ &= (0.85 \alpha^{0.06})^{1/(1/3-m)} \end{aligned} \quad (3.46)$$

where  $m$  is given by equations (3.31) and (3.33) or equations (3.32) and (3.34).

Equation (3.46) is applicable for  $\alpha < 6.3$ . For higher values of  $\alpha$ ,  $C_3 = 1.44$  and equation (3.46) becomes:

$$\frac{x}{\alpha d} = \left( \frac{1.43}{\alpha^{0.22}} \right)^{1/(1/3-m)} \quad (3.47)$$

The third boundary to consider is between the SDF and the terminal level region. This boundary can be estimated using equation (3.41) or equation (3.42).

These relations have been determined for  $D/d = 15$  and  $D/d = 25$  (figures 3.22 and 3.23). Examination of the plots indicates that the MDNF occupies a relatively small portion of the jet discharge; it does not extend more than about three times the jet nozzle diameter downstream (i.e.  $x = 3 d$ ). The MDFF exists downstream for a distance of about  $x = 0.5 \alpha d$  before reaching the SDF. This is true for  $\alpha > 4.5$ ; at lower values of  $\alpha$ , the jet conditions change from the MDNF to the SDF directly. This is likely due to the low values for the relative jet strength in this region. The exponents in the SDF for these jets will be close to the  $1/3$  power for the MDFF jets (distinguishing between the two is more difficult in this region).

### 3.5.11 Jet Widths

The jet width (as seen in plan view) data were separated into two groups for assessment:

- a) jets not experiencing surface effects (figures 3.24 and 3.25), and
- b) jets experiencing surface effects (Figure 3.26).

The transition between these two groups began at a relative jet strength of about  $\frac{\alpha^2 d}{D} = 2$ .

The data for the deep water jets (Figure 3.24) were first examined relative to the width equations of Pratte and Baines (1967) and Gordier (1959). Their width relations were developed to describe the jet width as a function of the distance downstream of the discharge nozzle. Gordier's equation provides a better fit to the data than the relation developed by Pratte and Baines.

The jet width data were examined in more detail to determine relations for the jet width as a function of the distance along the jet axis ( $\xi$ ). As correlations for the width data were much superior for the second relative jet strength parameter ( $\frac{\alpha^2 d}{D}$ ), the jet width relations will be discussed in terms of this parameter only.

Jet discharges with low values of  $\frac{\alpha^2 d}{D}$  were found to behave like deep water jets. Examination of the data indicated that the growth of the jet width is proportional to the square root of the distance along the  $\xi$  axis (Figure 3.25). Although this appears to contradict the cube root proportionality indicated by Pratte and Baines (1967) in equation (3.19), it should be noted that their data covered

values of  $\frac{\xi}{\alpha d}$  between 3 and 300. Examination of their data for values less than 20 (the upper limit investigated in this study) confirms the square root proportionality. Their data indicate that the transition between the two regions appears to occur at  $\frac{\xi}{\alpha d}$  values of about 10. The data obtained in this experiment did not go sufficiently far downstream to confirm this.

Coefficients of proportionality for each run were fitted to develop a jet width equation of the form:

$$\frac{W_z}{\alpha d} = C_4 \left( \frac{\xi}{\alpha d} \right)^{1/2} \quad (3.48)$$

For deep water jets ( $\frac{\alpha^2 d}{D} < 2$ ), the coefficient (C4) can be estimated by (Figure 3.27):

$$C_4 = C_5 = 1.1 - \frac{\alpha^2 d}{8 D} \quad (3.49)$$

Jet discharges with values of  $\frac{\alpha^2 d}{D} > 2$  (i.e. transition zone and shallow water jets) behave similarly to deep water jets only near the jet nozzle (the region of the jet flow not experiencing surface effects). This region was found to be confined to values of  $\frac{\xi}{\alpha d} < 1.5$  (Figure 3.26). The jet width in this region still holds to the square root proportionality with the coefficient again being defined by equation (3.49) to a limiting value of 0.66 for  $\frac{\alpha^2 d}{D} > 3.5$ . However, for

$\frac{\xi}{\alpha d} > 1.5$ , the jet width grows much faster than equations (3.48) and (3.49) would indicate; a further jet width function for the region dominated by surface effects is necessary.

The water surface restricts the height of the jet for shallow water jets. This forces the width of a shallow water jet to grow much faster than that for a deep water jet (Figure 3.26). The rate of growth was found to be proportional to the relative jet strength  $\left(\frac{\alpha^2 d}{D}\right)$  in a form similar to that for deep water jets:

$$\frac{W_z}{\alpha d} = C_5 \left(\frac{\xi}{\alpha d}\right)^n \quad (3.50)$$

In equation (3.50), the coefficient (C5) was also found to be given by equation (3.49), reaching a limiting value of 0.53 for  $\frac{\alpha^2 d}{D} > 4.5$ . The exponent (n) was found to be given by:

$$n = \frac{\alpha^2 d}{4 D} \quad (3.51)$$

for values of  $\frac{\alpha^2 d}{D} > 2$  (i.e. for the transition and shallow water jet regions).

After a period of rapid expansion, described by equations (3.50) and (3.51), the growth rate of the jet width decreased (Figure 3.26). This may have been due to wall effects from the flume. This is not considered likely as the greatest measured jet width (635 mm) was significantly less than the flume width (1220 mm). It is more likely due to a



significant decrease in jet entrainment as the jet velocity has declined considerably and approached that of the crossflow at this point. The data for the four strongest jets were examined and the maximum  $\frac{\xi}{\alpha d}$  value where equations (3.50) and (3.51) were applicable were noted. The point where limiting conditions are apparent can be estimated by:

$$\frac{\xi}{\alpha d} = \frac{22 D}{\alpha^2 d} \quad (3.52)$$

### 3.5.12 Jet Thickness

After a sufficiently large distance downstream of the jet nozzle, the jet thickness ( $W_y$ ) can be approximated by the difference between the inner and outer jet boundaries:

$$W_y = y_o - y_i \quad (3.53)$$

This is because the jet axis is nearly parallel with the x axis. However, near the nozzle, the jet axis is at a large angle with the x axis and the correct value for the jet thickness (normal to the jet axis) is given by:

$$W_y = \cos \theta (y_o - y_i) \quad (3.54)$$

A value for the angle ( $\theta$ ) can be determined from the derivative of the centreline profile equation:

$$\tan \theta = \frac{dy}{dx} = \frac{d}{dx} \left( \frac{y_c}{\alpha d} \right) = \frac{d}{dx} C_3 \left( \frac{x}{\alpha d} \right)^m \quad (3.55)$$

where  $C_3$  and  $m$  are the coefficient and exponent in the SDF equation (these could also be  $C_1$  and  $1/2$  in the MDNF equation or  $C_2$  and  $1/3$  in the MDFF equation). Thus:

$$\theta = \arctan \left( C_3 m \left( \frac{x}{\alpha d} \right)^{m-1} \right) \quad (3.56)$$

These corrections were made to the measured boundary data from this study (figures 3.28 and 3.29).

The only previous photographic analysis of jet thickness ( $W_y$ ) for jet discharges into crossflows was carried out by Pratte and Baines (1967). The jet thickness equation (3.18) from Pratte and Baines, expressing the jet thickness as a function of the distance downstream of the jet nozzle, was found to predict higher values than the thicknesses observed in this study (Figure 3.28).

Pratte and Baines also developed a relation for the jet thickness as a function of the distance along the jet centreline. Equation (3.19) indicates that the thickness grows proportionately with the  $1/3$  power of this distance. The jet thickness data from this study (Figure 3.29) were found to be reasonably well represented by this relationship. Near the jet nozzle (i.e. for  $\frac{\xi}{\alpha d} < 2.8$ ), Pratte and Baines

indicated another relationship for the jet thickness:

$$\frac{W_y}{\alpha d} = 0.39 \left( \frac{\xi}{\alpha d} \right)^{1.35} \quad (3.57)$$

For the data from this study, a similar, but higher, trend was observed near the jet nozzle.

From an analysis of the corrected thickness data, the form of equation for the thickness of deep water jets was found to be:

$$\frac{W_y}{\alpha d} = C_6 \left( \frac{\xi}{\alpha d} \right)^p \quad (3.58)$$

The values for the coefficient (C6) were found to have a dependency on the velocity ratio which was unique to each depth ratio (Figure 3.30). The values for the exponent (p) were also found to have a dependency on the velocity ratio which was unique to each depth ratio (Figure 3.31). The coefficient and exponent relationships for the two depth ratios examined in this study share common values when the velocity ratio has values in the order of 5 to 6.

Examination of the thickness data for a typical shallow water jet (Run 2113) in comparison with a typical deep water jet (Run 1234) indicates that the thickness of a shallow water jet grows until a limit is reached (Figure 3.32). This limiting thickness is reached as the jet approaches its terminal level.

### 3.6 Conclusions

a) Earlier work by others describing circular jet discharges into crossflows of infinite depth has identified three zones of flow:

- the potential core,
- the zone of maximum deflection, and
- the vortex zone.

This work has identified five zones of flow for circular jet discharges into crossflows of finite depth:

- the potential core,
- the momentum dominated near field,
- the momentum dominated far field,
- the surface dominated field, and
- the terminal level region.

b) Equations of the form:

$$\frac{y}{\alpha d} = \text{coefficient} \left( \frac{x}{\alpha d} \right)^{\text{exponent}}$$

are useful in evaluating the position of jet discharges into crossflows. From the examination of the data of other researchers in conjunction with those obtained in this dissertation, it is apparent that secondary effects are present for both deep water jet and shallow water jet discharges. As a result, neither the coefficient nor the exponent can be expected to have constant values.

c) This work utilized statistical analysis of boundary positions measured directly from six photographs of each run. Several of the previous studies by others made their measurements from boundaries drawn through a single photograph for each run; only two have evaluated more than a single photograph for each run. Turbulence provides significantly greater variance in the observed boundary position than did measuring error. It is estimated that up to 20 photographs would be needed to eliminate the effects of variance due to turbulence and provide an accurate determination of the jet boundary position at each station. In this work, this problem was overcome by conducting regression analysis through up to 20 jet boundary positions (each based on a six-photograph average).

d) As the potential core cannot be measured in a photographic investigation the **jet centreline penetration distance** was quantified:

$$Y_p = 0.53 \alpha d \quad (3.27)$$

For the range of relative jet strengths investigated ( $\frac{\alpha d}{D} < 0.6$ ), this distance was found to be independent of the depth of the crossflow.

e) Similar to the work of Wright (1977a), the zone of maximum deflection was found to be comprised of two jet

dominated regions: the **momentum dominated near field** (MDNF) and the **momentum dominated far field** (MDFP). The position of the jet centreline in the MDNF was found to be described by an equation of the form:

$$\frac{y_c}{\alpha d} = C_1 \left( \frac{x}{\alpha d} \right)^{1/2} \quad (3.6)$$

For the MDNF, the coefficient (C1) was found to be given by equation (3.28).

The position of the jet centreline in the MDFP was found to be described by an equation of the form:

$$\frac{y_c}{\alpha d} = C_2 \left( \frac{x}{\alpha d} \right)^{1/3} \quad (3.10)$$

For the MDFP, the coefficient (C2) was found to be given by equation (3.29).

f) Surface effects result in the suppression of the rate of progression of the jet across the flow. As a result, the exponent in the **surface dominated field** (SDF) centreline location equation is less than both the value of 1/2 for the MDNF and the value of 1/3 for the MDFP. The position of the jet centreline in the SDF was found to be described by an equation of the form:

$$\frac{y_c}{\alpha d} = C_3 \left( \frac{x}{\alpha d} \right)^m \quad (3.25)$$

For the SDF, the coefficient (C3) was found to be given by equation (3.29) up to a maximum value of 1.44. The exponent (m) was found to be given by equations (3.31) and (3.33).

g) After the jet passes through the first four zones of flow, it was observed to reach a relatively stable position. This position was maintained for some distance until it was dispersed by the turbulence of the free stream. The position of these **terminal levels** were found to be described by equations (3.35), (3.36) and (3.37). These equations are applicable up to maximum values of  $\frac{Y_i}{D} = 0.6$ ,  $\frac{Y_c}{D} = 0.8$  and  $\frac{Y_o}{D} = 1$ . The jet centreline and boundaries did not advance beyond these limits for the values of relative jet strength examined.

h) The MDNF was found to occupy a relatively small portion of the jet discharge; it did not extend downstream by more than about  $x = 3 d$  (figures 3.22 and 3.23). The MDFF was found to extend to about  $x = 0.5 \alpha d$  for jets where  $\alpha > 4.5$ . At lower values of  $\alpha$ , the jet conditions changed from the MDNF to the SDF directly.

i) The plan view widths of the jet discharges were not affected by the finite depth of flow for  $\frac{\alpha^2 d}{D} < 2$ .

The widths of these **deep water jets** were found to be described by an equation of the form:

$$\frac{W_z}{\alpha d} = C_4 \left( \frac{\xi}{\alpha d} \right)^{1/2} \quad (3.48)$$

For deep water jets, the exponent (1/2) is a constant. This is similar to that illustrated by the data of Pratte and Baines (1967) for  $\frac{\xi}{\alpha d} < 10$ . The coefficient (C4) was found to be given by equation (3.49) to a minimum value of 0.66.

j) When  $\frac{\xi}{\alpha d} < 1.5$ , the plan view widths for **transition zone jets** and **shallow water jets** (i.e. when  $\frac{\alpha^2 d}{D} > 2$ )

were found to be similar to those for deep water jets.

When  $\frac{\xi}{\alpha d} > 1.5$ , the plan view widths for transition zone jets and shallow water jets were found to grow at significantly higher rates than the 1/2 power indicated for deep water jets (Figure 3.26). The widths of these jets were found to be described by the equation:

$$\frac{W_z}{\alpha d} = C_5 \left( \frac{\xi}{\alpha d} \right)^n \quad (3.50)$$

where the coefficient C5 is given by equation (3.49) to a minimum value of 0.53 and the exponent (n) is given by equation (3.51).

k) The thickness (side view projection) of the deep water jet discharges were found to be slightly overestimated by equation (3.18) from Pratte and Baines (1967). The observed



thicknesses of the deep water jets were found to be given by equations of the form:

$$\frac{W_y}{\alpha d} = C_6 \left( \frac{\xi}{\alpha d} \right)^p \quad (3.58)$$

where the coefficient  $C_6$  and the exponent ( $p$ ) are indicated on figures 3.30 and 3.31, respectively.

1) Two relative jet strength parameters  $\left( \frac{\alpha d}{D} \right)$  and  $\left( \frac{\alpha^2 d}{D} \right)$  were identified in this section as dimensionless groups suitable for quantifying the effects of a finite free stream depth on jet discharges into crossflows. Examination of the work of Wright (1977a) indicated that the parameter  $\frac{\alpha d}{D}$  is preferable for describing the jet centreline profiles. Although the analysis of the data in this work corroborated this, it was found that the surface effects could also be correlated to the latter parameter  $\left( \frac{\alpha^2 d}{D} \right)$  for the SDF and the terminal level region. Additionally, the correlation of the jet width relations to  $\frac{\alpha^2 d}{D}$  were found to be superior. Further work is required to identify the relative importance of these two parameters.

Table 3.1 Range of parameters used in various photographic studies of jets in crossflow

Experiment	medium	runs	D/d	$\alpha$	x/d	$\frac{x}{\alpha d}$
Gordier (1959)	water	5	36	2.5 to 13.2	0.4 to 30	0.05 to 3.0
Crowe & Riesebieter (1967)	air	3	n/a	2.8 to 7.4	0 to 1.3	0 to 0.46
Pratte & Baines (1967)	air	6	128 to 196	5 to 35	3 to 1200	0.1 to 300
Margason (1968)	air	23	76	1.2 to 10.1	0 to 22	0 to 10
Chu & Goldberg (1974)	water	8	236	6.3 to 44	1 to 60	0.03 to 54
Abdelwahed & Chu (1974)	water	64	19 to 74	2.0 to 40	to 460	3 to 40
Wright (1977)	water	42	69 to 275	0.3 to 116	n/a	0.04 to 22
Chu (1985)	water	4	32	2.0 to 8.0	8 to 40	1 to 20
This work	water	13	16 and 24	2.3 to 13.1	1.3 to 41	0.1 to 18

Note: n/a indicates that the information was not available from the literature.

Table 3.2 Measurement precision and experimental error  
photographic investigation

Measurement	Precision	Experimental Values	Estimated Probable Error ( $\pm$ %)
depth of flow (mm)	1	174 to 300	< 1
jet position (mm)	1	9 to 298	1 to 20
flume flow (L/s)	0.1	47 to 83	1 to 2
jet flow (L/min)	0.25	4.0 to 12.8	2 to 6

Table 3.3 Range of conditions investigated

Run Number	Jet Diameter d (mm)	Channel Depth D (mm)	Jet Velocity U <sub>o</sub> (m/s)	Channel Velocity U (m/s)	D/d	$\alpha$ (= U <sub>o</sub> /U)	$\frac{\alpha d}{D}$	$\frac{\alpha^2 d}{D}$
1236	12.7	300	0.526	0.226	23.5	2.32	0.098	0.228
1231	12.7	298	0.658	0.220	23.5	2.99	0.127	0.381
1232	12.7	298	0.908	0.220	23.5	4.13	0.176	0.727
1233	12.7	298	1.158	0.220	23.5	5.27	0.225	1.184
1234	12.7	298	1.474	0.220	23.5	6.71	0.286	1.919
1235	12.7	298	1.737	0.220	23.5	7.91	0.337	2.666
1136	12.7	298	1.395	0.129	23.5	10.81	0.461	4.980
1135	12.7	298	1.684	0.129	23.5	13.05	0.556	7.258
2111	11.0	174	0.877	0.235	15.8	3.73	0.236	0.880
2112	11.0	174	1.228	0.235	15.8	5.22	0.330	1.723
2113	11.0	174	1.578	0.235	15.8	6.71	0.424	2.846
2114	11.0	174	1.929	0.235	15.8	8.20	0.518	4.251
2115	11.0	174	2.280	0.235	15.8	9.70	0.613	5.948

Table 3.4 Reynolds number data

Run Number	Temperature (°C)	$R_j = \frac{U_o d}{\nu}$	$R_d = \frac{U d}{\nu}$	$R_b = \frac{U D}{\nu}$
1236	15	5,900	2,500	6,000
1231	12	6,700	2,300	5,300
1232	12	9,300	2,300	5,300
1233	12	11,900	2,300	5,300
1234	12	15,100	2,300	5,300
1235	12	17,800	2,300	5,300
1136	15	15,600	1,400	3,800
1135	15	18,800	1,400	3,800
2111	15	8,500	2,300	3,600
2112	15	11,900	2,300	3,600
2113	15	15,200	2,300	3,600
2114	15	18,600	2,300	3,600
2115	15	22,000	2,300	3,600

Table 3.5 Maximum terminal levels and minimum jet strengths

Boundary	Maximum Terminal Level	Minimum Relative Jet Strength	
	$\frac{Y}{D}$	$\frac{\alpha d}{D}$	$\frac{\alpha^2 d}{D}$
Inner ( $Y_i$ )	0.6	0.48	3.9
Centreline ( $Y_c$ )	0.8	0.41	3.2
Outer ( $Y_o$ )	1.0	0.34	2.5

Figure 3.1 Wright's data for momentum dominated near field coefficient  $C_f$

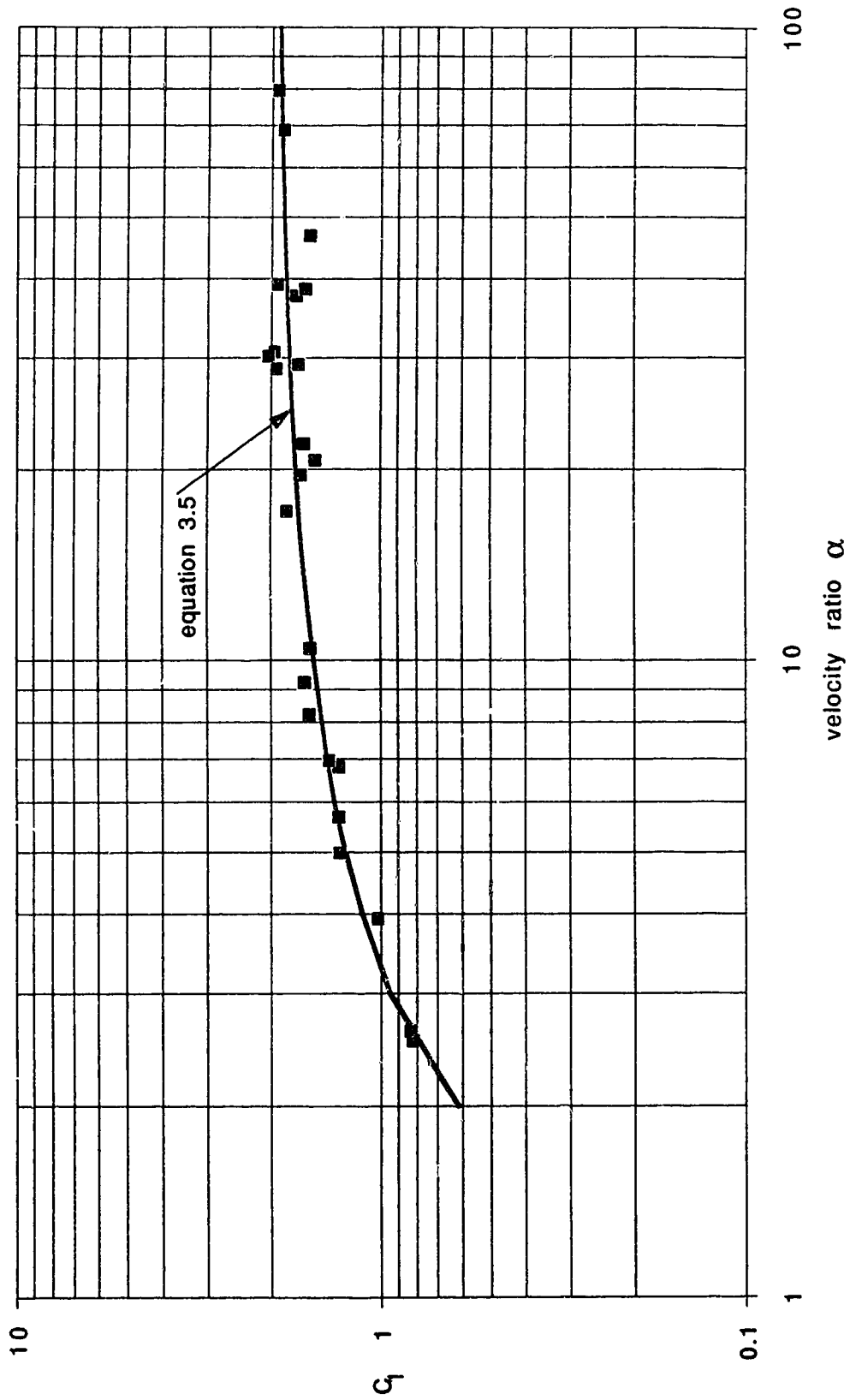


Figure 3.2 Wright's data for momentum dominated far field coefficient  $C_2$

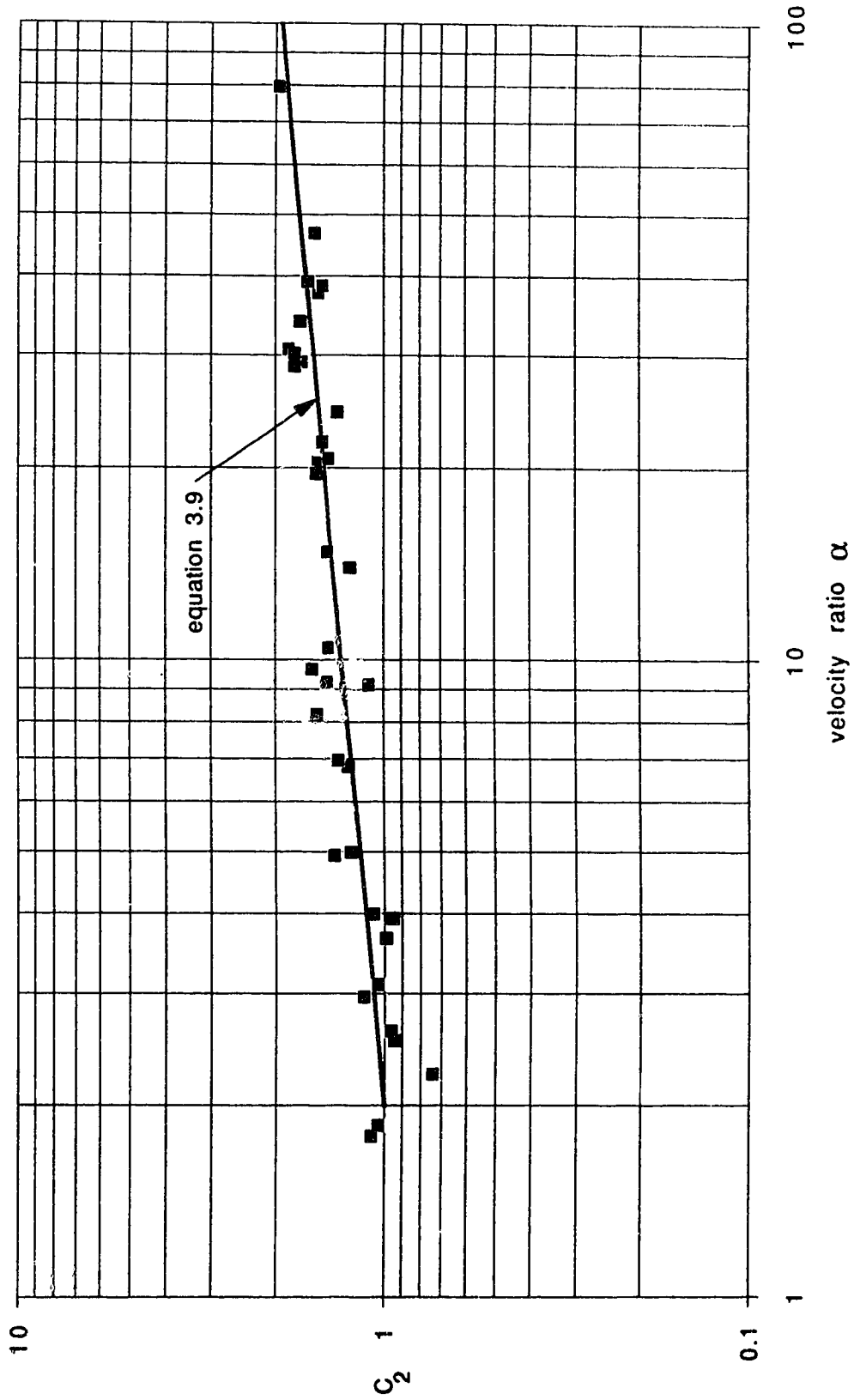




Figure 3.3 Boundary between momentum dominated near and far fields from Wright's equations

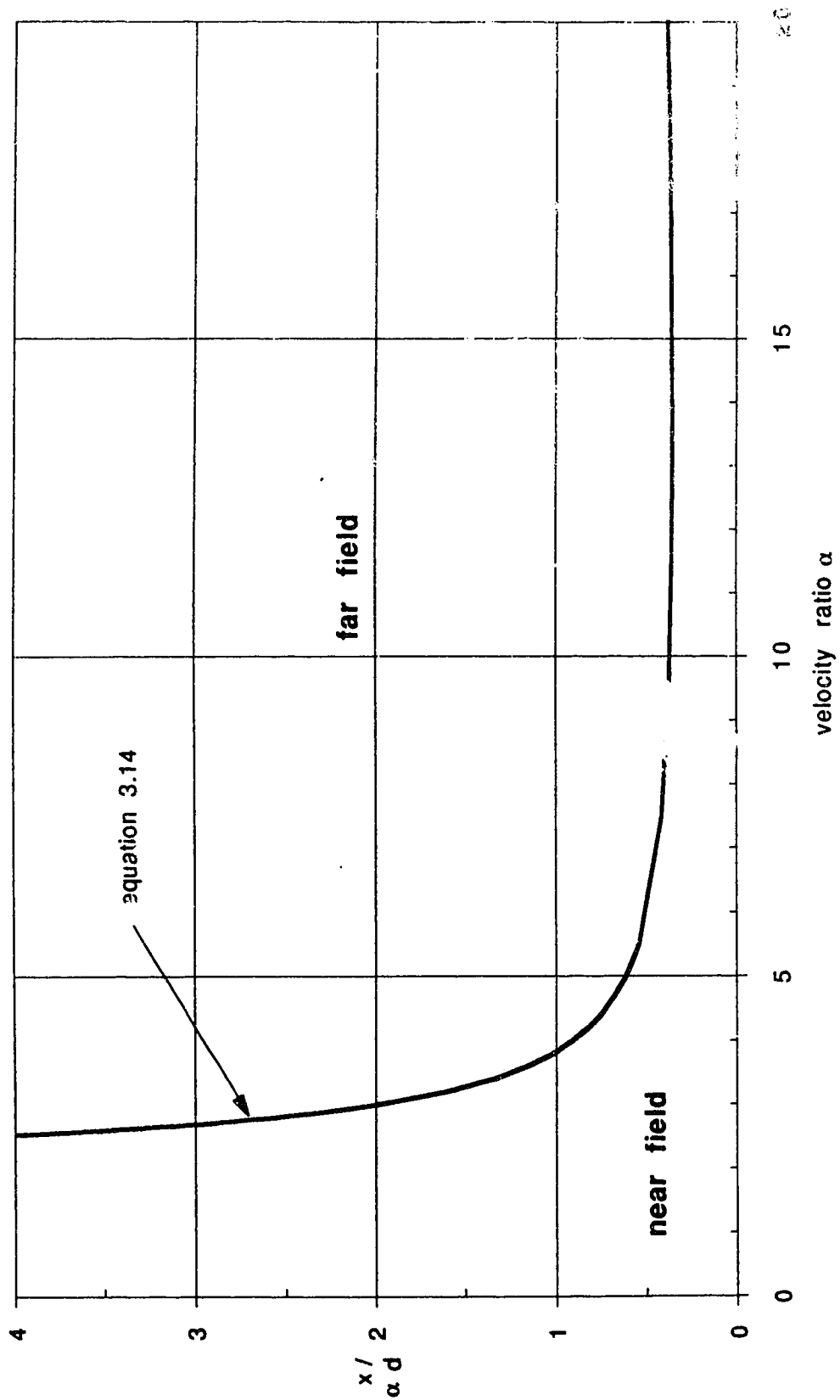


Figure 3.4 Wright's data for concentration centreline location

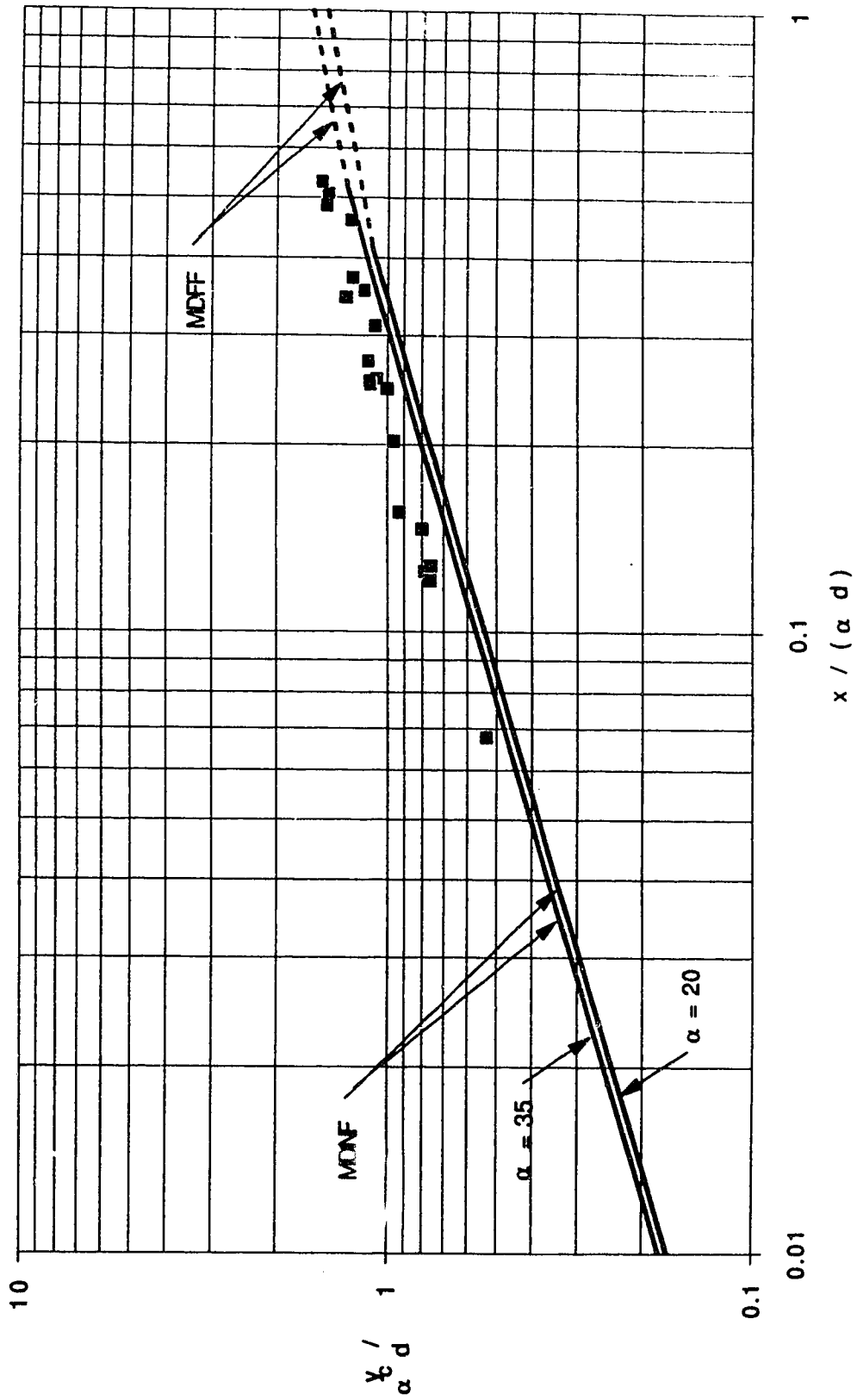


Figure 3.5 Boundary data for Run 1232 ( $\alpha d/D = 0.18$ )

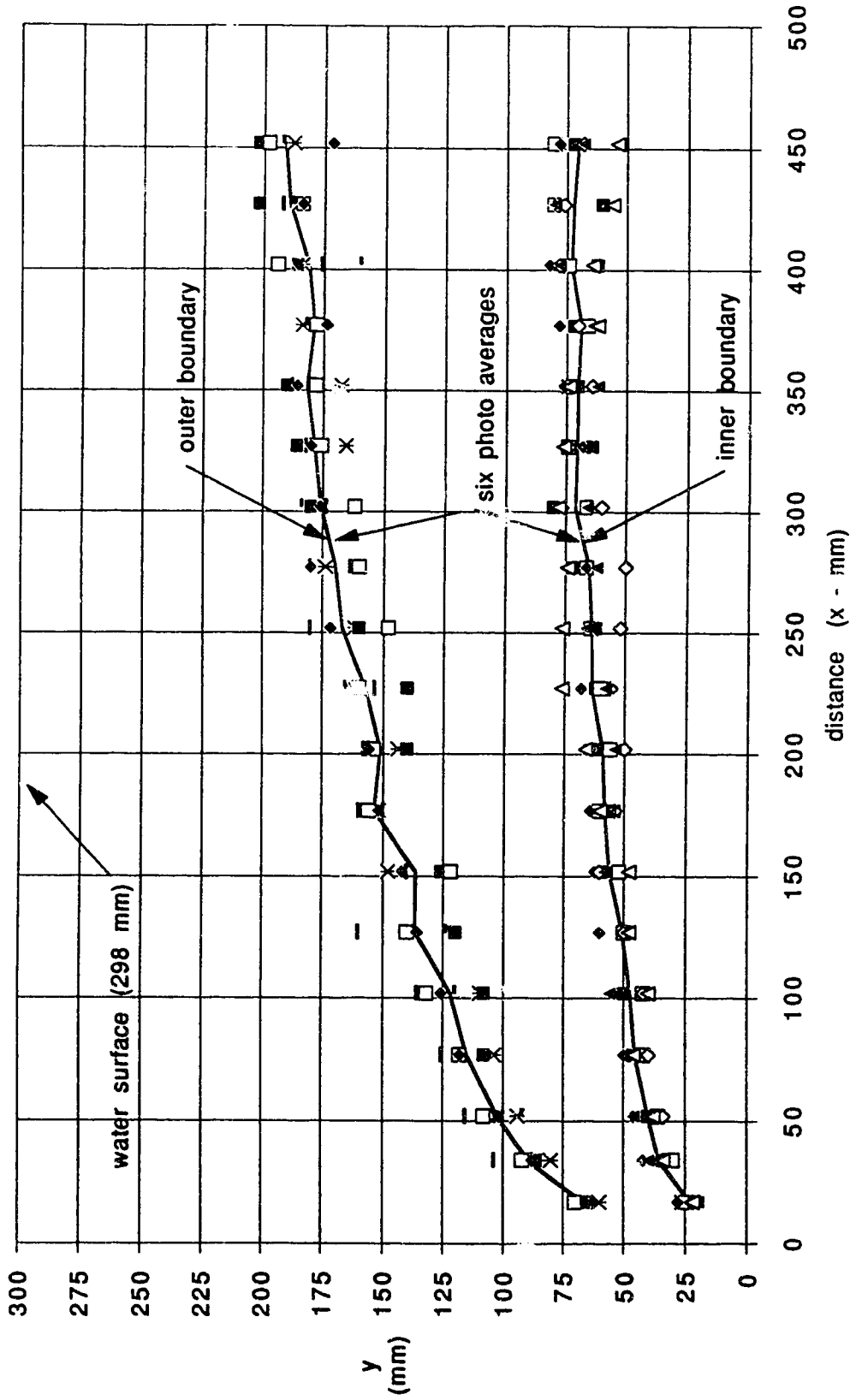


Figure 3.6 Boundary data for Run 1136 ( $\alpha d/D = 0.46$ )

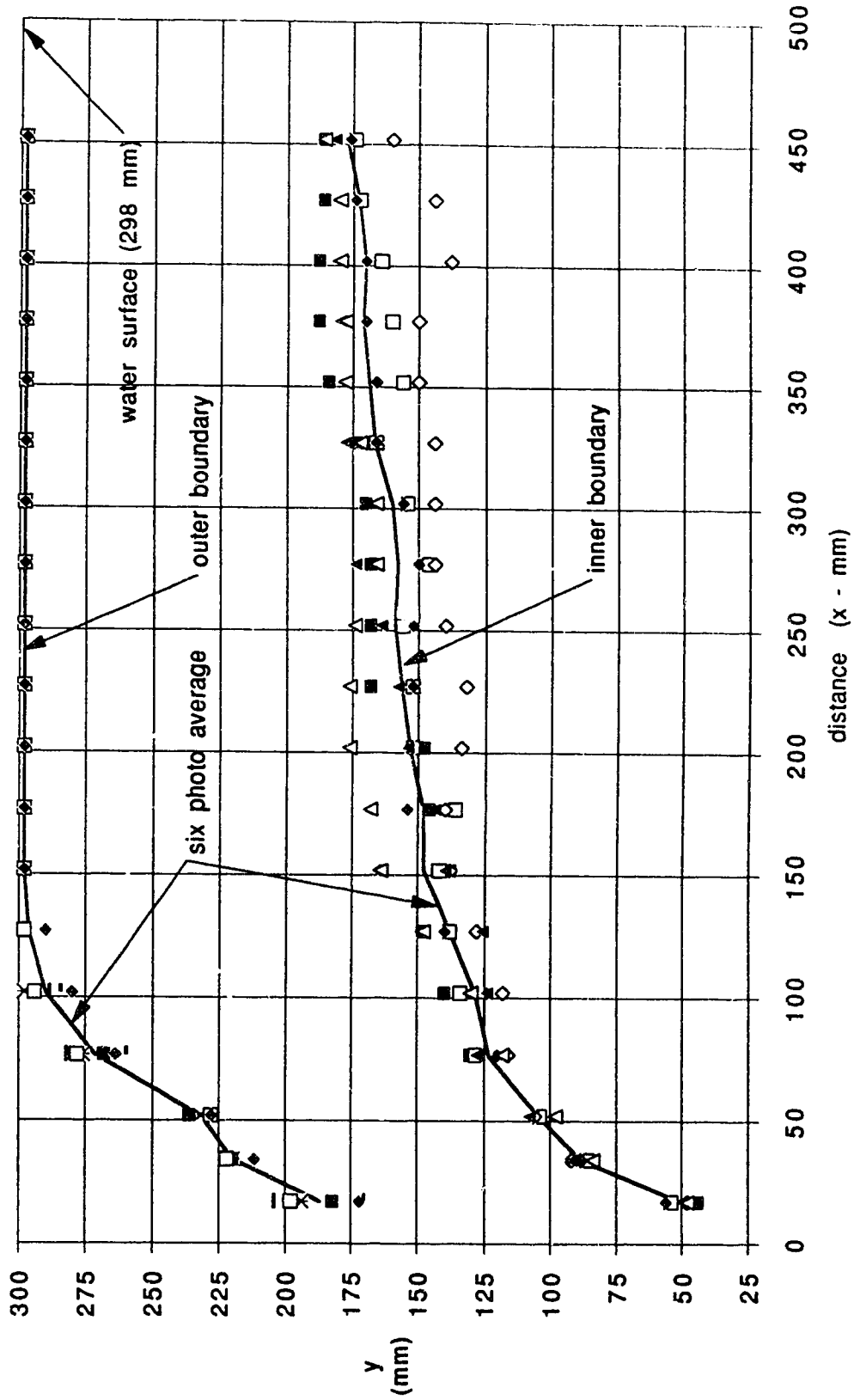


Figure 3.7 Width data for runs 1232 and 1136

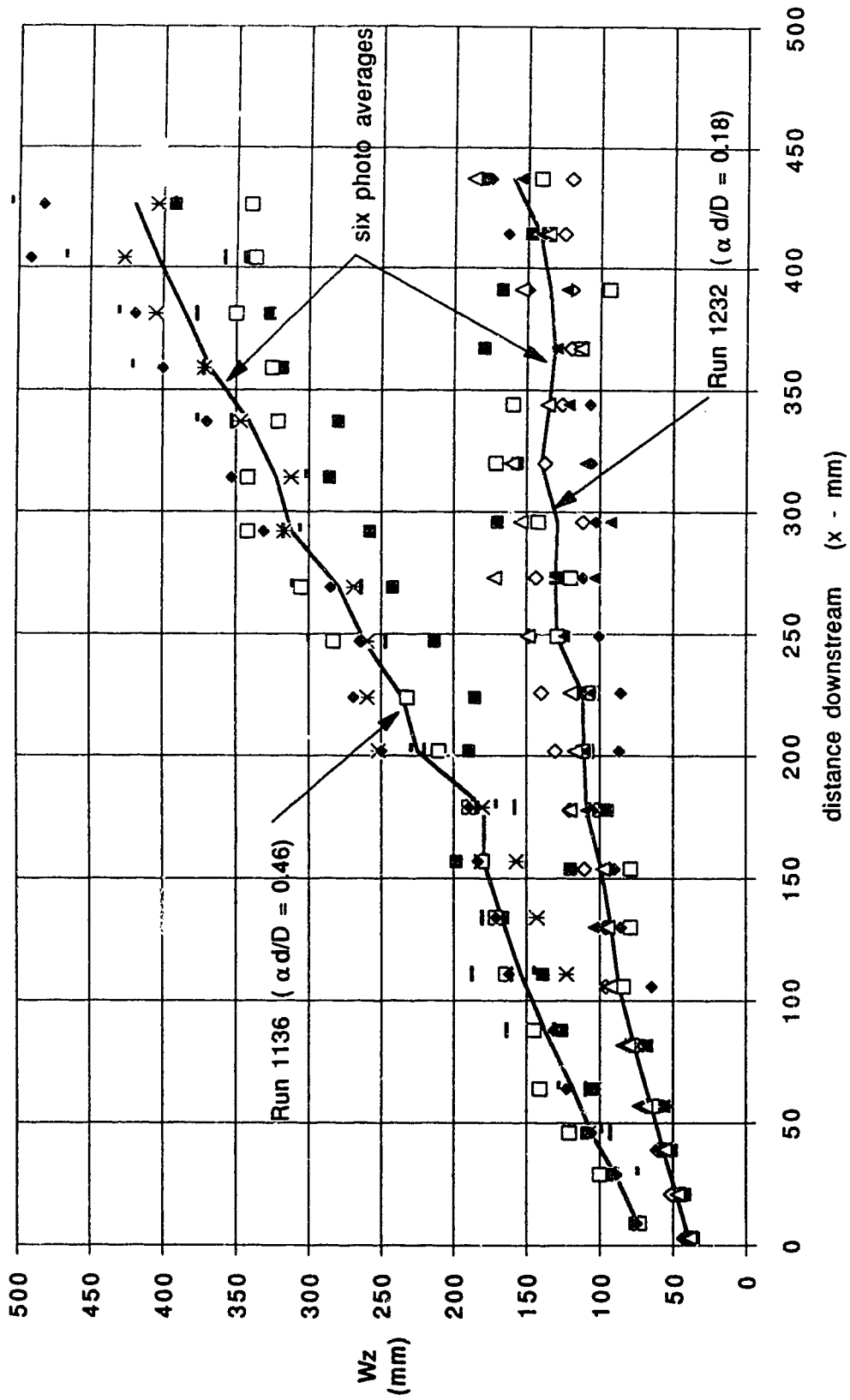


Figure 3.8 Variance and confidence interval of photographic measurements for inner boundary terminal level region of Run 1232

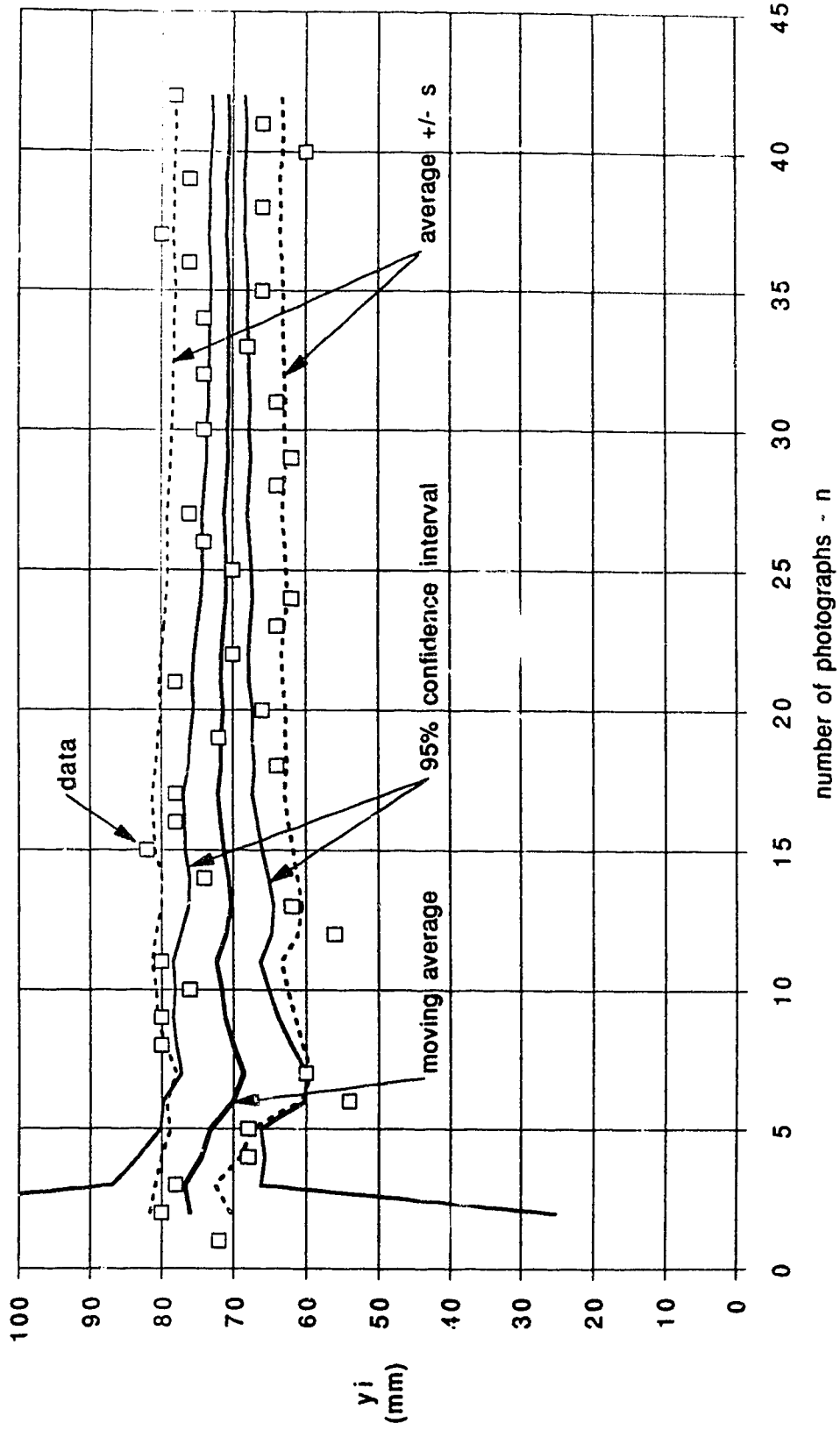


Figure 3.9 Inner boundary location for deep water jets

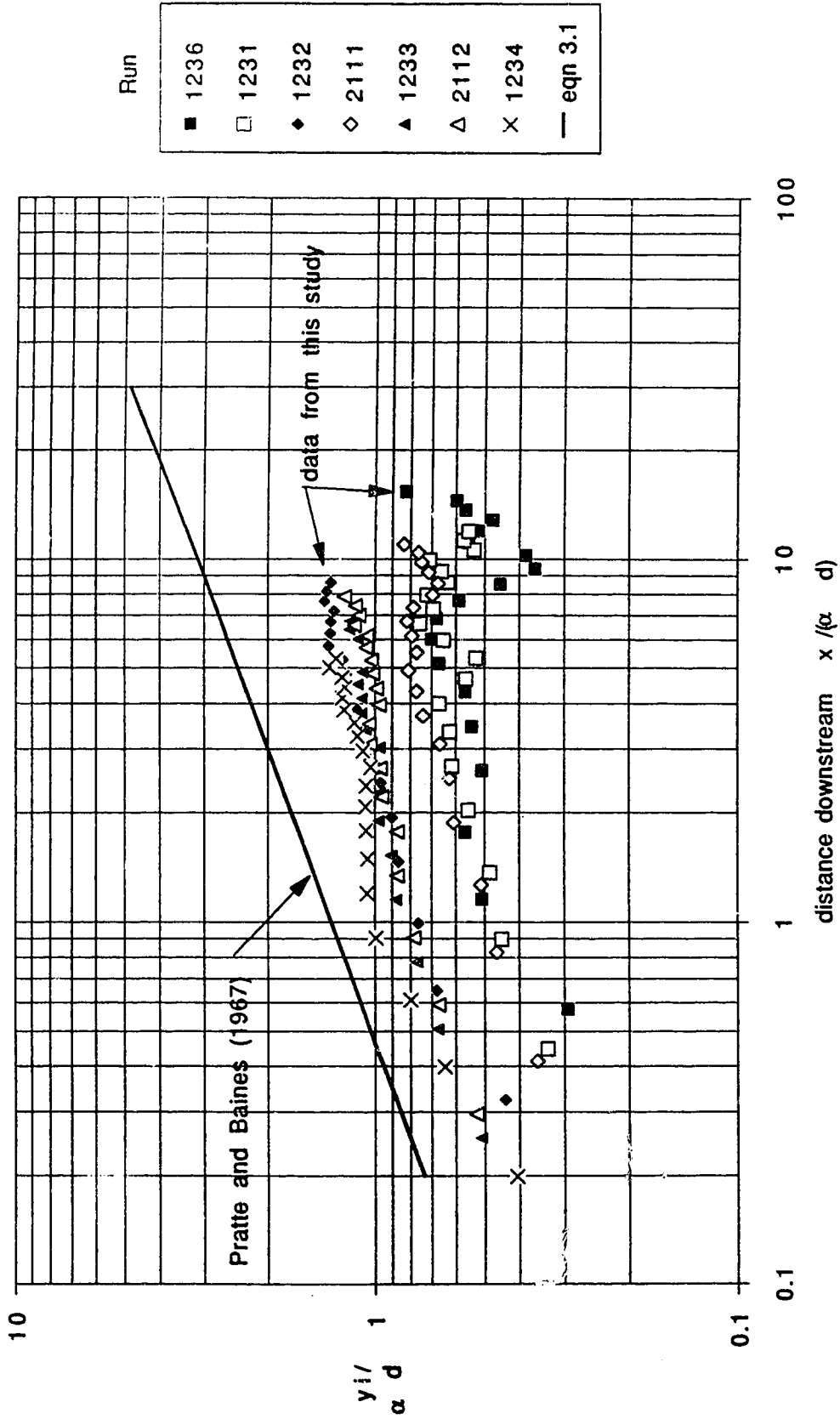


Figure 3.10 Outer boundary location for deep water jets

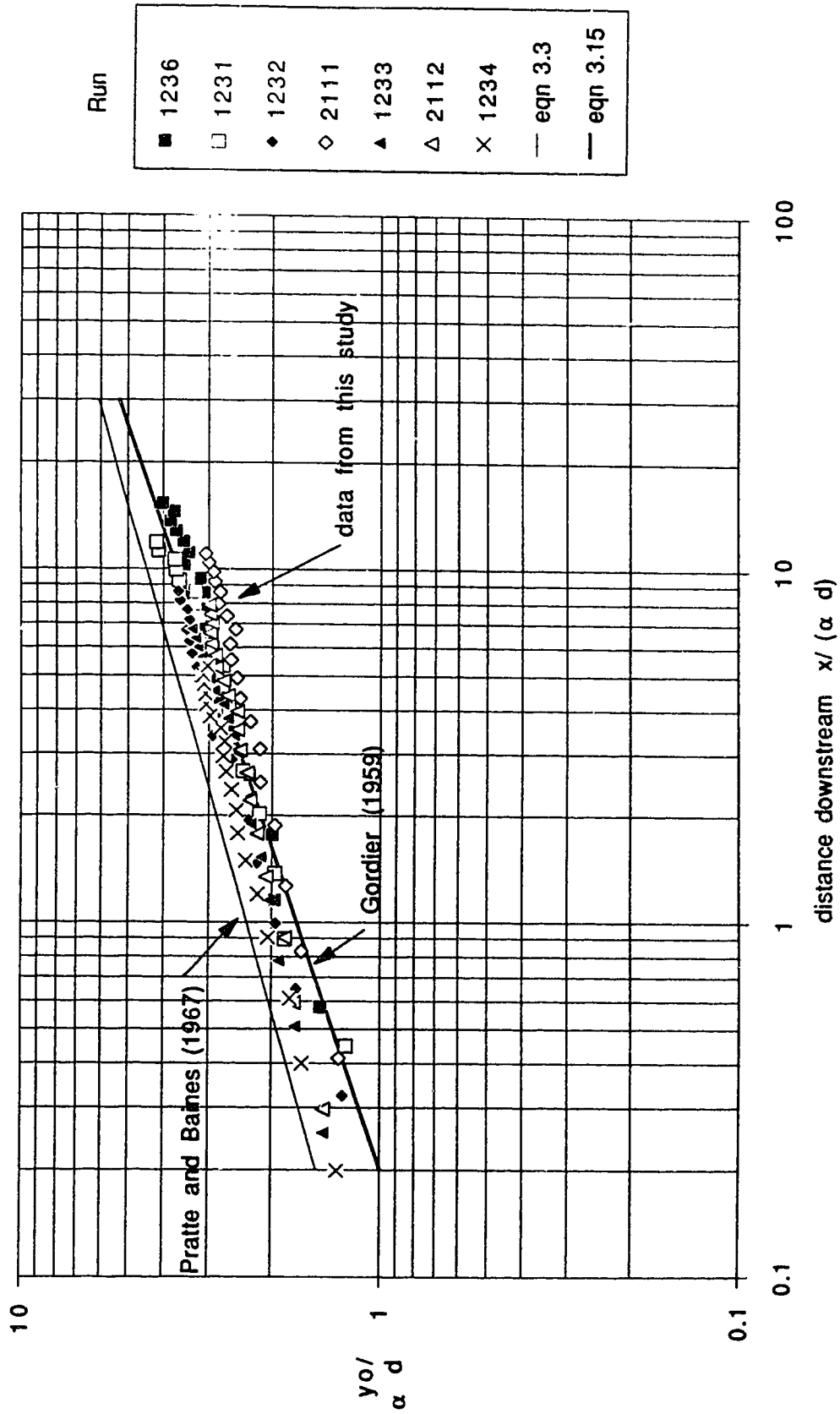




Figure 3.11 Jet centreline profile for deep water jets

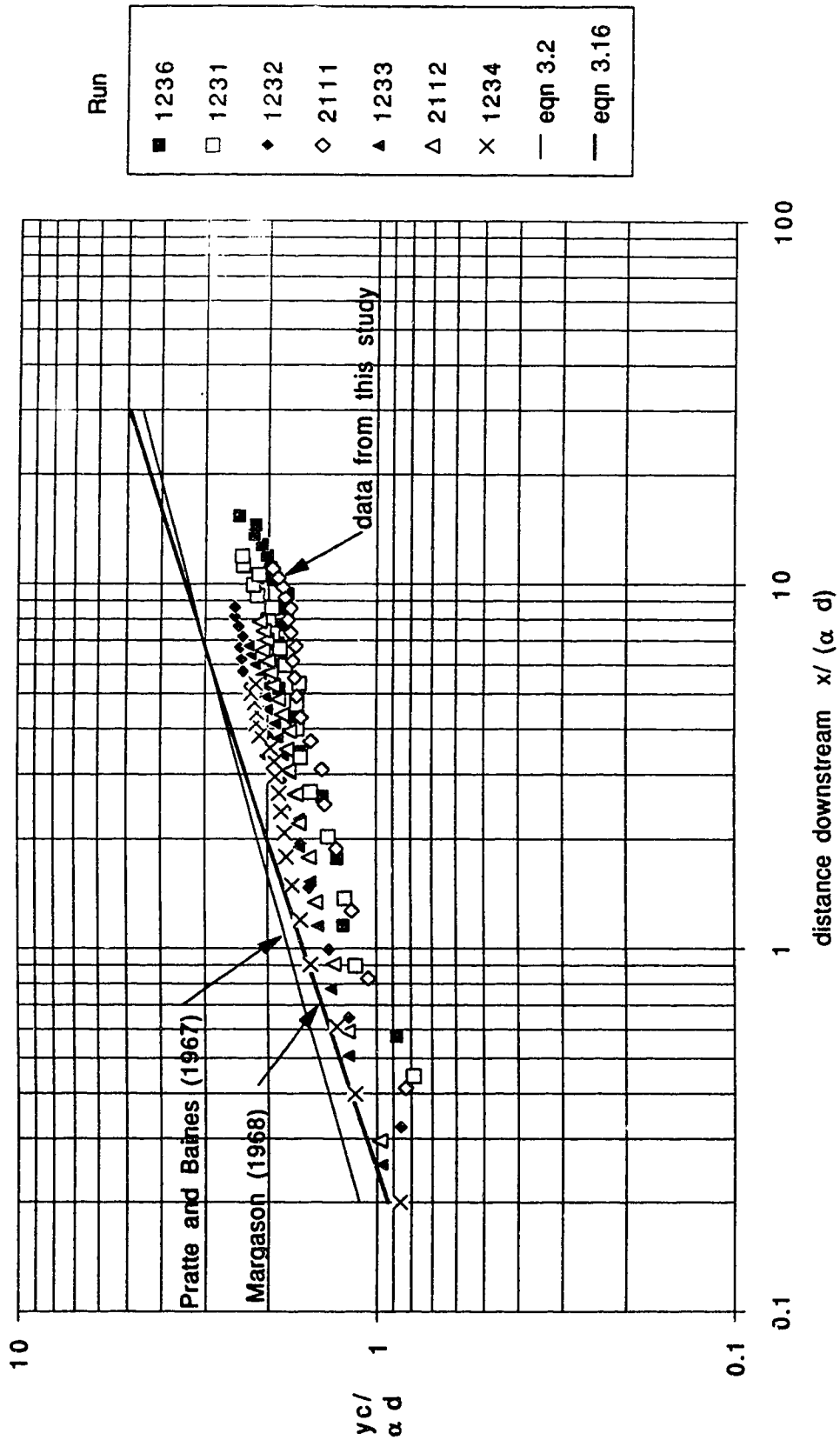


Figure 3.12 Jet centreline penetration distance

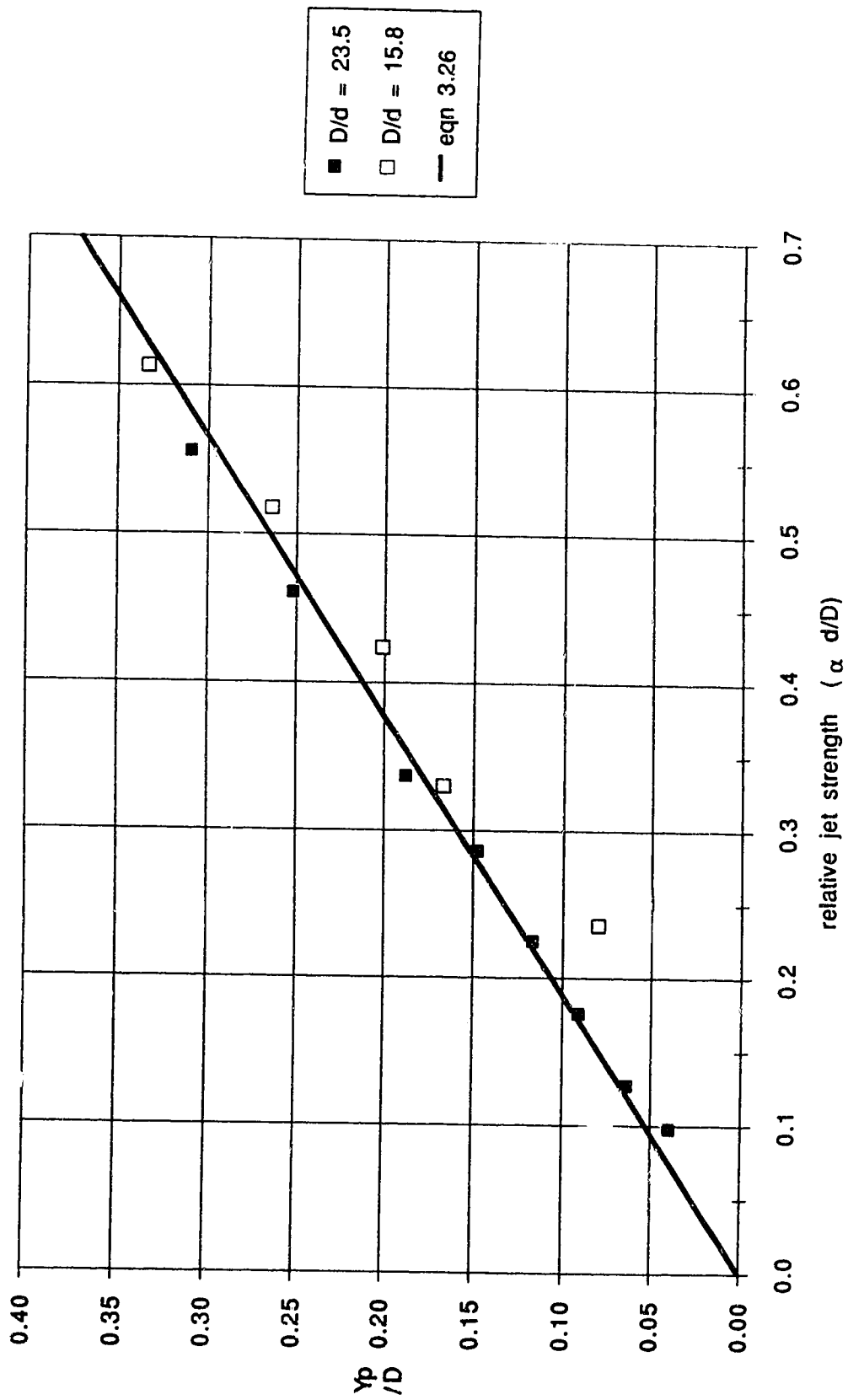


Figure 3.13 Momentum dominated near field coefficients

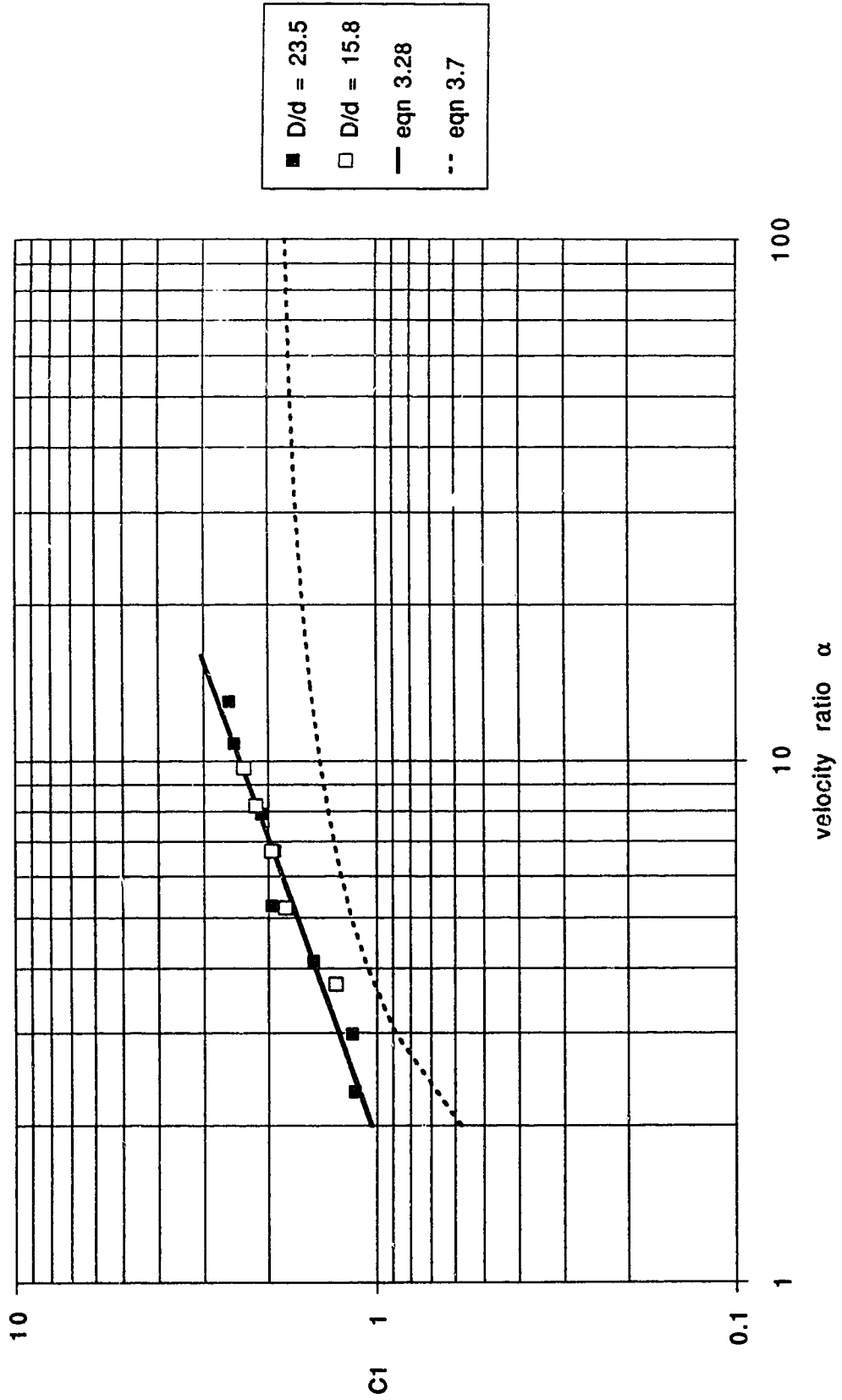


Figure 3.14 Momentum dominated far field coefficients

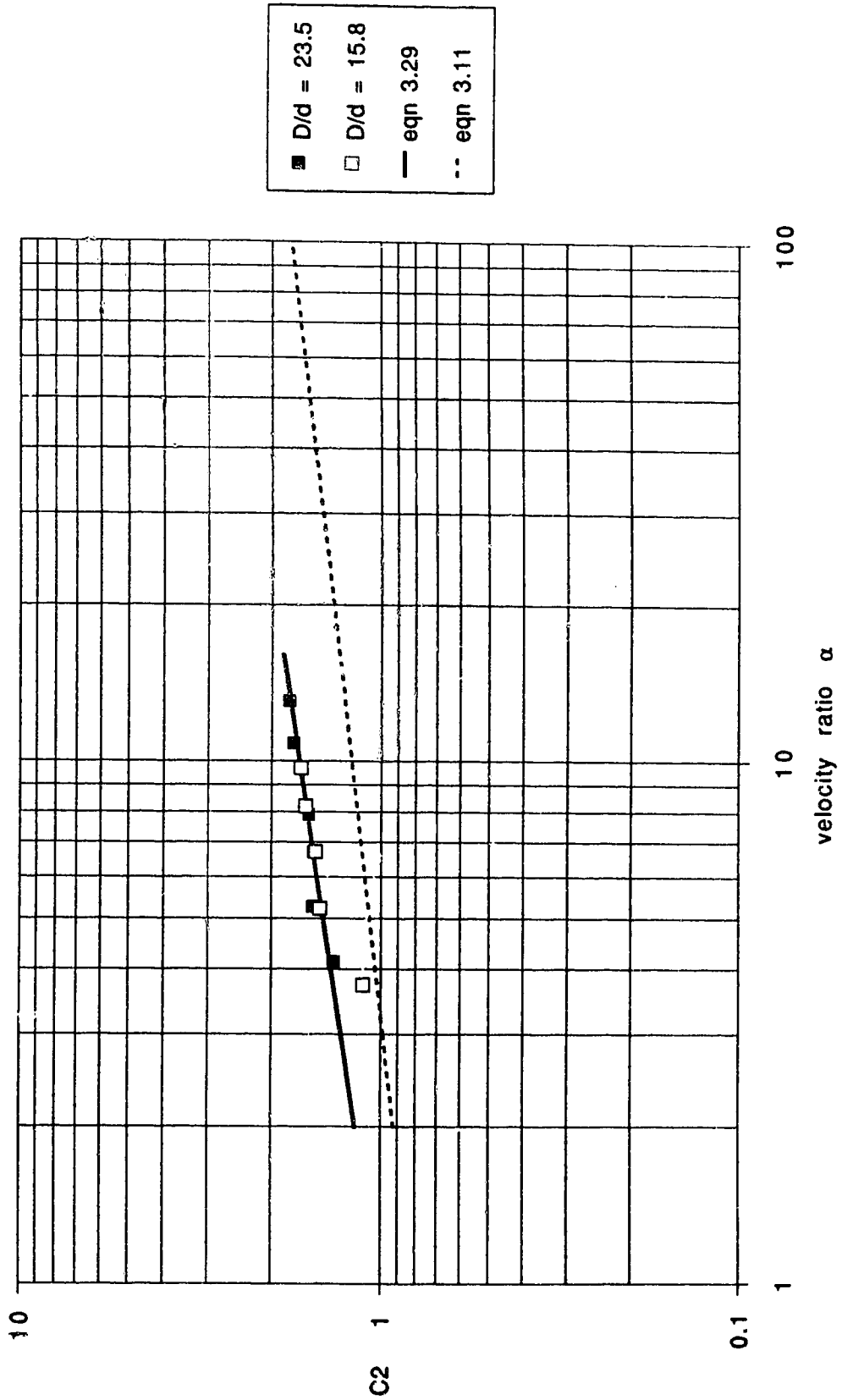


Figure 3.15 Surface dominated field coefficients

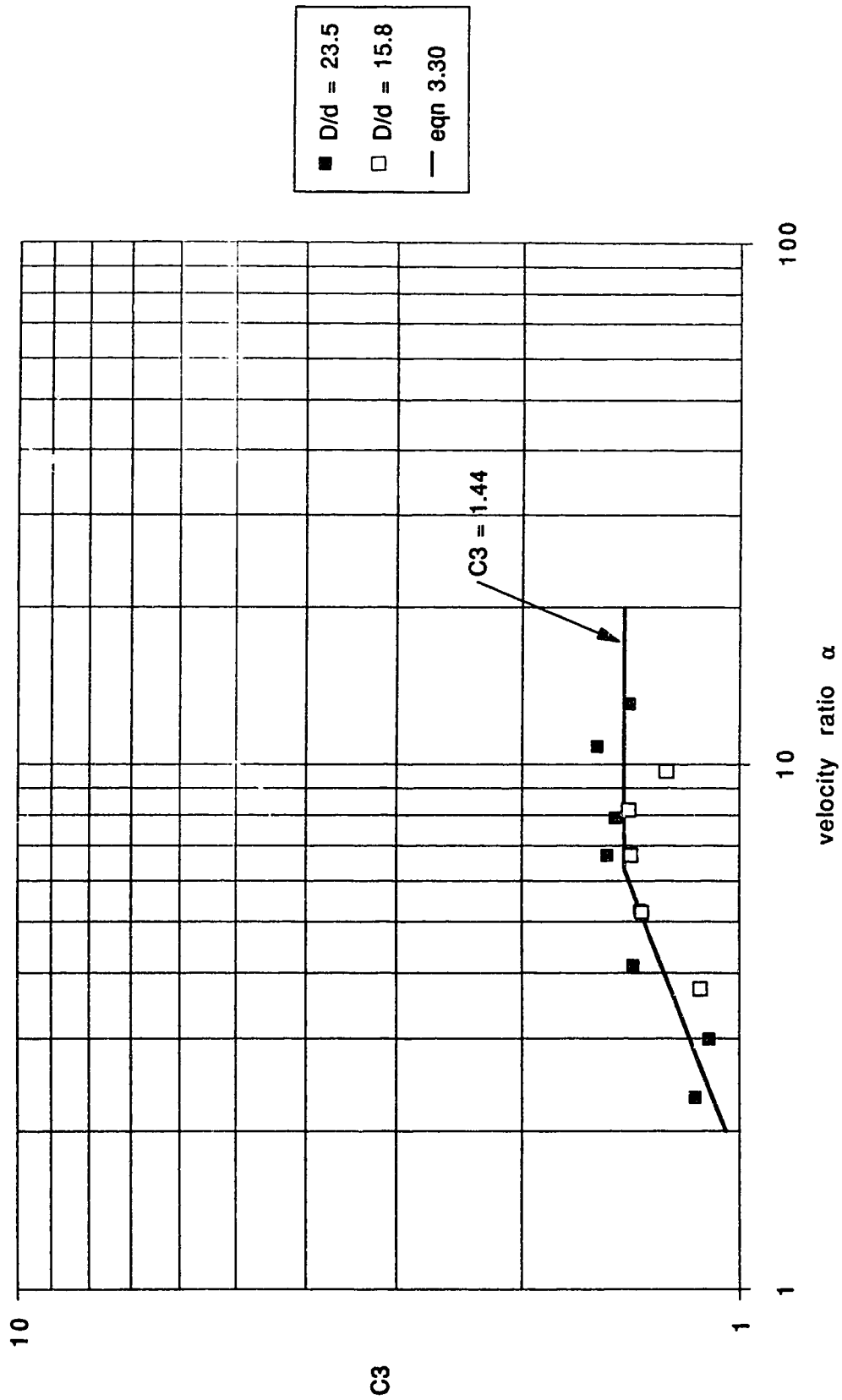


Figure 3.16 Surface dominated field exponents versus  $\frac{\alpha d}{D}$

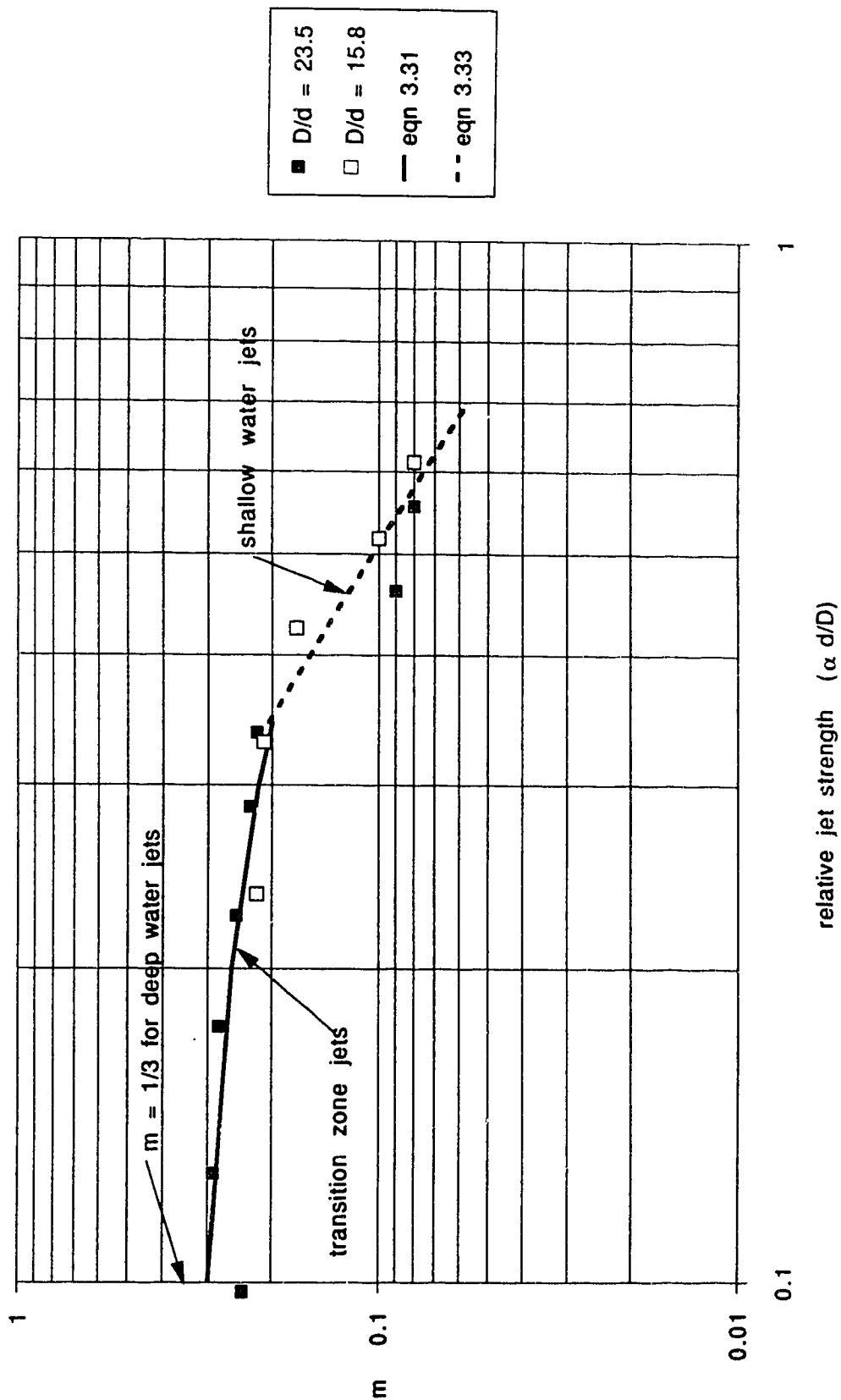


Figure 3.17 Surface dominated field exponents versus  $\frac{\alpha^2 d}{D}$

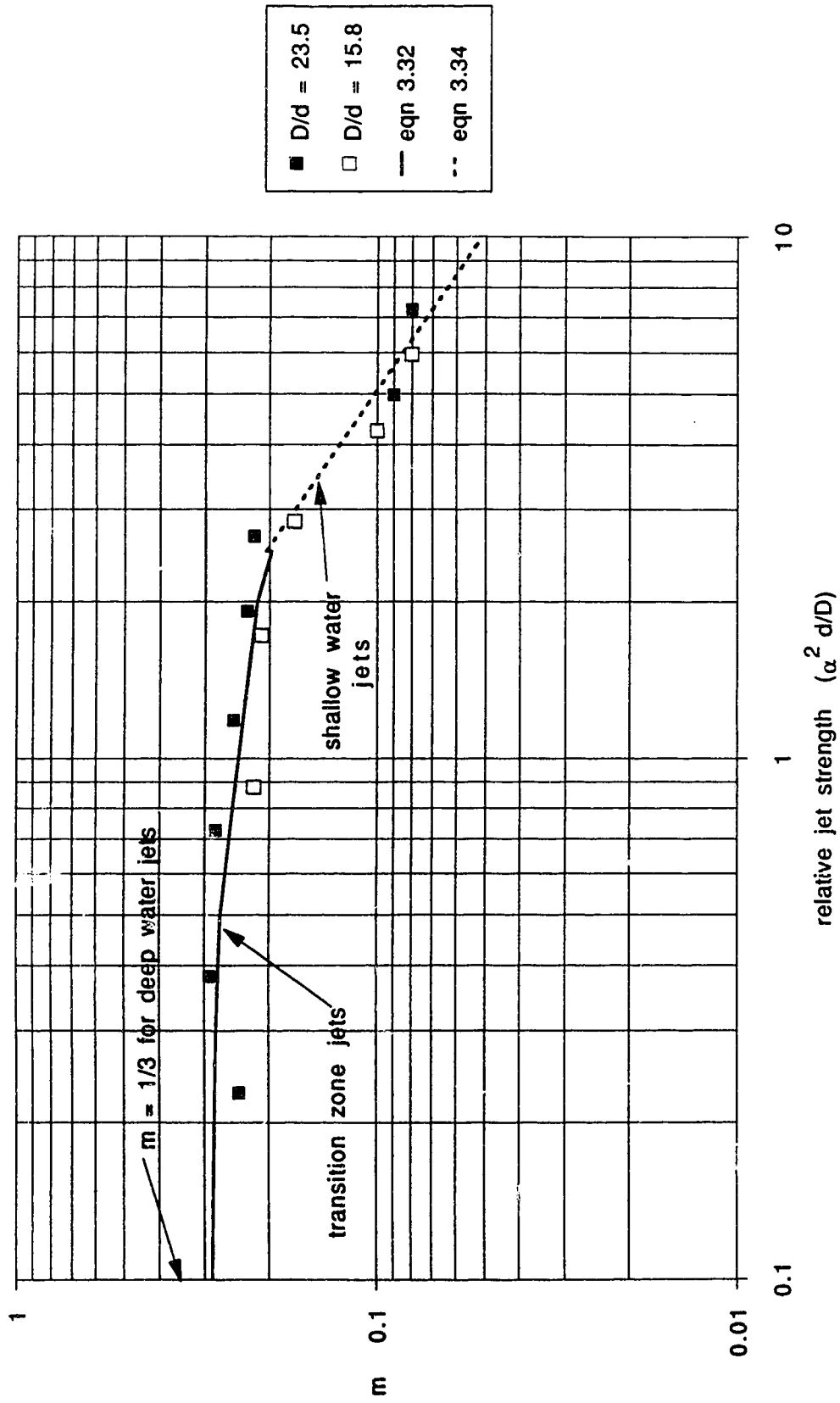


Figure 3.18 Jet terminal levels versus  $\frac{\alpha d}{D}$

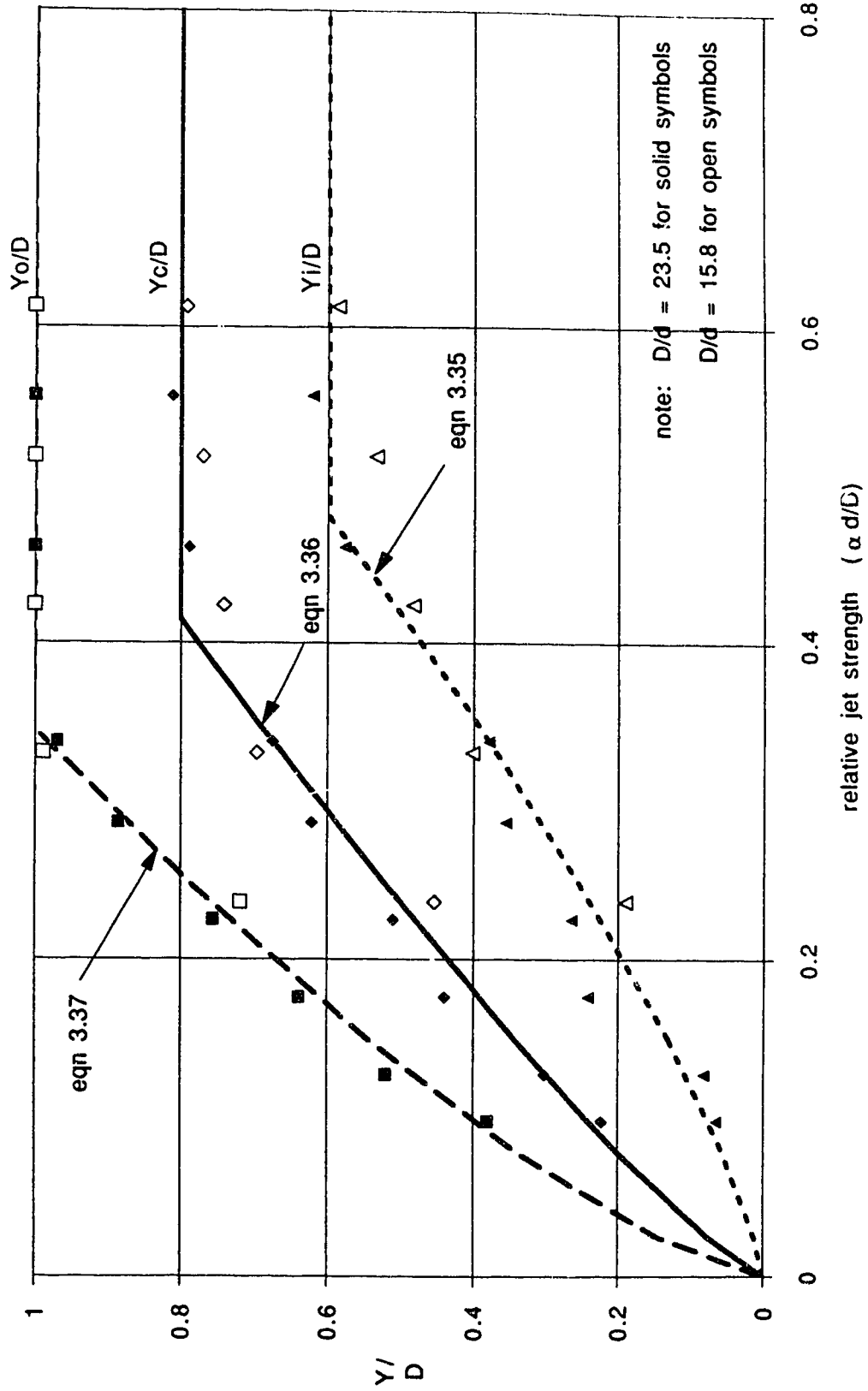




Figure 3.19 Jet terminal levels versus  $\frac{\alpha^2 d}{D}$

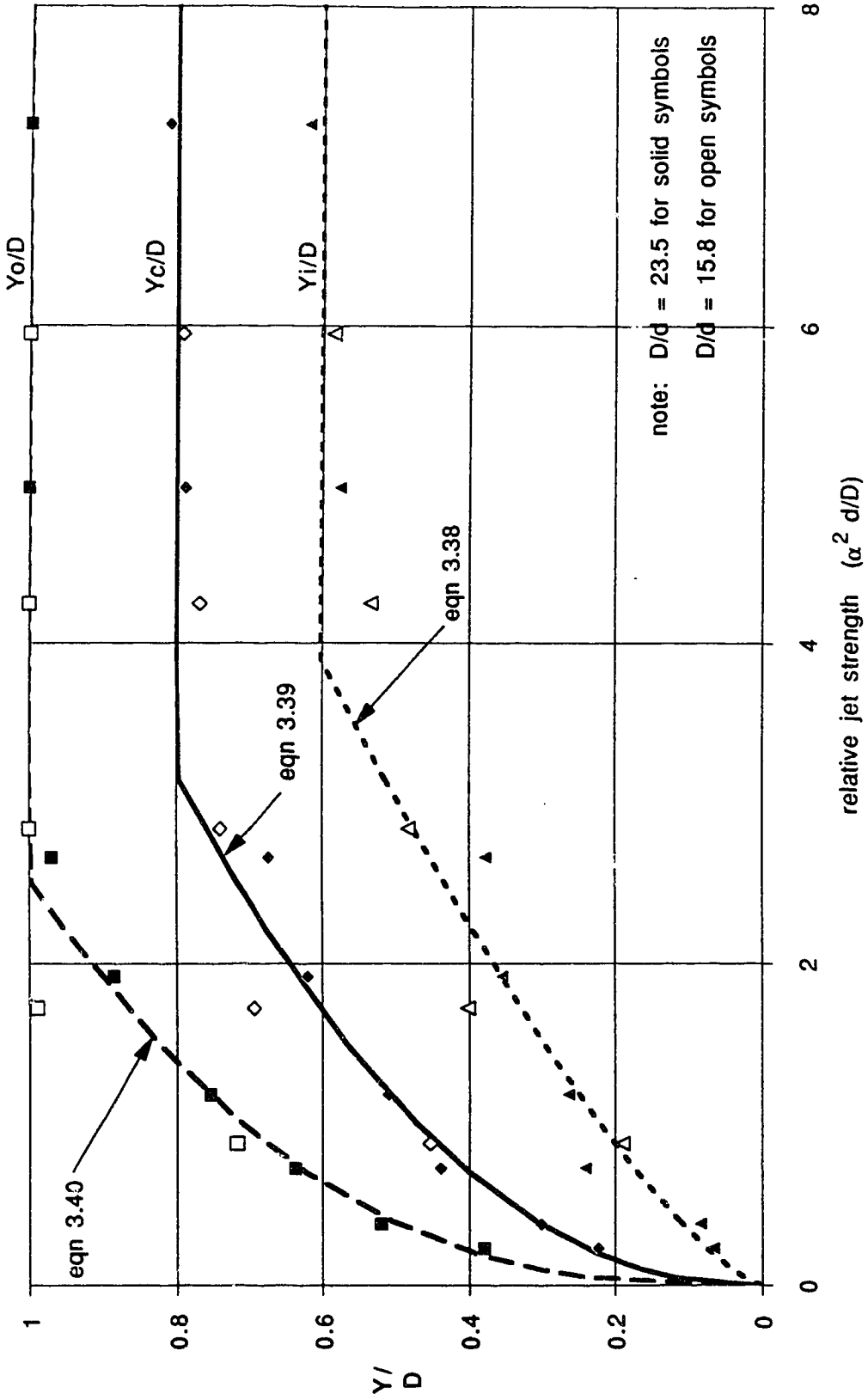


Figure 3.20 Terminal level distances versus  $\frac{\alpha d}{D}$

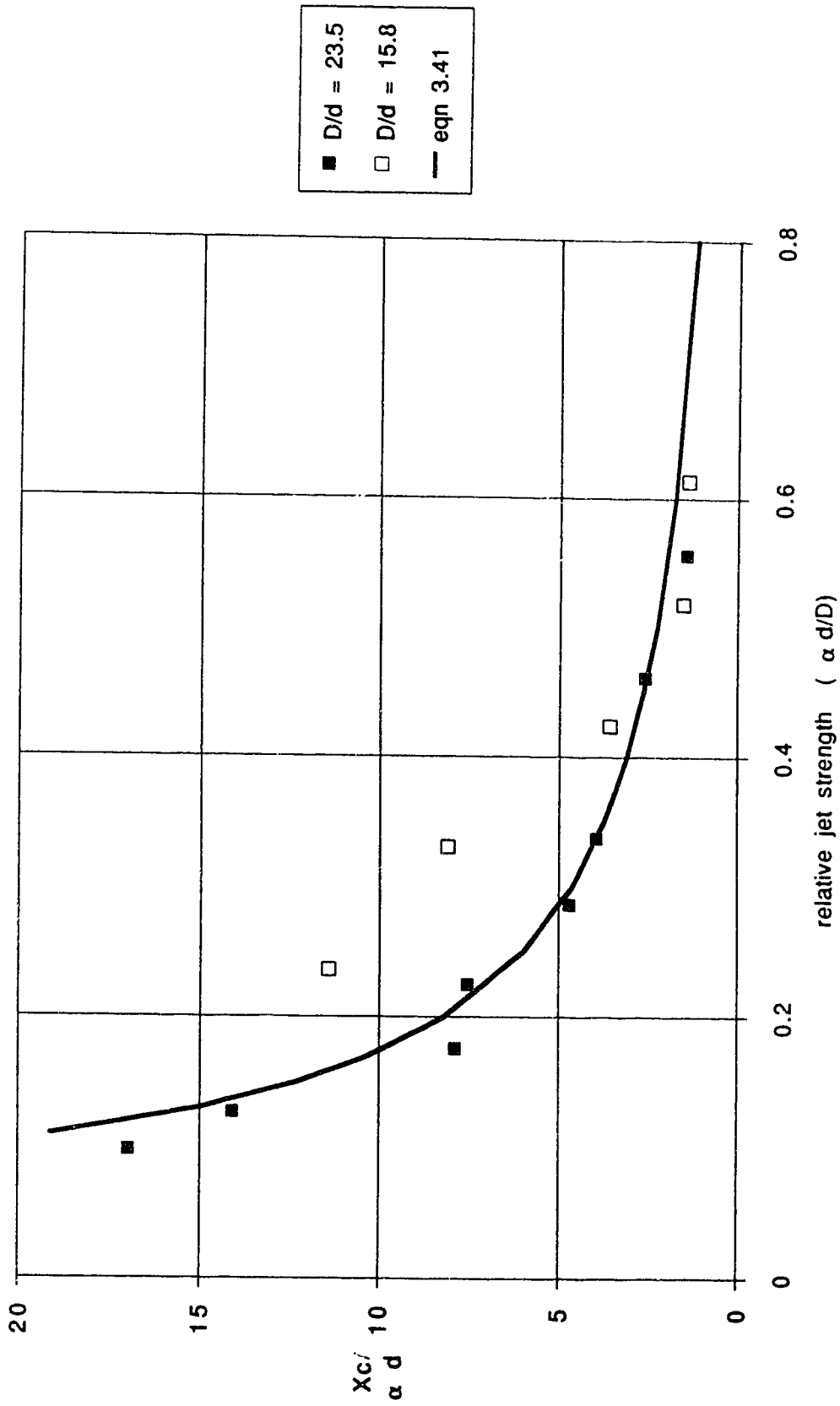


Figure 3.21 Terminal level distances versus  $\frac{\alpha^2 d}{D}$

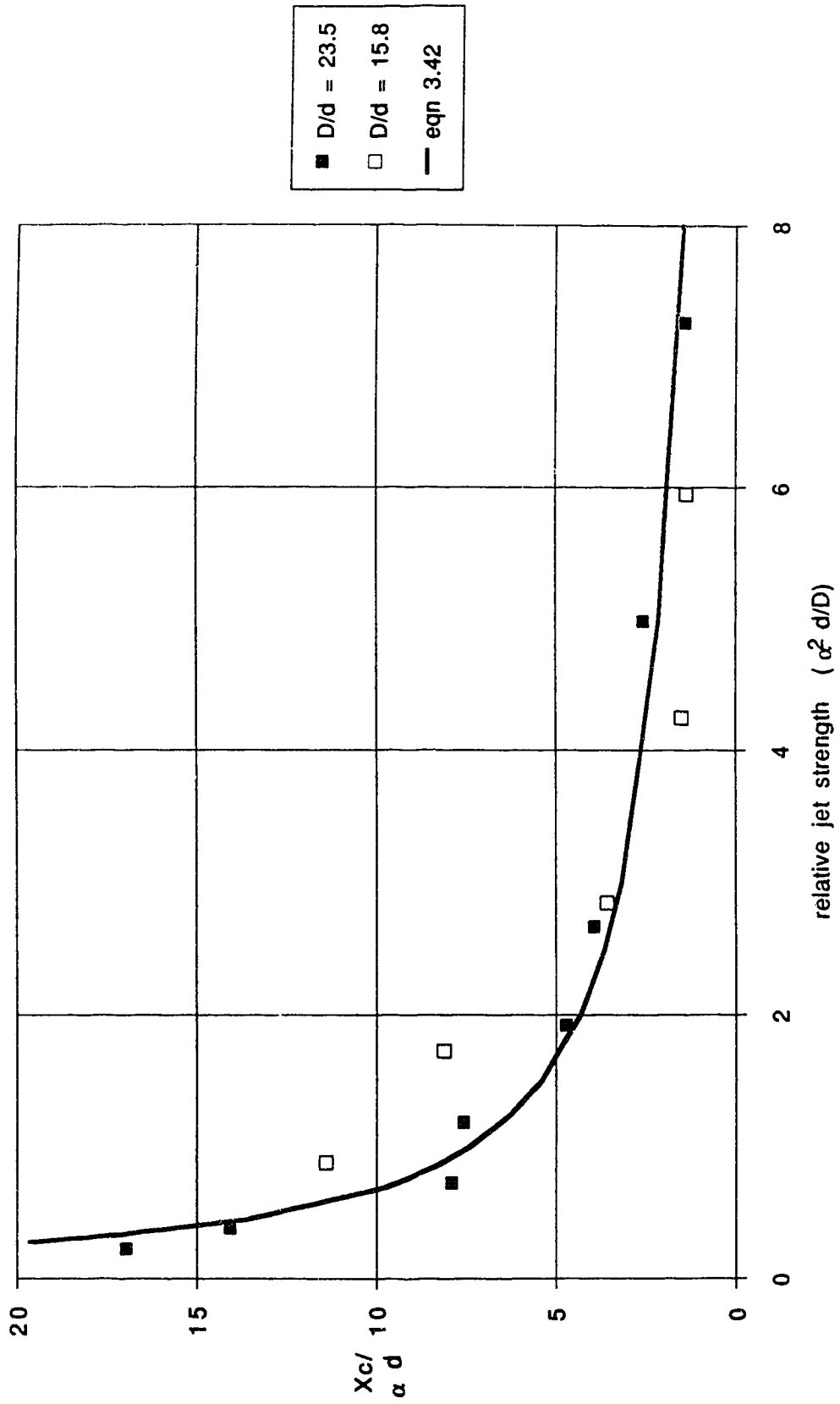


Figure 3.22 Shallow water jet discharges flow fields for  $D/d = 15$

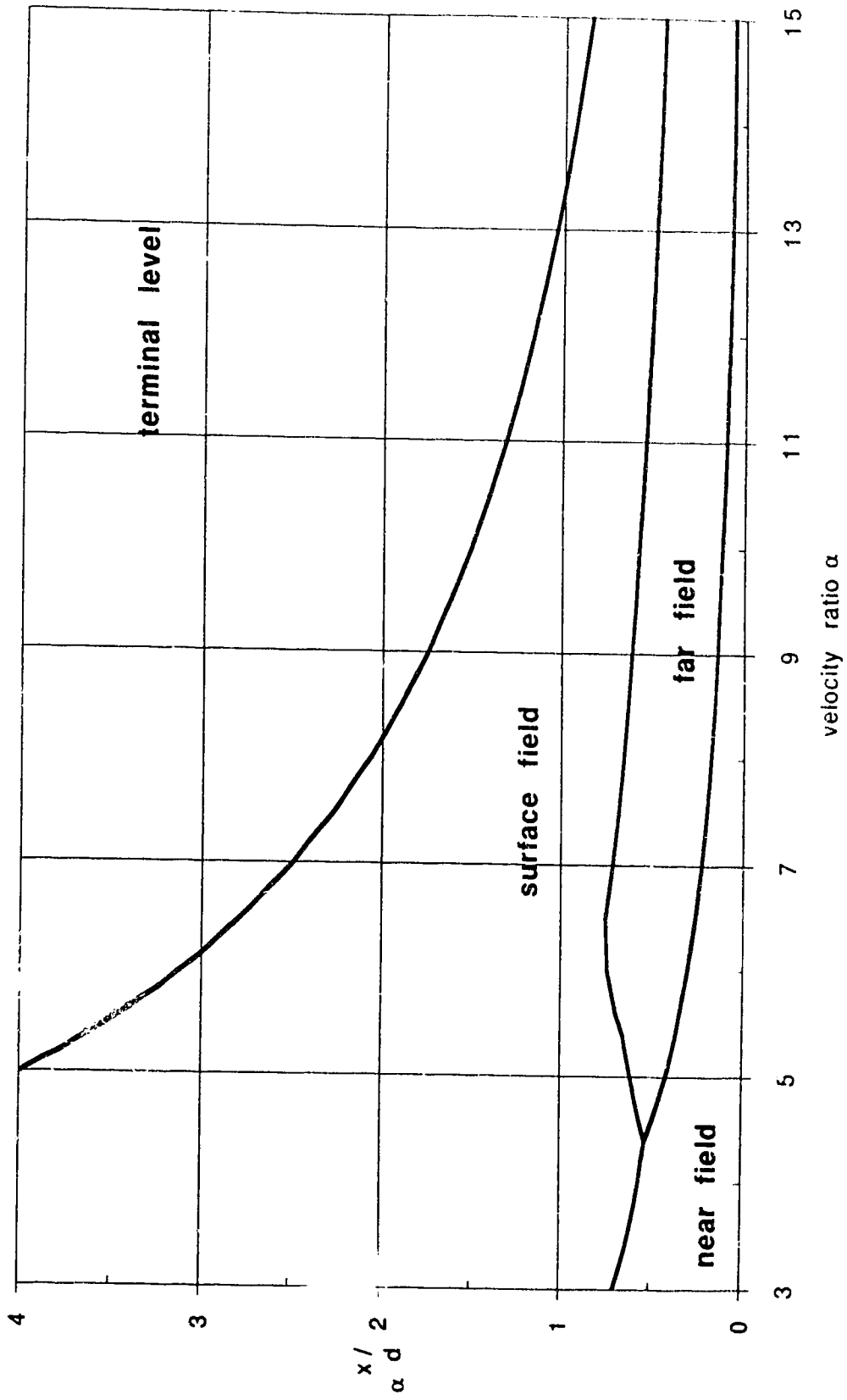


Figure 3.23 Shallow water jet discharges flow fields for  $D/d = 25$

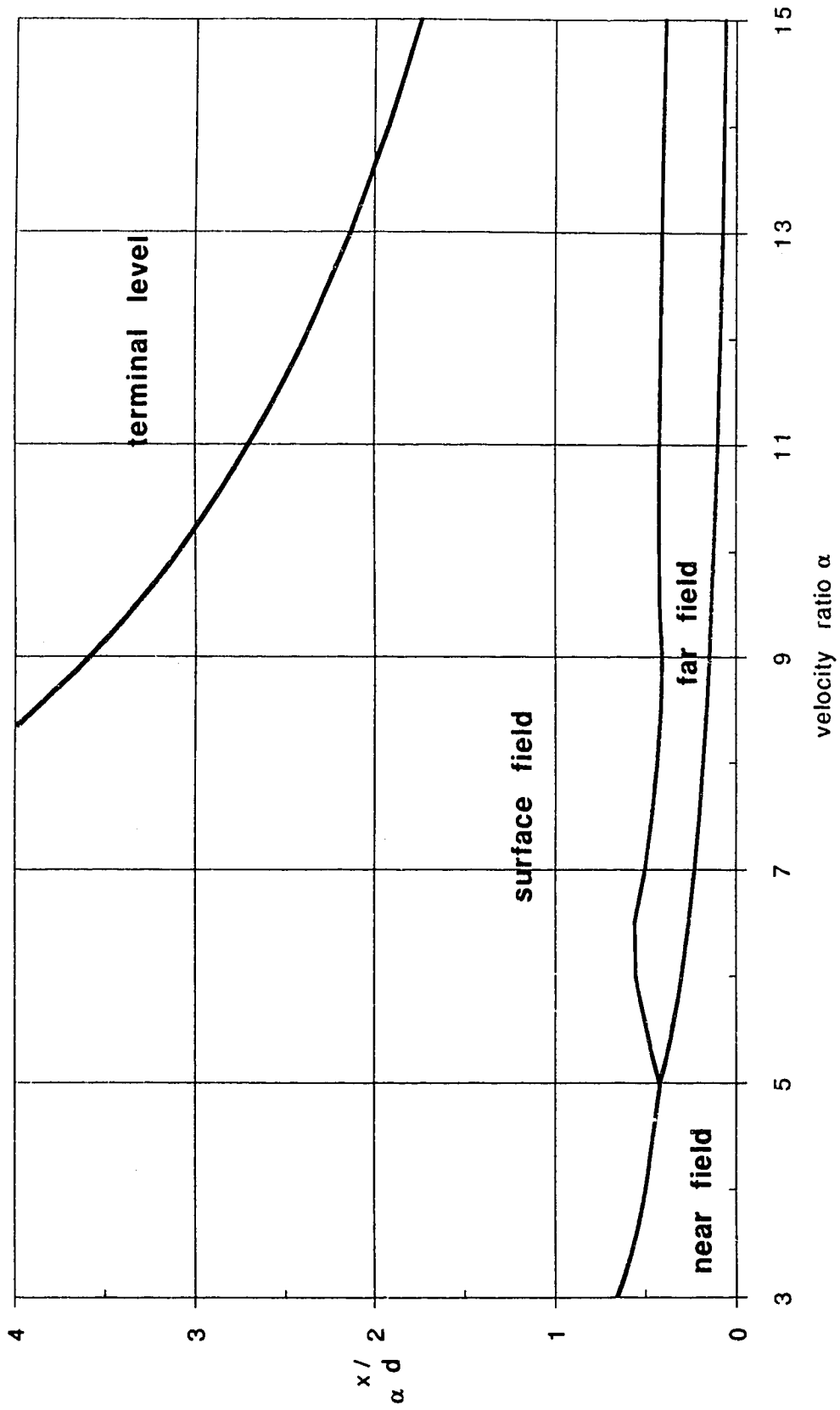


Figure 3.24 Jet widths for deep water jets

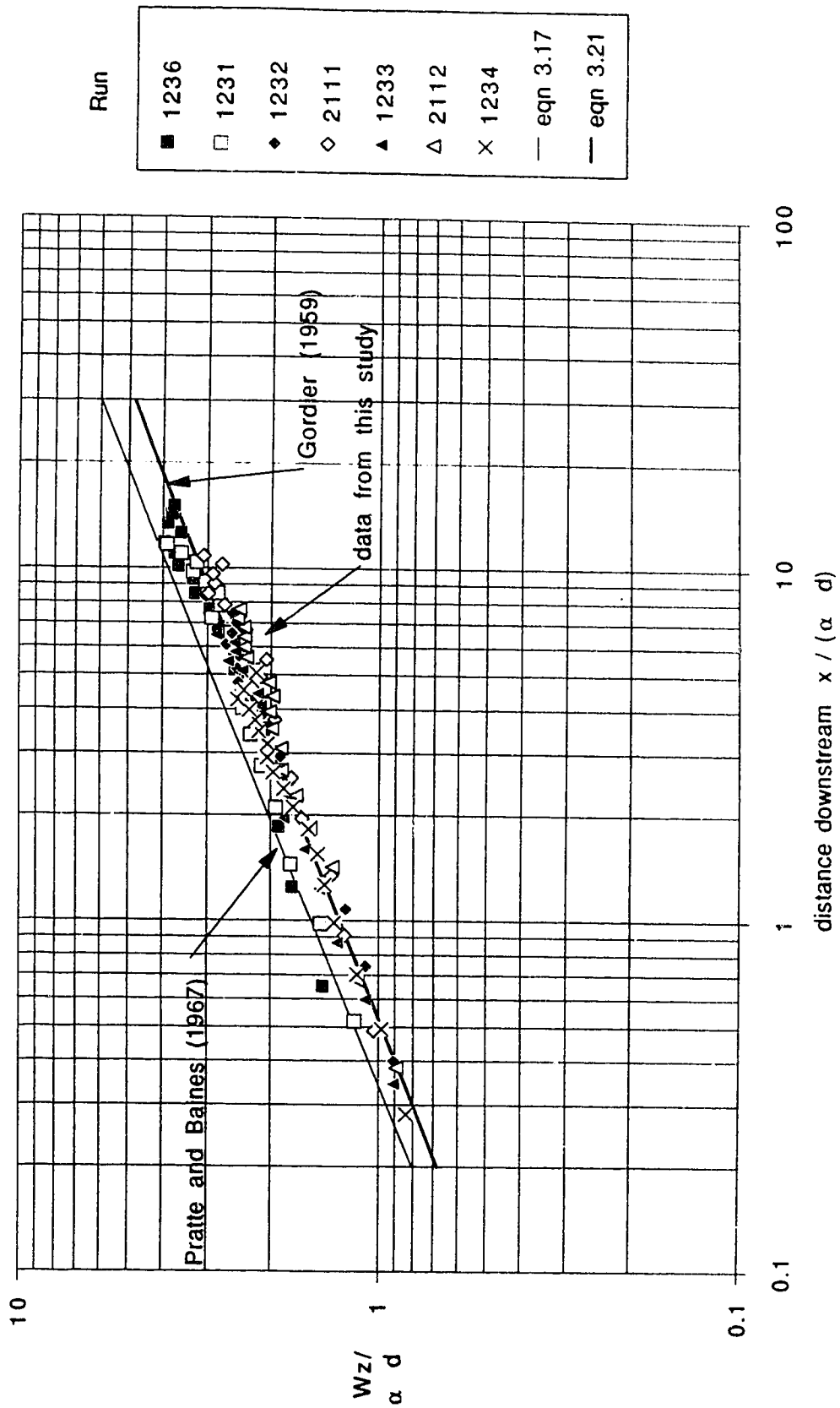


Figure 3.25 Jet width  $\left( \frac{\alpha^2 d}{D} < 2 \right)$

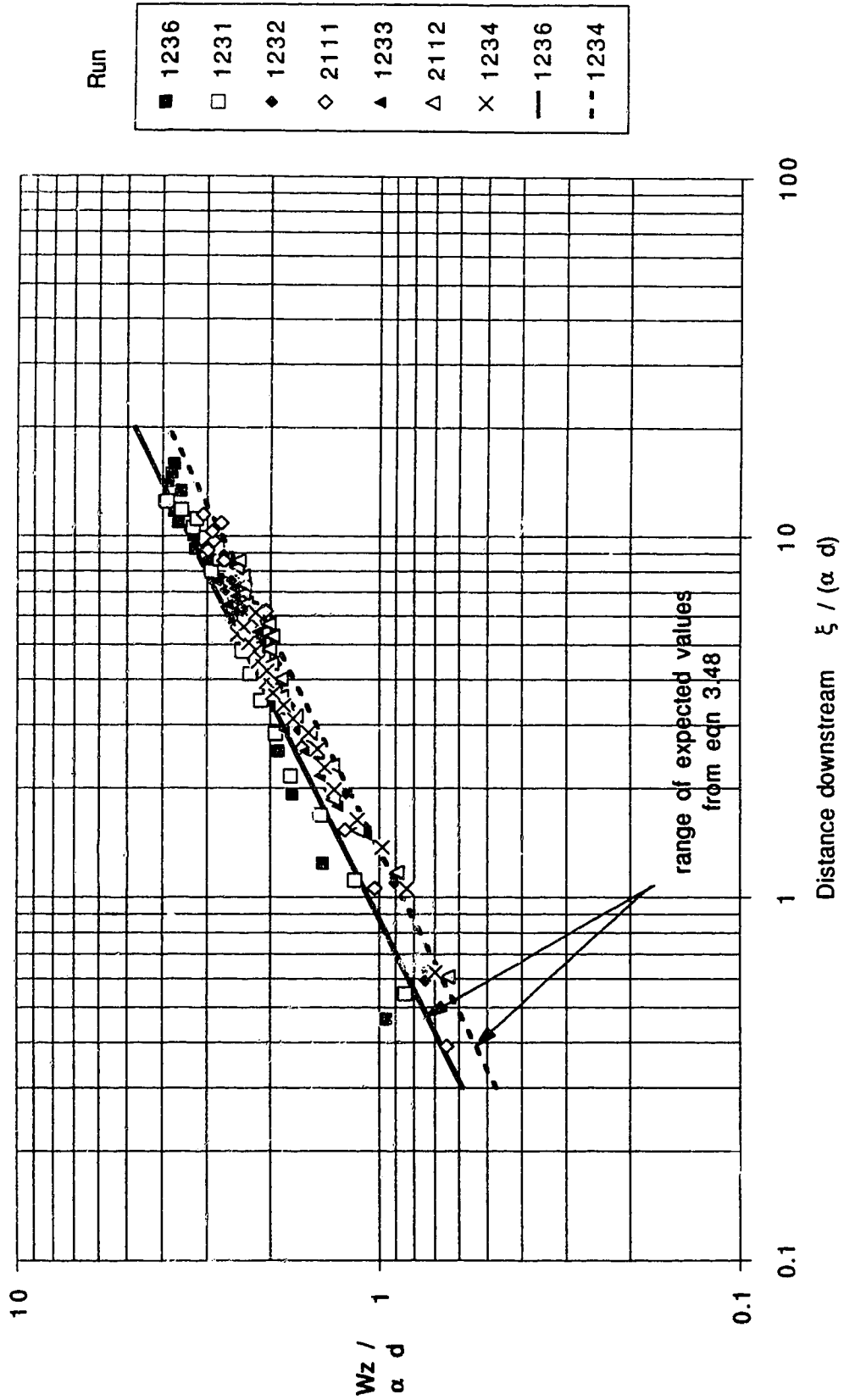


Figure 3.26 Jet width  $\left( \frac{\alpha^2 d}{L} > 2 \right)$

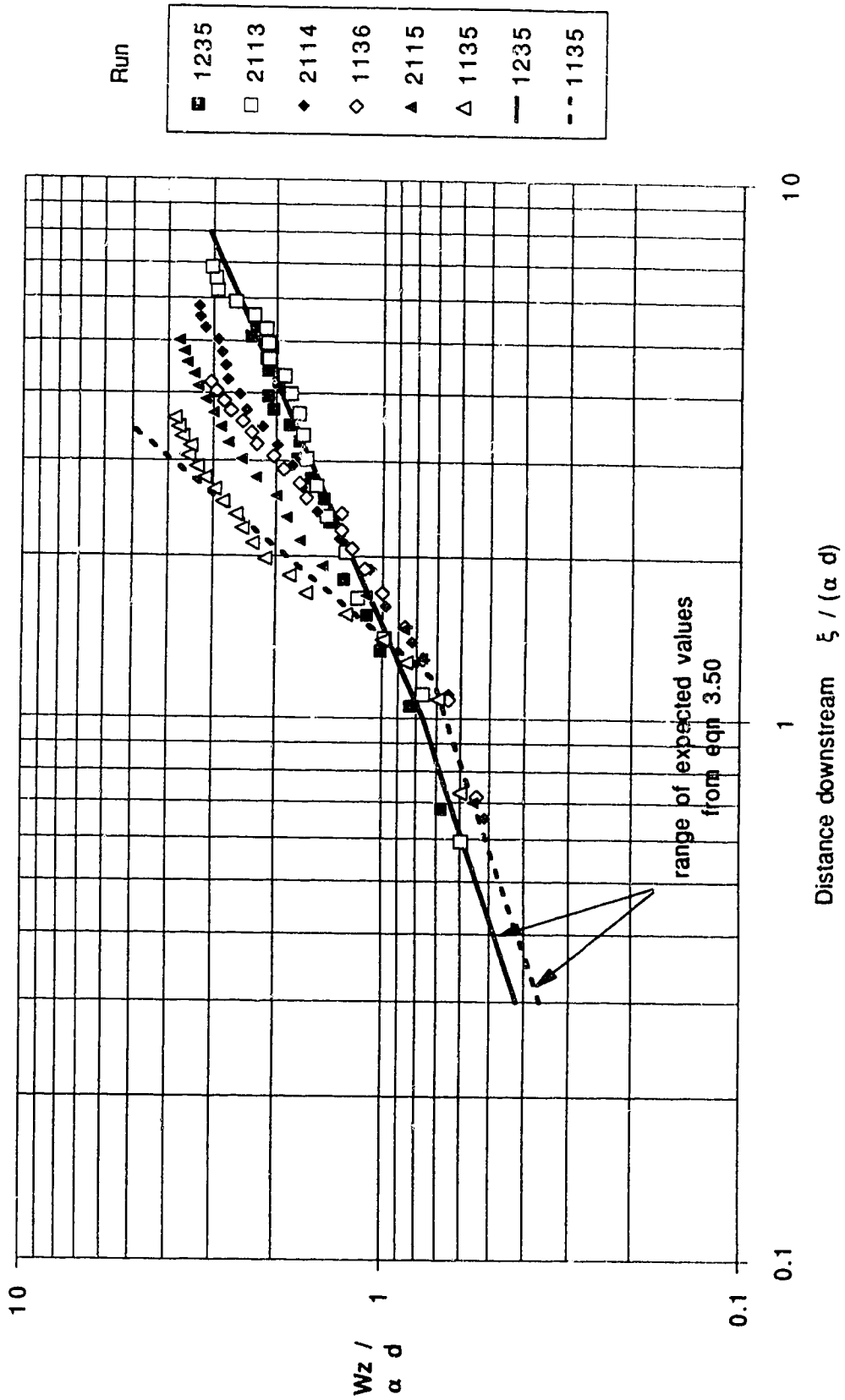




Figure 3.27 Jet width equations and coefficients

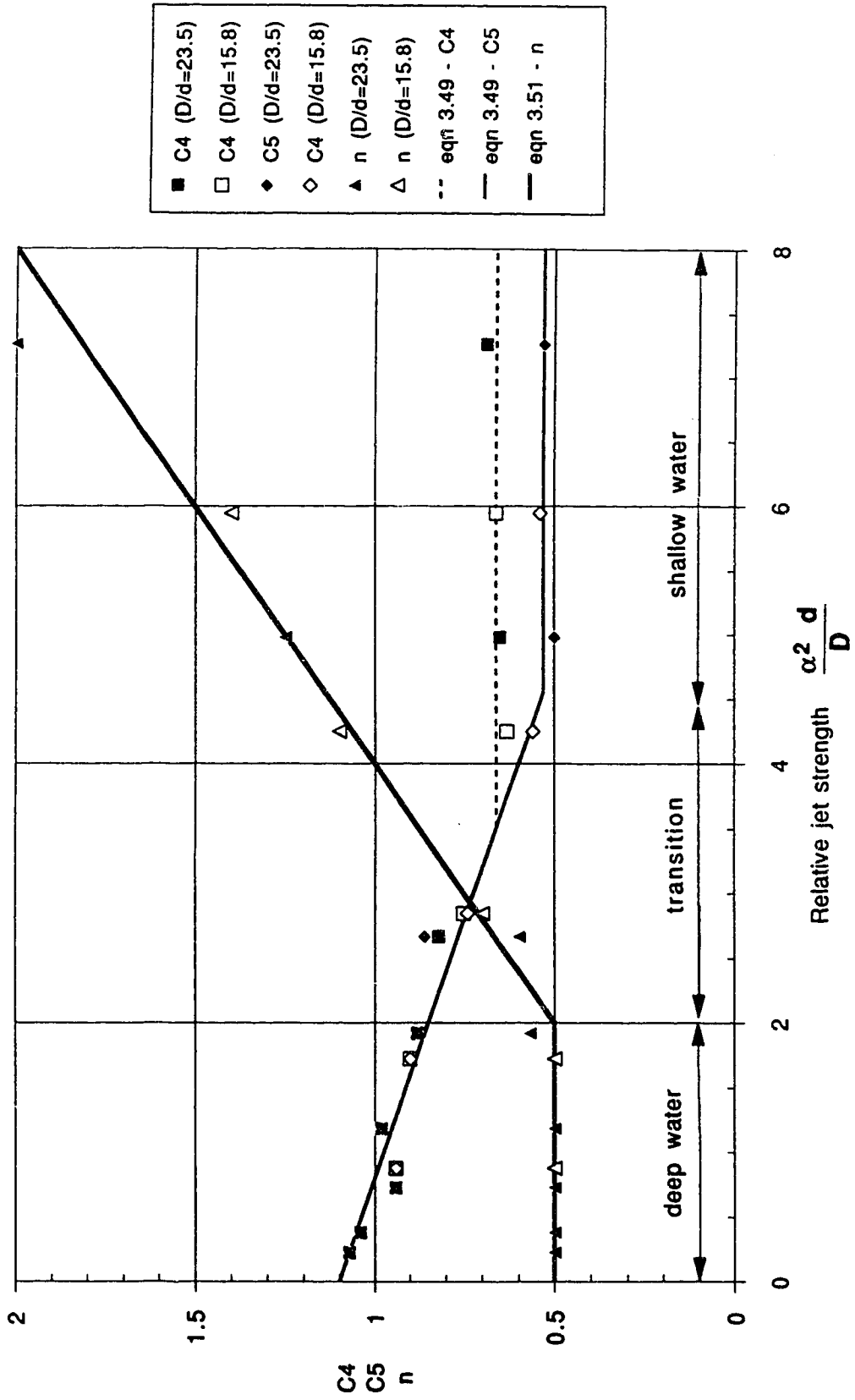


Figure 3.28 Jet thicknesses for deep water jets versus  $\frac{x}{\alpha d}$

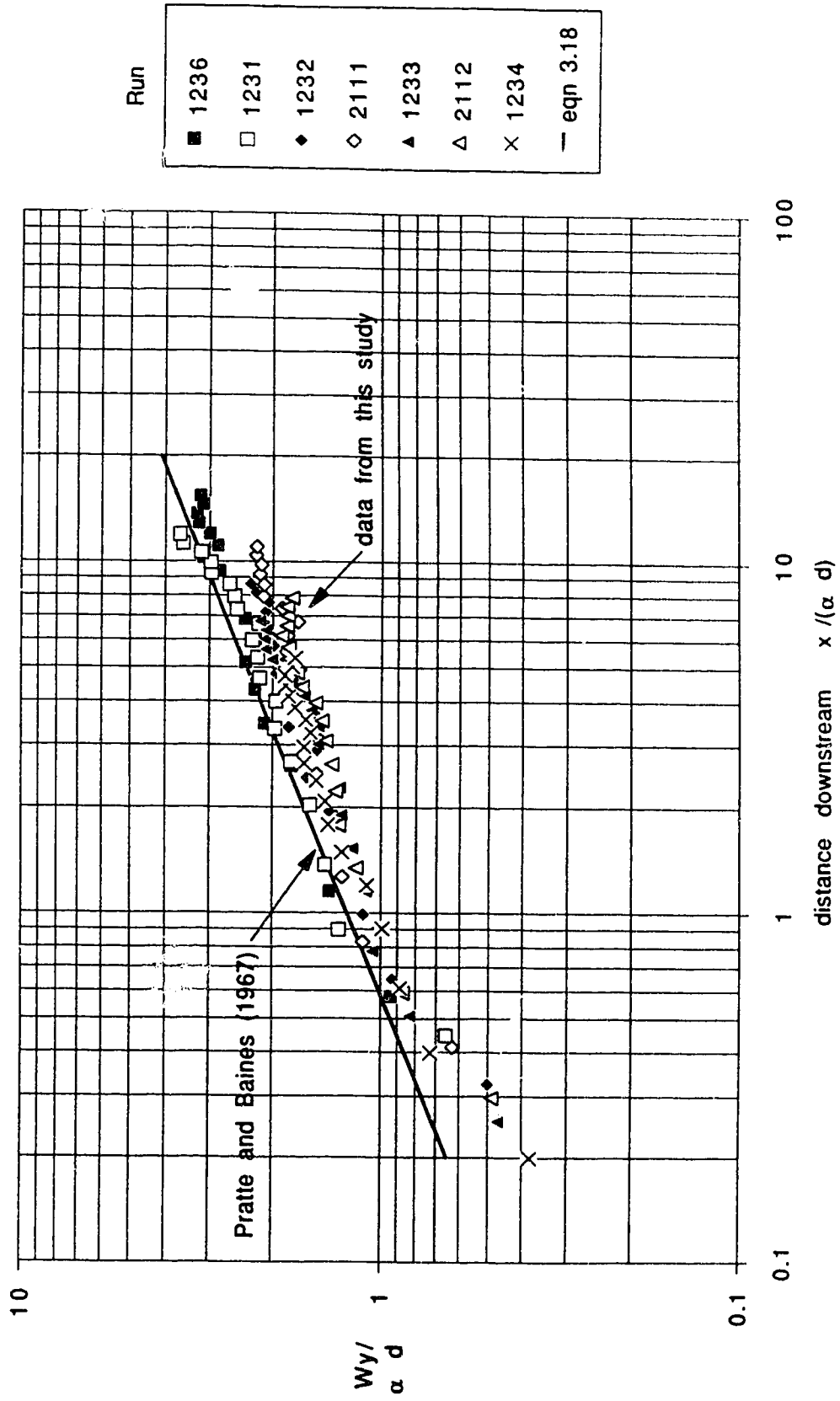


Figure 3.29 Jet thicknesses for deep water jets versus  $\frac{\xi}{\alpha d}$

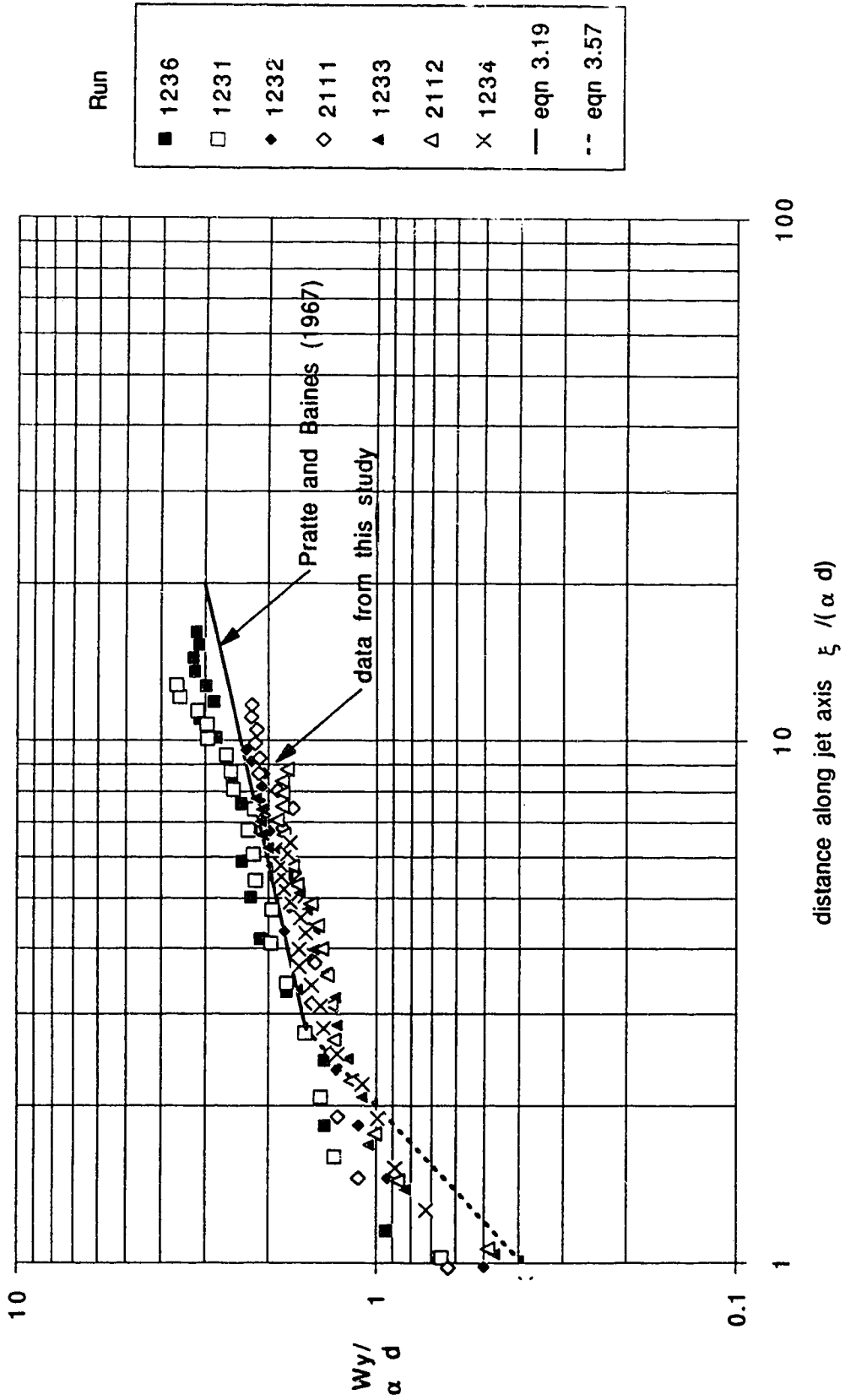


Figure 3.30 Thickness equation coefficients for deep water jets

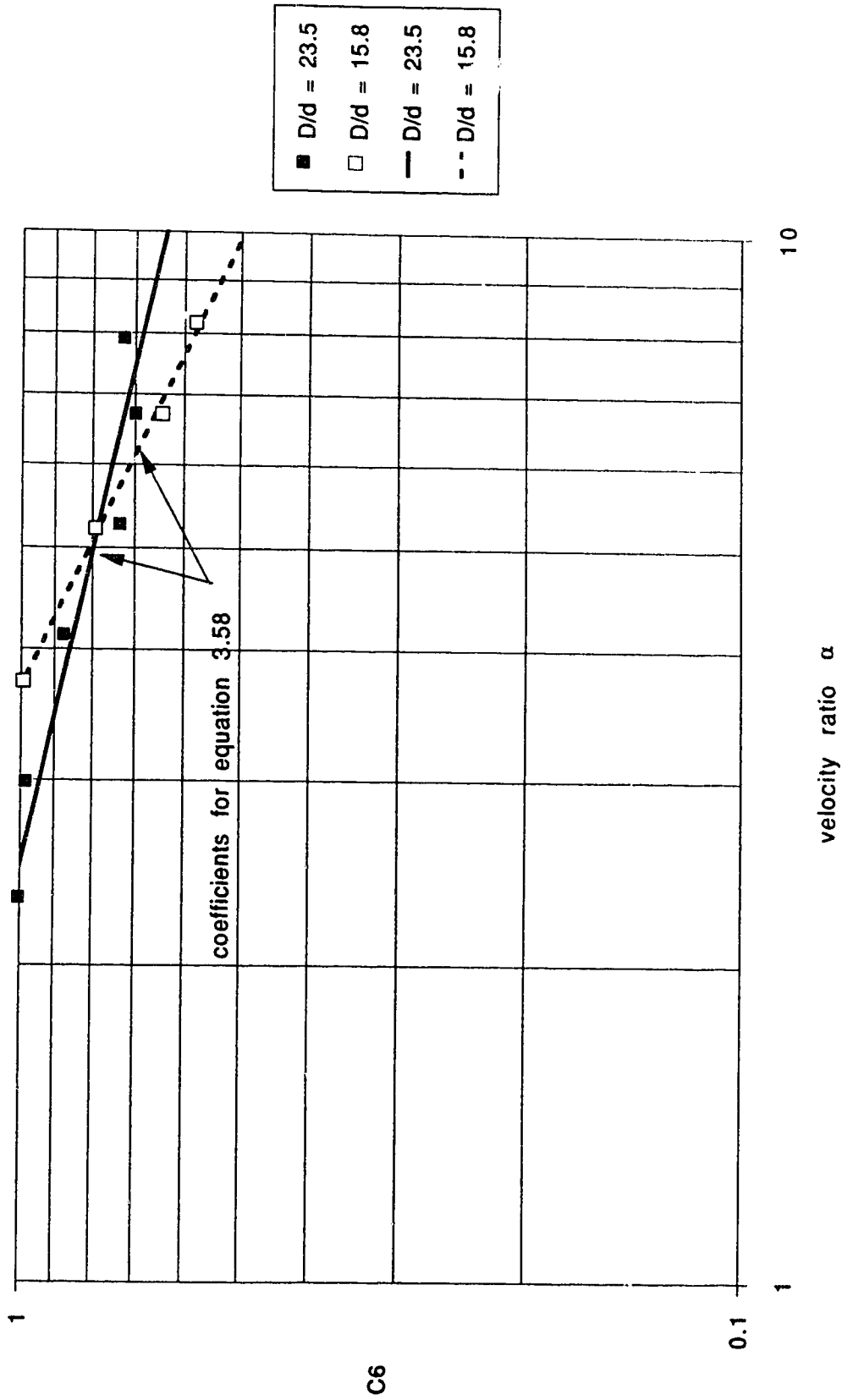


Figure 3.31 Thickness equation exponents for deep water jets

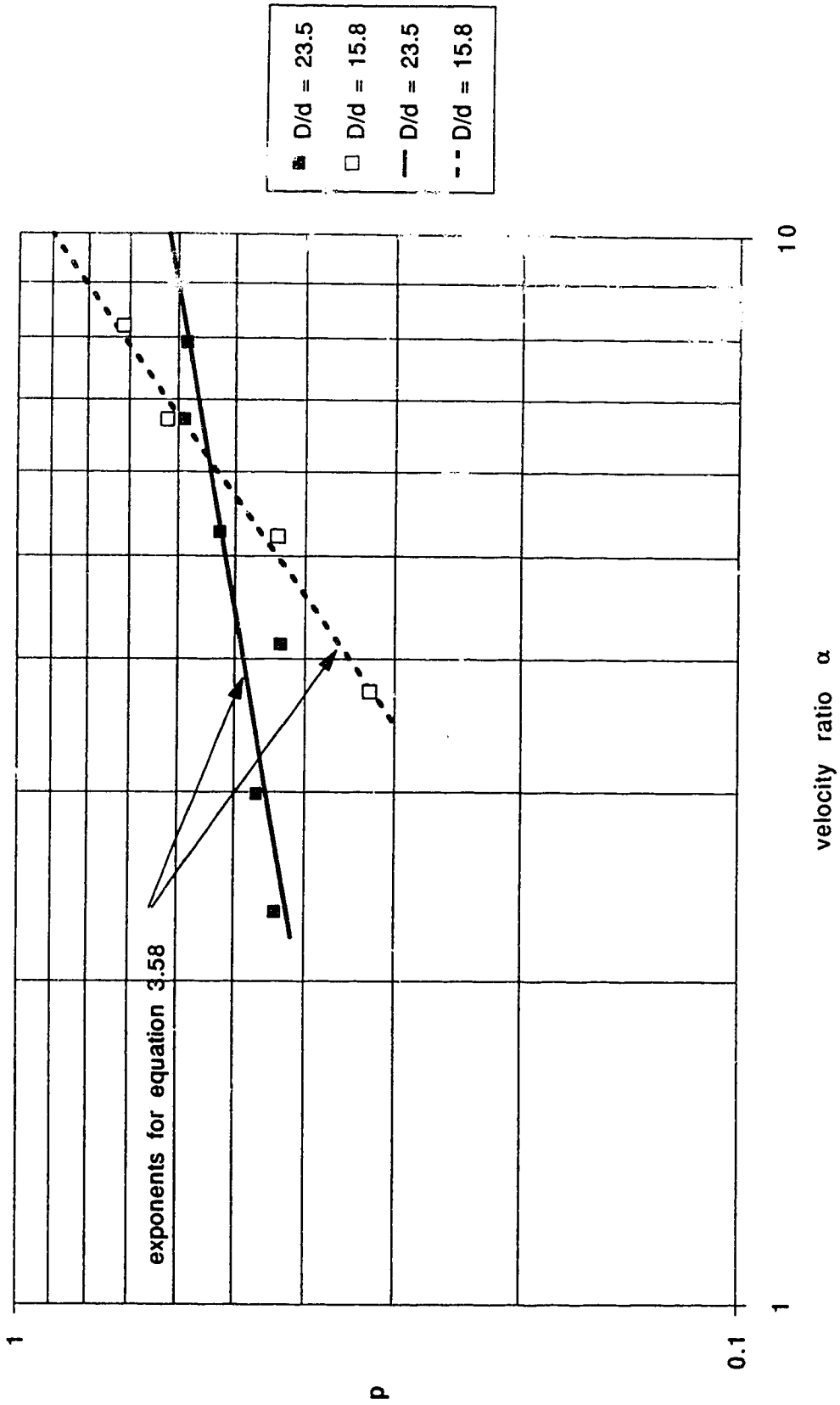
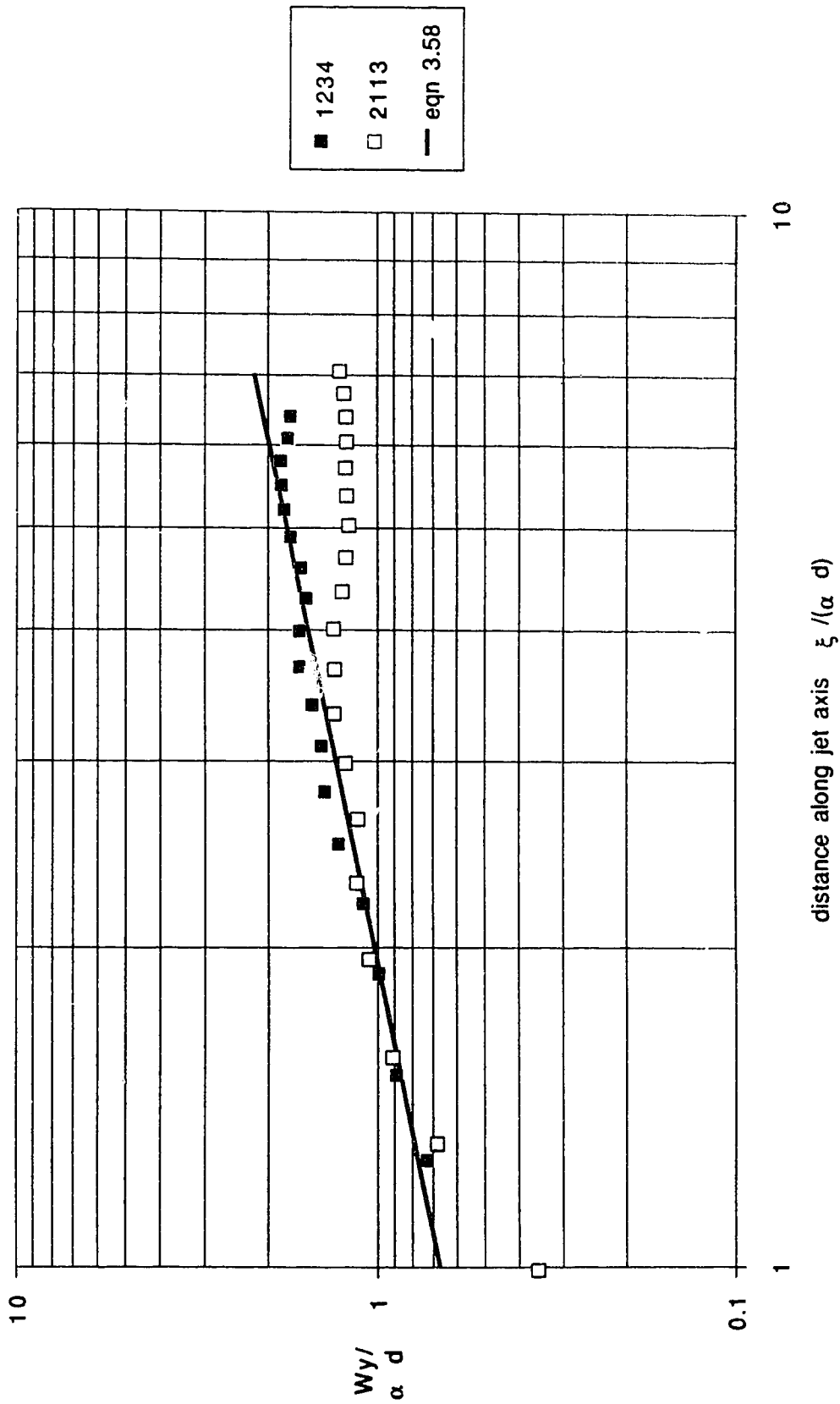


Figure 3.32 Jet thicknesses for selected deep water and shallow water jets



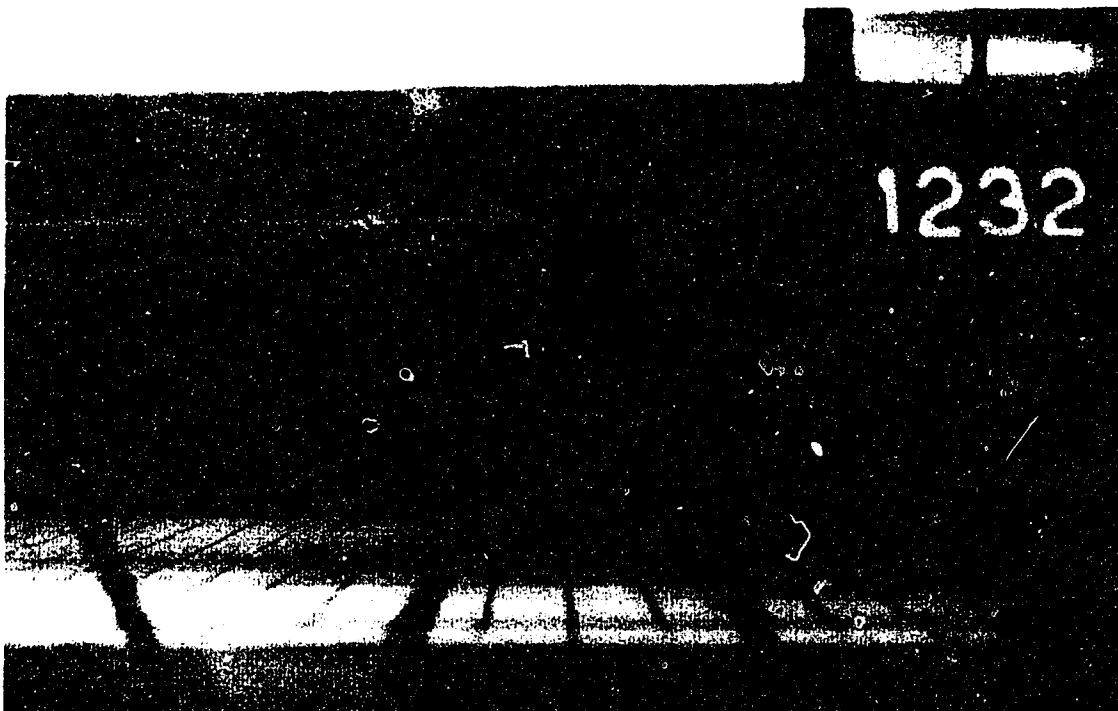


Plate 3.1 Typical side view photograph for Run 1232  
( $\frac{\alpha d}{D} = 0.18$ ); minimal surface effects are present.



Plate 3.2 Typical side view photograph for Run 1136  
( $\frac{\alpha d}{D} = 0.46$ ); surface effects are significant.

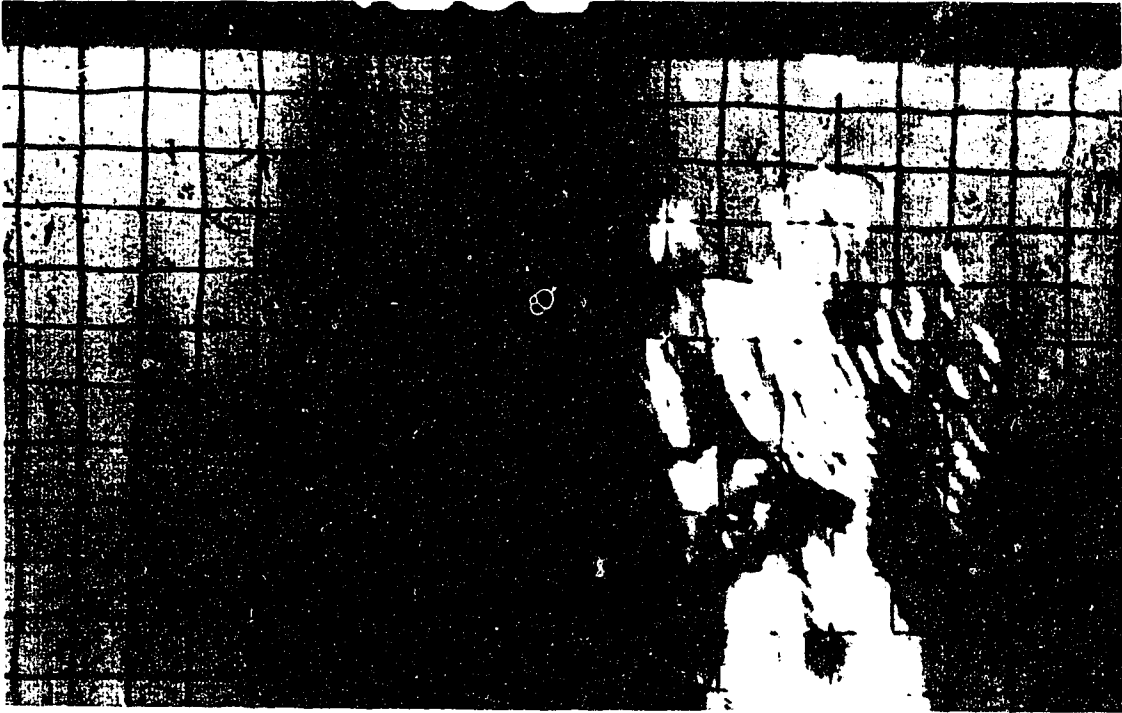


Plate 3.3 Typical plan view photograph for Run 1232  
( $\frac{\alpha d}{D} = 0.18$ ); minimal surface effects are present.

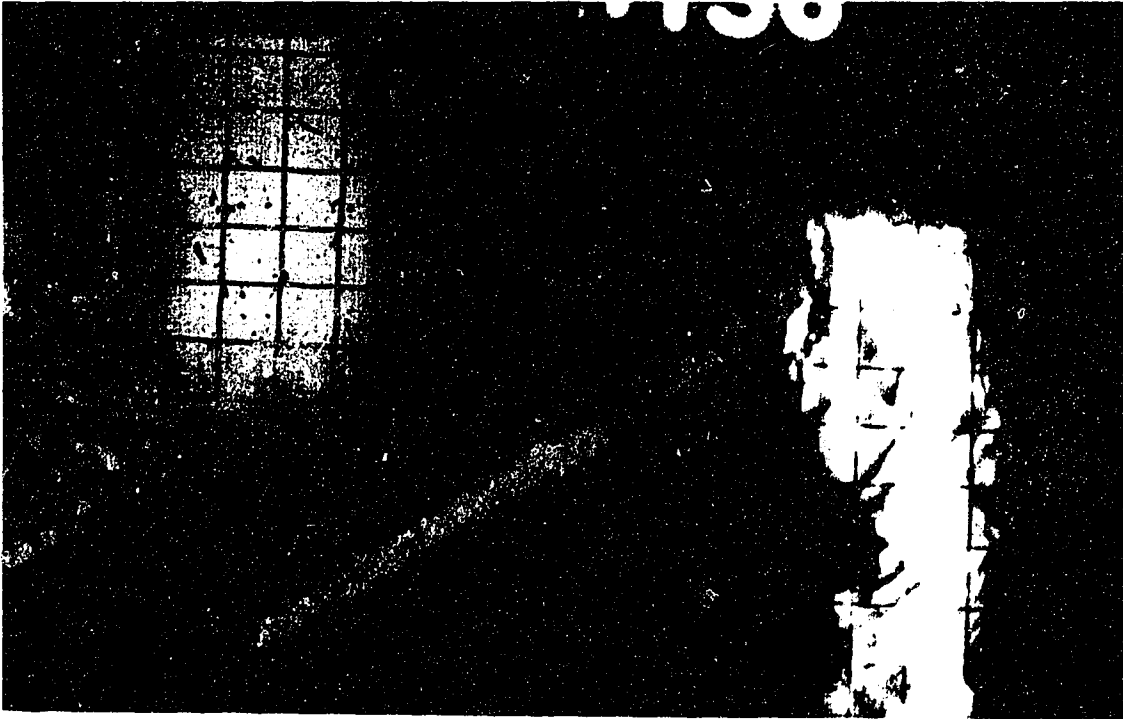


Plate 3.4 Typical plan view photograph for Run 1136  
( $\frac{\alpha d}{D} = 0.46$ ); surface effects are significant.



## CHAPTER 4

## A FIELD STUDY OF JET DILUTION IN A RIVER

4.1 General

Maximizing dilution is one of the primary objectives in the design of an outfall structure. The work in this chapter focusses on the development of dilution equations to quantify mixing in the near field of an effluent discharge.

Discharges in receiving waters are a turbulent flow phenomena that can have a wide range of geometrical configurations. Even in the restricted sense of effluent discharges in rivers, there are a large number of conditions to be considered (Table 4.1). The discharge may be non-buoyant, more dense or less dense than the receiving stream. The discharge may be perpendicular to, parallel with or at an inclined angle with the streamflow direction. It may be discharged vertically from the bottom, laterally from the side or in some other combination of location and direction. In addition to density differences, the receiving stream could appear infinitely deep to the discharge or it may exert wall effects or effects due to its finite depth. The velocity of the receiving stream relative to the discharge velocity is also an important factor; a crossflow enhances the turbulence and, hence, the dilution of the discharge.

The sections in this chapter discuss the literature which deals with the dilution of jet and buoyant jet discharges in quiescent ambients and the dilution of jet

discharges in crossflows. This literature provides the foundation for the axial dilution relationships developed in this investigation. The work also presents the results of a field program which was carried out to provide information on the dilution of jet discharges in a natural river. The analysis of the field and laboratory data results in the development of simple dilution equations which cover a wide range of discharge conditions.

#### **4.2 Jet Discharges in a Quiescent Ambient**

The discharge of a turbulent axially symmetrical jet in an infinite homogeneous quiescent ambient is one of the simpler jet discharge conditions to assess. Yet, in spite of the apparent simplicity, the analysis of this turbulence problem requires a rigorous effort to describe all of the characteristics of the flow. A number of papers have addressed (amongst other flow characteristics) the concentration distribution of a pollutant or tracer in such a discharge (Hinze and van der Hegge Zijnen, 1949; Forstall and Gaylord, 1955; Kristmanson and Danckwerts, 1961; Becker et al, 1967; Patrick, 1967; Birch et al, 1978; and Rajaratnam, 1979). Through the use of laboratory experiments, sometimes in conjunction with mathematical analysis, these researchers established that the dilution of the effluent concentration along the jet centreline could be estimated by fairly simple expressions (most of which are linear).

Hinze and van der Hegge Zijnen (1949) simplified the hydrodynamic equations for momentum, mass continuity and pollutant conservation to determine the following relation for the axial dilution along the jet centreline (Figure 2.1):

$$C_o / C_m = 0.190 \ x / d + 0.15 \quad (4.1)$$

where:  $C_o$  is the concentration at the jet nozzle,

$C_m$  is the maximum concentration in a section,

$x$  is the distance to the section, and

$d$  is the diameter of the jet nozzle.

This, and the subsequently described dilution equations, are not applicable in the potential core. In the potential core region, the centreline concentration remains unchanged from the concentration at the nozzle. Equation (4.1) indicates that the potential core has a length of about  $4.5 d$ ; the axial dilution ( $C_o/C_m$ ) has a value of 1 in this region. The relation in equation (4.1) was developed based on concentration data for a gas tracer in an air jet measured by Hinze and van der Hegge Zijnen (Figure 4.1).

Forstall and Gaylord (1955) examined the diffusion of jet discharges in water using salt (a 1% solution for the discharge) as a tracer. They found that the axial dilution could be expressed by:

$$C_o / C_m = 0.192 \ x / d \quad (4.2)$$

Kristmanson and Danckwerts (1961) used photographic methods to define the boundaries and dilution of an alkali jet discharging into an acidic water ambient (Table 4.2). They found that the axial dilution could be estimated by:

$$C_o / C_m = 0.209 \ x / d \quad (4.3)$$

Becker et al (1967) used a light-scatter technique to measure the mean concentrations and the turbulent concentration fluctuations for an air discharge marked with an oil aerosol. The axial dilution relation established in their work is:

$$C_o / C_m = 0.185 \ x / d - 0.44 \quad (4.4)$$

Experimental work for the dilution of a free jet was reported by Patrick (1967) to result in an axial dilution relation of:

$$C_o / C_m = 0.112 \ (x / d)^{1.18} \quad (4.5)$$

Patrick's is the only work which indicates a non-linear dilution relation for simple jet discharges.

Rajaratnam (1979) derived a dilution equation using the Integral Method. The relation for the axial dilution that he found was:

$$C_o / C_m = 0.187 \ x / d \quad (4.6)$$

The data for simple jet discharges from Hinze and van der Hegge Zijnen (1949), Forstall and Gaylord (1955), Becker et al (1967) and Patrick (1967) have been plotted for comparison (Figure 4.1). All of the data indicate little dilution up to the end of the potential core region. The data also indicate that (within experimental error) a single function could well represent the axial dilution relation in the region beyond the potential core.

Regression analyses of the data beyond the potential core indicate that the axial dilution illustrated by the four

data sets can be represented by the following power law relation:

$$C_o / C_m = 0.210 (x / d)^{0.966} \quad (4.7)$$

A linear relationship can also be fitted to the data:

$$C_o / C_m = 0.194 x / d \quad (4.8)$$

These regressions confirm the linear dilution relationship for jet discharges into quiescent ambients. Equations (4.7) and (4.8) also indicate that the potential core region has a length of about 5.1 d.

#### **4.3 Buoyant Jet Discharges in a Quiescent Ambient**

The dilution of buoyant discharges in quiescent ambients has received considerable interest over the years (Hinze and van der Hegge Zijnen, 1949; Abraham, 1960; Kamotani and Greber, 1972a and 1972b; Birch et al, 1978; and Kotsvinos, 1978). This dilution phenomenon is one of the primary mixing mechanisms for ocean outfalls. Hinze and van der Hegge Zijnen (1949) have presented data for a heated air jet discharge with a 30° C temperature excess (Figure 4.2 and Table 4.3). Abraham (1960) measured the dilution of pure water discharges into brine solutions of various densities. Kamotani and Greber (1972a and 1972b) measured the temperature decrease along the axis of a heated air jet with a temperature excess of 183° C. Birch et al (1978) presented dilution data for a methane jet discharge in air using a Raman spectrometer. These data show that buoyancy will result in increased dilution relative to simple jet

discharges. They also indicate that a non-linear dilution equation is likely.

The experiments conducted by Abraham (1960) confirmed a dilution relation of:

$$C_o / C_m = 0.103 F_o^{-2/3} (x/d + 2)^{5/3} \quad (4.9)$$

where  $F_o$  is the densimetric Froude number of the discharge:

$$F_o = \frac{U_o}{\sqrt{g \frac{\rho - \rho_o}{\rho_o} d}} \quad (4.10)$$

where:  $U_o$  is the velocity of the discharge,

$g$  is the acceleration due to gravity,

$\rho$  is the density of the ambient, and

$\rho_o$  is the density of the discharge.

Kotsovinos (1978) presented a more comprehensive dilution equation for jet/plume discharges:

$$C_o / C_m = 0.205 A \left( \frac{x}{d} \right) \left( 1 + 0.246 \left( \frac{x}{d} \right)^2 F_o^{-2} \right)^{1/3} \quad (4.11)$$

where:  $A = \left( \frac{\alpha_\infty}{\alpha_o} \right)^{1/3}$ ,

$\alpha_\infty$  is the ambient thermal expansion coefficient, and

$\alpha_o$  is discharge thermal expansion coefficient.

For simple jets, where  $A = 1$  and  $F_o = \infty$ , equation (4.11) becomes:

$$C_o / C_m = 0.205 x / d \quad (4.12)$$

With  $x/d$  sufficiently large, the momentum effects are negligible and equation (4.11) can be simplified to represent the dilution of pure plumes:

$$C_o / C_m = 0.128 F_o^{-2/3} (x/d)^{5/3} \quad (4.13)$$

Examination of equation (4.11) indicates that the dilution of a jet/plume discharge initially behaves like a jet. The flow will be primarily jet-like until about  $x/d = F_o/2$ . As the jet/plume progresses further upward, both jet and buoyancy processes affect the mixing. Beyond a distance of about  $x/d = 6 F_o$ , the dilution is primarily due to buoyancy effects.

#### **4.4 Jet Discharges in Crossflow**

Although a number of papers have investigated the location and the velocity distribution of jet discharges in crossflow, few have addressed the concentration distribution of a pollutant or tracer in this type of discharge (Figure 2.2). Patrick (1967), Kamotani and Greber (1972a and 1972b) and Wright (1977) have all conducted experimental work for various forms of jet and jet/plume discharges. Work on relative mass (or volumetric) flux (which is similar to axial dilution) has been conducted by Rajaratnam and Gangadhariah (1980).

Patrick (1967) carried out concentration measurements for non-buoyant jet discharges in a 150 mm by 450 mm wind tunnel (Table 4.4). The jet nozzles were mounted flush with the 150 mm wall and discharged normal to the direction of the

flow. Analysis of the concentration field was conducted using a nitrous oxide tracer. Twelve concentration profiles were measured for three jet nozzle diameters (3.25, 6.48 and 10.0 mm); the velocity ratio ( $\alpha$ ) for the flows ranged from 6.6 to 45.0.

Patrick found that, for any given jet discharge, the axial dilution could be related to the distance along the curvilinear jet axis ( $\xi$  - defined by the maximum concentrations) by a simple power law relation:

$$C_o / C_m = a (\xi / d)^b \quad (4.14)$$

Patrick found that his data could be adequately described if the exponent (b) had a constant value of 1.18 and the coefficient (a) had values given by:

$$a = [\exp (7.8 p - 1.856)]^{1.18} \quad (4.15)$$

In equation (4.15) the parameter p is the inverse of the velocity ratio (i.e.  $p = 1 / \alpha$ ). When  $p = 0$ , the jet is discharging into a quiescent ambient; here, equations (4.14) and (4.15) combine to yield equation (4.5).

Kamotani and Greber (1972a and 1972b) measured the longitudinal and transverse distribution of velocity, temperature and turbulence intensity for heated air discharges in a 710 mm square wind tunnel. In addition to the measurements of the free jet indicated on Figure 4.2, the axial decay of the temperature with distance along the jet axis for two jet discharges was presented. These jets had velocity ratio values of 3.91 and 7.72. As there was a temperature difference of 178° C at the jet nozzle, some



buoyancy effects were likely present in these discharges. From the information presented, the densimetric Froude numbers for these discharges were estimated to be in the range of 120 to 360 (Table 4.4).

Kamotani and Greber observed that the axial dilution is faster for jets in a crossflow than for the equivalent free jet. They found that the dilution near the nozzle was more rapid for the weaker jets (i.e. low  $\alpha$  values). However, further along the jet axis, there appeared to be little difference between the dilutions achieved by the two jets, although the dilutions achieved with crossflow discharges were both superior to that for the free jet.

Wright (1977a and 1977b) conducted experiments for buoyant and non-buoyant discharges in stratified and non-stratified crossflows. Wright's experimental arrangement involved towing the discharge orifice along the top of a stationary tank of water (with a width of 610 mm and a depth of 550 mm). Only a small portion of Wright's work was devoted to non-buoyant jet discharges in unstratified crossflows. Three series of runs were made with velocity ratios of 20.5, 30.0 and 36.2.

For the momentum dominated near field, Wright indicated an axial dilution relation of:

$$\frac{S_0 Q_0}{U l_m^2} = C_3 \frac{Y_c}{l_m} \quad (4.16)$$

where:  $S_o$  is the dilution ratio ( $C_o/C_m$ ),  
 $Q_o$  is the discharge flow rate,  
 $U$  is the velocity of the crossflow,  
 $l_m$  is the momentum length scale for the jet,  
 $y_c$  is the vertical distance above the bed, and  
 $C_3$  is a coefficient.

Wright (1977b) indicated that the coefficient ( $C_3$ ) had a constant value of about 0.35. Thus, the dilution of a jet discharge in the MDNF of a crossflow can be expressed as a function of the vertical coordinate by:

$$C_o / C_m = 0.395 \frac{y_c}{d} \quad (4.17)$$

Wright likely chose to relate the dilution to the vertical coordinate in his work as his investigation was developed for the study of ocean outfalls (where the primary direction of flow is in the vertical direction). To be more useful for discharges in rivers, this dilution relation should be presented as a function of the downstream direction. In order to do this, the equation for the location of the concentration centreline must be introduced:

$$\frac{y_c}{l_m} = C_1 \left( \frac{x}{l_m} \right)^{1/2} \quad (4.18)$$

Noting that Wright's (1977a) concentration data (shown on his Figure 5.16) supports a constant value of 2.35 for  $C_1$ , equation (4.18) can be rearranged to:

$$\frac{Y_c}{d} = 2.21 \alpha^{1/2} \left(\frac{x}{d}\right)^{1/2} \quad (4.19)$$

Combining equations (4.17) and (4.19) the dilution in the MDNF, based on Wright's work, would be:

$$C_o / C_m = 0.873 \left(\frac{\alpha x}{d}\right)^{1/2} \quad (4.20)$$

Beyond the momentum dominated near field is what Wright termed the momentum dominated far field. Here, Wright indicated that the axial dilution relation would have the form of:

$$\frac{S_o Q_o}{U l_m^2} = C_4 \left(\frac{Y_c}{l_m}\right)^2 \quad (4.21)$$

Wright (1977b) indicated that the coefficient ( $C_4$ ) had a constant value of 0.14. Therefore, the dilution of a jet discharge in the MDFF of a crossflow can be expressed as:

$$C_o / C_m = \frac{0.178}{\alpha} \left(\frac{Y_c}{d}\right)^2 \quad (4.22)$$

To present this dilution relation as a function of the downstream direction, the equation for the concentration centreline in the MDFF must be introduced:

$$\frac{Y_c}{l_m} = C_2 \left(\frac{x}{l_m}\right)^{1/3} \quad (4.23)$$

Wright's concentration data (shown on his Figure 5.17), coupled with similar data from Fan (1967), support the following relation for  $C_2$ :

$$C_2 = 1.21 \alpha^{1/6} \quad (4.24)$$

Incorporating equations (4.23) and (4.24) into equation (4.22) the dilution in the MDFP, based on Wright's work, would be:

$$C_n / C_m = 0.223 \left( \frac{\alpha x}{d} \right)^{2/3} \quad (4.25)$$

An interesting result of examining equations (4.20) and (4.25) is that jet dilution appears to be a function of  $\alpha x/d$ . The dilution appears to be governed by the square root function until  $\alpha x/d = 3600$ . This distance parameter has never been suggested before in the literature reviewed. Examination of the dilution data of Wright and others (where presented as a function of  $x/d$ ) indicate some validity for this relation (Figure 4.3).

Rajaratnam and Gangadhariah (1980) quantified the relative mass flux for discharges in a crossflow using water as the medium. They found that the relative mass flux of a jet discharge with a velocity ratio of  $\alpha = 23.4$  was represented by the equation:

$$m / m_0 = 0.42 \xi / d \quad (4.26)$$

where  $m$  is the mass flux at a distance  $\xi$  and  $m_0$  is the mass flux at the jet nozzle. In comparison, they indicated that the relative mass flux for a jet discharge into a quiescent ambient can be expressed by the relation:

$$m / m_0 = 0.32 x / d \quad (4.27)$$

Equation (4.27) has been derived by Albertson et al (1950) and has been verified experimentally by Ricou and Spalding (1961). From equations (4.26) and (4.27) it can be inferred

(assuming the equivalency of  $\xi$  and  $x$ ) that a jet discharge in a crossflow mixes more efficiently than a jet discharge into a quiescent ambient.

Rajaratnam and Gangadhariah also examined the relative mass flux of other jets with lower velocity ratios (2.73, 4.52 and 7.05). They found the relative mass flux to be a non-linear function:

$$m / m_0 = 0.54 (\xi / d)^{1.22} \quad (4.28)$$

Equations (4.26) and (4.28) indicate that the axial dilution of a jet in a crossflow is even more efficient for lower velocity ratios. This is similar to the findings of Kamotani and Greber (1972a and 1972b).

#### **4.5 Experimental Arrangement**

Field tests were carried out to determine the dilutions which could be achieved in a natural river. The main objective of the program was to obtain more data on the dilution of jet discharges in crossflows. Other objectives were to determine how well laboratory work could be scaled up to prototype conditions and to examine the effects of a finite depth of flow on jet mixing.

##### **4.5.1 River Conditions**

The experiments were conducted in the Lesser Slave River in northern Alberta (Figure 4.4). The Lesser Slave River is a relatively deep river which drains Lesser Slave Lake to the Athabasca River about 70 km away. Although the Lesser Slave

River meanders in an irregular fashion, it has a number of features which made it attractive for the field program:

- a) The flow rate is relatively steady since a major portion of the discharge is outflow from Lesser Slave Lake (the river's mean annual flow rate is  $53 \text{ m}^3/\text{s}$ ) over a weir. This meant that the crossflow would be reasonably steady during the period that concentrations within a given jet were being sampled.
- b) There are almost no bars or vegetative growth in the river. These features meant that the occurrence of additional turbulence due to bed forms would be minimized.
- c) The channel cross-section is well defined, deep and narrow. At the mean annual flow rate, the river has a surface width of 48 m, a hydraulic depth of 1.90 m and an average velocity of 0.58 m/s. This meant that a significant crossflow depth and velocity could be achieved.

A preliminary field program was conducted on 28 April 1988 to select the reach for the jet dilution field measurements. The site selected was near the left bank of the Lesser Slave River about 100 m downstream of the river's confluence with the Sauteaux River. The Sauteaux River is a tributary of the Lesser Slave River. The confluence is located about 21 km downstream from the outlet of Lesser Slave Lake. During the field trip, the Lesser Slave River's cross-section was surveyed at four locations about 20 m apart with a Raytheon depth sounder to confirm the uniformity of this relatively straight reach. Velocity measurements were

made using a Gurley velocity meter to identify the strength of the crossflow.

#### 4.5.2 Equipment

A considerable amount of field equipment had to be designed, fabricated and assembled prior to the second field trip on 13 to 16 June 1988 (Figure 4.5; plates 4.1 and 4.2). First, two 1200 mm by 2400 mm platforms were fabricated. Each platform had a steel bracket on each of the corners to hold a 50 mm diameter steel post which had a length of about 4 m. The posts had holes drilled 100 mm apart to allow them to be pinned to the platform and to allow the height to be adjusted to match any unevenness of the river bed. The platforms were floated into position, about 1500 mm apart, with the aid of a boat and the posts were then driven about 300 mm into the gravel river bed to provide a stable base for the jet discharge equipment and the scientific equipment.

The jet discharge equipment (Plate 4.1) comprised a 1/2 horsepower submersible sump pump (with an 11.6 amp, 115 volt electric motor) which was hung from the side of the platform and into the river (this pump had a flow capacity of up to 340 L/min). A 75 mm diameter Haliburton turbine flow meter and a 50 mm diameter gate valve were used to measure and control the pump's flow rate. Copper tubing and polyethylene piping (50 mm in diameter) connected the pump discharge to the jet nozzle. All bottom jets discharged with their outlets 150 mm above the river bed. Two outlet sizes were

used: the 50.4 mm diameter outlet was the same size as the copper discharge tubing, while the 34.5 mm diameter nozzle was a 50 mm by 32 mm copper reducer.

Rhodamine WT was the tracer dye used in this study. This dye was manufactured by duPont of Canada Ltd. and was supplied as a 20% solution. Rhodamine WT has a specific gravity of 1.19. The dye was mixed in 100 L batches in a plastic garbage pail to achieve jet nozzle concentrations in the order of 70 ppb to 250 ppb, depending on the jet dilution expected (density difference would not be a factor at these nozzle concentrations).

The dye was introduced into the jet discharge line by an ISCO peristaltic pump which could generate a flow rate (regardless of the discharge head) of 2.9 L/min. The length of the discharge pipeline (about 3 m) was sufficient to allow complete mixing of the dye before the nozzle outlet.

The sampling line was comprised of copper and surgical rubber tubing (Plate 4.2). A 2 m length of 13 mm diameter copper tubing, with a 13 mm by 9 mm reducer soldered to one end, was bent so that concentration samples would be taken from a relatively small portion of the flow about 100 mm ahead of the vertical position of the sampler. The sample was conveyed a further 2.5 m through surgical rubber tubing, drawn by another ISCO peristaltic pump. The sample was then discharged through a Turner Model 10 Field Fluorometer equipped with a continuous flow cuvette system. After passing through the fluorometer, the sample flow was



discharged to the surface of the river well away from the jet.

All power to the system was supplied by a 2000 Watt (16.7 amps at 120 volts) gasoline powered electrical generator. The power to the scientific equipment was passed through a voltage equalizer to minimize the voltage fluctuations in this equipment.

#### **4.5.3 Sampling Procedures**

Sample readings were taken by selecting the appropriate range on the fluorometer and recording the instrument's reading in a field book. The readings were also recorded on a strip chart recorder for later evaluation in the office.

In operation, it would take about 10 s to 15 s for the flow from a new sampling point to pass through the tubing and the fluorometer. A further 4 s was allowed after selecting the appropriate fluorometer scale to allow the instrument to register readings in the selected range. The strip chart recorder was then run for about 15 s while the fluorometer's scales were read and recorded in the field book. The 15 s reading was found to be of sufficient duration to allow a reasonable time-averaged concentration to be made.

The concentration fluctuation of the measurements varied, being small in the middle of the jet (where the concentrations were high) and great at the periphery (where concentrations were low). A sample averager, comprised of a 300 mm length of 50 mm diameter plastic piping, was used as a

means of time averaging the sample for Jet 1. It was found that, although the fluctuations were reduced somewhat, the time between samples had to be large in order to ensure that the sample averager was sufficiently flushed between sampling points. As it was easy enough to time average the strip chart traces when they were made without this device, the sample averager was not used for the other three jets.

Rhodamine WT dye is visually detectable in clean (tap) water at concentrations of 10 ppb. The Turner fluorometer can measure concentrations of Rhodamine WT as low as 0.01 ppb. During the 28 April 1988 field trip, a 20 L sample of Lesser Slave River water was taken to calibrate the fluorometer and to measure the background fluorescence back at the laboratory. The laboratory work indicated that this river water had a background fluorescence of 0.044 ppb (Figure 4.6).

Background fluorescence had a greater impact on the concentration readings during the June field trip. It was found that the river's background fluorescence levels of 0.2 ppb to 0.8 ppb were much higher than those measured in April. This was probably due to the greater microbiological activity - the water temperature in April was close to freezing while the water temperature in June was about 15° C. The background fluorescence varied throughout the day but showed no consistent trend either temporally (i.e. time of day) or spatially (i.e. near the bed versus near the surface).

Concentration distributions were measured for three jets discharging from the bottom of the river and for one jet discharging from the side. For the bottom jet discharges, concentrations were measured at three sections. For each section, a vertical concentration profile was first measured at the jet centreline and then a horizontal concentration transect was measured at the depth where the vertical concentration profile was at a maximum. This was followed by two further vertical concentration profiles, measured on either side of the first vertical, to more completely describe the concentration field at the cross-section. In addition to the concentration measurements throughout the jet, readings were taken at the beginning and the end of most transects with the dye supply shut off in order to estimate the level background fluorescence (all readings presented in this work have had background fluorescence deducted).

Concentrations were sampled at four sections for the side jet discharge. Only one profile and one transect were measured for each section. First, the horizontal transect was sampled at the same elevation as the jet nozzle and, more or less, perpendicular to the jet centreline. Next, a vertical concentration profile was sampled at the location of the maximum concentration in the horizontal transect.

#### **4.5.4 Experimental Error and Variance**

There were a number of sources of error to be considered in the field program (Table 4.5). No effort to quantify

these potential errors was made due to time constraints for the field work. The errors were larger than those typical of laboratory investigations as the equipment had to be capable of being transported and installed in a harsher environment. Based on the field program experience, it can be concluded that future field work could be conducted with reduced measurement error for length (this work only used tape measures for the lateral and downstream distances) and  $< 5\%$  for flow and concentration measurements.

#### **4.6 Results and Analysis**

##### **4.6.1 Conditions Investigated**

Concentration measurements were sampled at about 300 locations for the four jet discharge conditions investigated. These data (corrected to eliminate background fluorescence) are presented in Appendix C. The jets had nozzle diameters of 34.5 mm and 50.4 mm and had velocity ratios which ranged from 3.68 to 6.99 (Table 4.6). Concentration measurements were made as far as  $68 \xi/d$  downstream of the nozzle. The depth of flow for the bottom jet discharges was in the range of 762 mm to 889 mm. The velocity of flow (measured using the Gurley meter at 0.2, 0.6 and 0.8 times the depth of flow from the water surface) had values ranging from 0.79 m/s to 0.88 m/s. The work presented earlier in Chapter 3 indicates that jets having values of  $\alpha \cdot d/D > 0.34$  would be affected by a finite

depth of flow. Based on this, only Jet 2, with  $\alpha \cdot d/D = 0.32$ , would possibly be affected by the water surface.

#### **4.6... Maximum Concentration Along Jet Axis**

Examination of the field test data indicated that a power law relation could be fit through the data for any given jet discharge condition (Figure 4.7). This could also be done using the data from the works of Patrick (1967), Kamotani and Greber (1972a and 1972b) and Wright (1977). A power law relation in the form of equation (4.14) was fitted to the data for each of the simple jets and crossflow jets where concentration measurements had been taken. Values for the coefficient (a) and the exponent (b) were determined for 28 discharge conditions. The results of the regression analyses are contained in Appendix B. These regressions (having  $0.89 < r^2 < 1.0$ ) all had a high degree of correlation.

It was found that neither the coefficient nor the exponent had constant values (figures 4.8 and 4.9). Further analysis indicated that curves could be made to fit the dilution equation parameters as a function of  $p$  (the inverse of the velocity ratio). In addition to the previously mentioned sources for discharges in crossflows, these curves fit the laboratory data from Hinze and van der Hegge Zijnen (1949), Forstall and Gaylord (1955), Becker et al (1967) and Patrick (1967), for discharges in quiescent ambients, at  $p = 0$ . They also fit the data obtained from the Lesser Slave

River field program very well. Both the laboratory data and the field data appear to conform to the same trend lines, although the overlap is limited to the region around  $p = 0.15$  ( $\alpha = 6$ ). For values of  $p$  greater than 0.15, the relationships rely primarily on the field trip data. Although the jets of Kamotani and Greber are affected to some extent by density, they have high densimetric Froude numbers (indicating that they behave more like a jet than a plume). These jets also tend to corroborate the trends at high  $p$  values. More field work would be desirable to confirm the relations at the higher  $p$  values and to extend the range of overlap at the lower  $p$  values.

The effect of the finite depth of flow becomes evident upon examination of the dilution equation parameters for the side jet discharge (Jet 4 with  $a = 0.408$  and  $b = 1.086$  for  $p = 0.148$ ) and for the bottom discharge Jet 2 (with  $a = 2.567$  and  $b = 0.631$  for  $p = 0.143$ ). If there were no surface effects, then the dilution equation parameters would be expected to be the same. However, the parameters for the side discharge jet (which was unaffected by the finite depth of flow) fit the trend curves well while those for the bottom discharge jet did not. The bottom discharge jet exhibited rapid initial mixing which became inhibited as the jet flow came into contact with the water surface (Figure 4.7). Hence, the higher value for the coefficient ( $a$ ) and the lower value for the exponent ( $b$ ) for Jet 2 on figures 4.8 and 4.9.

The dilution data indicate that jets in crossflow are more efficient at mixing than simple jet discharges. This was determined by examining the relative dilution of crossflow jets in comparison with that for a simple jet (i.e.  $C_o / C_m$  for the crossflow jet divided by  $C_o / C_m$  for a simple jet) to see the relation between the velocity ratio and the relative dilution (Figure 4.10).

A strong jet discharging into a weak crossflow (represented on Figure 4.10 by  $p = 0.1$ ) mixes much like a simple jet near the nozzle. Then, as the flow progresses along the axis, the mixing improves due to the effects of the crossflow. A weak jet discharging into a strong crossflow (represented on Figure 4.10 by  $p = 0.3$ ) mixes rapidly near the nozzle, as the crossflow effects are felt immediately, and then mixes more slowly. The maximum degree of mixing appears to occur at  $p = 0.18$  when the crossflow jet consistently has 3.5 times the dilution of a simple jet. Based on this, it would be best to initially consider a jet discharge of  $p = 0.18$  ( $\alpha = 5.6$ ) in the design of outfall diffusers for discharging to a river.

The majority of the literature examined has evaluated dilution as a function of either the vertical distance above the discharge nozzle or the distance along the jet's curvilinear axis. The distance parameter  $\alpha x/d$  has been presented as another possible distance parameter to correlate jet dilution. Dilution relative to this parameter is examined in detail in Section 5.

#### 4.7 Conclusions

a) A power law relation, in the form of  $C_o/C_m = a (\xi/d)^b$ , could be fitted to the concentration data for both the laboratory studies (by others) and the field work (this investigation) with a high degree of correlation. The coefficient (a) and the exponent (b) were found to be functions of the inverse of the velocity ratio ( $p = 1/\alpha$ ) as indicated on figures 4.8 and 4.9.

b) The dilution equation parameters determined using data from both previous laboratory investigations and the Lesser Slave River field program conform to the same trend lines. The extent of overlap for the laboratory and the field program data values is limited to the region in the vicinity of  $p = 0.15$ . The relationships depend primarily on the Lesser Slave River field program data for values of  $p > 0.15$ . More field work assessing jets in crossflows of these higher strengths is necessary to better confirm the relationships for a and b. More field work should be conducted for weaker crossflows (i.e. at lower values of p) in order to extend the range of overlap between field and laboratory work.

c) A finite depth of flow can significantly affect the dilution that a jet can achieve. When the depth is a factor, the coefficient (a) will be higher and the exponent (b) will



be lower. This is because the jet mixes more rapidly initially (hence, the high value for the coefficient) and then mixes more slowly as the jet flow contacts the water surface (hence, the low value for the exponent). This is exemplified by the dilution equation parameters for Jet 2 indicated on figures 4.8 and 4.9.

d) The axial dilution of a jet discharge in a crossflow is superior to that of a jet discharge in a quiescent ambient. This observation was made by Kamotani and Greber (1972a and 1972b), was confirmed by the laboratory analysis of mass flux by Rajaratnam and Gangadhariah (1980), and was confirmed again by the concentration measurements of the Lesser Slave River field program. The axial dilution equation parameters identified in this work indicate that the mixing is the most efficient (at 3.5 times that for a free jet) when the velocity ratio is 5.6 (Figure 4.10).

Table 4.1 Characteristics of jet discharges in crossflows

Characteristic	Possible Conditions
1. outlet shape	plane circular
2. outlet streamlines	nozzle orifice
3. outlet location	bed side other (e.g. surface)
4. outlet orientation	vertical angle lateral angle
5. turbulence of discharge	low (laminar: $R_j < 4000$ ) high (turbulent: $R_j > 4000$ )
6. buoyancy of discharge	non-buoyant (jet) positive buoyancy (dense jet) weak negative buoyancy (jet/plume) strong negative buoyancy (plume)
7. ambient flow direction	quiescent ambient co-flowing crossflowing angled
8. ambient flow depth	infinite (deep water) finite (shallow water)
9. relative turbulence (ambient versus discharge)	low high

Table 4.2 Parameters from selected studies of jet discharges in quiescent ambients

Work	Medium	Tracer	Nozzle Type	d mm	U <sub>o</sub> m/s	R <sub>j</sub>	Distance x/d
Hinze and van der Hegge Zijnen (1949)	air	town gas	orifice	25	40	67,000	40
Forstall and Gaylord (1955)	water	salt	nozzle	6.35/ 9.53	n/a	n/a	36
Kristmanson and Dankwerts (1961)	water	acid/base	orifice	3.2	1.9	12,000	110
Becker et al (1967)	air	oil aerosol	nozzle	6.35	130	54,000	42
Patrick (1967)	air	nitrous oxide	nozzle	8.03	n/a	n/a	74

Note: n/a indicates that the information was not available from the literature

Table 4.3 Parameters from selected studies of buoyant jet discharges in quiescent ambients

Work	Discharge	Nozzle Type	d mm	U <sub>o</sub> m/s	F <sub>o</sub>	R <sub>j</sub>	Distance x/d
Hinze and van der Hegge Zijnen (1949)	hot air in air	orifice	25	40	252	55,000	40
Abraham (1960)	water in brine	pipe	15-25	0.1-0.7	1-6	1770-8650	27
Kamotani and Greber (1972a)	hot air in air	nozzle	6.35	6-9	30-45	1100-1700	70
Birch et al (1978)	methane in air	tube	6.35	3.2	65	16,000	75

Table 4.4 Parameters from selected studies of jet discharges in crossflows

Work	Medium	Nozzle Type	d mm	U m/s	$\alpha$	D/d	F <sub>0</sub>	Distance $\xi/d$
Patrick (1967)	air	nozzle	3.25-10	≈ 8	6.5-45	45-138	∞	59
Kamotani and Greber (1972a)	air	nozzle	6.35	6-9	3.9 & 7.7	112	120-360	70
Wright (1977)	water	orifice	8	0.019-0.039	21-36	69	∞	48
Hodgson (this work)	water	nozzle	34.5-50.4	0.79-0.88	3.7-7.0	18-22	∞	68

Table 4.5 Measurement precision and experimental error  
field dilution study

Measurement	Precision	Experimental Values	Estimated Probable Error ( $\pm$ )
depth of flow (mm)	1	762 to 914	< 3 mm
jet nozzle diameter (mm)	0.4	34.5 and 50.4	< 0.5 mm
vertical position (mm)	1	-11 to 904	< 3 mm
transverse position (mm)	3	-48 to 1324	< 6 mm
downstream position (mm)	3	62 to 2064	< 6 mm
jet discharge (L/min)	0.7	235 to 390	< 5%
crossflow velocity (m/s)	0.001	0.790 to 0.884	< 5%
concentration (ppb)	0.01	0.1 to 33.4	< 5%

Table 4.6 Jet discharge conditions in the  
Lesser Slave River field program

Jet	1	2	3	4
Source	bottom	bottom	bottom	side
d (mm)	50.4	34.5	34.5	34.5
D (mm)	889	762	762	914
D/d	17.6	22.1	22.1	n/a
$U_o$ (m/s)	3.255	5.730	4.188	5.324
U (m/s)	0.884	0.820	0.820	0.790
$\alpha$	3.68	6.99	5.11	6.74
$R_j$	144,000	173,000	127,000	161,000
$R_d$	39,000	25,000	25,000	24,000
$\alpha \cdot d/D$	0.21	0.32	0.23	n/a
$\alpha^2 d/D$	0.77	2.21	1.18	n/a

Figure 4.1 Dilution ratios for jet discharges into quiescent ambients

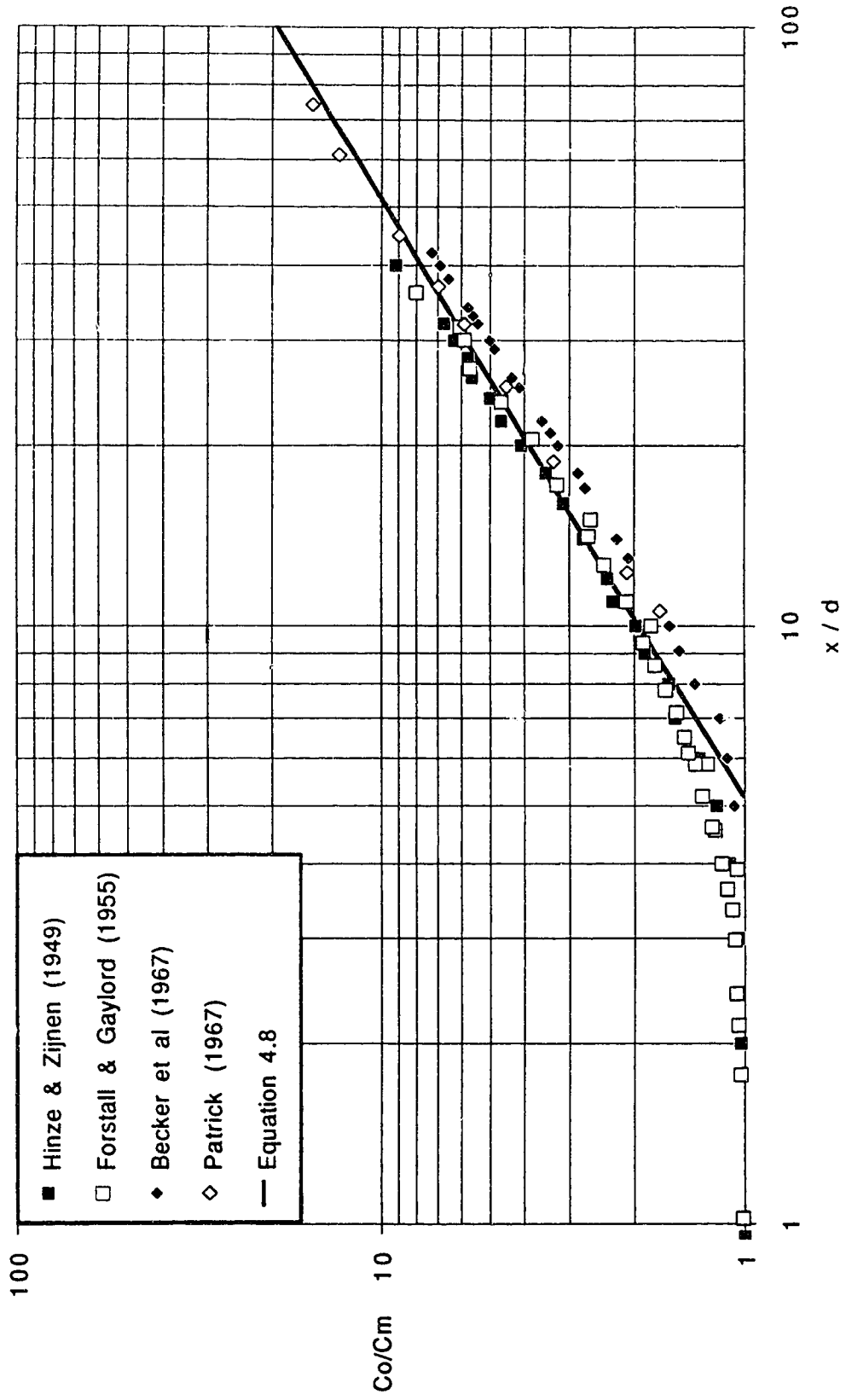




Figure 4.2 Dilution ratios for buoyant jet discharges into quiescent ambients

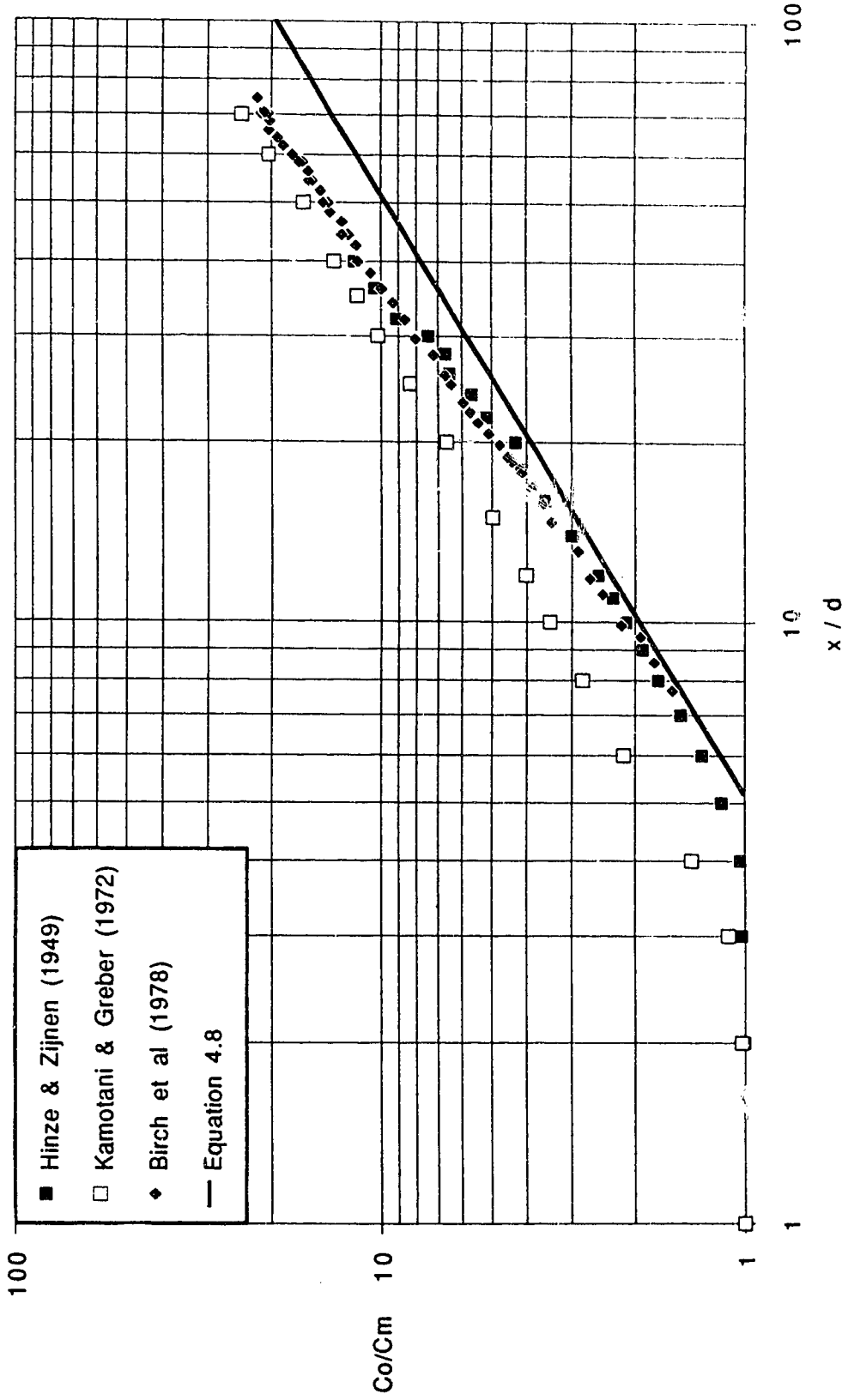
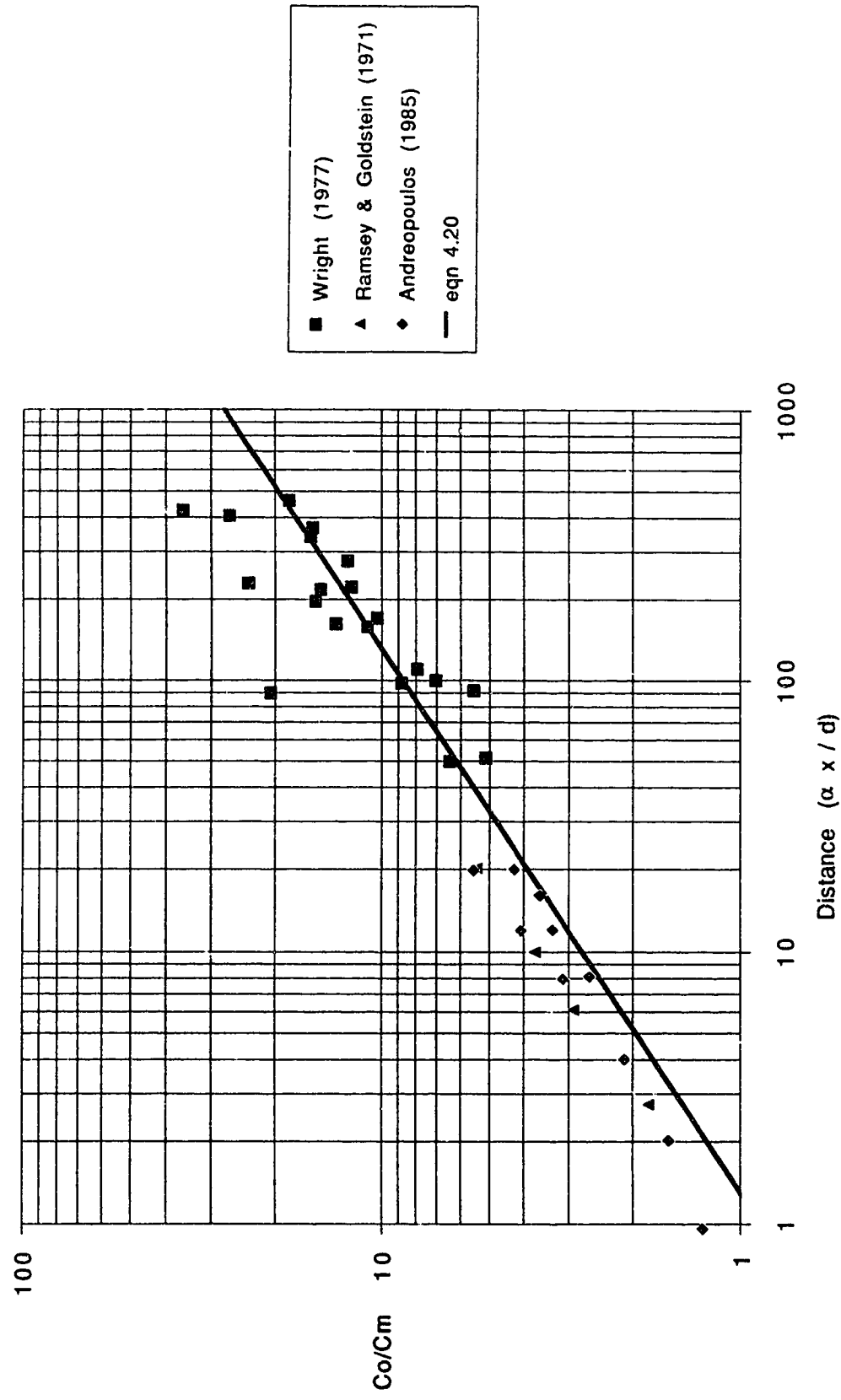


Figure 4.3 Published data for jet dilution versus downstream direction



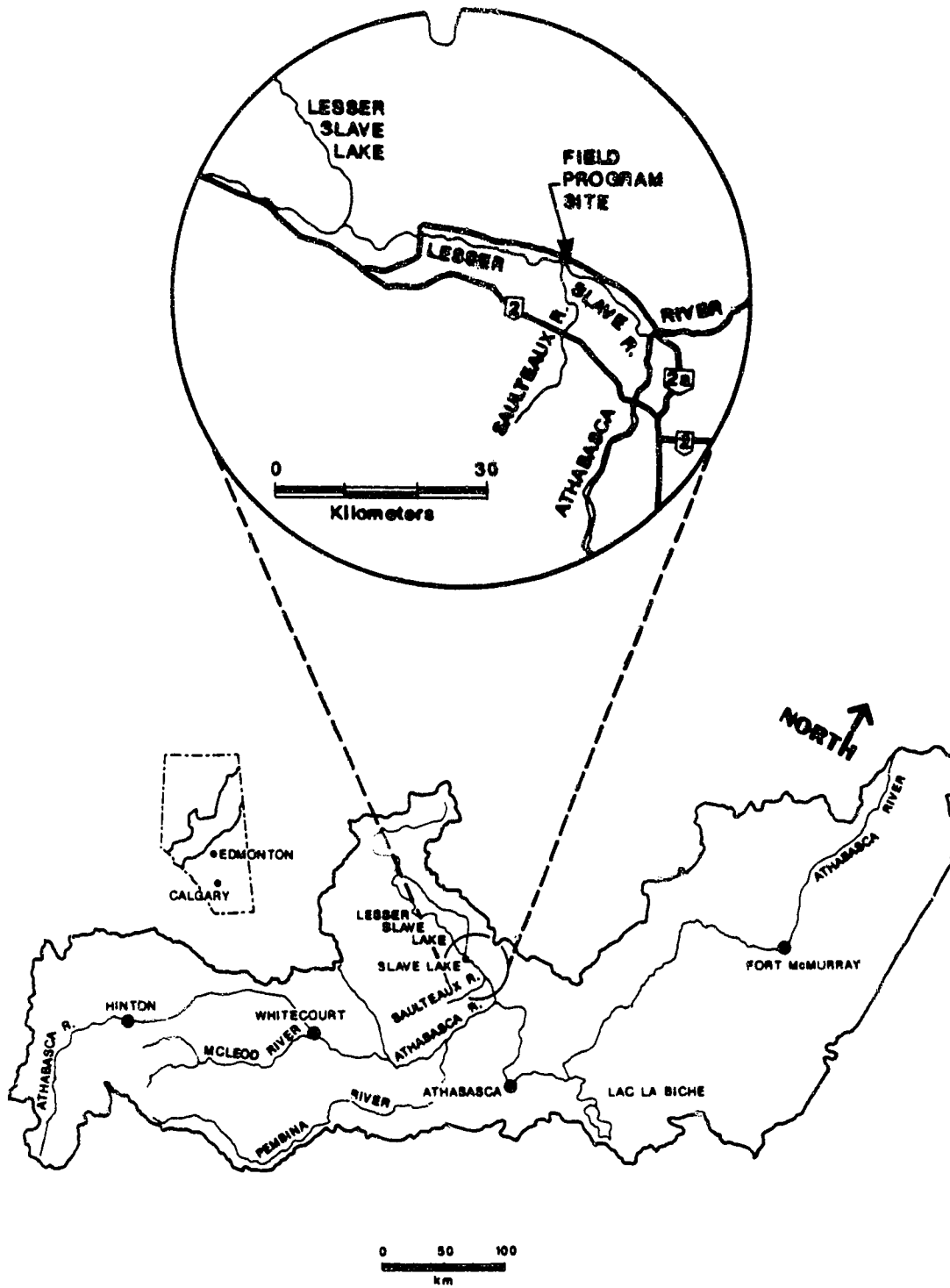


Figure 4.4 Lesser Slave River Location Plan

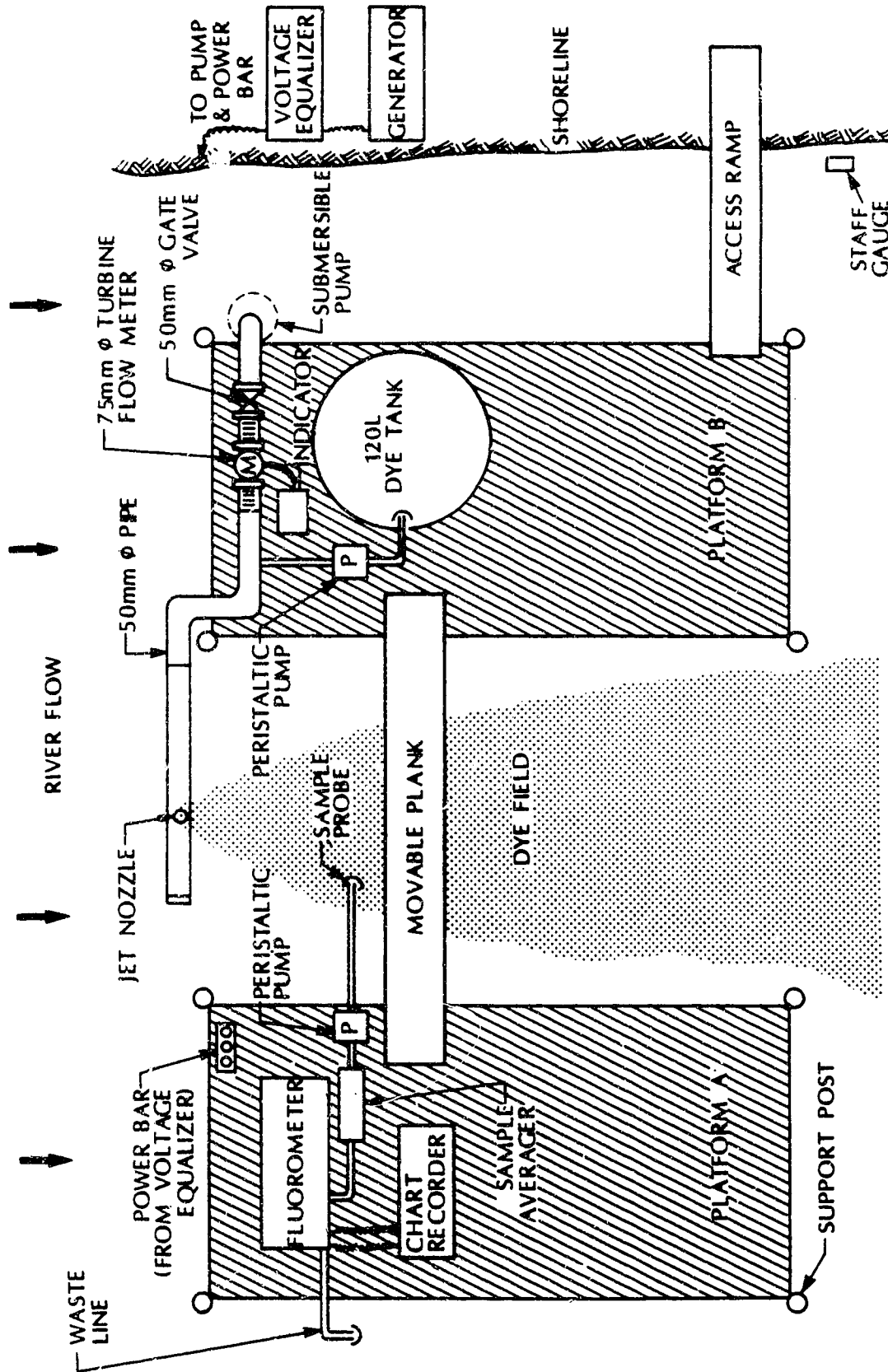


Figure 4.5 Field Program Equipment Schematic

Figure 4.6 Fluorometer calibration - field study

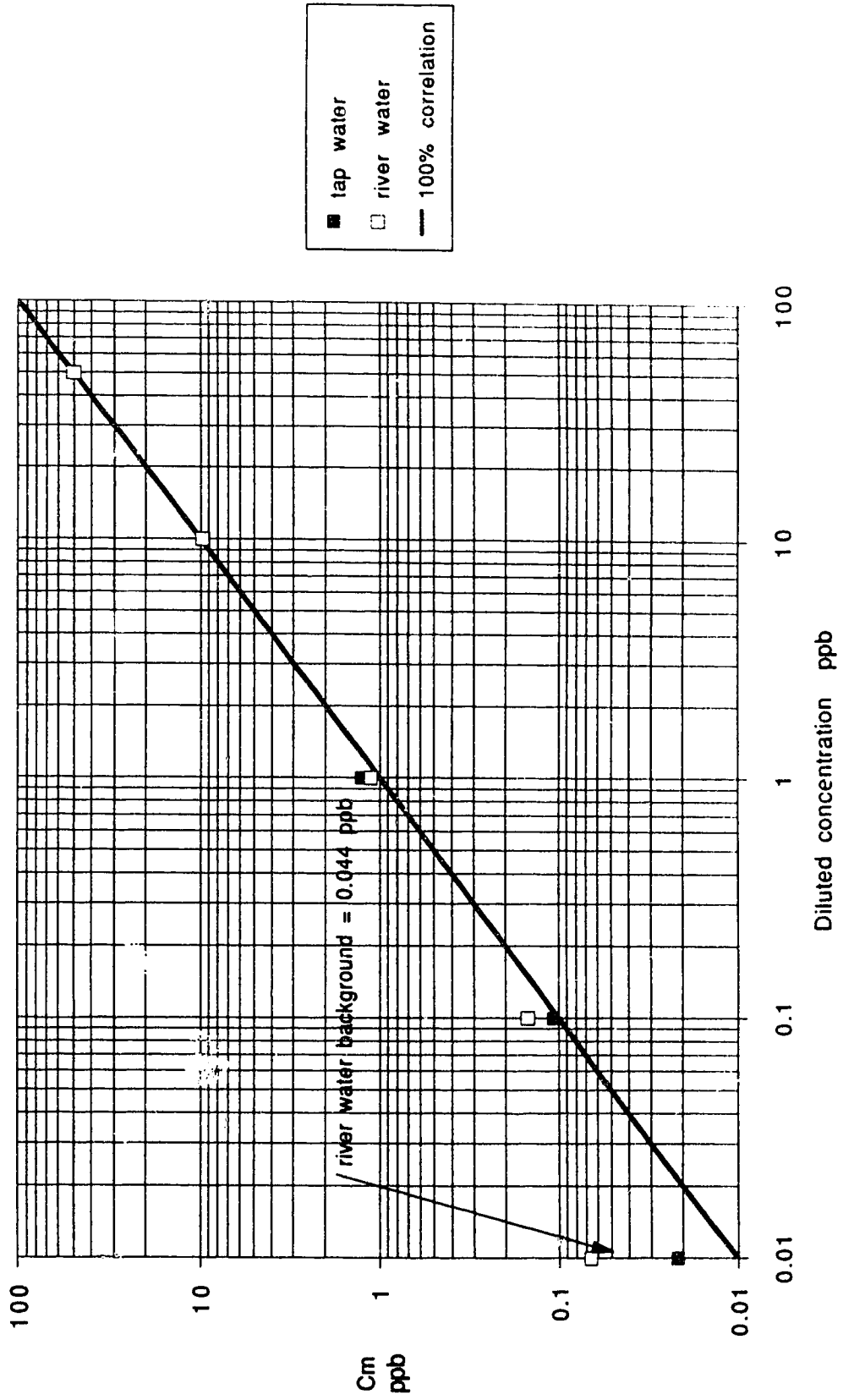


Figure 4.7 Dilution ratios for discharges with low velocity ratios

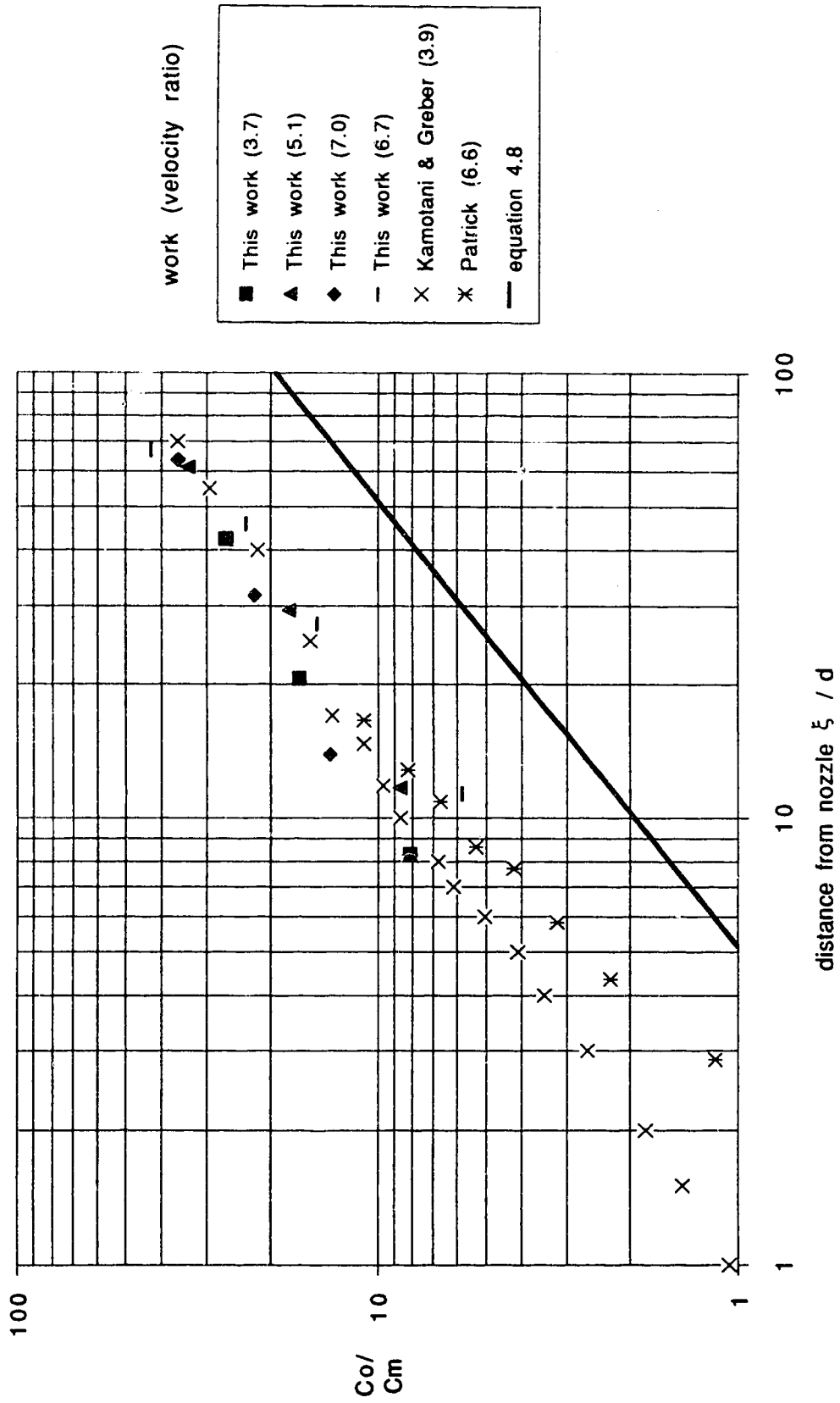


Figure 4.8 Dilution equation parameters - coefficient a

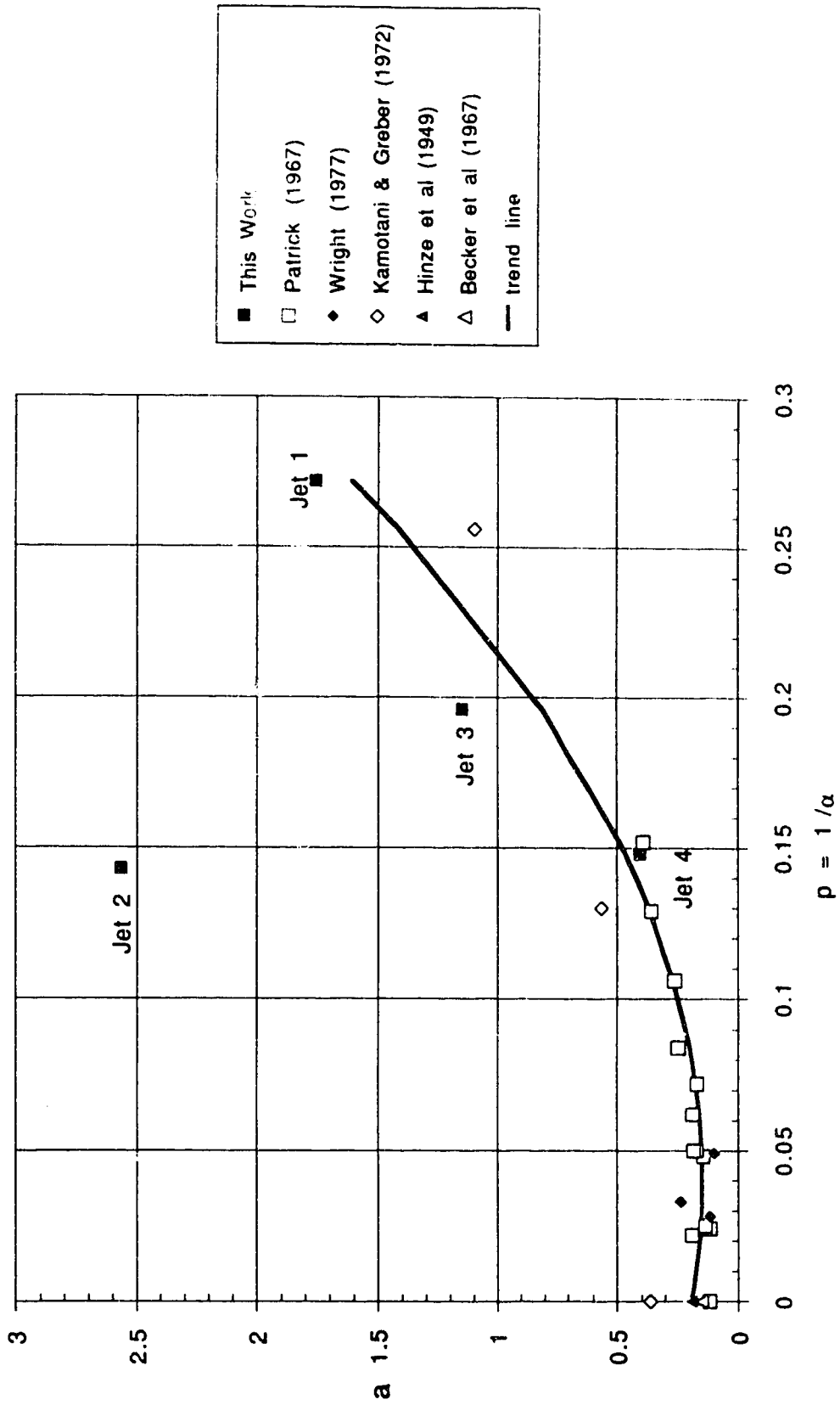


Figure 4.9 Dilution equation parameters - exponent b

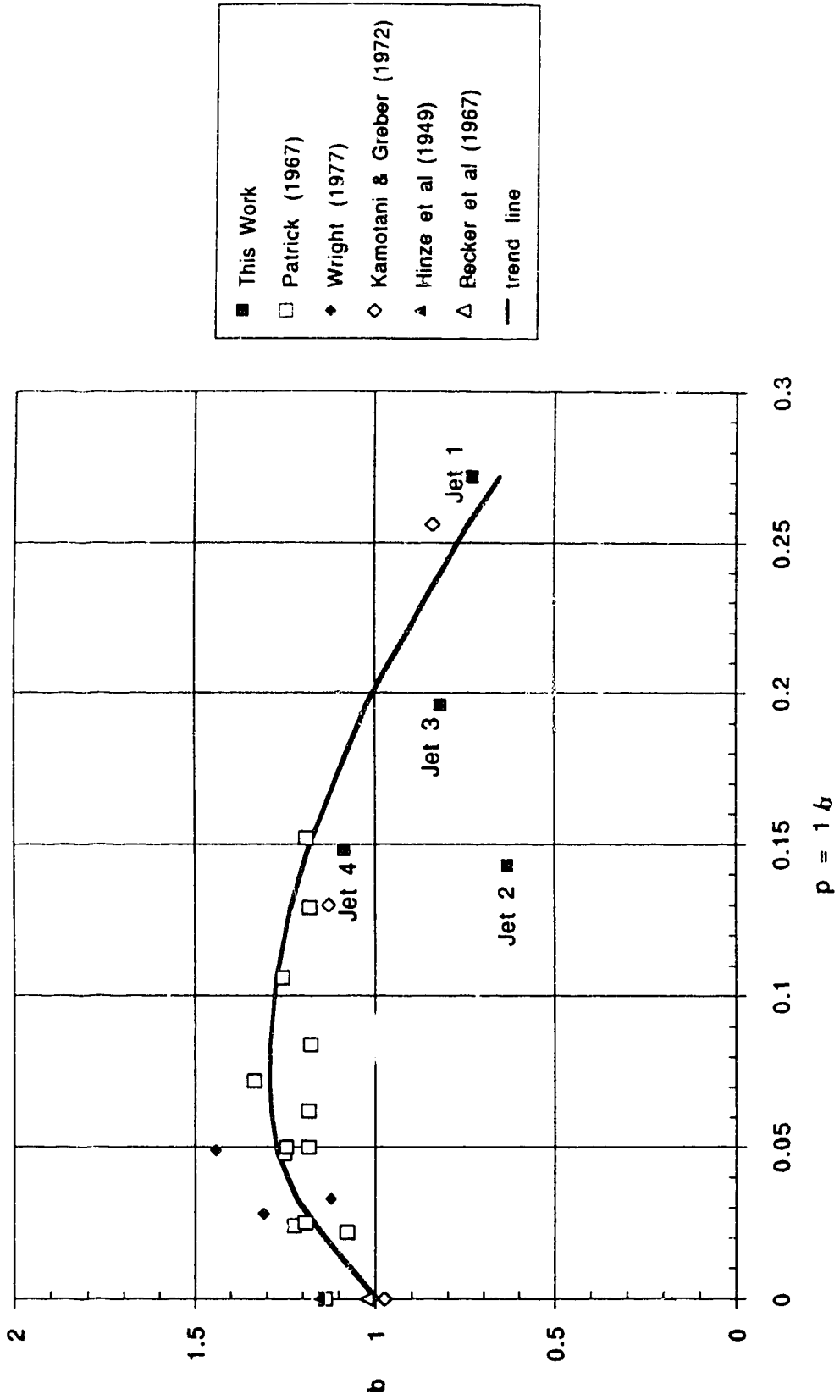




Figure 4.10 Comparison of dilution ratios

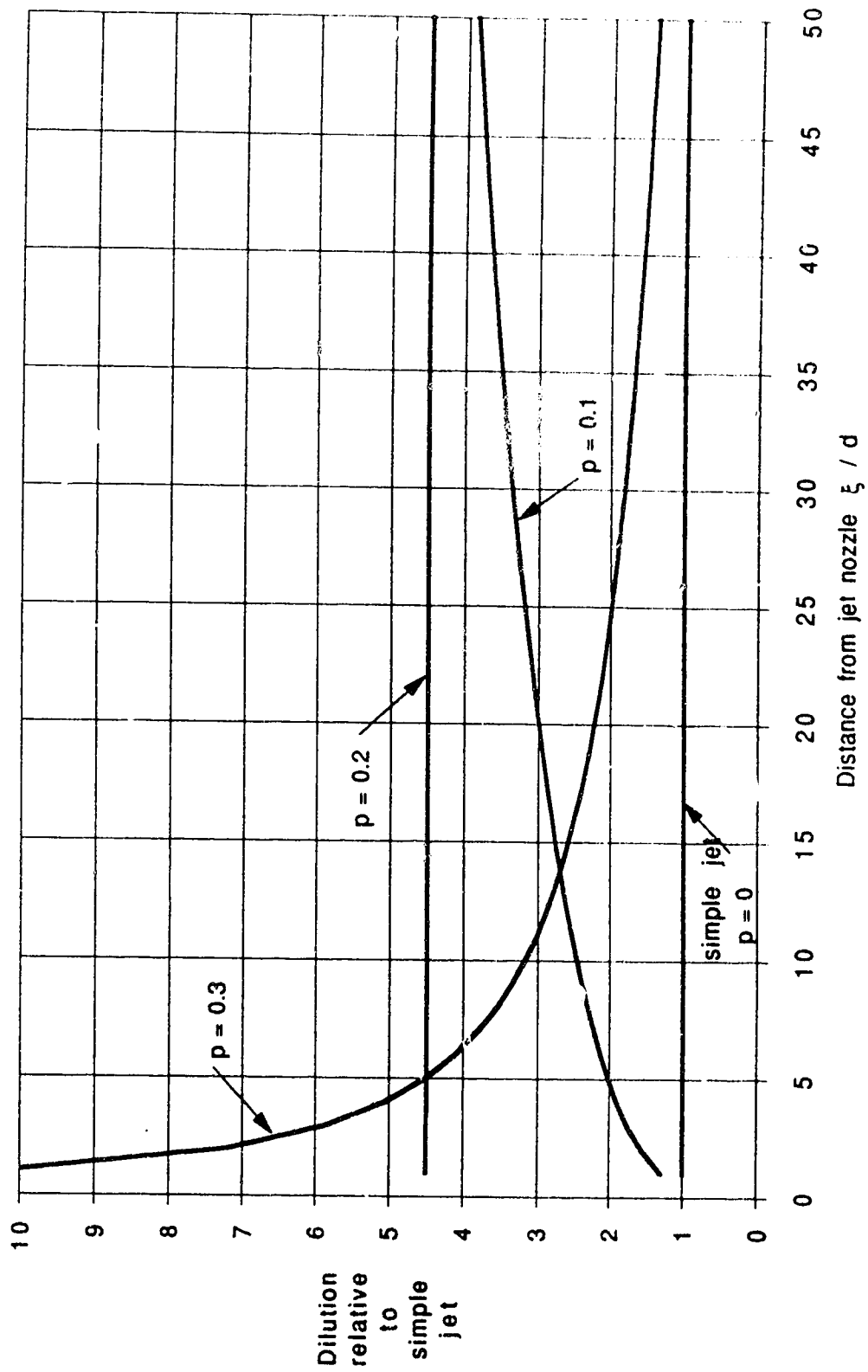




Plate 4.1 Jet discharge equipment: dye tank with peristaltic pump connected to discharge line; gate valve, flow meter and readout/totalizer; pump is submerged off to the right.

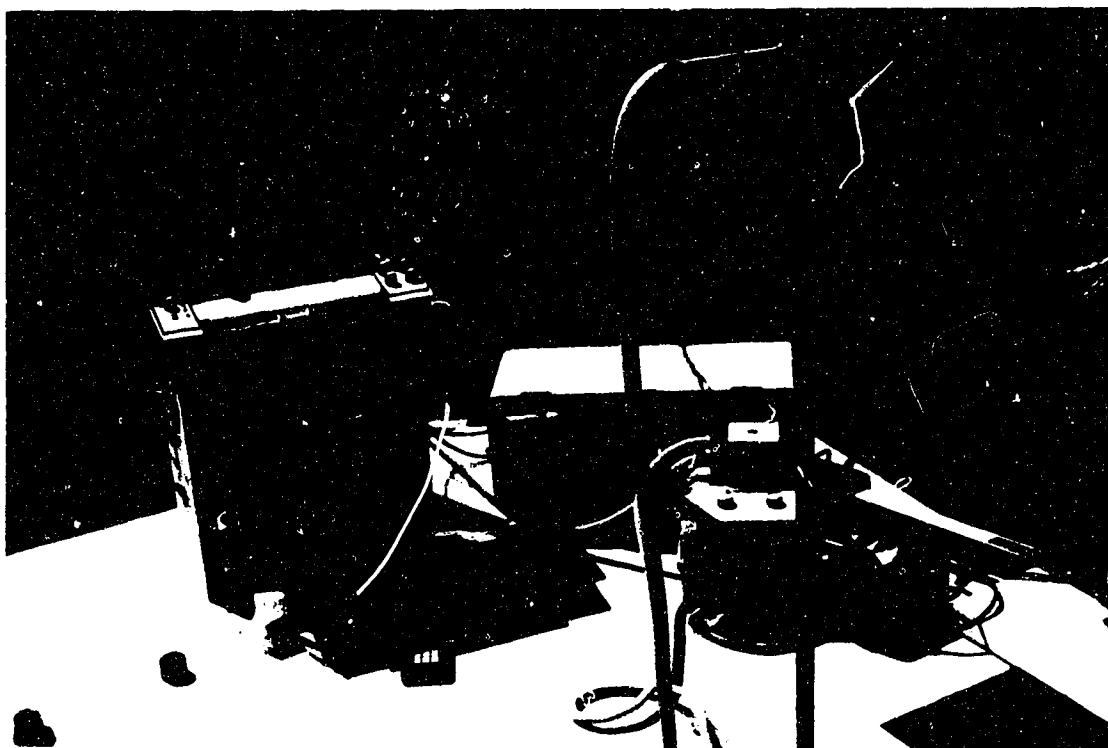


Plate 4.2 Sampling equipment: copper and rubber tubing, peristaltic pump, fluorometer and chart recorder.

## CHAPTER 5

## A LABORATORY STUDY OF JET DILUTION IN CROSSFLOWS

5.1 General

The literature review and field investigation discussed previously in chapters 2 and 4 provided much insight on the dilution of jet discharges in crossflows. The field work and the review of other laboratory work indicated that jet dilution could be quantified by a simple power law relation:

$$C_o / C_m = a (\xi / d)^b \quad (4.14)$$

where:  $C_o$  is the concentration at the jet nozzle,  
 $C_m$  is the maximum concentration in a section,  
 $\xi$  is the distance to the section along the  
 curvilinear axis,  
 $d$  is the diameter of the jet nozzle,  
 $a$  is a dilution coefficient, and  
 $b$  is a dilution exponent.

For jets discharging into crossflows of infinite depth, the values for the coefficient ( $a$ ) and the exponent ( $b$ ) were found to be functions of the inverse of the velocity ratio (i.e.  $p = 1/\alpha = U/U_o$ , where  $U$  is the crossflow velocity and  $U_o$  is the jet discharge velocity at the nozzle).

In addition to equation (4.14), other dilution relations were derived in Chapter 4 based on the work of Wright (1977a and 1977b). These were developed to quantify jet dilution relative to the more appropriate direction for effluent discharges into rivers (i.e. in terms of the distance

downstream of the discharge nozzle). These relations indicate that jet dilution is a function of the dimensionless downstream distance  $\alpha x/d$ :

$$C_o / C_m = 0.873 (\alpha x/d)^{1/2} \quad (4.20)$$

$$C_o / C_m = 0.223 (\alpha x/d)^{2/3} \quad (4.25)$$

Equation (4.20) was developed for the momentum dominated near field (MDNF) and equation (4.25) was developed for the momentum dominated far field (MDFF).

The work in this chapter builds on the findings of Chapter 4. A laboratory study was carried out to provide additional information on jets having velocity ratios of  $\alpha < 10$  (i.e.  $p > 0.10$ ). In addition, the experiment was carried out for three depth to diameter ratios ( $D/d$ ) in order to identify the effects of the finite depth of flow on the dilution of shallow water jets.

## **5.2 Experimental Arrangement**

### **5.2.1 Flume Conditions**

The experiment was conducted in a rectangular water channel at the University of Alberta's T. Blench Hydraulics Laboratory. The channel was the same one used in the photographic analysis and is described in Section 3.4.1. In this set of runs, the jet flows were produced by a larger (a 1/3 horsepower Jacuzzi model SP125-JX) pump equipped with a bypass line and a constant head tank. The jet discharge fluid was mixed in a 900 L tank located adjacent to the

flume. Bypassed flow from the bypass line and overflow from the head tank returned to this tank. The flow rates of the jet discharge were controlled by a valve on the bypass line and a valve between the constant head tank and the jet nozzle. A Fischer rotameter was used to measure the flow rate of the jet nozzle.

The jet velocities were determined from the measured jet flow rates and the jet nozzle diameter. Each nozzle was machined from a 30 mm long, 25 mm diameter brass plug. The crossflow velocities were determined from the flume flow conditions and velocity profiles measured at a vertical near the jet nozzle. Boundary layer profiles for the flume flow conditions were measured prior to and after the experiment using a propeller-type velocity meter (figures 5.1 and 5.2). Analysis of the turbulent boundary layer, based on the results of work on flow past a flat plate (Schlichting, 1979), indicated that the boundary layer was fully developed for the 100 series runs. The analysis also indicated that the boundary layer for the 200 and 300 series runs was about 40% developed. The measured velocity distributions confirm that these levels of development have occurred.

### **5.2.2 Sampling Procedures**

Rhodamine WT was used as the tracer in this study. The characteristics of this organic dye have been described in Section 4.5.3. Two Turner model 10 Field Fluorometers, equipped for flow-through sampling, were used to measure the

tracer concentrations. Both fluorometers were calibrated to diluted standards over a range of 0.1 ppb to 150 ppb (Figure 5.3). The initial background fluorescence and that of tap water were found to be the same since the flume water came from the municipal water distribution system. Values for background fluorescence during the fluorometer calibration were found to be less than 0.1 ppb. Examination of the calibration plot indicates that the fluorescence measurements were affected by adsorption onto the tubing in the sampling lines at concentrations of less than 0.5 ppb. As a result, the experiments were designed to provide concentration measurements of more than 1 ppb at all sampled locations. In addition, concentration measurements were made for periods of sufficient duration to allow the adsorption or desorption period to be eliminated.

The fluorometer calibration work indicated that the fluorescence is a linear function of tracer concentration that covers a range of at least three orders of magnitude. For all runs, the concentrations in the dye tank ( $C_0$ ) and the concentrations in the jet discharge ( $C$ ) were measured with one fluorometer. This eliminated the need to continually recalibrate the fluorometer over the course of the experiment. As the sump for the flume would gradually become contaminated with tracer during the course of making a run, the second fluorometer was used to continuously monitor the flume background fluorescence. For each run, the two fluorometers were calibrated to common measurements of

background fluorescence. In order to minimize the effect of flume background fluorescence, the tracer concentration in the sump was never allowed to exceed 15% of the maximum concentration at a section.

Concentrations were measured at a minimum of eight points for each section using a 2.44 mm inside diameter sampling probe. Concentration distributions were first measured in a vertical line at the flume centreline in order to find the maximum centreline concentration. Concentrations for horizontal transects were also measured for several of the more downstream sections to ensure that the concentration maximum did not shift away from the centreline and to determine whether or not the jet discharge was bimodal. A sufficient number of concentration measurements were made to allow the concentration distribution to be mapped for the most downstream section of each run in the 300 and 100 series (figures 5.4 through 5.11).

The turbulence of the jet discharges resulted in significant concentration fluctuations in the measured concentration at all sampling points. Concentration fluctuations at each sampling point were measured and recorded by connecting the fluorometer output channels to a two channel chart recorder. The chart data were then analysed to determine the time-averaged concentrations. The magnitude of the concentration fluctuations varied greatly, being small in the vicinity of the maximum and large at the periphery of the jet. There was little fluctuation in the

background fluorescence. The concentrations at sampling points were recorded for a duration which varied from two to eight minutes. The duration used was proportional to the magnitude of the concentration fluctuation. As the focus of this work was to determine the maximum concentrations, the low turbulence in the region of the maximums meant that time-averaging was relatively easy.

Most of the jet discharges shifted to the left (viewing downstream) of the jet centreline due to secondary currents in the flume. These currents persistently advected the tracer material to the left by as much as 25% of the distance along the curvilinear axis. This effect was most significant for the weaker jets in the 200 series runs. Horizontal transects were made whenever the maximum concentration away from the jet centreline was expected to be greater than 5% more than the centreline maximum. This eliminated any gross overestimation of the jet dilution at that section.

All of the jets were sufficiently weak that the vorticity did not result in jet **bifurcation** (the splitting of the jet discharge into two distinctly separated vortices). However, two of the jet discharges (runs 103 and 104) were **bimodal** (i.e. had two concentration maximums, greater than the maximum of the centreline profile, which were located equidistant from the jet centreline). When a jet was found to be bimodal, additional transects were made to determine the bimodal peak concentrations as well as the maximum concentration for the centreline vertical.



### **5.2.3 Experimental Error and Variance**

There were a number of potential sources of error to be considered in this laboratory analysis. A summary of these have been presented in Table 5.1. All measuring errors were minimal. The depth, the vertical location and the transverse location were measured with point and traverse gauges, equipped with verniers, and have the reading precisions indicated in Table 5.1. The jet nozzle diameters were measured with calipers. The rotameter was calibrated by timing the filling of a 9.80 L bottle. The crossflow velocities were determined by depth averaging the velocity profiles (measured at 14 points) at the jet nozzle. The main source of error was in the concentration measurements. The fluorometer calibration indicated that the variation in the concentration measurements was less than 5% of the expected (diluted) concentrations. The probable error may be less than this as some of the indicated error could be due to the dilution of the dye in making the standards.

## **5.3 Results and Analysis**

### **5.3.1 Conditions Investigated**

Concentrations were sampled at up to eight sections for the ten jet discharge conditions investigated. More than 1400 concentration measurements were made. These data (corrected to eliminate background fluorescence) are

presented in Appendix D. The jet nozzles used in these runs had diameters of either 10.7 mm or 19.0 mm (Table 5.2). Velocity ratios ranged from 1.5 to 10.5 and the depth to diameter ratios were 15.7, 23.3 and 41.3. Concentration measurements were made as far as  $\xi/d = 107$  downstream of the jet nozzle; values for  $\alpha x/d$  ranged from 1.1 to 990.

### 5.3.2 Maximum Concentrations

#### **Dilution Ratios for Centreline Maximums**

The jet discharge concentration ( $C_0$ ) and the maximum concentration at each section ( $C_m$ ) were used to determine the **dilution ratio** for each section ( $S_0 = C_0/C_m$ ). These ratios were first evaluated in terms of the distance along the curvilinear axis ( $\xi/d$ ) defined by the concentration maximums (figures 5.12, 5.13 and 5.14).

The dilution data typically could be represented by a power law relation like equation (4.14) in the initial stages of the discharge. However, the dilution in the latter stages did not increase as rapidly. This is because the initial stage is dominated by entrainment in the jet discharge which is similar to (and more efficient than) that of a simple jet while the latter stage is dominated by vortex entrainment. The extent of the **jet entrainment zone** appears to be proportional to the velocity ratio. For the runs observed, the transition appeared to be at values of  $\xi/d$  between 15 and 25. The dilution ratios at the end of this zone had values in the order of 10:1 to 20:1. The dilution ratios in the

**vortex entrainment zone** tended to converge to some value at  $\xi/d = 100$  for each flume flow condition. For the 300 series runs, the dilutions appear to be converging on a dilution ratio of 50:1 at  $\xi/d = 100$  (Figure 5.12). For the 100 series runs, the common dilution ratio at  $\xi/d = 100$  would be about 30:1 (Figure 5.14).

The general applicability of the power law relation would be severely limited due to the apparent differences in the rates of mixing relative to the jet curvilinear axis. As a result, the dilution data were examined relative to the downstream distance parameter  $\alpha x/d$  indicated in equations (4.20) and (4.25). Presented in this fashion, a more generally applicable relationship for jet dilution is apparent (figures 5.15, 5.16 and 5.17). The data can be fitted by a single dilution relation with a high degree of correlation (Figure 5.18):

$$C_o / C_m = 1.09 (\alpha x/d)^{0.56} \quad (5.1)$$

This relation is valid for dimensionless downstream distances covering three orders of magnitude (i.e.  $1.1 < \alpha x/d < 990$ ).

Equations (4.20) and (4.25) indicate that the transition between the MDNF and MDFF would occur at  $\alpha x/d = 3600$ . The dilution data did not extend far enough downstream to allow the differentiation between these two flow regions. A single trend line was found for the region examined.

Examination of Figure 5.18 for all of the dilution data indicates that there are three areas where there is potential for deviation from equation (5.1):

- a) For the weaker ( $\alpha d/D < 0.20$ ) jets, there is a tendency to mix at rates superior to that indicated in equation (5.1) at the downstream end of the discharge. This is likely because there is additional mixing due to boundary layer turbulence.
- b) The relationship for the nine runs where  $1.5 < \alpha < 8.0$  conformed to the trend line. The dilution data for the one run where  $\alpha > 8.0$  (Run 303, where  $\alpha = 10.5$ ) indicated that dilution was less in the initial stages and then tended to conform to the trend line at higher values of  $\alpha x/d$ .
- c) Even when the jets became bimodal (i.e. runs 103 and 104) the centreline maximums still conformed to the trend line. However, areas of lower dilution existed away from the centreline in the vicinity of the bimodal peaks.

The field dilution data from the work described in Chapter 4 were examined relative to equation (5.1). The data, having downstream distance values of  $22 < \alpha x/d < 408$ , have greater scatter than the laboratory data. Although they corroborate the relation, the field data appear to indicate greater mixing than the laboratory data (Figure 5.19). This is likely due to the greater turbulence in the river's boundary layer.

#### **Bimodal Concentration Distributions**

Bimodal concentration distributions were found to exist only in runs 103 and 104. The only jet strength parameter which could identify these occurrences was  $\alpha d/D$ . This parameter had values between 0.06 and 0.28 for the eight jet discharges which remained **unimodal** (i.e. had only one point

of maximum concentration located on or near the centreline of each section). The two runs which did become bimodal had values of 0.36 and 0.43 for  $\alpha d/D$ . As a result, the transition between unimodal and bimodal jet discharges appears to be a result of the finite depth of flow, occurring for  $\alpha d/D$  somewhere between 0.28 and 0.36. This corresponds well with the results of the photographic analysis in Chapter 3 which indicated that surface effects begin to occur when  $\alpha d/D = 0.34$ .

Photographs were taken to illustrate the range of jet discharge conditions examined (plates 5.1 to 5.6). The side view photographs were taken at a relatively fast shutter speed (1/30 s) to illustrate the jet position and the turbulence structure. The jet for Run 101 does not come near the water surface while, for Run 104, the jet contacts the surface before  $x/d = 15$ . The plan view photographs were taken with both short and long exposure times (1/15 s and 15 s) to illustrate the jet turbulence, the mean jet position and the jet dilution (the grid size is 50 mm by 50 mm). Run 102 was clearly unimodal and Run 104 was clearly bimodal. These observations required the information provided by the long exposure time photographs and the detailed concentration measurements.

When a jet discharge is sufficiently strong to become bimodal it does so quickly. For Run 103, the concentration distributions at four sections (where  $54 < \alpha x/d < 280$ ) were examined in detail: all were bimodal. For Run 104, three

sections (where  $41 < \alpha x/d < 99$ ) were examined in detail: all were bimodal.

It would be expected that the bimodal peak concentrations at a given section would have equal values. However, due to the secondary currents inherent in the flume, the observed bimodal peaks were quite different. The left peak was always higher than the right peak due to the leftward bias of the flume. As a result, the bimodal peak concentration was taken as the average of the two peaks. There was an insufficient number of bimodal jet discharges examined to establish a relationship between the jet strength and the ratio of the bimodal peaks to the centreline maximum. The measurements for the bimodal distributions indicated that the average **bimodal ratio** (the average of the two bimodal peaks divided by the centreline maximum) was about 1.3 for Run 103 ( $\alpha d/D = 0.36$ ) and about 1.5 for Run 104 ( $\alpha d/D = 0.43$ ). Intuitively, the bimodal ratio would have a value of 1.0 for all unimodal jets (i.e. where  $\alpha d/D$  has a value in the order of 0.3) and would increase as the jet strength increases.

### 5.3.3 Centreline Profiles

The concentration measurements in the laboratory provided another means to quantify the jet centreline position (Figure 5.20). The entire data set was fitted by the equation:

$$\frac{y_c}{\alpha d} = 1.46 \left( \frac{x}{\alpha d} \right)^{0.26} \quad (5.2)$$

This trend line represents the data from the 300 series and 100 series out to  $\frac{x}{\alpha d} = 10$ . Beyond this distance, the centreline data for the two series begin to diverge with the centreline being lower for the shallower (100 series) runs. The suppression of vertical growth of the jets in the 100 series is likely due to the finite depth of flow.

The centreline data for the 200 series runs fall below the trend line. These centreline observations are likely the result of the low jet strength (the two runs were the weakest jets examined). This is to be expected since previous work discussed in Chapter 3 indicated that there is tendency for global jet centreline equations to overpredict for weaker jets.

The centreline positions determined from the field program ( $D/d \approx 18$  and  $22$ ) were also plotted on Figure 5.20. They tend to corroborate the laboratory data for the 200 series runs ( $D/d \approx 16$ ).

#### 5.3.4 Jet Widths

The width of the jet discharge is of importance for setting the jet spacing of diffuser outfalls. These structures typically comprise a number of nozzles discharging across a portion of the river. The concentration data were of sufficient accuracy to allow the determination of the jet widths where the concentration is 50% of the maximum

concentration at that section (i.e.  $C/C_m = 0.5$ ). This is sufficient for setting the spacing of the jets. The interaction of adjacent jets is less than what would be indicated by the superposition of the concentrations of the adjacent jets (see Appendix E for a detailed analysis of jet interaction).

The width data for both the unimodal and the bimodal jet discharges were examined as a function of the downstream distance (figures 5.21 and 5.22). The jet widths can be quantified by the following relations:

$$\frac{W_z}{\alpha d} = 1.20 \left( \frac{x}{\alpha d} \right)^{0.29} \quad (5.3)$$

$$\frac{W_z}{\alpha d} = 0.98 \left( \frac{\xi}{\alpha d} \right)^{0.36} \quad (5.4)$$

Both equations (5.3) and (5.4) were found to provide adequate representations of the data. Although the jet widths observed in the field (taken from the work described in Chapter 4) exhibited more scatter, they corroborate both of the relations developed from the laboratory data.

### 5 Jet Thicknesses

The concentration data were examined to determine the thickness of the jet discharge at each section between the points where  $C/C_m = 0.5$  (figures 5.23 and 5.24). Correction factors, outlined in Section 3.5.12, were applied to the jet thickness data as they were measured in the vertical plane. This means that the thicknesses indicated on figures 5.23 and



5.24 are normal to the jet axis and not in the vertical plane.

The thickness data (as well as the width data in Section 5.3.4) for both unimodal and bimodal jets were examined relative to the assumption that the centreline maximum was  $C_m$ . For bimodal jets, this would result in thicknesses and widths which are somewhat greater than if the bimodal peak concentrations were used to determine  $C_m$ .

The jet thickness for the discharges examined can be represented by the following relations:

$$\frac{W_y}{\alpha d} = 0.78 \left( \frac{x}{\alpha d} \right)^{0.52} \quad (5.5)$$

$$\frac{W_y}{\alpha d} = 0.78 \left( \frac{x}{\alpha d} \right)^{0.37} \quad (5.6)$$

$$\frac{W_y}{\alpha d} = 0.36 \left( \frac{\xi}{\alpha d} \right)^{1.28} \quad (5.7)$$

$$\frac{W_y}{\alpha d} = 0.60 \left( \frac{\xi}{\alpha d} \right)^{0.46} \quad (5.8)$$

The two pairs of equations were found to provide adequate representations of the data. The equations indicate some form of two zone growth. In the near zone, the growth in jet thickness is rapid. The thickness is expressed as a function of the distance downstream by equation (5.5) and as a function of the distance along the curvilinear axis by equation (5.7). The thickness does not grow as rapidly in the far zone and is represented by equations (5.6) and (5.8).

The transition between the two zones appears to occur at

$$\frac{x}{\alpha d} = 1 \text{ or } \frac{\xi}{\alpha d} = 2.$$

The jet thicknesses observed in the field (taken from the work described in Chapter 4) corroborate both sets of relations developed from the laboratory data.

#### 5.4 Conclusions

a) The jet dilution data was well represented by a power law relation along the curvilinear ( $\xi/d$ ) axis like equation (4.14) in the initial stages of the discharge (the **jet entrainment zone**). The representation did not hold into the **vortex entrainment zone** where the jet effects diminish and give way to vortex mixing. The transition between these two zones occurred at values of  $15 < \xi/d < 25$  with the length of the first zone being proportional to the jet strength. The dilution ratios at the transition were in the order of 10:1 to 20:1.

b) The dilution ratios in the vortex entrainment zone tended to converge to some value at  $\xi/d = 100$  for each flume flow condition. For the 300 series runs ( $D/d = 41.3$ ), this value was 50:1; for the 100 series runs ( $D/d = 15.7$ ), this value was 30:1.

c) The jet dilution was more generally represented as a function of  $\alpha x/d$  (Figure 5.18). Equation (5.1) represents all of the laboratory data for downstream distances covering three orders of magnitude ( $1.1 < \alpha x/d < 990$ ). The dilution data from the field work (Figure 5.19) corroborates equation (5.1).

d) The eight jets where  $0.06 < \alpha d/D < 0.28$  were found to be **unimodal** (i.e. had concentration distributions with single peaks). The two jet discharges where  $\alpha d/D$  had values 0.36 and 0.43 had **bimodal** (i.e. twin peaks) concentration distributions. Although centreline dilution ratios for these discharges were well represented by equation (5.1), the bimodal peak concentrations were significantly greater.

e) The bimodal peak concentrations were not identical due to secondary currents in the flume. The average **bimodal ratio** (i.e. the bimodal peak concentration divided by the centreline maximum concentration) was about 1.3 for  $\alpha d/D = 0.36$  and 1.5 for  $\alpha d/D = 0.43$ . More work is required to determine a relationship for the bimodal ratio.

f) The concentration centreline can be represented by equation (5.2) for values of  $\frac{x}{\alpha d}$  up to about 10 (Figure 5.20). Beyond this distance, the centreline profiles were more significantly affected by the finite depth of flow.

g) The width of the jet between points where  $C/C_m = 0.5$  is important for setting the jet spacing in a diffuser outfall. Available data were used to develop jet width relations (figures 5.21 and 5.22). Equations (5.3) and (5.4) both provide adequate representations of the data.

h) The jet thickness data indicate two zones of growth (figures 5.23 and 5.24). Near the jet nozzle, the growth of jet thickness is rapid and faster than that for simple jets. Further away, the growth in jet thickness is slower than the initial rate. The transition between these two zone appears to occur at  $\frac{x}{\alpha d} = 1$  or  $\frac{\xi}{\alpha d} = 2$ .

Table 5.1 Measurement precision and experimental error  
laboratory dilution study

Measurement	Precision	Experimental Values	Estimated Probable Error ( $\pm$ )
depth of flow (mm)	0.1	168 and 442	< 1%
jet nozzle diameter (mm)	0.025	10.7 and 19.0	< 1%
vertical position (mm)	0.1	14 to 431	< 1 mm
transverse position (mm)	0.3	0 to $\pm 120$	< 1 mm
downstream position (mm)	< 1	14.3 to 1026	< 1 mm
jet discharge (L/min)	0.05	2.70 to 6.83	< 2%
crossflow velocity (m/s)	0.001	0.120 and 0.171	< 2%
concentration (ppb)	0.01	1 to 141	< 5%

Table 5.2 Conditions investigated in laboratory dilution study

Run Number	Jet Diameter d (mm)	Channel Depth D (mm)	Jet Velocity U <sub>o</sub> (m/s)	Channel Velocity U (m/s)	D/d	$\alpha =$ U <sub>o</sub> /U	$\frac{\alpha d}{D}$	$\frac{\alpha^2 d}{D}$	R <sub>j</sub> = $\frac{U_o d}{V}$
101	10.7	168	0.500	0.171	15.7	2.93	0.19	0.55	5,300
102	10.7	168	0.751	0.171	15.7	4.39	0.28	1.23	7,950
103	10.7	168	0.980	0.171	15.7	5.73	0.36	2.09	10,400
104	10.7	168	1.170	0.171	15.7	6.84	0.43	2.98	12,400
201	19.0	442	0.175	0.120	23.3	1.46	0.06	0.09	3,300
202	19.0	442	0.356	0.120	23.3	2.96	0.13	0.38	6,690
300	10.7	442	0.500	0.120	41.3	4.17	0.10	0.42	5,300
301	10.7	442	0.652	0.120	41.3	5.44	0.13	0.71	6,910
302	10.7	442	0.849	0.120	41.3	7.07	0.17	1.21	8,990
303	10.7	442	1.266	0.120	41.3	10.55	0.26	2.69	13,400

Figure 5.1 Boundary layer velocity distribution for 200 and 300 series runs

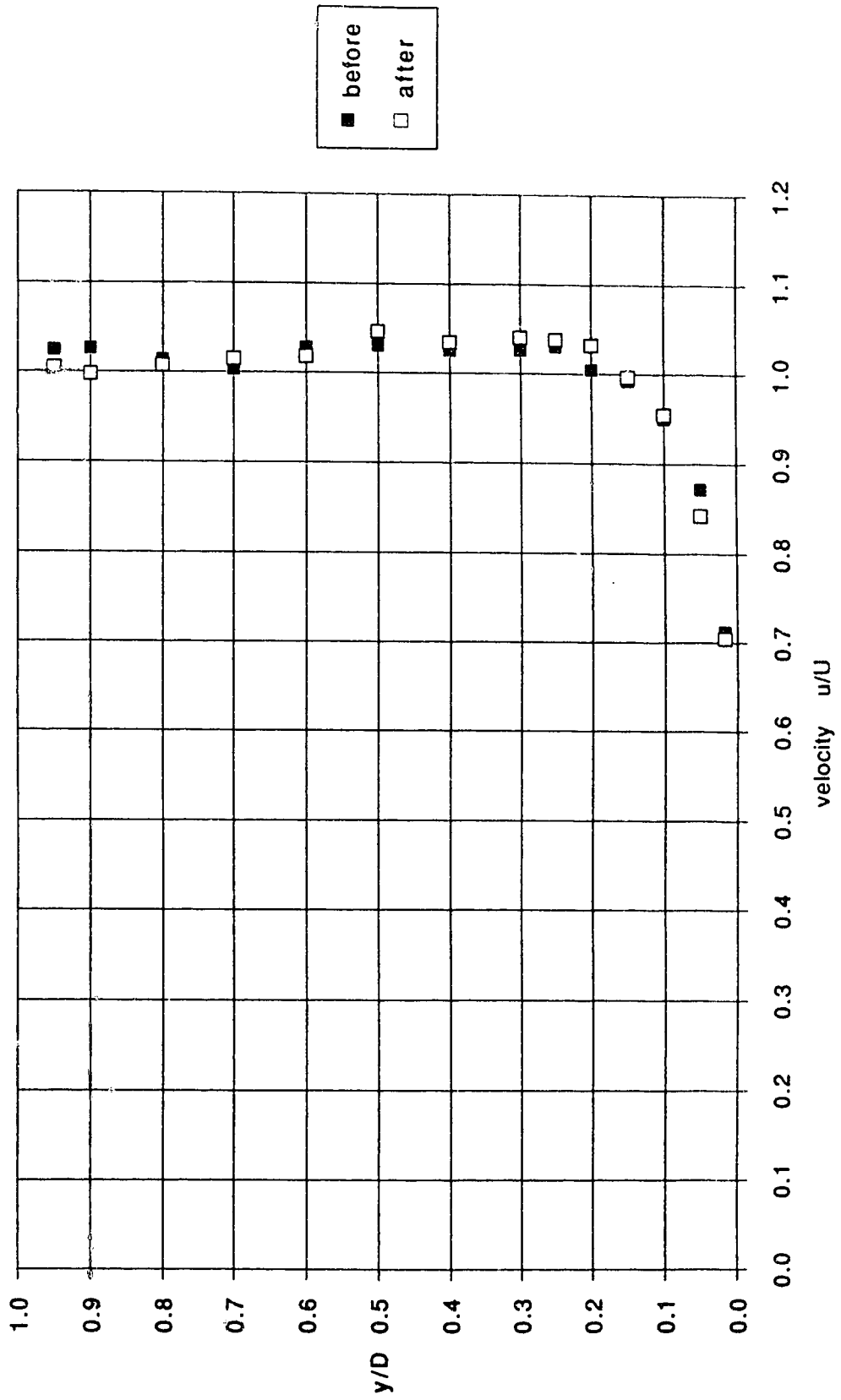


Figure 5.2 Boundary layer velocity distribution for 100 series runs

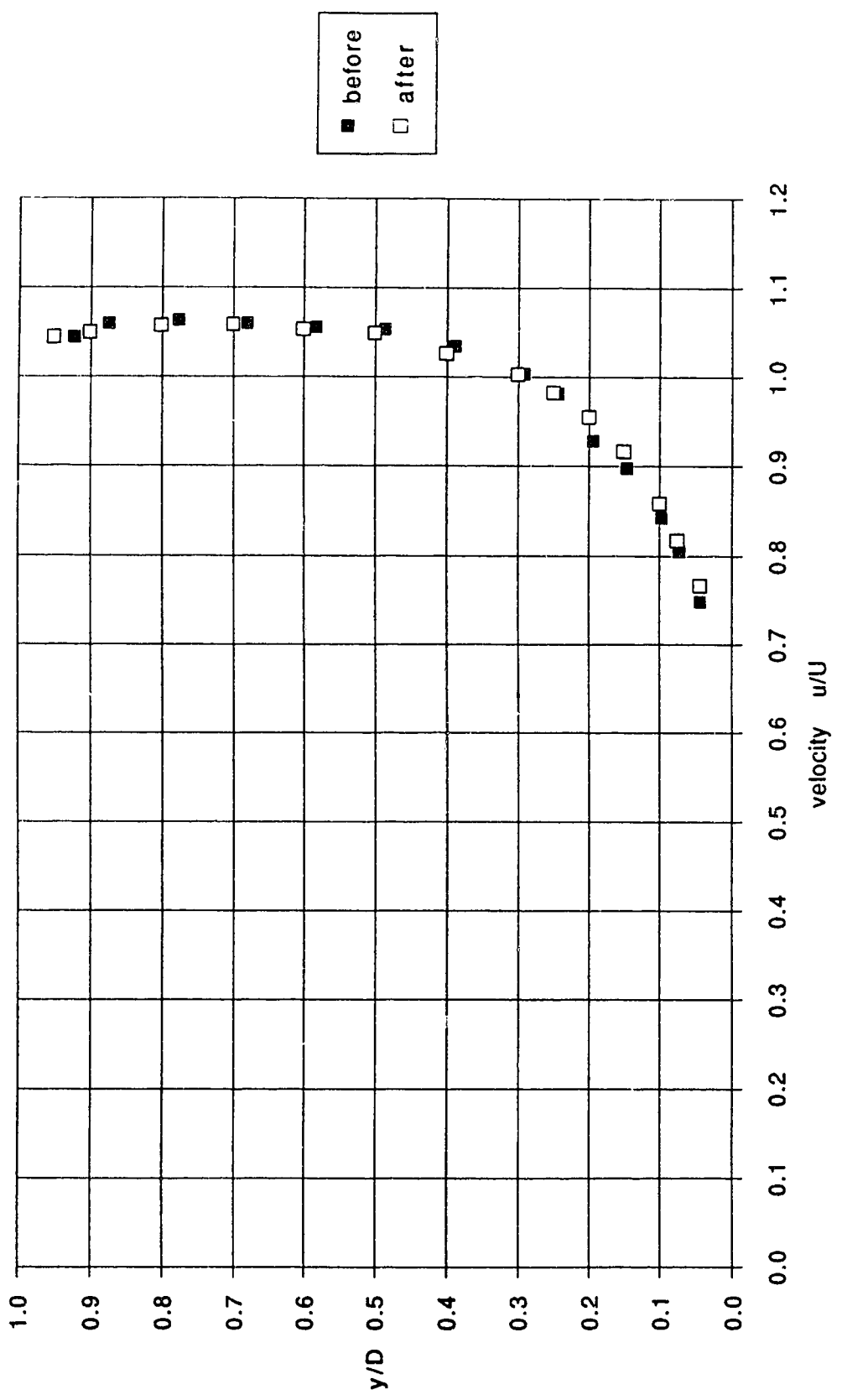




Figure 5.3 Fluorometer calibration - laboratory study

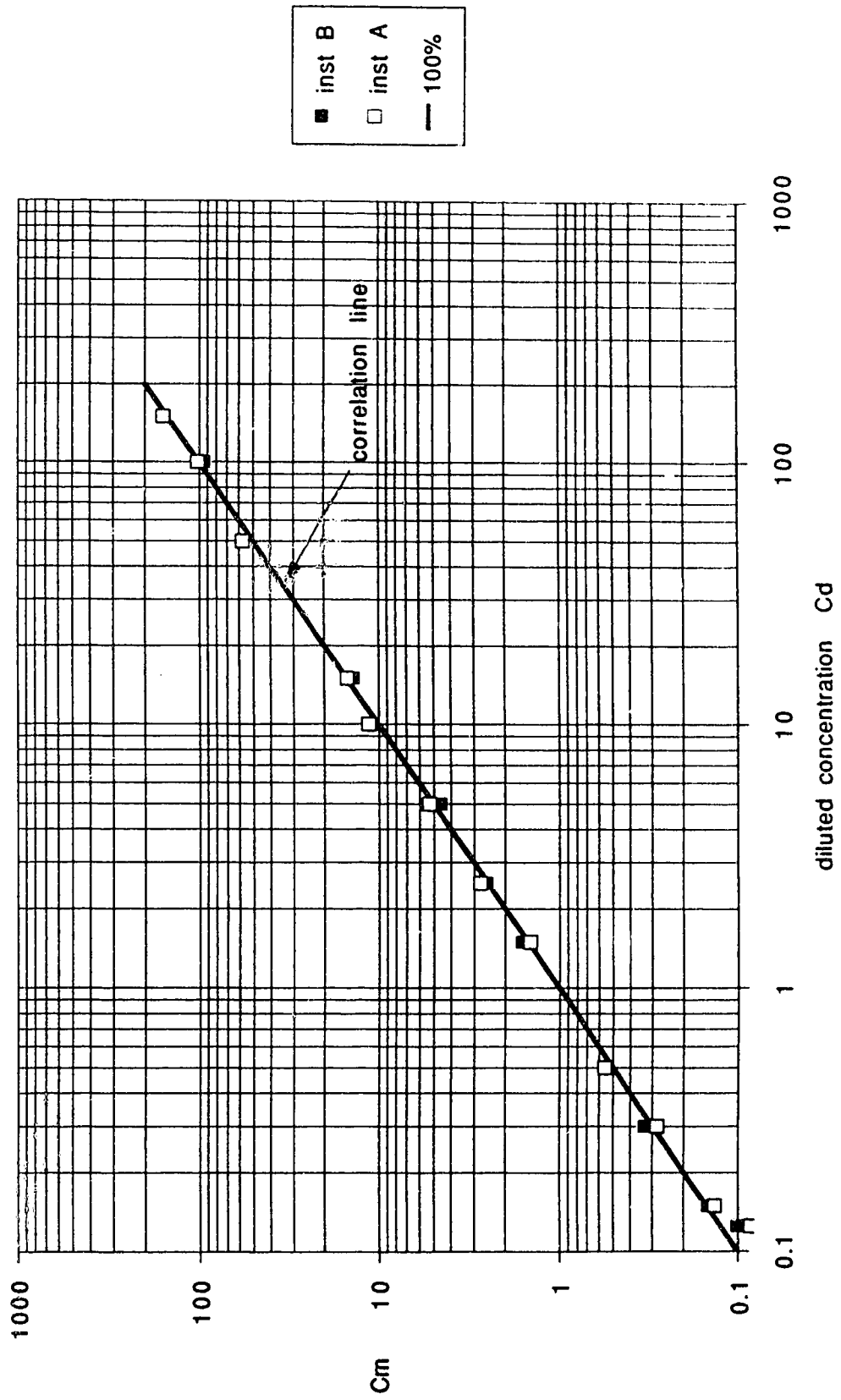




Figure 5.5 Concentration distribution for Run 301 -  $x/d = 95$

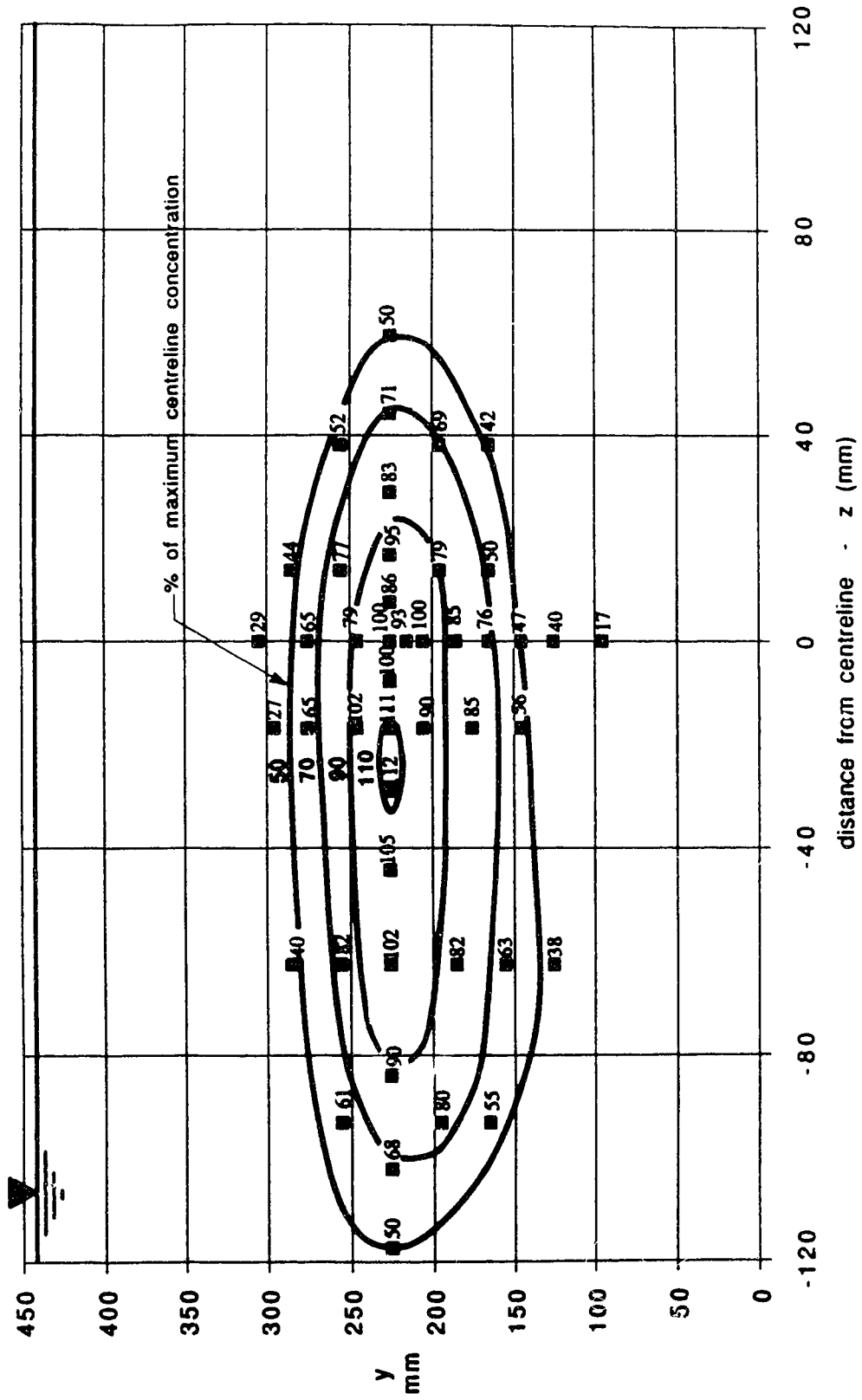


Figure 5.6 Concentration distribution for Run 302 -  $x/d = 95$

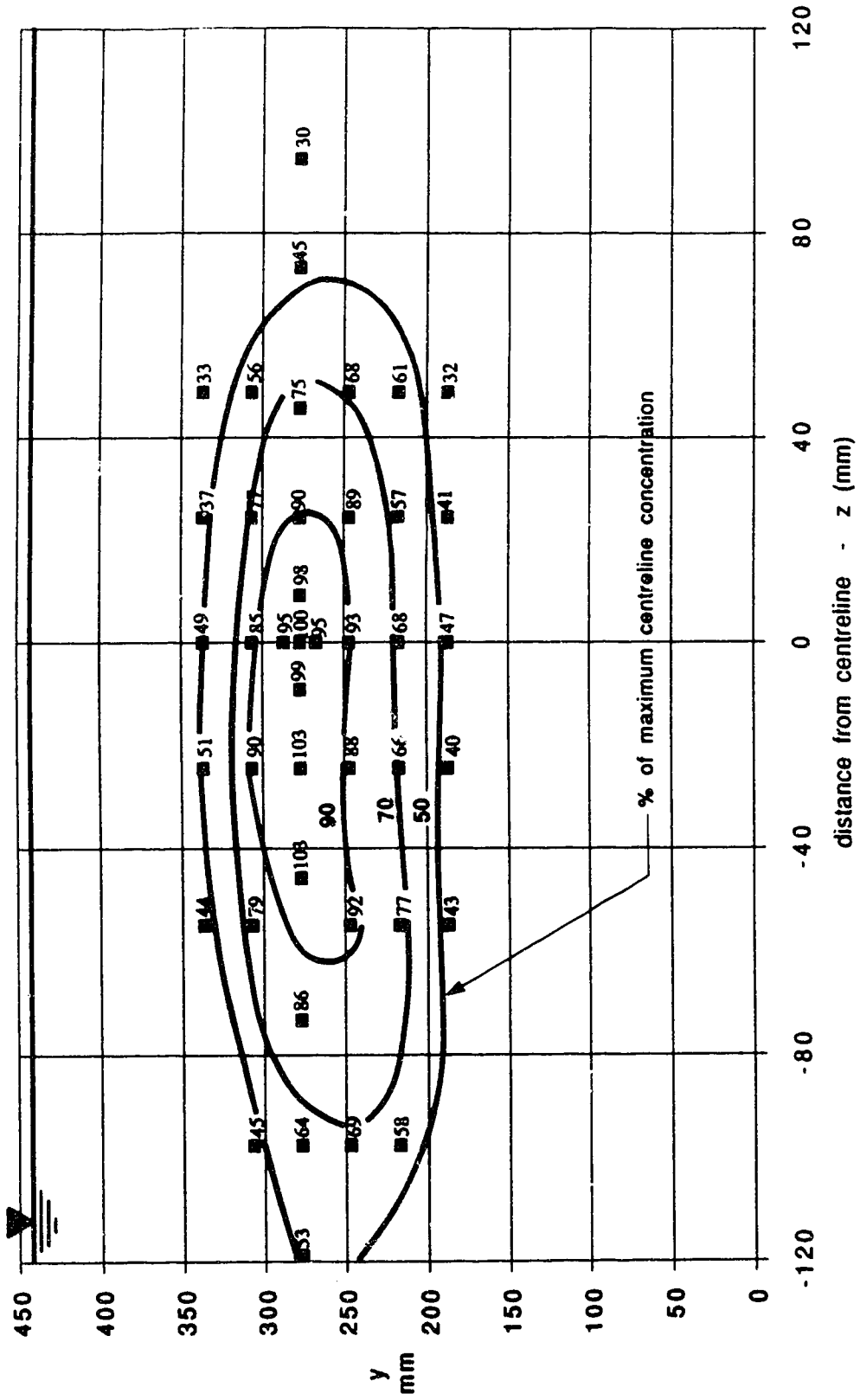


Figure 5.7 Concentration distribution for Run 303 -  $x/d = 95$

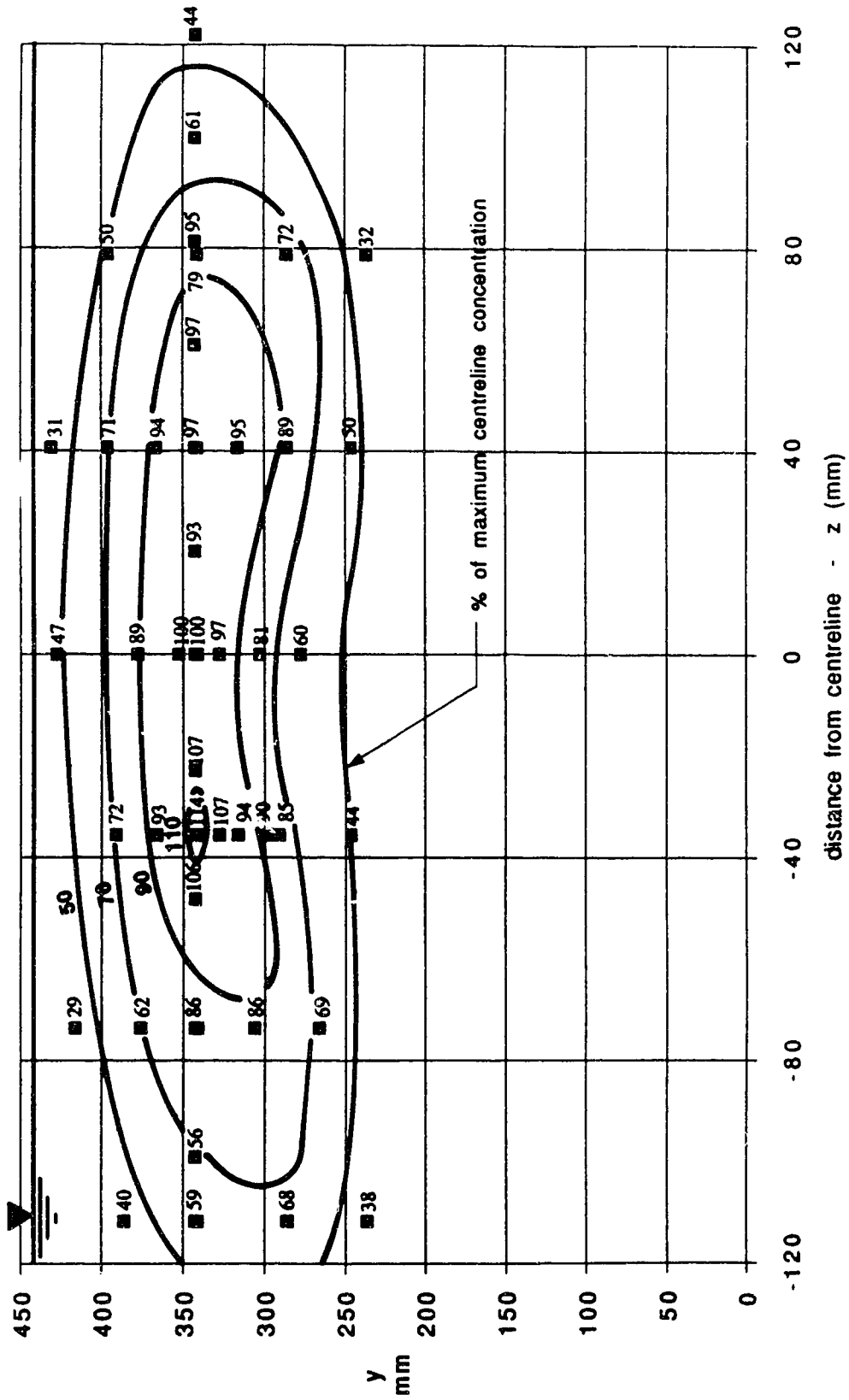


Figure 5.8 Concentration distribution for Run 101 -  $x/d = 95$

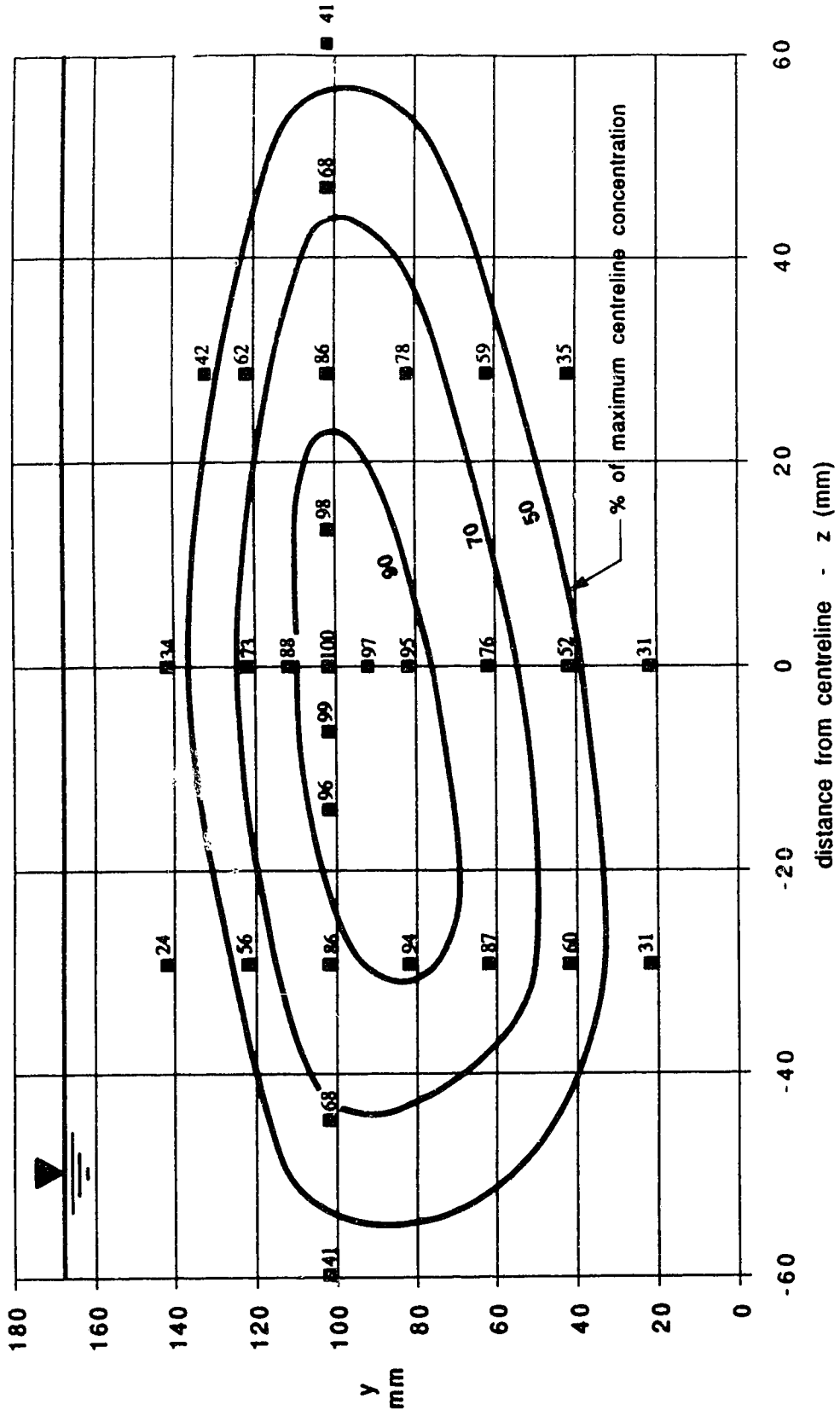


Figure 5.9 Concentration distribution for Run 102 -  $x/d = 50$

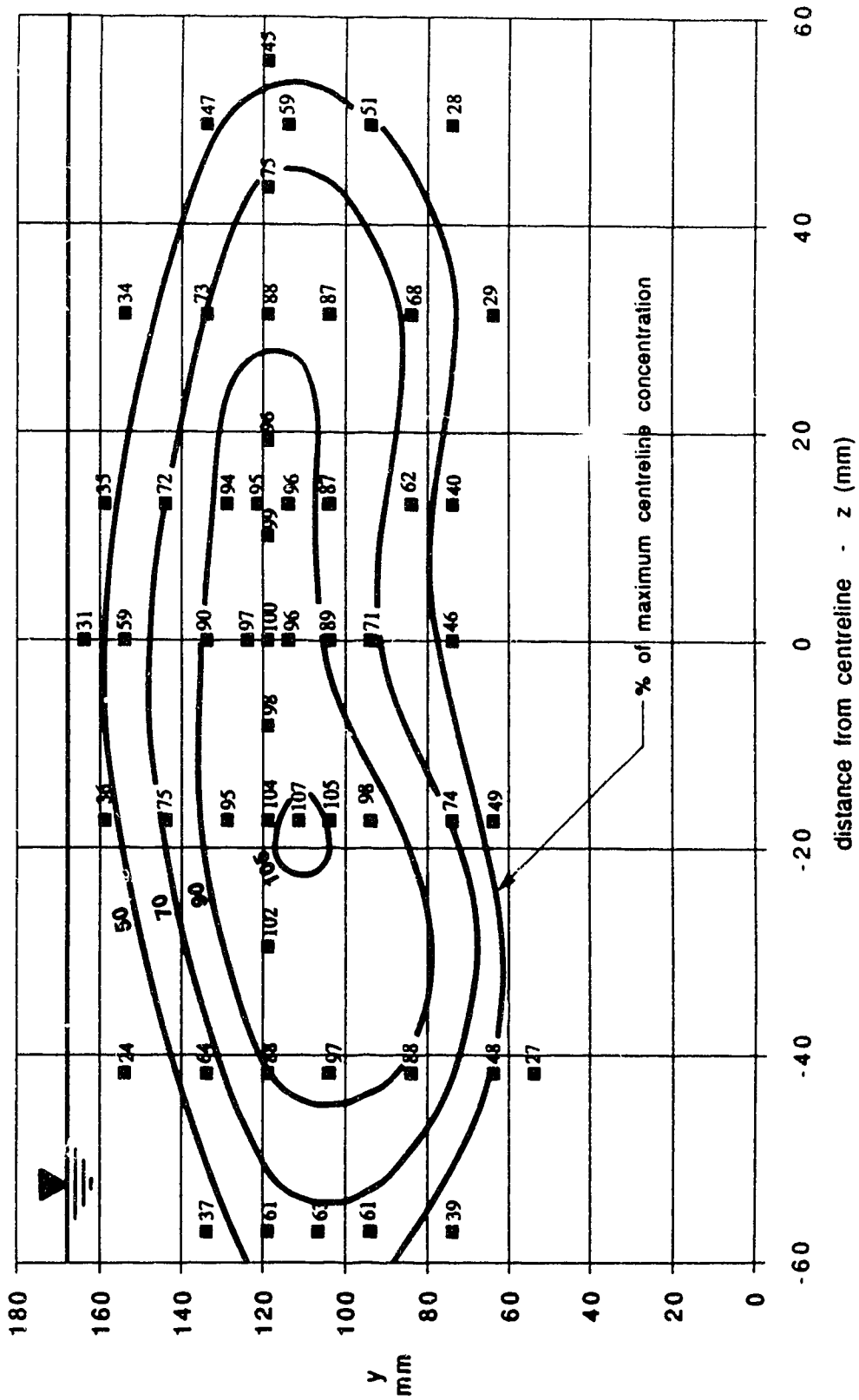
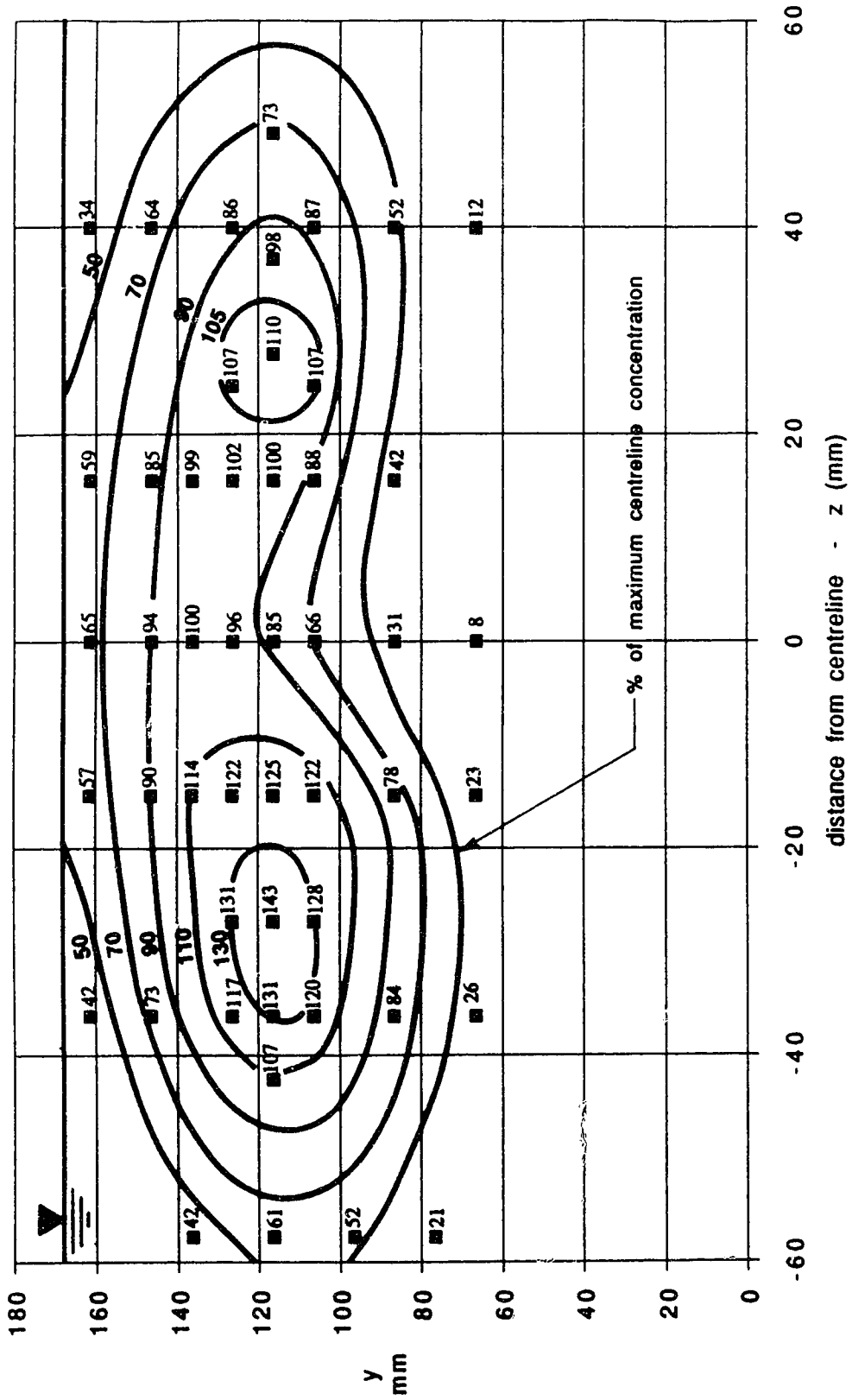


Figure 5.10 Concentration distribution for Run 103 -  $x/d = 30$



180  
160  
140  
120  
100  
80  
60  
40  
20  
0

y  
mm

-60 -40 -20 0 20 40 60

distance from centreline - z (mm)

— % of maximum centreline concentration



Figure 5.11 Concentration distribution for Run 104 -  $x/d = 15$

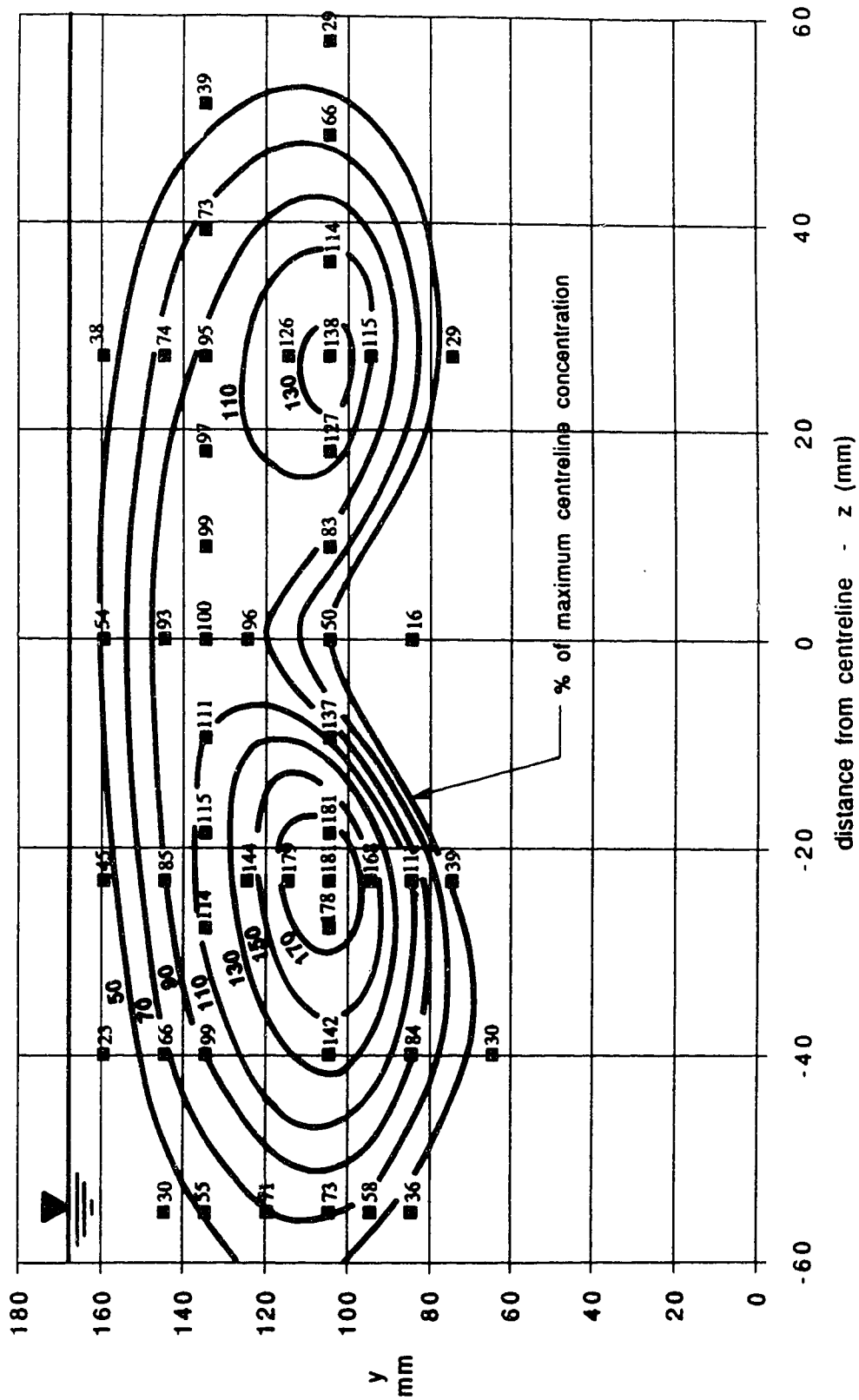


Figure 5.12 Centreline dilution ratios along curvilinear axis - 300 series runs -  $D/d = 41.3$

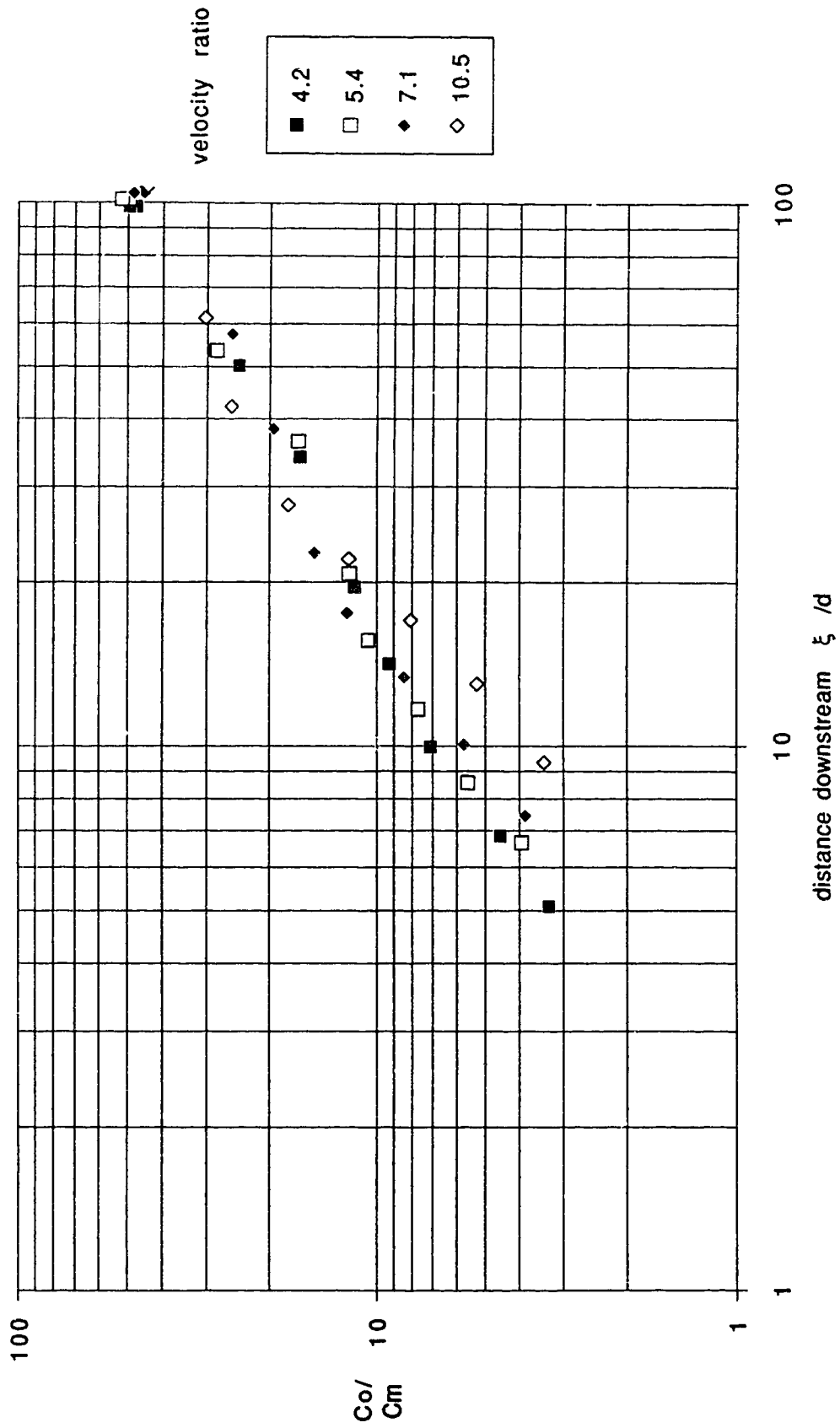


Figure 5.13 Centreline dilution ratios along curvilinear axis - 200 series runs -  $D/d = 23.3$

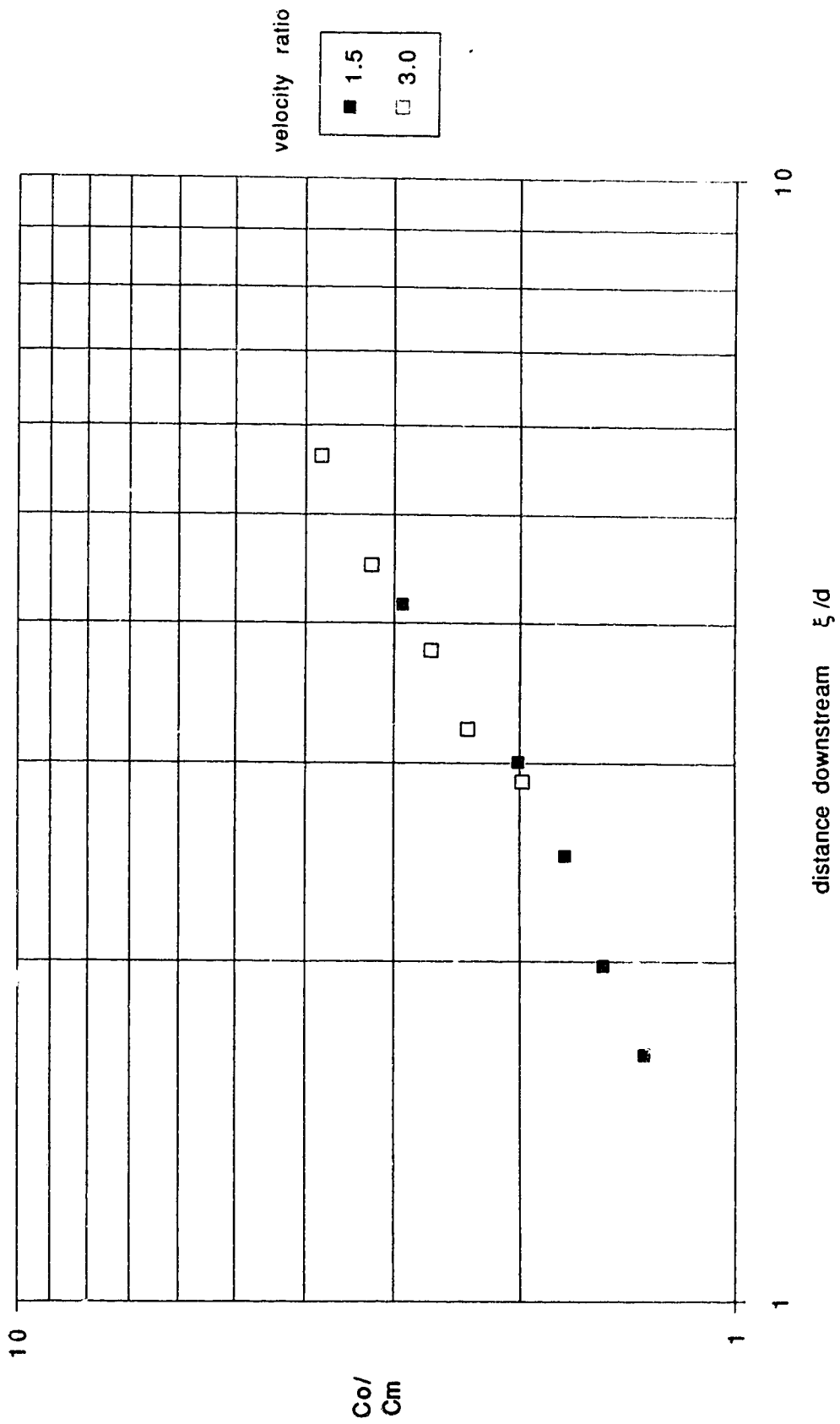


Figure 5.14 Centreline dilution ratios along curvilinear axis - 100 series runs -  $D/d = 15.7$

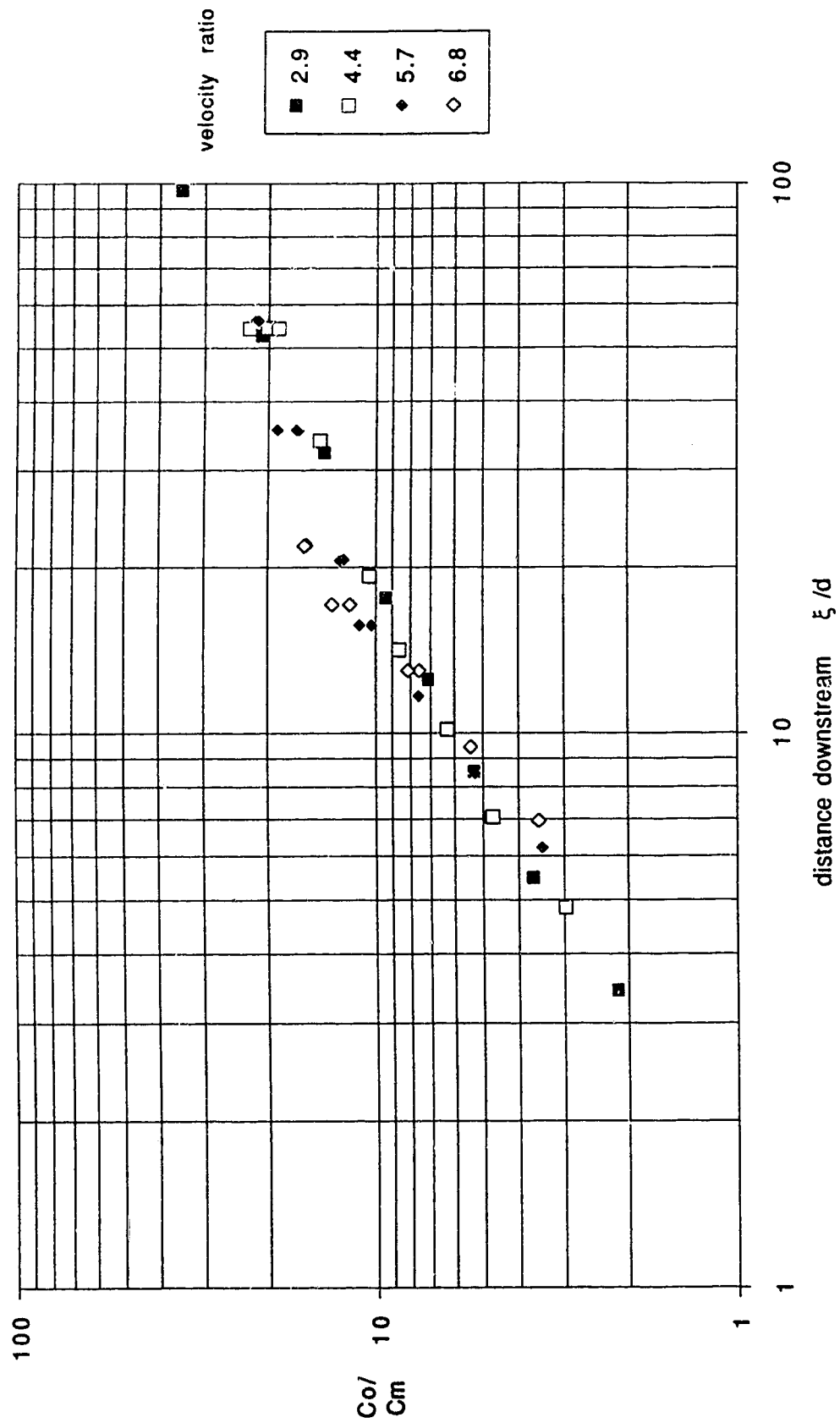


Figure 5.15 Centreline dilution ratios for 300 series runs ( $D/d = 41.3$ )

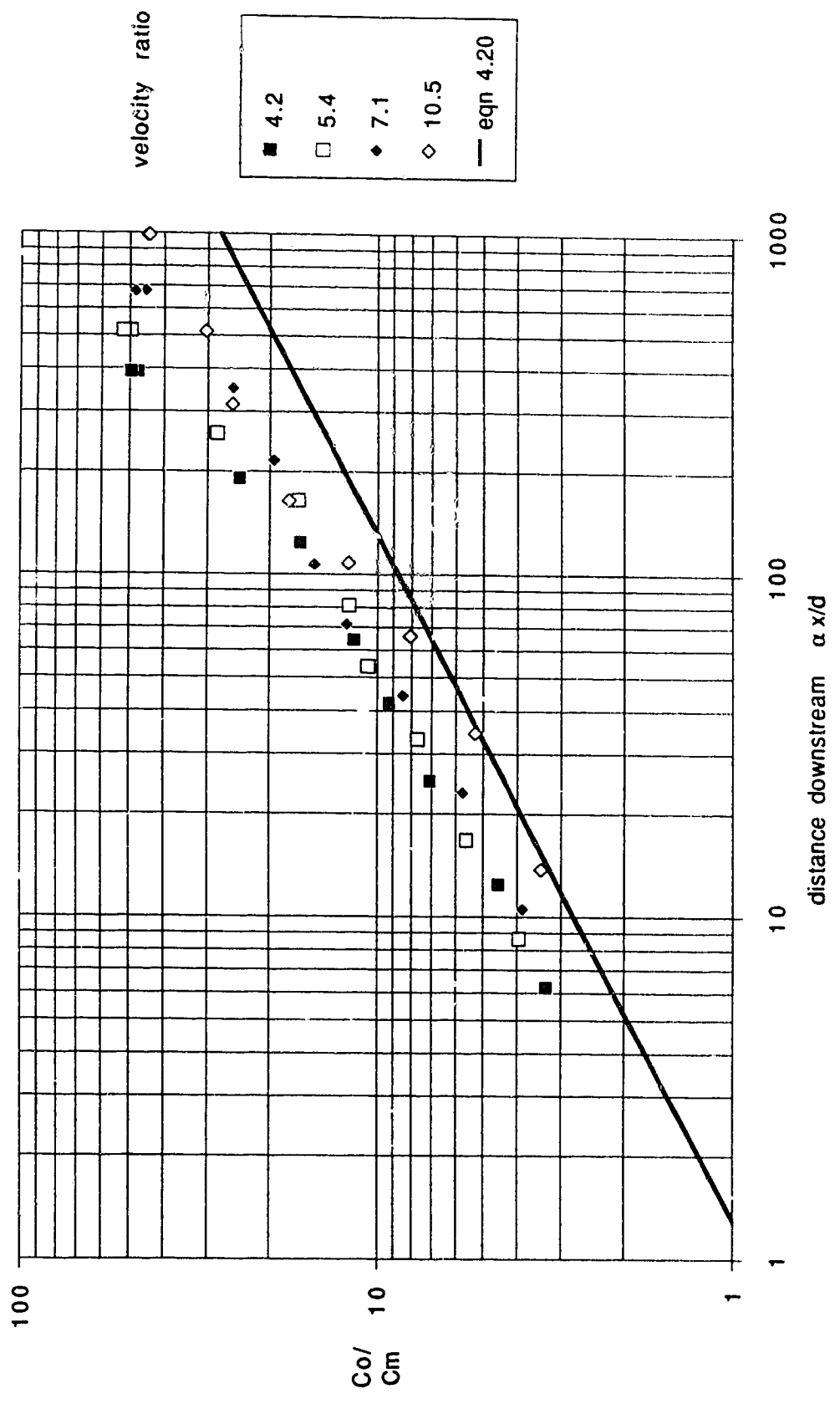


Figure 5.16 Centreline dilution ratios for 200 series runs ( $D/d = 23.3$ )

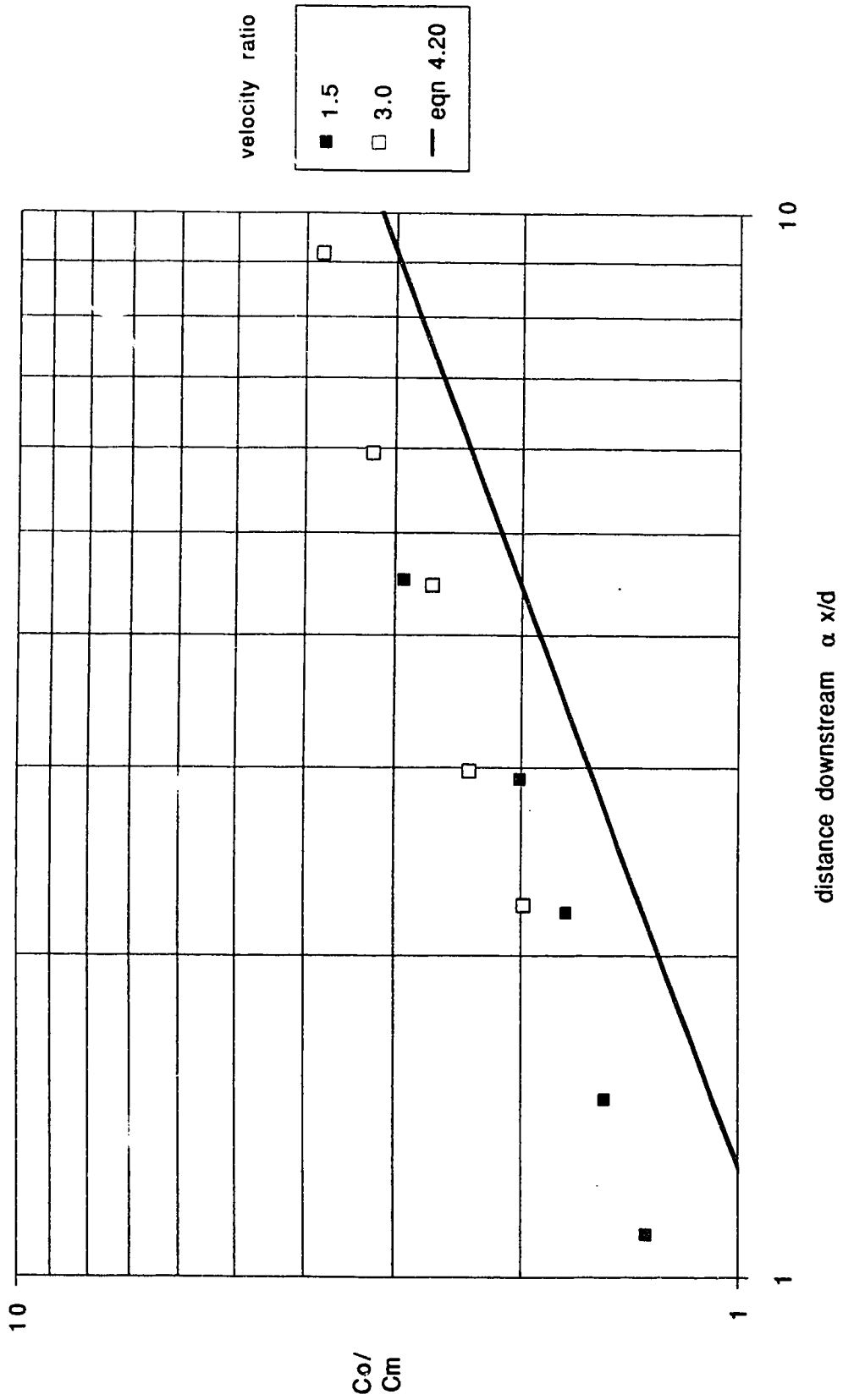


Figure 5.17 Centreline dilution ratios for 100 series runs ( $D/d = 15.7$ )

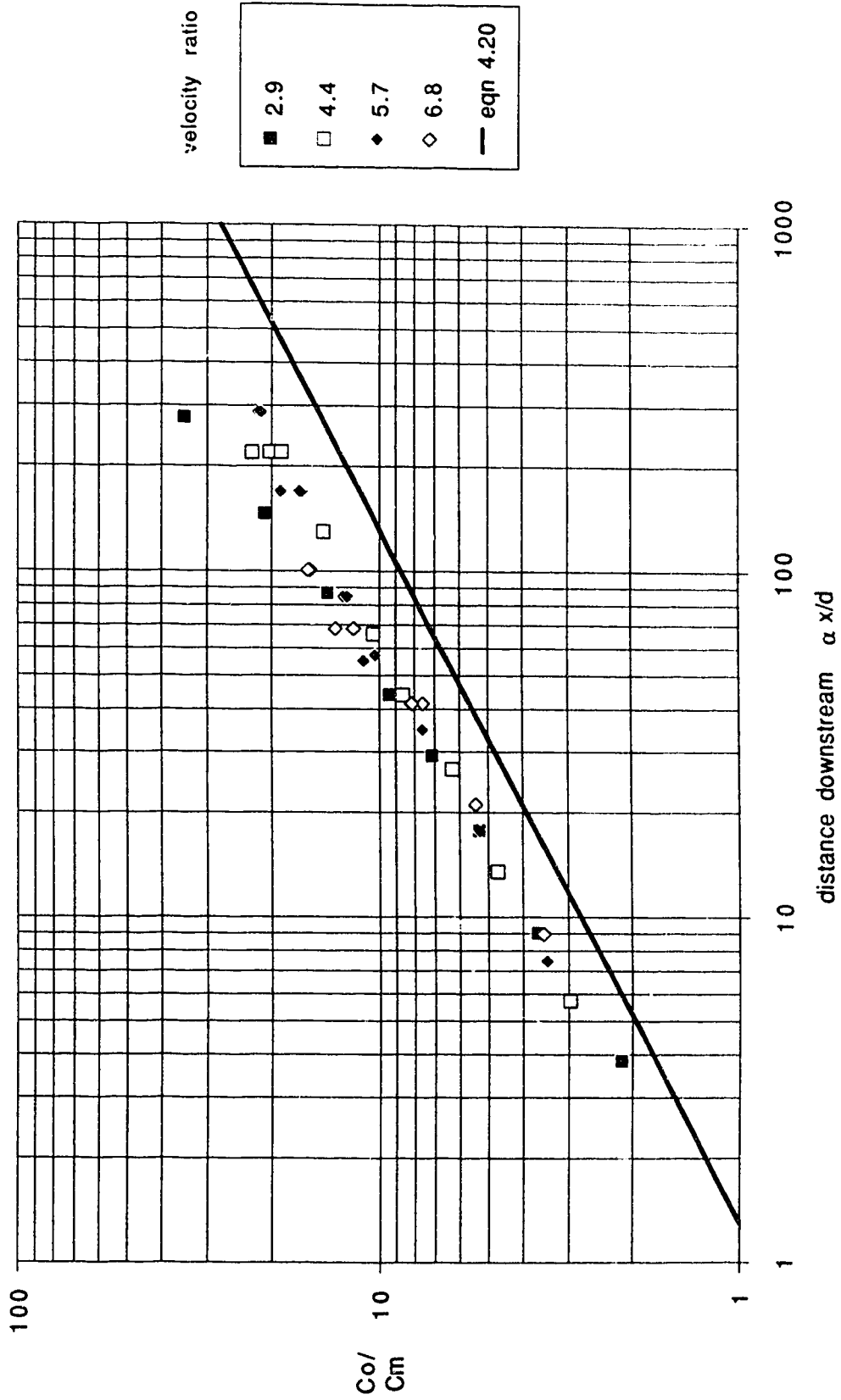
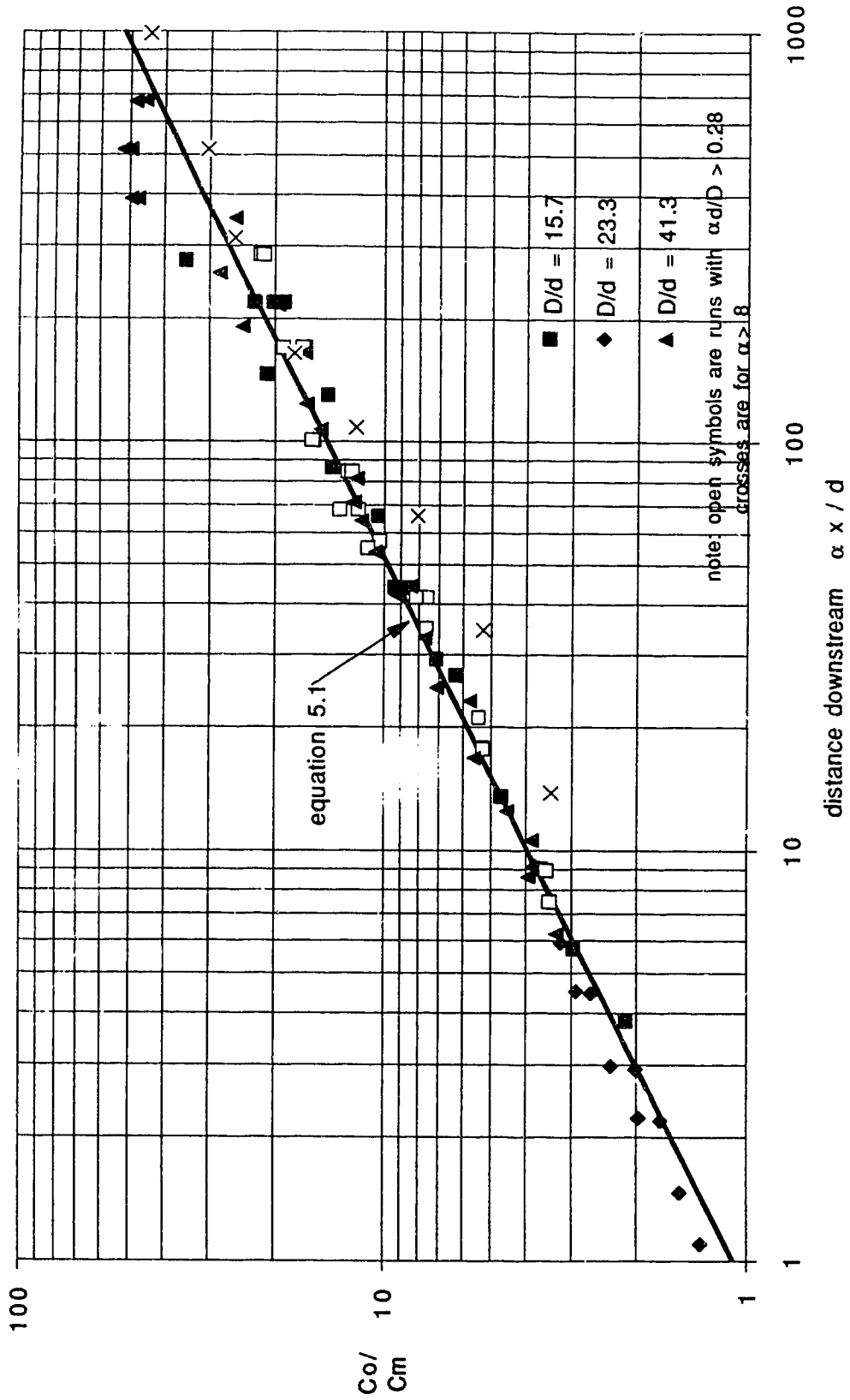


Figure 5.18 Centreline dilution ratios - all runs



1000

100

10

1

distance downstream  $\alpha x / d$

$C_o / C_m$



Figure 5.19 Comparison of field and laboratory dilution ratios

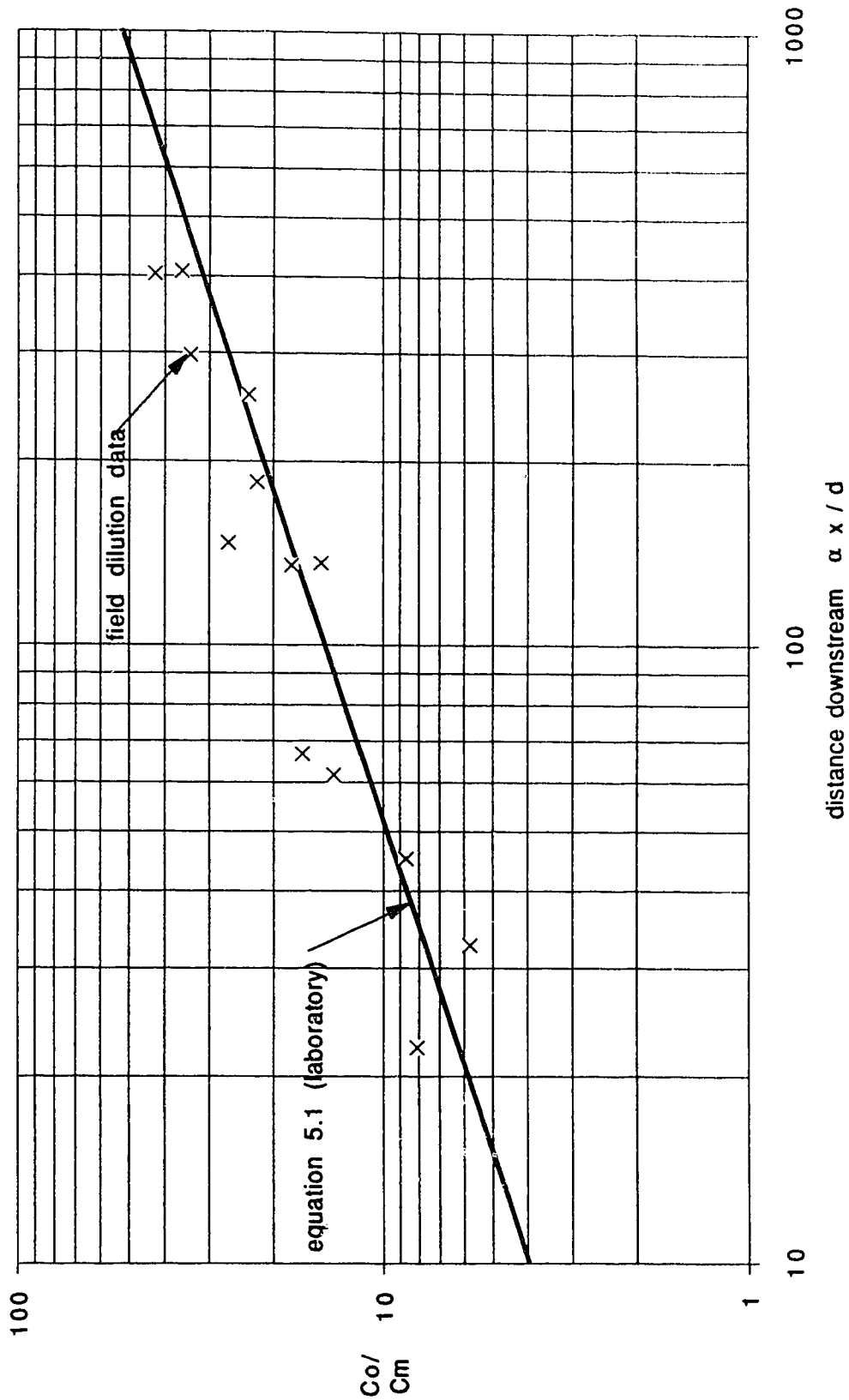


Figure 5.20 Concentration centreline locations

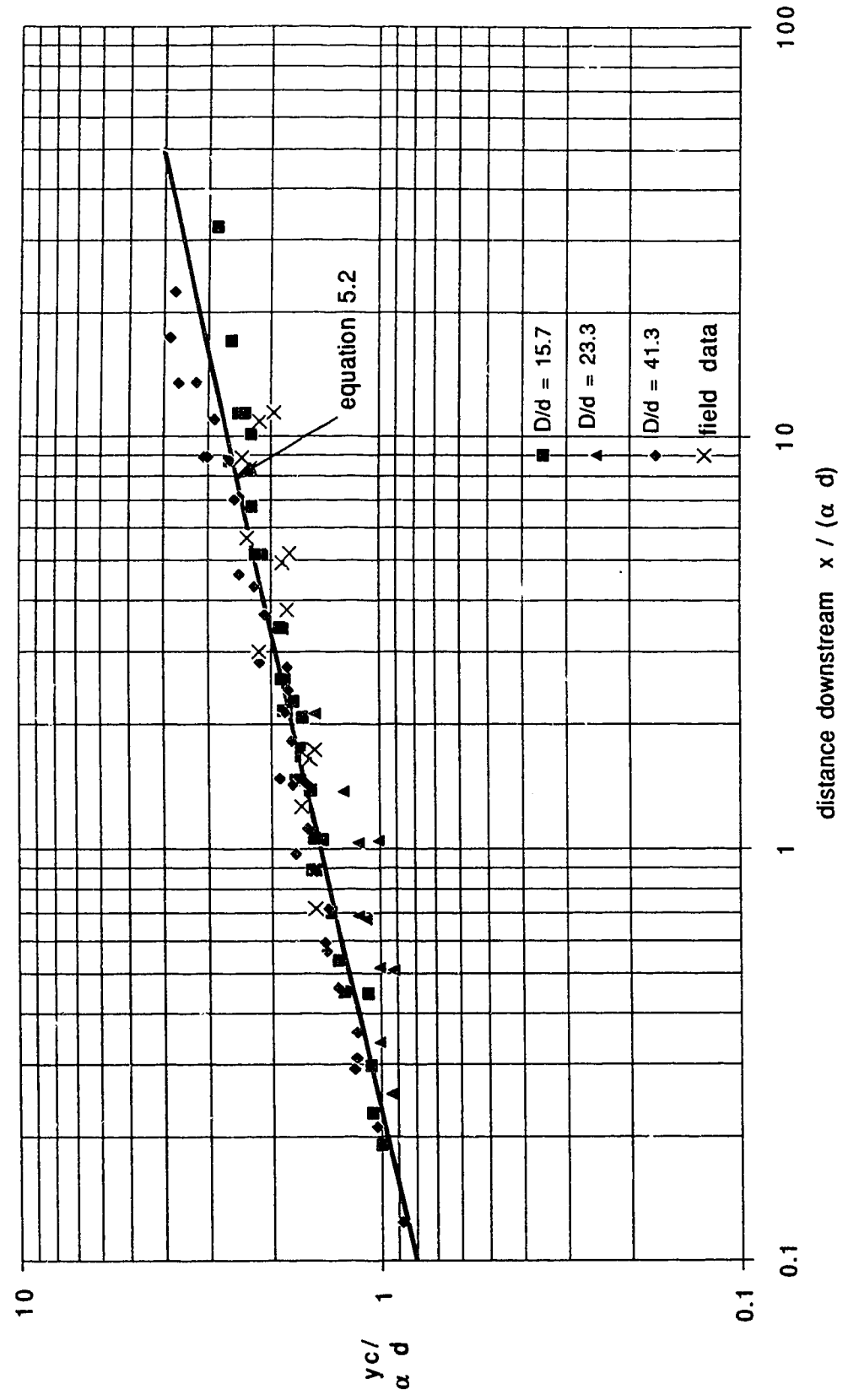


Figure 5.21 Jet width: data for 50% concentration location

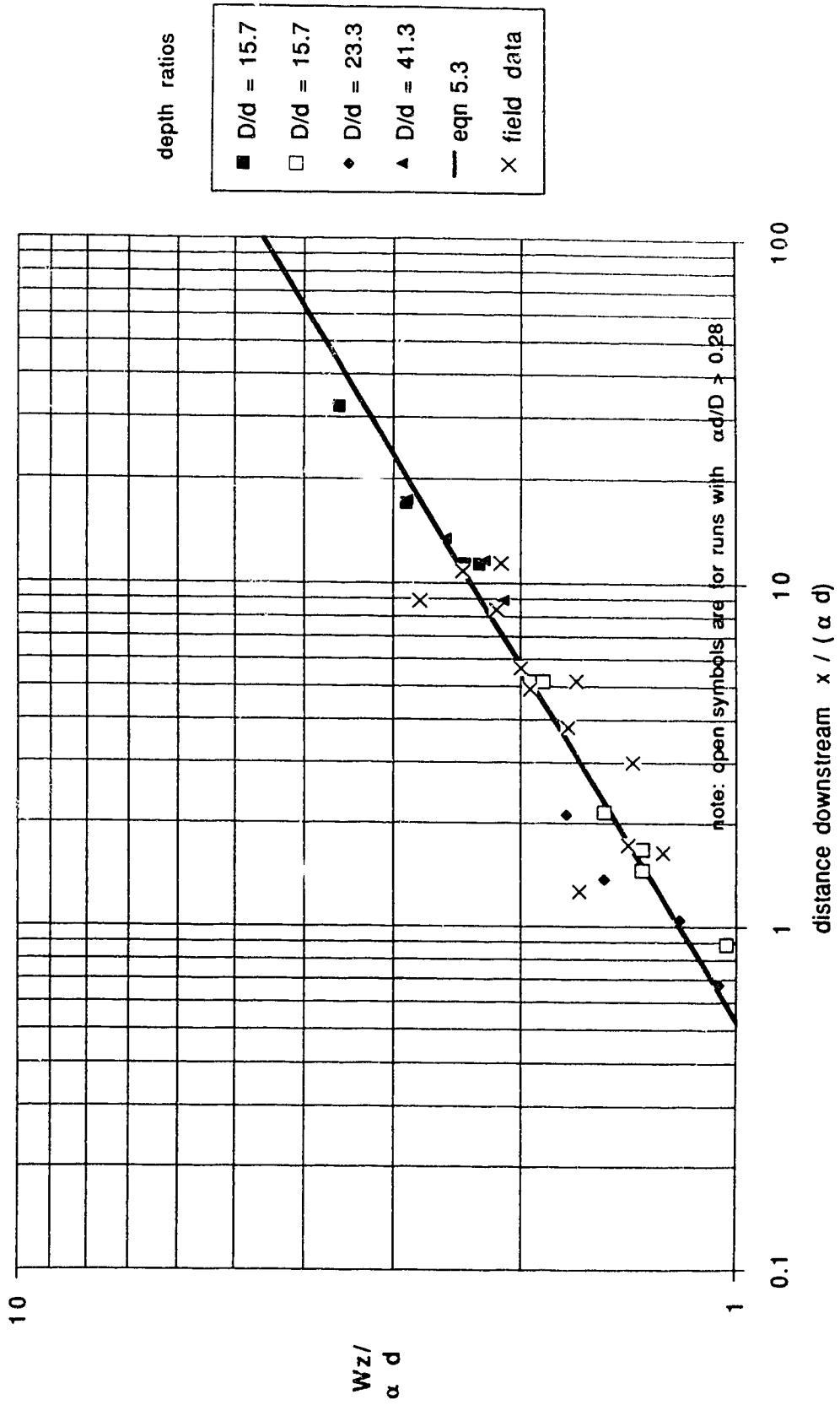


Figure 5.22 Jet width along curvilinear axis

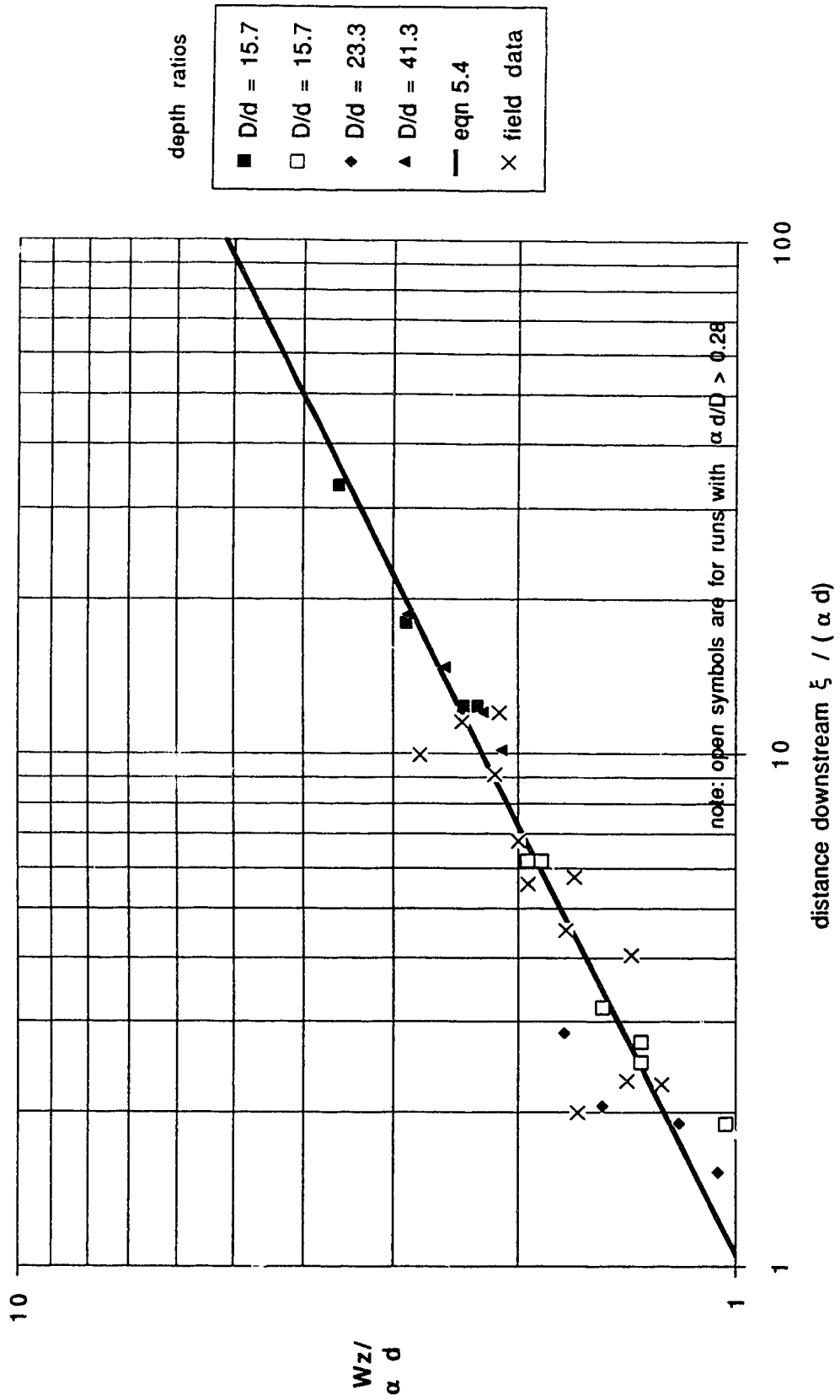


Figure 5.23 Jet thickness data for 50% concentration location

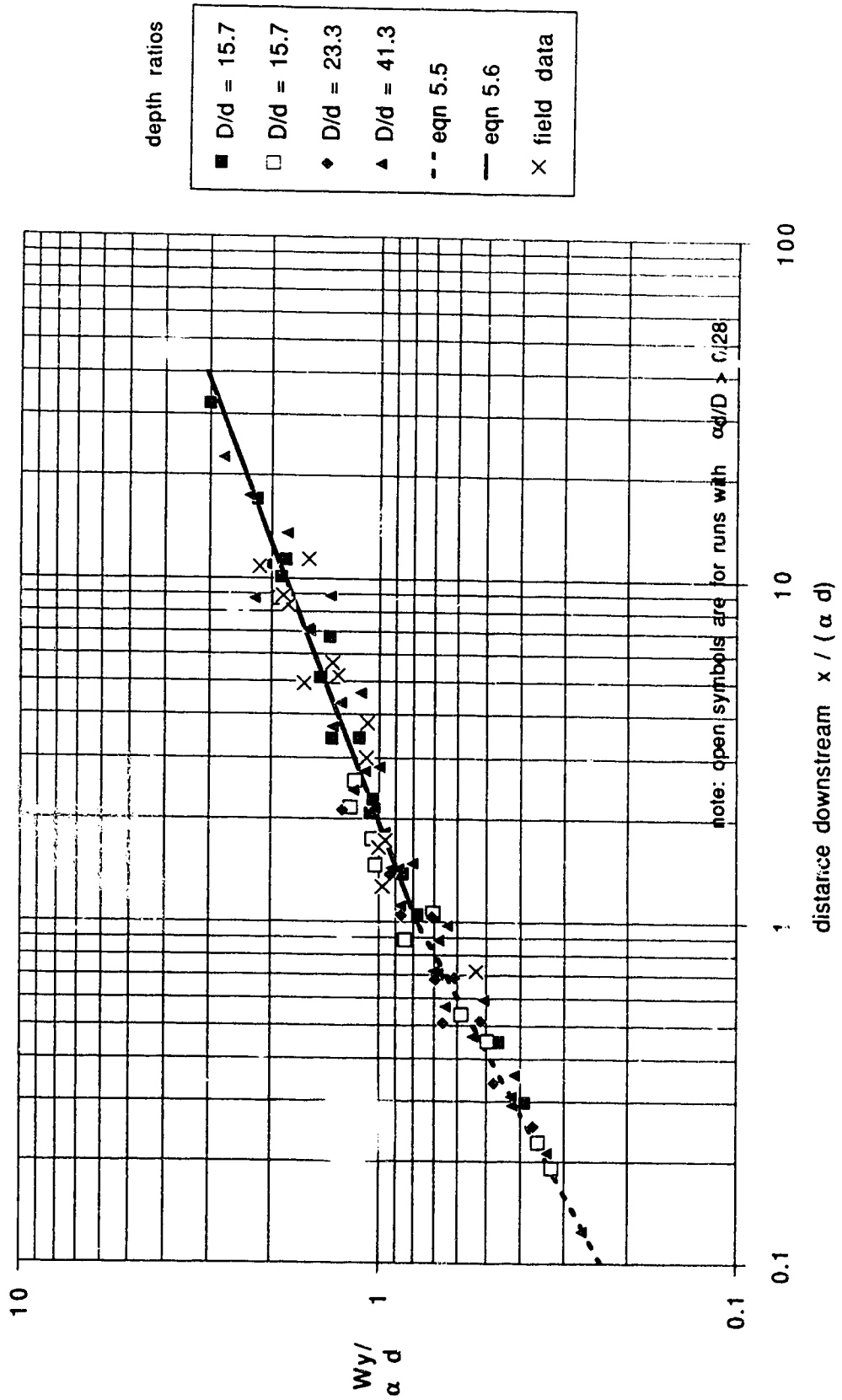
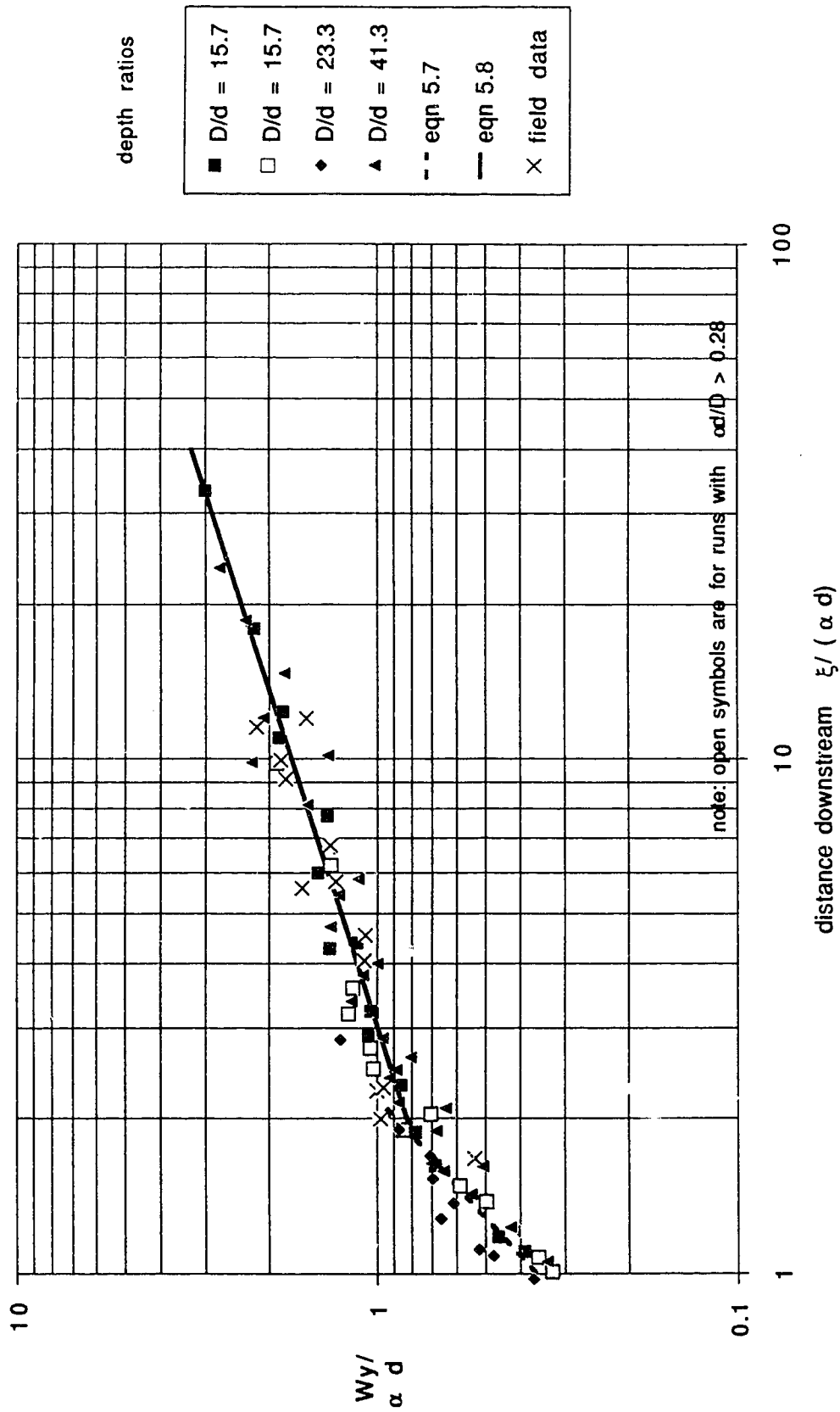


Figure 5.24 Jet thickness along curvilinear axis



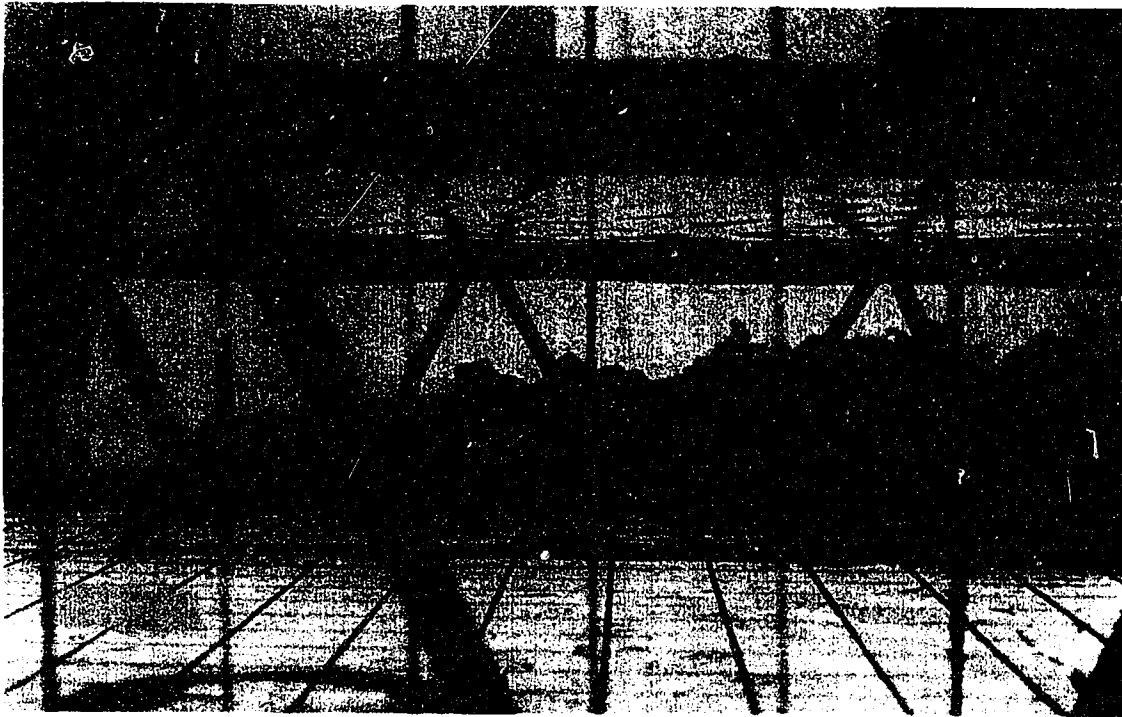


Plate 5.1 Side view of Run 101 (exposure time = 1/30 s)

$$D/d = 15.7; \quad \alpha = 2.9; \quad \frac{\alpha d}{D} = 0.19.$$

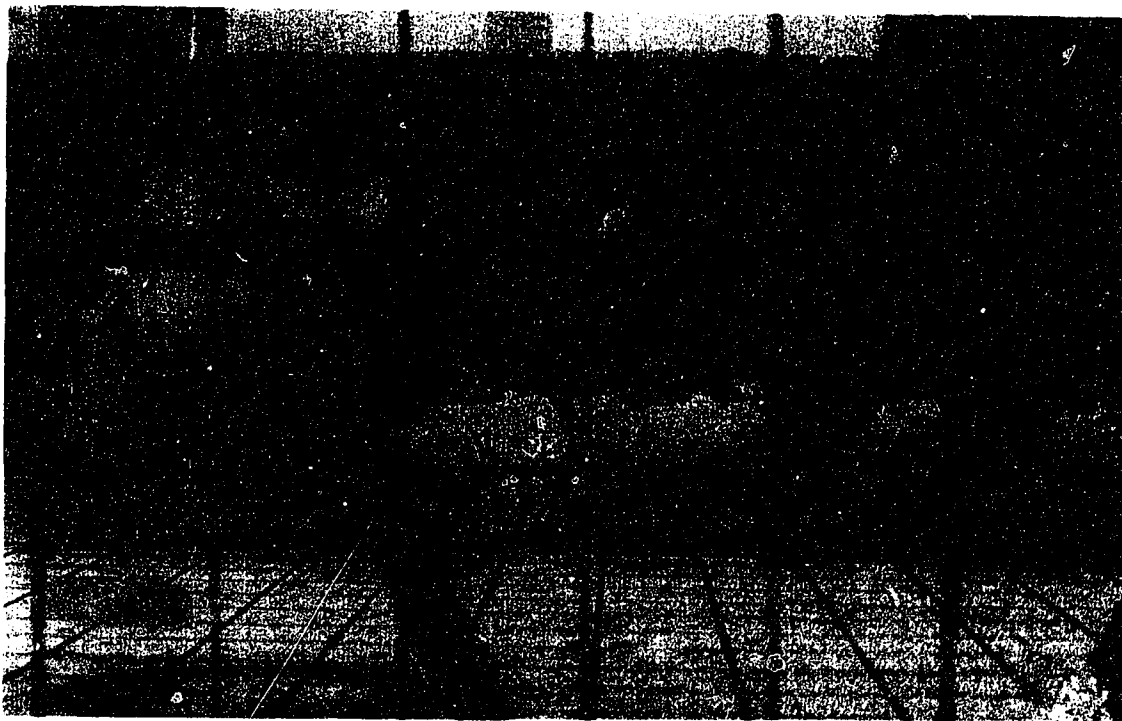


Plate 5.2 Side view of Run 104 (exposure time = 1/30 s)

$$D/d = 15.7; \quad \alpha = 6.8; \quad \frac{\alpha d}{D} = 0.43.$$

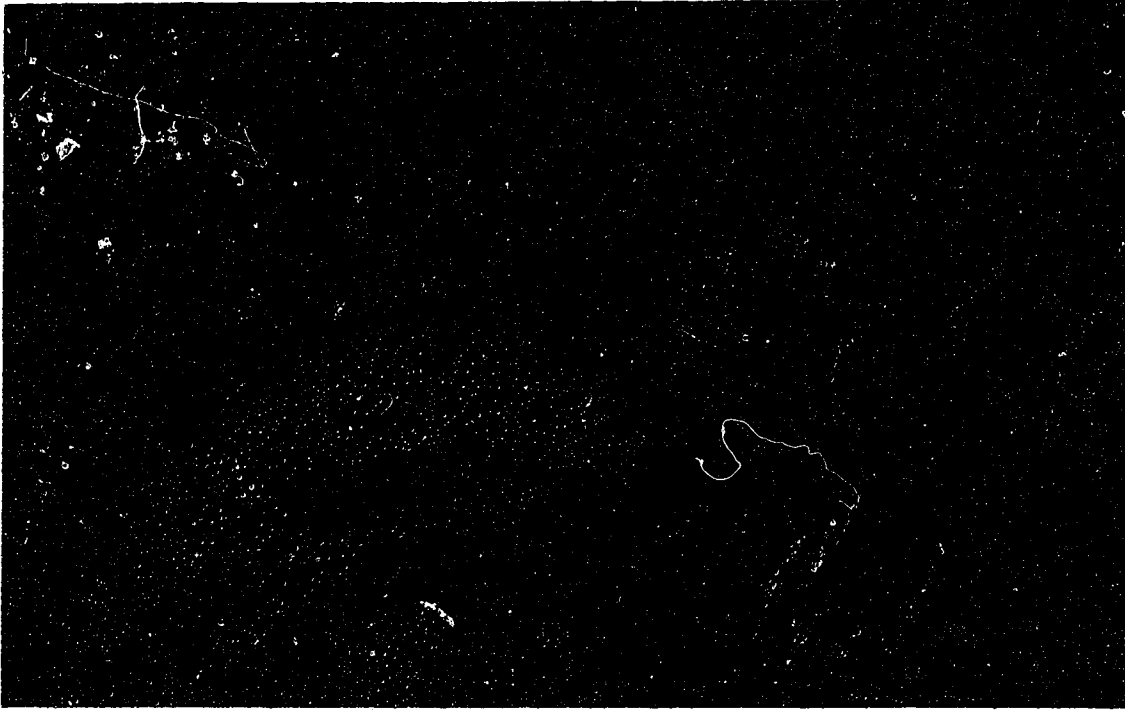


Plate 5.3 Plan view of Run 102 (exposure time = 1/15 s)

$$D/d = 15.7; \quad \alpha = 4.4; \quad \frac{\alpha d}{D} = 0.28.$$

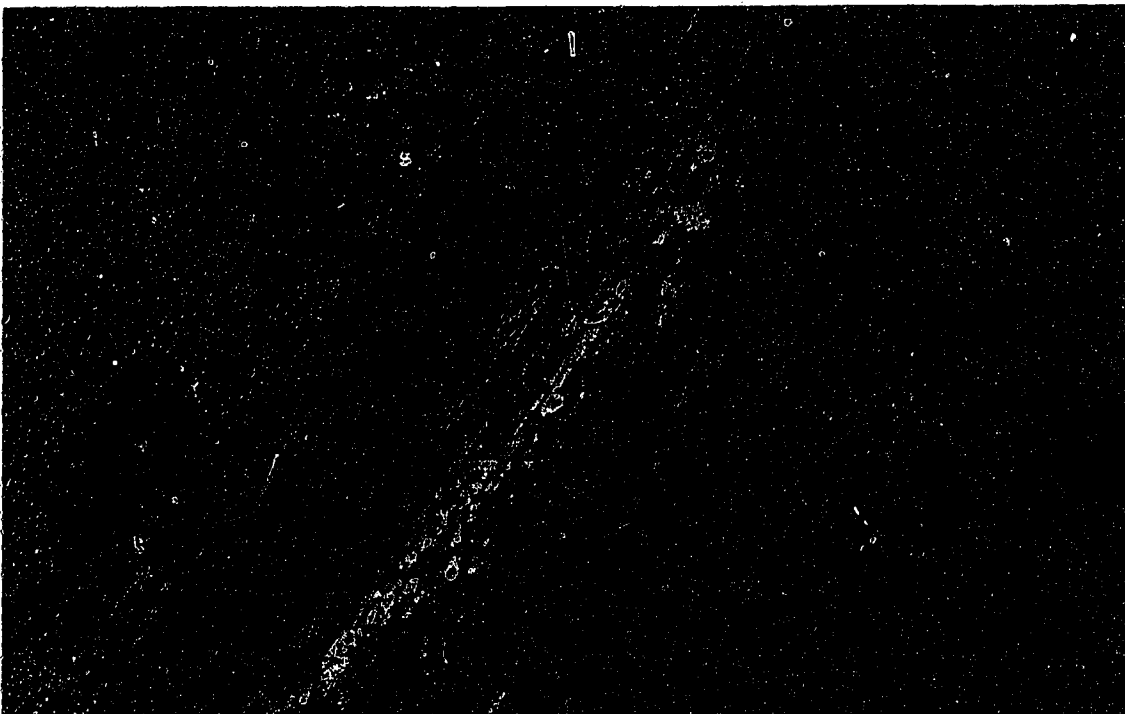


Plate 5.4 Plan view of Run 102 (exposure time = 15 s)

$$D/d = 15.7; \quad \alpha = 4.4; \quad \frac{\alpha d}{D} = 0.28.$$



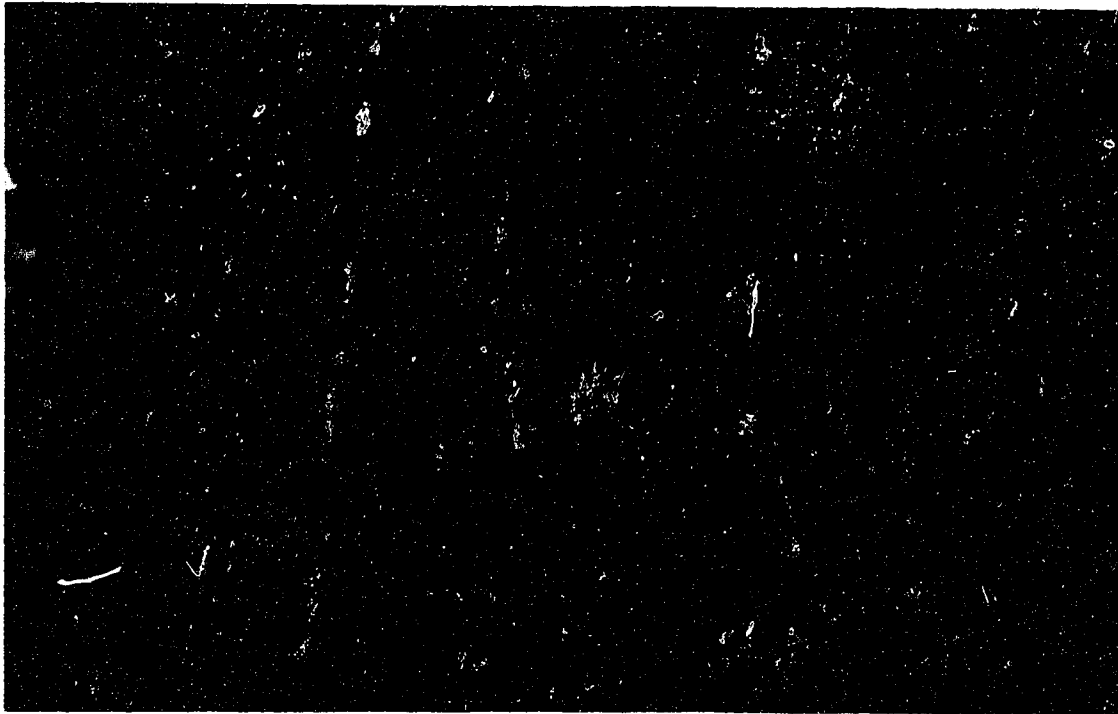


Plate 5.5 Plan view of Run 104 (exposure time = 1/15 s)

$$D/d = 15.7; \quad \alpha = 6.8; \quad \frac{\alpha d}{D} = 0.43.$$

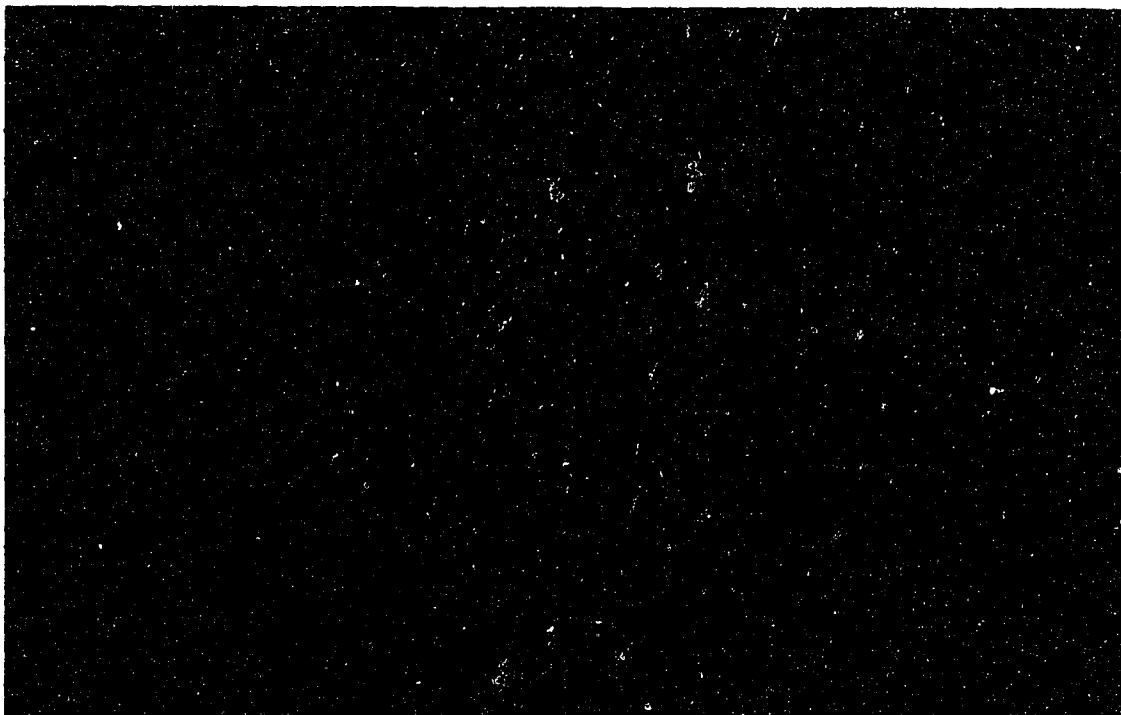


Plate 5.6 Plan view of Run 104 (exposure time = 15 s)

$$D/d = 15.7; \quad \alpha = 6.8; \quad \frac{\alpha d}{D} = 0.43.$$

## CHAPTER 6

### FAR FIELD CONSIDERATIONS

#### 6.1 General

When an effluent is discharged to a river, it is affected by a number of phenomena which tend to disperse the discharge. These processes have been described in a number of previous works (Beltaos, 1978a; Fischer et al, 1979; Hodgson, 1981; Elhadi et al, 1984). The processes include:

**advection:** the transport of the effluent by the current;

**molecular diffusion:** the movement of matter on a molecular scale; these random motions move the effluent from areas of high concentration to areas of low concentration;

**turbulent diffusion:** the movement of material due to the random fluctuations of a fluid in turbulent flow; these motions also move material from areas of high concentration to areas of low concentration; in rivers, the dispersive effect of turbulent diffusion is far more significant than that due to molecular diffusion;

**differential advection:** the spreading due to the uneven advection of the effluent which results from the non-uniform velocity distributions in rivers; these velocity distributions can occur due to the vertical velocity gradient (due to the stream bed alone or in conjunction with an ice cover) and the transverse velocity gradient which would occur due to the varying depths across the river's cross-section;

**secondary currents:** lateral circulation of the flow, as a river progresses downstream, can be induced by the shape of the cross-section or the curvature of the channel's alignment; these currents can advect the effluent across the width of the river; and

**momentum and buoyancy effects:** the momentum of the effluent discharge will enhance the initial mixing of an effluent discharge; buoyancy has the potential to either increase or decrease the initial mixing and the vertical diffusion of the effluent; most far field analyses assume that buoyancy effects are negligible; means to determine if this is the case have been presented in Chapter 2.

Because of the number and complexity of these processes, it is difficult to precisely model river mixing. However, using a number of simplifying assumptions, a variety of mixing models have been developed.

The **mixing zone** is the far field region of predominate interest in most receiving stream assessments. Various subregions within the mixing zone have been identified by Gowda (1980 and 1984). In his work, Gowda presented the concepts of the **mixing length**, the **crossing length**, the **limited use zone** and the **zone of passage**. He developed relations and procedures for determining these for the particular case of a point source bank outfall. The basis for Gowda's work was the analytical solution for two dimensional dispersion of a steady state point source effluent discharge to a receiving stream.

In this chapter, the analytical solutions to the dispersion equations for point source and line source outfalls are reviewed. These equations are then used to provide simple expressions to describe the various regions in the mixing zone. The concentration distribution equations for both outfall types are used to extend Gowda's analysis and to provide simple expressions for the mixing length, the crossing length and the boundaries of the limited use zone (Figure 6.1).

## 6.2 Transverse Mixing Equations

### 6.2.1 The Governing Equation

The general three dimensional pollutant conservation equation for turbulent flows in streams can be written as (Holley et al 1972; Elhadi et al, 1984):

$$\frac{\partial C}{\partial t} + \frac{\partial uC}{\partial x} + \frac{\partial vC}{\partial y} + \frac{\partial wC}{\partial z} = \frac{\partial}{\partial x} (D_m + \epsilon_x) \frac{\partial C}{\partial x} + \frac{\partial}{\partial y} (D_m + \epsilon_y) \frac{\partial C}{\partial y} + \frac{\partial}{\partial z} (D_m + \epsilon_z) \frac{\partial C}{\partial z} \quad (6.1)$$

where: C is the concentration at some point (x, y, z, t),  
 t is the time,  
 x is the distance downstream of the outfall,  
 y is the distance above the river bed,  
 z is the lateral distance from the reference bank,  
 u is the local velocity in the x direction,  
 v is the local velocity in the y direction,

$w$  is the local velocity in the  $z$  direction,  
 $D_m$  is the molecular diffusion coefficient,  
 $\epsilon_x$ ,  $\epsilon_y$  and  $\epsilon_z$  are the turbulent diffusion coefficients  
 in the  $x$ ,  $y$  and  $z$  directions, respectively.

On the left hand side of equation (6.1) are the unsteady term and the three convective terms. On the right hand side of the equation are the three diffusive terms which account for both molecular and turbulent diffusion. This equation can be simplified by making the following assumptions:

a) the flow conditions of both the streamcourse and the effluent discharge are steady (i.e.  $\frac{\partial(\quad)}{\partial t} = \frac{\partial C}{\partial t} = 0$ ).

b) the velocity along any streamline (the  $x$  direction) is constant (i.e.  $\frac{\partial u}{\partial x} = 0$ ); thus:

$$\frac{\partial uC}{\partial x} = u \frac{\partial C}{\partial x} + C \frac{\partial u}{\partial x} = u \frac{\partial C}{\partial x}$$

c) the effluent is evenly distributed over the depth in any vertical in the flow and there are no vertical velocity components in the flow (i.e.  $\frac{\partial C}{\partial y} = 0$ ;  $v = 0$ ;  $\frac{\partial v}{\partial y} = 0$ ); thus:

$$\frac{\partial vC}{\partial y} = v \frac{\partial C}{\partial y} + C \frac{\partial v}{\partial y} = 0$$

d) there are no transverse velocity components in the flow (i.e.  $w = 0$ ;  $\frac{\partial w}{\partial z} = 0$ ); thus:

$$\frac{\partial wC}{\partial z} = w \frac{\partial C}{\partial z} + C \frac{\partial w}{\partial z} = 0$$

e) the flow is turbulent (with turbulent diffusion being much greater than molecular diffusion):

$$\epsilon_x \gg D_m; \epsilon_y \gg D_m; \text{ and } \epsilon_z \gg D_m$$

f) the change in longitudinal diffusion is small relative to the convective transport of the effluent.

$$\frac{\partial}{\partial x} (\epsilon_x) \frac{\partial C}{\partial x} \ll u \frac{\partial C}{\partial x}$$

With these six simplifying assumptions, equation (6.1) becomes:

$$u \frac{\partial C}{\partial x} = \frac{\partial}{\partial z} (\epsilon_z) \frac{\partial C}{\partial z} \quad (6.2)$$

If both sides of equation (6.2) are integrated with respect to the depth of flow, the depth-averaged concentrations (which can be represented by a sample taken at any depth at a location  $(x, z)$  if assumption c holds true) can be used. Thus:

$$h u \frac{\partial C}{\partial x} = \frac{\partial}{\partial z} (h \epsilon_z) \frac{\partial C}{\partial z} \quad (6.3)$$

Yotsukura and Cobb (1972) introduced the streamtube concept as a means to simplify the analysis. This concept overcomes the analytical difficulties which arise when a river has widths which vary over the distance downstream. With the streamtube concept, the distance across the river is expressed in terms of the cumulative flow rate  $(q)$ :

$$q = \int_0^z h u dz \quad (6.4)$$

Since: 
$$\frac{\partial}{\partial z} = \frac{\partial q}{\partial z} \frac{\partial}{\partial q} = h u \frac{\partial}{\partial q} \quad (6.5)$$

equation (6.3) becomes:

$$\frac{\partial C}{\partial x} = \frac{\partial}{\partial q} h^2 u \epsilon_z \frac{\partial C}{\partial q} \quad (6.6)$$

Yotsukura and Cobb also indicated that the diffusion factor ( $K = h^2 u \epsilon_z$ ) is reasonably constant across any channel cross-section. Thus:

$$\frac{\partial C}{\partial x} = K \frac{\partial^2 C}{\partial q^2} \quad (6.7)$$

Equation (6.7) is a second-order linear homogeneous partial differential equation. Solutions to equation (6.7) for both point source and line source outfalls have been presented in the literature (Yotsukura and Cobb, 1972; Fischer et al, 1979; Elhadi et al, 1984).

Equation (6.7) and its solutions are powerful in that they provide efficient means for the analysis of river mixing. However, some of the assumptions made earlier do not hold true for all rivers. River cross sections are rarely rectangular. As a result, the assumption of a constant diffusion factor is not likely to hold true. Recognizing this, much of the subsequent work has been directed toward developing equation (6.6) further for numerical solution. Yotsukura and Sayre (1976) extended the analysis by introducing an orthogonal curvilinear coordinate system which would account for the curvature of bends in a stream. If:

$$m_x = 1 \pm \frac{z}{r} \quad (6.8)$$

where the sign depends on the direction of the bend, then equation (6.6) becomes:

$$\frac{\partial C}{\partial x} = \frac{\partial}{\partial q} m_x h^2 u \epsilon_z \frac{\partial C}{\partial q} \quad (6.9)$$

Equation (6.9) must be solved numerically. Yotsukura and Sayre (1976) presented an explicit finite difference algorithm for solving this equation. This formulation is relatively easy to program but suffers from numerical instability unless a very short distance interval is used (Beltaos, 1978a).

Lau and Krishnappan (1981) presented an implicit finite difference solution for equation (6.9). They concluded that including the cross-sectional variation of  $m_x h^2 u$  can be very important in determining the concentration distribution. They also concluded that the inclusion of the longitudinal variation of the cross-sectional average of  $\epsilon_z$  is more important than considering  $\epsilon_z$  as variable across the width of the section.

Leimkuhler et al (1975) presented one of the earlier papers on finite element method solution procedures for river mixing. Solanki (1988) solved equation (6.9) using two new higher order upwinding elements in conducting his finite element analyses. He found these models to be superior to using standard linear finite elements or implicit finite difference schemes. Although the models promise powerful simulation capabilities for river mixing, the computational requirements for the finite element models were high.

### **6.2.2 General Dispersion Equations**

The governing equation (6.9) for the mixing of an effluent in a receiving stream has been developed in the



previous section and by several others (Yotsukura and Sayre, 1976; Lau and Krishnappan, 1981; Elhadi et al, 1984). Yotsukura and Cobb (1972) and Yotsukura and Sayre (1976) indicated that, if the quantity  $m_x \epsilon_z u h^2$  has about the same value over the width of the stream and the channel is essentially prismatic, then equation (6.9) can be simplified to account for differential advection:

$$\frac{\partial C}{\partial x} = m_x \epsilon_z u h^2 \frac{\partial^2 C}{\partial q^2} = D_z \frac{\partial^2 C}{\partial q^2} \quad (6.10)$$

where  $D_z$  is the constant of diffusion.

If the diffusion coefficient ( $\epsilon_z$ ) is assumed to be constant within the mixing zone, the constant of diffusion can be written in terms of the average properties for the cross section to account for differential advection:

$$D_z = \psi \overline{\epsilon_z} U H^2 = E_z U H^2 \quad (6.11)$$

where:  $\psi$  is the shape velocity factor,

$\overline{\epsilon_z}$  is the reach-averaged diffusion coefficient,

$U$  is the average velocity for the cross section,

$H$  is the average depth for the cross section, and

$E_z$  is the transverse mixing (or dispersion)

coefficient for the reach.

In the foregoing, the shape velocity factor is given by:

$$\psi = \frac{1}{Q} \int_0^Q m_x \left(\frac{u}{U}\right)^2 \left(\frac{h}{H}\right)^3 dq \quad (6.12)$$

where  $Q$  is the total flow rate.

Typical values for  $\psi$  range from 1.0 for straight wide rectangular channels to 3.0 or more for highly sinuous streams (Beltaos, 1978a).

### 6.2.3 Dispersion Downstream of Point Source Outfalls

The concentration at any point downstream of a point source outfall can be determined by an analytical solution to the differential equation (6.10). For the case of the steady state discharge of a neutrally buoyant effluent at a point in a stream flowing at a steady rate, the concentration at any point downstream can be determined by:

$$C(\phi, p) = C_b + \frac{C_a}{\sqrt{4\pi\phi}} \sum_{n=-\infty}^{n=+\infty} \left[ \exp\left\{-\frac{(2n+p_s-p)^2}{4\phi}\right\} + \exp\left\{-\frac{(2n+p_s+p)^2}{4\phi}\right\} \right] \quad (6.13)$$

where:  $C(\phi, p)$  is the concentration at location  $(\phi, p)$ ,

$C_b$  is the background concentration,

$C_a$  is the increase in the mixed concentration due to the effluent:

$$\left( C_a = \frac{C_e Q_e}{Q + Q_e} \approx \frac{C_e Q_e}{Q} \text{ where } Q_e \ll Q \right),$$

$C_e$  is the effluent concentration,

$Q_e$  is the effluent discharge rate,

$Q$  is the stream flow rate,

$\phi$  is the dimensionless distance downstream:

$$\left( \phi = \frac{E_z x}{W^2 U} \right),$$

$W$  is the width of the stream,

$n$  is the number of reflections or images,

$p$  is the location of the point in the cross section, expressed in terms of relative flow (i.e.  $p=q/Q$ ) with respect to the near bank, and  $p_s$  is the outfall location in the cross section.

With equation (6.13), the concentrations can be in mg/L or any other set of consistently used units. The reference bank for the dimensionless distances  $p$ ,  $p_s$  and  $q$  must also be used consistently.

Equation (6.13) requires the use of a small number of images (e.g. it is usually only necessary to evaluate the summation from, say,  $n=-3$  to  $n=+3$ ). The equation is applicable for distances of  $x > W$  downstream of the outfall. This restriction is due to a mathematical constraint; the computed concentration approaches  $\infty$  as  $x$  approaches 0.

#### 6.2.4 Dispersion Downstream of Line Source Outfalls

The concentration at any point downstream of a line source outfall can be determined by an analytical solution to the differential equation (6.10). For the case of the steady state discharge of a neutrally buoyant effluent from a line source extending a width ( $w$ ) from the bank into a stream flowing at a steady discharge, the concentration at any point downstream can be estimated by:

$$C(\xi, p) = C_b + \frac{C_a}{2w} \sum_{n=-\infty}^{n=+\infty} \left[ \operatorname{erf} \left\{ \frac{(2n+w-p)}{\sqrt{2\xi}} \right\} + \operatorname{erf} \left\{ \frac{(2n+w+p)}{\sqrt{2\xi}} \right\} \right] \quad (6.14)$$

where:  $w$  is the outfall width (i.e from  $p = 0$  to  $p = w$ ), and  
 $\xi$  is the dimensionless distance downstream:

$$\left( \xi = 2 \phi = \frac{2 E_z x}{W^2 U} \right).$$

If we use the mixing length ( $X_m$ ) for a bank outfall as the reference length:

$$X_m = \frac{W^2 U}{2 E_z} \quad (6.15)$$

the expression:

$$\xi = 2 \phi = \frac{x}{X_m} \quad (6.16)$$

can be used to provide additional meaning to the denominator of the  $\text{erf}\{ \}$  terms in equation (6.14). Using equation (6.16), equation (6.14) can be rewritten as:

$$C(x, p) = C_b + \frac{C_a}{2 w} \sum_{n=-\infty}^{n=+\infty} \left[ \text{erf} \left\{ \frac{(2n+w-p)}{\sqrt{2x/X_m}} \right\} + \text{erf} \left\{ \frac{(2n+w+p)}{\sqrt{2x/X_m}} \right\} \right] \quad (6.17)$$

In equation (6.17), locations where  $x/X_m < 1$  are within the mixing zone and the concentrations are  $C(x, p) \geq C_b$ ; for locations where  $x/X_m > 1$ ,  $C(x, p) = C_m = C_b + C_a$  (i.e. the river is completely mixed).

### 6.3 Mixing Lengths

In assessing the environmental impact of an effluent discharge, one of the most important hydraulic characteristics of the streamcourse is the distance from the outfall to the cross section where the effluent has become completely mixed. This distance is called the **mixing length** ( $X_m$ ). The

reach of the river from the outfall to the section where mixing is complete is called the **mixing zone**. Within the mixing zone the variations in concentration are great and, for a proper environmental assessment, should be considered in detail.

The analytical equations (6.13) and (6.17) for concentrations within the mixing zone can be manipulated to determine the mixing length for point source and line source outfalls. The criterion to determine when "complete" mixing has occurred can be defined by the concentrations at the bank furthest from the outfall (i.e. where  $p = 1$ ). When the concentration at the far bank becomes some significant portion (e.g. 90%, 95% or 99%) of the completely mixed concentration, then for practical purposes, the effluent can be considered to be completely mixed. Using this definition (i.e.  $1 - \delta$ , where  $\delta$  is the mixing criterion), simple mixing length equations can be developed.

### 6.3.1 Point Source Discharges

Using the concentration equation for point source outfalls (6.13), the ratio of the far bank concentration to the completely mixed concentration can be written for a finite number of terms as:

$$\frac{C(\phi, p) - C_b}{C_a} = \text{criteria} = 1 - \delta =$$

$$\frac{1}{\sqrt{4\pi\phi}} \sum_{n=-k}^{n=+k} \left[ \exp \left\{ \frac{-(2n+p_s-p)^2}{4\phi} \right\} + \exp \left\{ \frac{-(2n+p_s+p)^2}{4\phi} \right\} \right] \quad (6.18)$$

Expanding the summation terms in equation (6.18) to determine the concentrations at the far bank (i.e.  $p = 1$ ) using the terms from  $n = -2$  to  $n = +2$  (i.e.  $k = 2$ ) gives:

$$\begin{aligned} n = -2: & \quad \exp \left\{ \frac{-(p_s-5)^2}{4\phi} \right\} + \exp \left\{ \frac{-(p_s-3)^2}{4\phi} \right\} \\ n = -1: & \quad \exp \left\{ \frac{-(p_s-3)^2}{4\phi} \right\} + \exp \left\{ \frac{-(p_s-1)^2}{4\phi} \right\} \\ n = 0: & \quad \exp \left\{ \frac{-(p_s-1)^2}{4\phi} \right\} + \exp \left\{ \frac{-(p_s+1)^2}{4\phi} \right\} \\ n = +1: & \quad \exp \left\{ \frac{-(p_s+1)^2}{4\phi} \right\} + \exp \left\{ \frac{-(p_s+3)^2}{4\phi} \right\} \\ n = +2: & \quad \exp \left\{ \frac{-(p_s+3)^2}{4\phi} \right\} + \exp \left\{ \frac{-(p_s+5)^2}{4\phi} \right\} \end{aligned}$$

In the above,  $p_s$  must be less than 1 (it will likely be less than 0.5). The results of this evaluation will show that  $4\phi$  will have a maximum value of about 2 as  $x$  approaches the end of the mixing zone. As a result, the  $\exp\{ \}$  terms with  $(p_s-5)$  and  $(p_s+5)$  in the numerator will approach 0. Therefore, these terms and all other terms generated by higher values of  $n$  can be ignored. The use of  $k = 2$  is sufficiently accurate to determine the characteristic lengths for point source outfalls. Thus, by summing the significant terms of the expansion, the characteristic length equation is:

criteria =  $1 - \delta =$

$$\frac{\exp\left\{\frac{-(p_s-3)^2}{4\phi}\right\} + \exp\left\{\frac{-(p_s-1)^2}{4\phi}\right\} + \exp\left\{\frac{-(p_s+1)^2}{4\phi}\right\} + \exp\left\{\frac{-(p_s+3)^2}{4\phi}\right\}}{\sqrt{\pi\phi}} \quad (6.19)$$

By setting the value for the criteria to 0.90, 0.95 or 0.99, equation (6.19) can be solved iteratively to develop a simple mixing length equation of the form:

$$X_m = \frac{\phi_m W^2 U}{E_z} \quad (6.20)$$

Thus, the mixing length for a point source outfall is a function of the hydraulic properties of the river (as indicated in equation 6.20) and the location of the outfall (Table 6.1).

From the values of the dimensionless mixing length ( $\phi_m$ ) indicated in Table 6.1, it can be seen that the mixing length for a mid-stream outfall is 1/4 that for a bank outfall. However, note that if the outfall is not exactly at mid-stream the mixing length rapidly increases. The precise siting of a point source outfall is crucial if the enhanced mixing suggested by the equations is to be achieved. Siting an outfall within 5% of mid-stream would result in reducing the mixing length to about 60% of that for a bank outfall (Figure 6.2).

The dimensionless mixing length for the 99% criterion is about 45% greater than that for the 95% criterion. This

indicates that the mixing in the latter part of the mixing zone is gradual. Also note that, for a bank outfall, a 98.5% criterion would give a  $\phi_m$  value of about 0.5. This supports equation (6.15) and the validity of the assumption to ignore the terms for  $n > 2$ .

### 6.3.2 Line Source Discharges

Using the concentration equation for line source outfalls (6.17), the ratio of the far bank concentration to the completely mixed concentration can be written for a finite number of terms as:

$$\frac{C(X,p) - C_b}{C_a} = \text{criteria} = 1 - \delta =$$

$$\frac{1}{2w} \sum_{n=-k}^{n=+k} \left[ \operatorname{erf} \left\{ \frac{(2n+w-p)}{\sqrt{2x/X_m}} \right\} + \operatorname{erf} \left\{ \frac{(2n+w+p)}{\sqrt{2x/X_m}} \right\} \right] \quad (6.21)$$

Expanding the summation terms in equation (6.21) for  $n = -2$  to  $n = +2$  (i.e.  $k = 2$ ) to determine the concentrations at the the far bank (i.e.  $p = 1$ ) gives:

$$\begin{aligned} n = -2: & \quad \operatorname{erf} \left\{ \frac{w-5}{\sqrt{2x/X_m}} \right\} + \operatorname{erf} \left\{ \frac{w-3}{\sqrt{2x/X_m}} \right\} = -\operatorname{erf} \left\{ \frac{5-w}{\sqrt{2x/X_m}} \right\} - \operatorname{erf} \left\{ \frac{3-w}{\sqrt{2x/X_m}} \right\} \\ n = -1: & \quad \operatorname{erf} \left\{ \frac{w-3}{\sqrt{2x/X_m}} \right\} + \operatorname{erf} \left\{ \frac{w-1}{\sqrt{2x/X_m}} \right\} = -\operatorname{erf} \left\{ \frac{3-w}{\sqrt{2x/X_m}} \right\} - \operatorname{erf} \left\{ \frac{1-w}{\sqrt{2x/X_m}} \right\} \\ n = 0: & \quad \operatorname{erf} \left\{ \frac{w-1}{\sqrt{2x/X_m}} \right\} + \operatorname{erf} \left\{ \frac{w+1}{\sqrt{2x/X_m}} \right\} = -\operatorname{erf} \left\{ \frac{1-w}{\sqrt{2x/X_m}} \right\} + \operatorname{erf} \left\{ \frac{1+w}{\sqrt{2x/X_m}} \right\} \\ n = +1: & \quad \operatorname{erf} \left\{ \frac{w+1}{\sqrt{2x/X_m}} \right\} + \operatorname{erf} \left\{ \frac{w+3}{\sqrt{2x/X_m}} \right\} = \operatorname{erf} \left\{ \frac{1+w}{\sqrt{2x/X_m}} \right\} + \operatorname{erf} \left\{ \frac{3+w}{\sqrt{2x/X_m}} \right\} \end{aligned}$$



$$n = +2: \quad \epsilon = \operatorname{erf}\left\{\frac{w+3}{\sqrt{2x/X_m}}\right\} + \operatorname{erf}\left\{\frac{w+5}{\sqrt{2x/X_m}}\right\} = \operatorname{erf}\left\{\frac{3+w}{\sqrt{2x/X_m}}\right\} + \operatorname{erf}\left\{\frac{5+w}{\sqrt{2x/X_m}}\right\}$$

In the above,  $w$  must be less than 1 (it will likely be less than 0.5). It is also known that the maximum value for  $\sqrt{2x/X_m}$  is  $\sqrt{2}$  which occurs as  $x$  approaches the mixing length. As a result,  $\operatorname{erf}(\ )$  terms with  $(5-w)$  and  $(5+w)$  in the numerator will approach a value of 1 and will cancel each other. Therefore, these terms and all other terms generated by higher values of  $n$  can be ignored. Using  $k = 2$ , and by noting that  $2\phi = x/X_m$ , the characteristic lengths of the mixing zone for line source outfalls can be determined from:

$$\text{criteria} = 1 - \delta = \frac{\operatorname{erf}\left\{\frac{3+w}{\sqrt{4\phi}}\right\} - \operatorname{erf}\left\{\frac{3-w}{\sqrt{4\phi}}\right\} + \operatorname{erf}\left\{\frac{1+w}{\sqrt{4\phi}}\right\} - \operatorname{erf}\left\{\frac{1-w}{\sqrt{4\phi}}\right\}}{w} \quad (6.22)$$

Equation (6.22) can be solved iteratively to determine the dimensionless mixing length ( $\phi_m$ ) for various outfall widths (Table 6.2). From these values it can be seen that the mixing length for a line source outfall is not much different from that for a point source outfall until  $w$  and  $p_s$  exceed 0.2 (Figure 6.2). When a line source outfall extends to midstream, the mixing length is only about 10% to 15% less than that for a point source bank outfall. Thus, the value of diffuser outfalls is not for shortening the mixing length (it is more for establishing the initial dilution).

#### 6.4 Crossing Lengths

For some distance downstream of an outfall, the concentrations along the shoreline opposite of the outfall bank will remain at background levels. As the plume spreads, the concentrations along this bank eventually begin to increase. The distance from the outfall section to the point where a noticeable increase exists is defined as the **crossing length**.

The characteristic length equations (6.19) and (6.22) can be used to determine the crossing lengths for point source outfalls and line source outfalls. The criterion to determine when the plume has crossed to the far bank (i.e.  $p = 1$ ) is when concentrations increase to some percentage (e.g. 10%, 5% or 1%) of the completely mixed concentration (Figure 6.1). Using this definition (i.e.  $\delta$ , where  $\delta$  is the mixing criterion), simple relations for the crossing length can be developed.

##### 6.4.1 Point Source Discharges

For point source outfalls, the crossing length ( $X_c$ ) can be determined from:

$$X_c = \frac{\phi_c W^2 U}{E_z} \quad (6.23)$$

Using an iterative solution to the characteristic length equation (6.19), values for the dimensionless crossing length ( $\phi_c$ ) can be determined (Table 6.3 and Figure 6.2). From these

values, it can be seen that the crossing length for a mid-stream outfall is 1/4 that for a bank outfall (note that crossing lengths for point sources near mid-stream are not as sensitive to the outfall location as mixing lengths are). It can also be seen that varying the crossing length criterion changes the crossing lengths significantly as concentrations are increasing slowly in the vicinity of the crossing point. From tables 6.1 and 6.3 it can be seen (using the 5% and the 95% criteria) that the crossing length is about 15% of the mixing length.

#### **6.4.2 Line Source Discharges**

The crossing length can be determined for line source outfalls by using an iterative solution to equation (6.22). Values of  $\phi_c$  for line sources of various width ( $w$ ), extending from the bank toward the far shore of the stream, were determined for the three levels of criteria (Table 6.4). From these, it can be seen that crossing lengths for line source outfalls are greater than those for point source outfalls. Again, varying the crossing criterion changes the crossing length significantly. Examination of tables 6.2 and 6.4 indicates that the crossing length to mixing length ratio of 0.15, determined above for point source outfalls, holds approximately true for line sources with widths ( $w$ ) up to 0.2. For outfalls extending further toward midstream, the ratio appears to be about 0.1.

## 6.5 Limited Use Zone Concepts

### 6.5.1 Definitions

The limited use zone (LUZ) concept was developed by Gowda (1980 and 1984) as a means to facilitate water quality management in receiving streams. The LUZ concept enables a detailed rational examination of the mixing zone and allows the development of consistent policy and assessment procedures. The LUZ concept can facilitate the interaction between the government and those applying for a permit to discharge an effluent to a receiving stream.

The mixing zone comprises the zone of passage (ZOP) and the limited use zone (figures 6.1 and 6.2). The **zone of passage** is the portion of the width of the river (in terms of flow) where pollutant concentrations must be within the limits set out in the receiving stream guidelines (i.e.  $C < C_g$ ). This portion of the river must be preserved as a suitable habitat for biota. It is necessary to maintain the ZOP in the receiving stream throughout the year in order to ensure the safe movement of various species of fishes during their migration periods. The ZOP should be maintained even during non-migratory periods so that the enroute environment is not degraded.

The **limited use zone** is the portion of the width of the river (in terms of flow) where pollutant concentrations may exceed receiving stream guidelines (i.e.  $C > C_g$ ). The maximum width (i.e.  $p_1 = q_1/Q$ ) of the LUZ is a matter of other

environmental considerations and should be designated as water resource management policy. A width in the range of  $0.2 < p_1 < 0.4$  has been considered reasonable in other applications (Gowda, 1980; SIEC, 1985; Saskatchewan Environment and Public Safety, 1988).

The longitudinal extent of the LUZ must also be controlled. The **LUZ length** ( $X_s$ ) is the distance from the outfall to the point where the shoreline concentration reaches the receiving stream guideline ( $C_s$ ). The **maximum permissible LUZ length** ( $X_p$ ) is prescribed considering both existing and future water users along the bank (Figure 6.1).

#### 6.5.2 LUZ Boundary (Critical Point) Constraints

The first consideration in outlining the LUZ is to determine the critical point. For a designated LUZ boundary ( $p_1 = q_1/Q$ ), the concentration profile along the boundary will be at background levels until the plume has spread to the boundary (Figure 6.3). The concentration will then gradually increase until it reaches a maximum and afterward it will gradually decrease to the mixed concentration as the end of the mixing zone is approached. The **critical point** is the point along the LUZ boundary where the concentration profile reaches a maximum value. Here, the derivative of the concentration profile is zero (i.e.  $dC/dx = 0$ ). The concentration at the critical point is called the **critical concentration** ( $C_i$ ) and distance from the outfall to the critical point is called the **critical length** ( $X_1$ ).

### Point Source Bank Outfalls

For a point source outfall discharging to a stream with no background concentrations, equation (6.13) can be written to consider a finite number of terms:

$$C(\phi, p) = \frac{C_a}{\sqrt{4\pi\phi}} \sum_{n=-k}^{n=+k} \left[ \exp\left\{\frac{-(2n+p_s-p)^2}{4\phi}\right\} + \exp\left\{\frac{-(2n+p_s+p)^2}{4\phi}\right\} \right] \quad (6.24)$$

If equation (6.16) is used to define the distance downstream, the  $n = -1$  to  $n = +1$  terms for a point source bank outfall ( $p_s = 0$ ) along the LUZ boundary (i.e.  $p = p_1$ ) can be written:

$$C(X, p_1) = \frac{C_a}{\sqrt{2\pi}} \sqrt{\frac{X_m}{x}} \left[ \exp\left(\frac{-(2-p_1)^2}{2x/X_m}\right) + 2\exp\left(\frac{-p_1^2}{2x/X_m}\right) + \exp\left(\frac{-(2+p_1)^2}{2x/X_m}\right) \right] \quad (6.25)$$

Equation (6.25) does not include terms for  $n = 2$  or higher. It should be noted that  $x/X_m$  is always less than 1 in the mixing zone and that  $p_1$  would usually be in the range of 0.2 to 0.4. Thus,  $\exp(\ )$  terms with  $(4-p_1)$  and  $(4+p_1)$  in the numerator approach 0. Therefore, using  $k = 1$  (as in equation 6.25) would be sufficiently accurate to determine critical point conditions.

Gowda (1980 and 1984) developed relations for the critical concentration and the critical length for a point source bank outfall.

$$C_1 = \frac{C_a}{2.066 p_1} \quad (6.26)$$

$$X_1 = p_1^2 X_m = \frac{p_1^2 W^2 U}{2 E_z} \quad (6.27)$$

These can be derived using equation (6.24) and the  $n = 0$  terms only. Confining the analysis to  $n = 0$  is reasonable as equation (6.27) indicates that the maximum value for  $x/X_m$  would be 0.16 (for  $p_1 = 0.4$ ). Examination of equation (6.25) again indicates that  $\exp(\ )$  terms with  $(2-p_1)$  and  $(2+p_1)$  in the numerator would also approach 0. Thus, equations (6.26) and (6.27) are sufficiently accurate for application.

### **Line Source Outfalls**

Expressions to determine the critical concentration and the critical length can be developed for line source outfalls from equation (6.17). Writing the equation for the case where there is no background concentration, using the  $n = 0$  terms only, the concentration along the LUZ boundary is:

$$C(x, p_1) = \frac{C_a}{2 w} \left[ \operatorname{erf} \left\{ \frac{(w-p_1)}{\sqrt{2x/X_m}} \right\} + \operatorname{erf} \left\{ \frac{(w+p_1)}{\sqrt{2x/X_m}} \right\} \right] \quad (6.28)$$

The use of the  $n = 0$  terms only is reasonable assuming that the critical length for line source outfalls is similar to that for point source bank outfalls. Examination of equation (6.17) indicates that terms for  $k = 1$  and higher approach a value of 1 and cancel each other.

The maximum concentration along the LUZ boundary ( $p = p_1$ ) would occur when  $dC/dX = 0$ . Differentiating equation (6.28) gives (note:  $\frac{d}{dx} \operatorname{erf}(u) = \frac{2}{\sqrt{\pi}} \exp(-u^2) \frac{du}{dx}$  and

$\operatorname{erf}(-u) = -\operatorname{erf}(u)$ ):

$$0 = \frac{C_a}{\sqrt{\pi} w} \left[ \exp\left\{\frac{-(p_1+w)^2}{2 x/X_m}\right\} \left\{\frac{-(p_1+w)\sqrt{X_m/2}}{2 x^{3/2}}\right\} - \exp\left\{\frac{-(p_1-w)^2}{2 x/X_m}\right\} \left\{\frac{-(p_1-w)\sqrt{X_m/2}}{2 x^{3/2}}\right\} \right]$$

Eliminating  $\frac{-C_a}{\sqrt{\pi} w} \left\{\frac{\sqrt{X_m/2}}{2 x^{3/2}}\right\}$  gives:

$$\exp\left\{\frac{-(p_1+w)^2}{2 x/X_m}\right\} \{p_1+w\} = \exp\left\{\frac{-(p_1-w)^2}{2 x/X_m}\right\} \{p_1-w\}$$

Taking the natural logarithm of both sides gives:

$$\frac{-(p_1+w)^2}{2 x/X_m} + \ln(p_1+w) = \frac{-(p_1-w)^2}{2 x/X_m} + \ln(p_1-w)$$

Expanding the squared terms and rearranging again will allow the critical length to be determined:

$$x_1 = \frac{2 p_1 w X_m}{\beta} = \frac{p_1 w w^2 U}{E_z \beta} \quad (6.29)$$

where:  $\beta$  is the outfall width factor ( $\beta = \ln(p_1+w) - \ln(p_1-w)$ )

The concentration at the critical point can be estimated by using the value for  $X_1/X_m$  indicated in equation (6.29) in equation (6.28):

$$C_1 = \frac{C_a}{2w} \left[ \operatorname{erf}\left\{\frac{(p_1+w) \beta^{1/2}}{2\sqrt{p_1 w}}\right\} - \operatorname{erf}\left\{\frac{(p_1-w) \beta^{1/2}}{2\sqrt{p_1 w}}\right\} \right] \quad (6.30)$$

### 6.5.3 Shoreline Concentration Constraints

For point source bank outfalls and line source outfalls, the concentration along the shoreline of the outfall bank is a maximum at the outfall. The concentration decreases along



the shoreline until it reaches the mixed concentration at the downstream end of the mixing zone (Figure 6.3). At some point along the shoreline the concentration should reach the receiving stream guideline concentration ( $C_s$ ). The distance from the outfall to this point is defined as the **LUZ length** ( $X_s$ ).

### **Point Source Bank Outfalls**

Although Gowda did address the LUZ length in his work, he did not develop an explicit relation for this length. A simplified expression can be developed for the LUZ length by writing the first two terms ( $n = 1$ ) of equation (6.24) for the concentrations along the shoreline (i.e.  $p = 0$ ):

$$C(x,0) = \frac{2 C_a}{\sqrt{2\pi}} \sqrt{\frac{X_m}{x}} \left[ \exp\{0\} + 2 \exp\left\{-\frac{2 X_m}{x}\right\} \right] \quad (6.31)$$

Ignoring the second  $\exp\{ \}$  term in equation (6.31) as being small gives:

$$C(x,0) = \frac{C_a}{1.253} \sqrt{\frac{X_m}{x}} \quad (6.32)$$

By definition, when  $C(x,0) = C_s$ ,  $x = X_s$ . Thus, the LUZ length can be estimated by:

$$X_s = \left(\frac{C_a}{C_s}\right)^2 \frac{X_m}{1.571} = \left(\frac{C_a}{C_s}\right)^2 \frac{W^2 U}{\pi E_z} \quad (6.33)$$

Substituting  $X_s/X_m$  from equation (6.33) into equation (6.31) results in:

$$C = \frac{C_a}{1.253} \sqrt{\frac{X_m}{x}} \left[ 1 + 2 \exp\left\{-\pi \left(\frac{C_s}{C_a}\right)^2\right\} \right] \quad (6.34)$$

$$X_s = \left(\frac{C_a}{C_s}\right)^2 \frac{X_m}{1.571} \left[1 + 2 \exp \left\{-\pi \left(\frac{C_s}{C_a}\right)^2\right\}\right]^2 \quad (6.35)$$

Equation (6.35) is a more accurate approximation for the LUZ length.

#### **Line Source Outfalls**

There appears to be no way in which to derive an explicit relation for the LUZ length of a line source outfall. To find the LUZ length, one can derive an approximate equation for the shoreline concentrations from equation (6.17):

$$C(x,0) = \frac{C_a}{w} \left[ \operatorname{erf} \left\{ \frac{2+w}{\sqrt{2x/X_m}} \right\} + \operatorname{erf} \left\{ \frac{w}{\sqrt{2x/X_m}} \right\} - \operatorname{erf} \left\{ \frac{2-w}{\sqrt{2x/X_m}} \right\} \right] \quad (6.36)$$

To determine  $X_s$ , equation (6.36) must be solved iteratively to determine the distance ( $x$ ) where  $C(x,0) = C_s$ .

#### **6.5.4 Determining Allowable Effluent Concentration**

Once the critical point concentration ( $C_1$ ) has been determined, it is compared with the receiving stream guideline ( $C_s$ ). If it is greater, an adjusted allowable effluent concentration ( $C_{ea}$ ) can be estimated from:

$$C_{ea} = C_e \frac{C_s}{C_1} \quad (6.37)$$

If the estimated LUZ length ( $X_s$ ) is longer than the permissible LUZ length ( $X_p$ ) then the adjusted allowable effluent concentration can be estimated from:

$$C_{ea} = C_e \frac{C_s}{C(X_p, 0)} \quad (6.38)$$

## 6.6 Conclusions

a) The **mixing length** ( $X_m$ ) for a point source outfall is dependent on the hydraulic properties of the river and the location of the outfall. Although the mixing length for a mid-stream outfall is 1/4 that for a bank outfall, a mid-stream outfall would have to be precisely sited in order to achieve the enhanced degree of mixing suggested. Siting a point source outfall within 5% of mid-stream would result in a mixing length which is about 60% of that for a bank outfall.

b) The mixing lengths achieved by line source outfalls are about 10% to 15% less than that for a point source bank outfall. Thus, the value of a diffuser outfall is not for shortening the mixing length. It is for establishing initial dilution.

c) Mixing lengths are sensitive to the criteria used to define them. This is because mixing occurs more slowly in the latter portion of the mixing zone.

d) The **crossing length** ( $X_c$ ) for a point source outfall is about 15% of the mixing length. The crossing length to mixing length ratio is sensitive to the criterion used.

e) The crossing lengths for line source outfalls are greater than those for point source outfalls. The ratio of the crossing length to the mixing length varies from about 0.15 for short diffusers to about 0.1 for diffusers extending to near mid-stream.

f) The analytical equations for the mixing of point source and line source effluent discharges can be manipulated to quantify the extent of various subregions within the mixing zone. One of these subregions, the **limited use zone**, is of considerable importance for receiving stream analysis.

g) If a **maximum permissible width** ( $p_1$ ) is set for the limited use zone, then the location (the **critical length** -  $X_1$ ) of the **critical point** and the **critical concentration** ( $C_1$ ) at that point can be determined explicitly for both point source bank outfalls and line source outfalls.

h) An explicit expression to determine the distance that the limited use zone extends along the shoreline (the **LUZ length** -  $X_s$ ) can be derived for point source bank outfalls. This distance must be determined by iteration for line source outfalls.

Table 6.1 Dimensionless mixing lengths ( $\Phi_m$ ) for point source outfalls

Location of Outfall ( $p_s$ )	Mixing Criterion		
	0.90	0.95	0.99
0.0 (bank)	0.304	0.374	0.537
0.1	0.298	0.369	0.532
0.2	0.282	0.352	0.515
0.3	0.250	0.320	0.483
0.4	0.186	0.255	0.418
0.5 (mid-stream)	0.076	0.093	0.134

Table 6.2 Dimensionless mixing lengths ( $\Phi_m$ ) for line source outfalls

Width of Outfall ( $w$ )	Mixing Criterion		
	0.90	0.95	0.99
0.0 (bank)	0.304	0.374	0.537
0.1	0.302	0.372	0.536
0.2	0.297	0.367	0.531
0.3	0.288	0.358	0.522
0.4	0.275	0.346	0.510
0.5 (mid-stream)	0.258	0.328	0.493
0.6	0.234	0.305	0.469
0.7	0.203	0.273	0.437
0.8	0.157	0.227	0.391
0.9	0.087	0.151	0.314
1.0	0.0	0.0	0.0

Table 6.3 Dimensionless crossing lengths ( $\phi_c$ ) for point source outfalls

Location of Outfall ( $p_3$ )	Crossing Criterion		
	0.10	0.05	0.01
0.0 (bank)	0.066	0.055	0.039
0.1	0.061	0.050	0.035
0.2	0.049	0.040	0.027
0.3	0.036	0.029	0.021
0.4	0.025	0.021	0.015
0.5 (mid-stream)	0.017	0.014	0.010

Table 6.4 Dimensionless crossing lengths ( $\phi_c$ ) for line source outfalls

Width of Outfall ( $w$ )	Crossing Criterion		
	0.10	0.05	0.01
0.0 (bank)	0.066	0.055	0.039
0.1	0.064	0.053	0.036
0.2	0.060	0.048	0.034
0.3	0.052	0.041	0.028
0.4	0.043	0.033	0.022
0.5 (mid-stream)	0.033	0.025	0.016
0.6	0.023	0.017	0.011
0.7	0.014	0.010	0.006
0.8	0.007	0.005	0.003
0.9	0.002	0.001	0.001
1.0	0.0	0.0	0.0

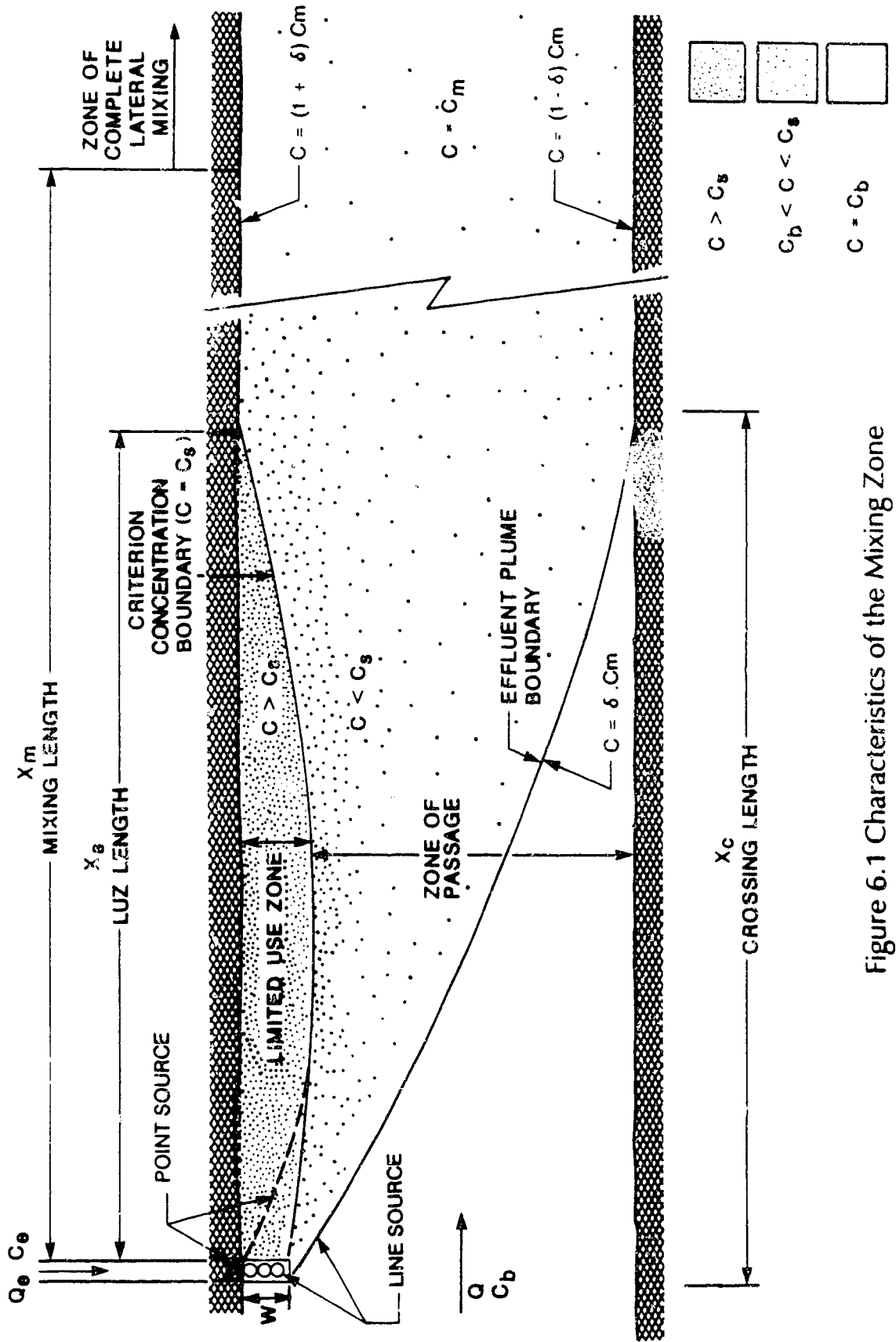
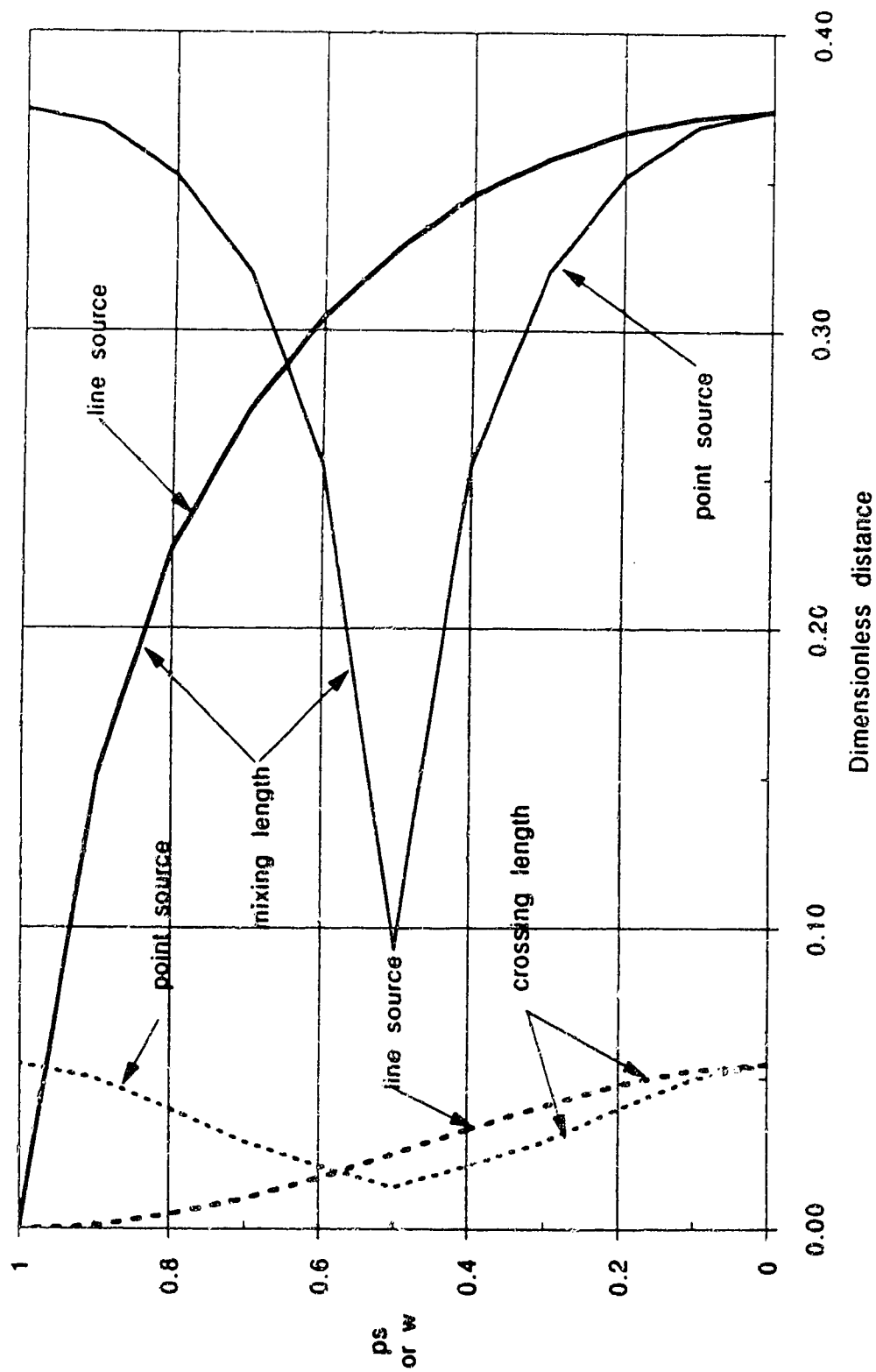


Figure 6.1 Characteristics of the Mixing Zone

Figure 6.2 Dimensionless mixing and crossing lengths - 95% and 5% criteria





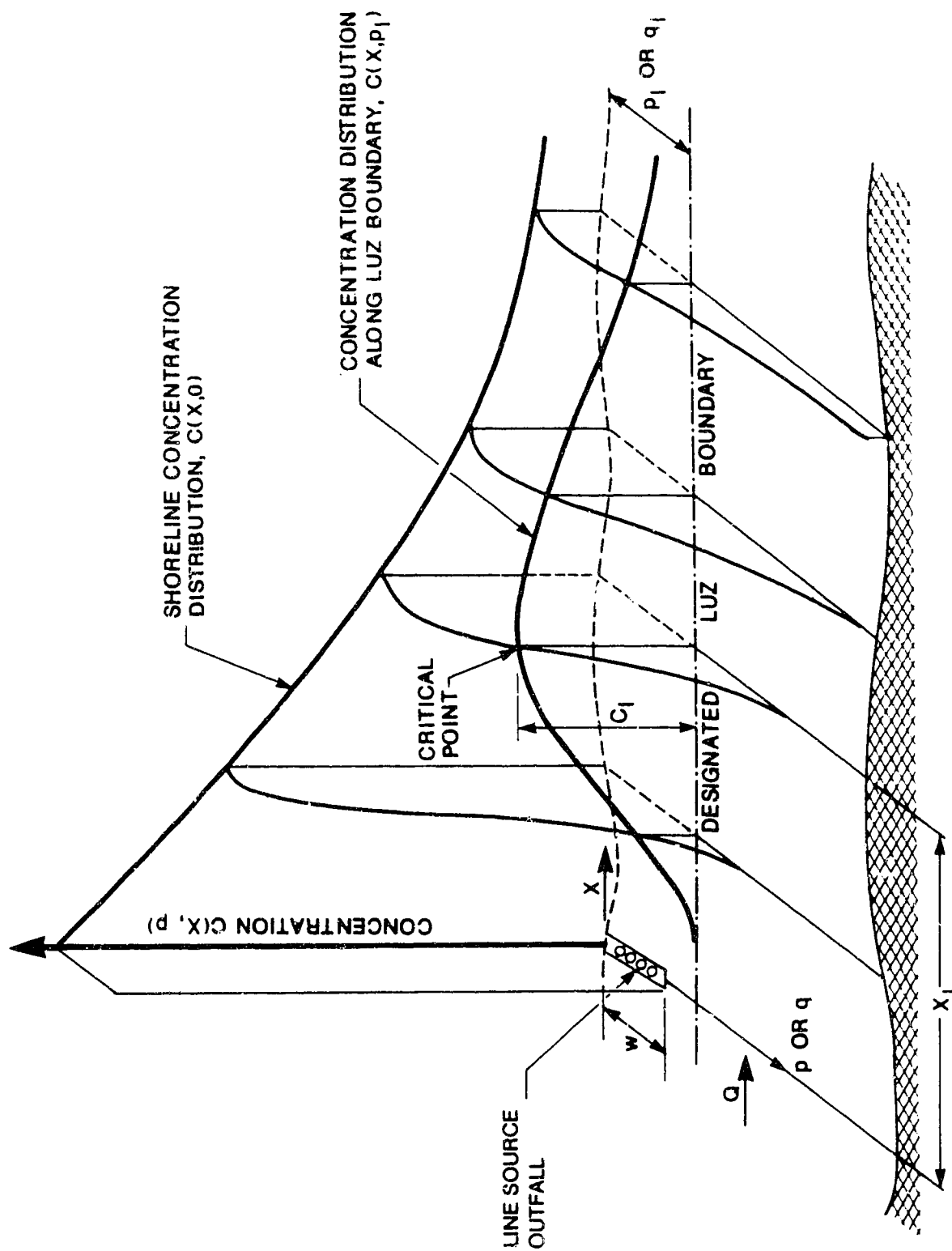


Figure 6.3 Limited Use Zone and Critical Point

## CHAPTER 7

### THE DESIGN OF JET DIFFUSER DISCHARGES IN RIVERS

#### 7.1 General

The designer of effluent outfall structures for rivers needs to consider the near field mixing phenomena. Traditionally, outfall designs have paid little attention to this flow region under the assumption that near field mixing is rapid relative to the mixing zone length. However, as effluent standards often permit discharge concentrations which are greater than receiving stream guidelines, near field mixing should be an important factor in outfall design. This is because receiving stream guidelines now often impose constraints on the extent of the limited use zone. More importantly, these constraints are more severe than what can be determined or assured by river (passive plume) mixing processes.

With this in mind, A. A. Aquatics (1987) developed procedures for initial dilution zone analysis. These procedures were based on knowledge of jet dilution and the mixing zone which was available at that time. Several constraints on jet discharges were identified and simplified procedures were outlined so that an effective outfall design could be achieved relatively easily. These concepts were applied during 1988 in the design of the diffuser outfall for

Daishowa Canada Ltd.'s Peace River Pulp Mill on the Peace River.

In this chapter, the constraints which must be considered in the design of a jet diffuser outfall are outlined. These build on the work of A. A. Aquatics (1987) incorporating the additional knowledge developed in this dissertation. The application of these procedures is then demonstrated by examining the design of Daishowa's jet diffuser outfall.

## **7.2 Constraint Considerations**

The design of an outfall facility requires the consideration of a broad spectrum of information and constraints:

- a) effluent characteristics
  - design flows (initial/ultimate; seasonal variation)
  - water quality (effluent standards; expected performance and variability)
- b) river conditions
  - seasonal flows
  - extreme flows (for both open water and ice cover seasons)
  - river hydraulics (at outfall site and downstream)
    - cross-sectional velocity and depth distributions (at and near the outfall site)
    - average velocity, depth and width (downstream)
    - water levels (rating curves and extreme levels)

- morphological characteristics (bed and bank material and erosional characteristics)
- c) environmental concerns
  - receiving stream guidelines (environmental impacts)
  - construction period constraints (fish spawning and migration periods)
- d) construction requirements
  - procedures (construction berms or wet trench methods)
  - construction period water levels
  - costs
- e) diffuser design considerations
  - cavitation (maximum jet velocity)
  - jet nozzle size and flow rate
  - jet spacing (interference considerations)
  - general and local scour (depth of cover and discharge port elevations)
  - materials of construction (corrosion concerns)

The work in this dissertation covers most of the activities in item e) above. The following sections provide a discussion of how the results of this work can be applied to this design area. In order to develop an understanding of all aspects of effluent discharges to a river system, the reader is left to pursue the literature on river engineering, hydrology, environmental science and other sources.

### 7.2.1 Cavitation

**Cavitation** in a flowing fluid is the local vaporization (i.e. boiling) of the fluid as it encounters a velocity discontinuity. Such a discontinuity exists at the outlet of a jet nozzle discharging into a quiescent or moving ambient. The vapour pockets form at random and generate high pressures (both locally and for a short duration) when the bubbles collapse. Cavitation first manifests itself in the form of noise. If jet velocities are increased beyond the level where cavitation noise is first noticed, the cavitation can result in severe physical damage to the nozzle.

The potential for cavitation can be quantified by the cavitation index ( $\sigma$ ):

$$\sigma = \frac{p_0 - p_v}{\rho_0 U_0^2 / 2} \quad (7.1)$$

where:  $p_0$  is the ambient pressure at the jet nozzle ( $p_0 = \rho g H$ ),

$p_v$  is the vapour pressure of the effluent,

$\rho_0$  is the density of the effluent,

$\rho$  is the density of the ambient fluid,

$U_0$  is the jet exit velocity,

$g$  is the gravitational constant, and

$H$  is the depth of water above the jet nozzle.

Rouse (1953) conducted experiments on cavitation in jet discharges. For jets discharging through nozzles, he found that intermittent periods of cavitation begin to occur at  $\sigma$  values as high as 0.7; cavitation noise begins to steadily occur when the cavitation index has a value of about 0.55.

Subsequent studies on jets by Rouse (1966) indicated that cavitation damage to the nozzle is not likely to occur until the locations of the bubble collapses are in the vicinity of the nozzle itself. He indicated that physical damage to a nozzle begins to occur when the cavitation index has a value of less than 0.2.

In the application of this knowledge to jet diffuser design, the cavitation index equation (7.1) can be rearranged to give the maximum allowable jet discharge velocity:

$$U_0 < \sqrt{\frac{2}{\rho_0 \sigma} (\rho g H - p_v)} \quad (7.2)$$

Values for the maximum acceptable jet discharge velocity, based on equation (7.2), have been determined for jets discharging into water of various depths (Figure 7.1). These are for conditions where the jet and the ambient are at the same temperature. The velocities are more strongly dependent on depth than temperature in the range of values expected in Alberta rivers. The maximum allowable velocities were between 4 m/s (at 1 m depth) and 18 m/s (at 10 m depth).

For some effluents, any cavitation of the discharge is undesirable because it may cause foaming at levels where noise and physical damage do not occur. This would be particularly important in effluents where foaming agents are present (e.g. pulp mill effluents). This phenomena has not been examined in this work. It is an area where experiments with pulp mill effluents would provide useful information.

Until such work is done, the cavitation criteria should be applied conservatively.

### 7.2.2 Jet Nozzle Size

It would be desirable to maximize the diameter ( $d$ ) of the jet nozzle in order to minimize the number of ports in a diffuser. The first step (setting the maximum discharge velocity) was discussed in the previous section. After determining the maximum value for  $U_0$ , the size and the number of ports can be determined based on the river's depth and velocity in the immediate vicinity of the outfall at the design low flow condition. In many environmental studies, design low flow has been taken to be the seven consecutive day low flow event which occurs, on average, once every ten years (Nemerow, 1974; Krenkel and Novotny, 1980). For simplicity, this design low flow event is termed the 7Q10. The objective should be to utilize all of the flow depth during this low flow condition knowing that, at greater flow depths and flow velocities that come with higher river discharges, the dilution will be superior.

The diameter constraint proposed in A. A. Aquatics (1987) was based on rearranging the outer boundary equation from Pratte and Baines (1967) so that the jet did not come into contact with the water surface. Based on the experimental and field work described in this dissertation, the constraints should be:

$$\frac{\alpha d}{H} < 0.3 \quad (7.3)$$

$$2 < \alpha < 8 \quad (7.4)$$

$$l_m \gg l_b \quad (7.5)$$

$$l_M > H \quad (7.6)$$

The first constraint better achieves the intentions of A. A. Aquatics. Based on experimental work, the jet discharge will not interact strongly with the water surface and will remain unimodal as long as equation (7.3) is satisfied. As a result, the jet centreline dilutions ( $C_o/C_m$ ) predicted by equation (5.1) can be used:

$$\frac{C_o}{C_m} = 1.09 \left( \frac{\alpha x}{d} \right)^{0.56} \quad (5.1)$$

Bimodal discharges (i.e. where  $\frac{\alpha d}{H} > 0.3$ ) would also be acceptable but, the higher concentration at the bimodal peaks (in the order of 60% to 80% more than the centreline maximum) must be taken into consideration.

The second constraint relates to two aspects of applicability. The lower limit of velocity ratio ( $\alpha$ ) is to ensure that the jet does not remain attached to the river bed. The upper limit is to restrict the discharge condition to the range of velocity ratios where the laboratory and field investigation results were found to be applicable.

The third and fourth criteria relate to the discharge of thermal effluents. These ensure the prevention of density stratification. The third criterion ensures that the momentum of the jet governs the effluent discharge's initial



dilution. At some point after the jet momentum region, the mixing then begins to be dominated by the crossflow and, later, by the vortices in the deflected jet discharge. The fourth criterion ensures that buoyancy is never the major factor in the mixing.

### 7.2.3 Jet Spacing

After the maximum discharge velocity has been determined, the nozzle diameter and the number of ports in the jet diffuser can be selected. The jet spacing must be determined to ensure that the jets do not significantly overlap. The spacing should be set so that the desired degree of dilution (initial dilution zone requirements are typically 20:1) is achieved downstream each individual port during the design low flow condition. First, the distance downstream of the port is determined from equation (5.1). Then, the 50% width equation is used for the downstream distance to determine the minimum jet spacing:

$$\frac{W_z}{\alpha d} = 1.20 \left( \frac{x}{\alpha d} \right)^{0.29} \quad (5.3)$$

The peripheries (i.e. where  $C/C_m < 0.5$ ) of adjacent jets can overlap as they will not result in any decrease in the expected dilution prior to that point (Appendix E). Beyond this point, the flow fields will begin to interact significantly and the dilutions expected from the analysis of a single jet could decrease. If there is sufficient width

available in the river, the port spacing could be increased to provide enhanced mixing potential.

#### **7.2.4 Other Considerations**

Relative to the work covered in this dissertation, there are two other factors to consider in the design of a jet diffuser:

##### ***dilution in the far field***

The far field dilution will likely still be of importance even if the initial dilution zone objectives are achieved. The region of influence for the effluent discharge should be determined. Included in this analysis should be the contributions from other dischargers in the river system.

##### ***dilutions achieved at other flow rates***

The flows in a river system are constantly changing on a day to day basis. The design of a jet diffuser is based on the expected effluent discharge conditions at a design low flow condition. The additional degree of dilution achievable at river flow rates greater than this condition should be quantified. These conditions would be important in the assessment of long term and chronic effects of the effluent discharge.

There has been some resistance to the use of the design low flow concept; the rationale being that the ecosystem will, at some point, experience flow conditions less than the design low flow. The writer does not condone deviating from the design low flow concept as there would be no consistent

basis by which good design could be carried out and evaluated. However, recognizing that the 7Q10 event is not the worst event that the ecosystem could experience, the design of an effluent diffuser should also determine the consequences of the more severe events. This does not mean that the water quality guidelines should be blindly applied (the guidelines are usually designed for the prevention of chronic effects during sustained exposure). Rather, knowledge of the ecosystem and the critical components of the effluent should be considered. If the effects of the effluent discharge under the extreme conditions are not acute, then the discharge should be considered adequate.

### **7.3 Application of Design Principles - A Case History**

Over the past five years, Daishowa Canada Company Ltd. developed a Kraft pulp mill adjacent to the Peace River. The mill site is located adjacent to the west bank of the river about 19 km downstream of the Town of Peace River. The mill is designed to have a pulp production rate of 1000 ADT/d (air dried tonnes per day). In the future, the mill has the mill site area and the wood resources to potentially double its production. Most of the environmental studies were completed by the end of 1987 and much of the design of the mill was carried out during 1988. The mill construction was completed and the mill commenced operation during 1990.

**Effluent Conditions**

The mill's effluent diffuser was to consider the discharge of effluent from both the initial and ultimate pulp mill configurations. The parameters of importance for designing the jet diffuser structure were:

effluent discharge rate:  $Q_e = 0.58 \text{ m}^3/\text{s}$  (initial)  
 $1.16 \text{ m}^3/\text{s}$  (ultimate)

temperature of the effluent:  $T_e = 30 \text{ }^\circ\text{C}$

The jet diffuser structure was to be sized for the ultimate flow rate and the outfall was to be installed initially with one half of the diffuser ports blinded off.

**River Conditions**

The Peace River is one of the larger rivers in Alberta. The river's mean annual flow rate is about  $1800 \text{ m}^3/\text{s}$ . Flows in the river have been significantly modified since the completion of the W. A. C. Bennett dam in British Columbia in 1972. A hydrologic analysis was carried out and it was found that the river experiences minimum flows during the months of September through March. Due to the operation of the dam, the mean freeze-up date has been delayed by about one month to December. It is now possible for the winter minimums to occur during open water conditions.

The relevant river conditions in the immediate vicinity of the effluent discharge are:

<u>Characteristic</u>	<u>7010</u>	<u>mean annual</u>
flow (m <sup>3</sup> /s)	550	1800
section depth (m)	1.84	2.84
section velocity (m/s)	0.82	1.28
section width (m)	364	495
local depth (m)	2.9	4.6
<u>local velocity (m/s)</u>	<u>1.1</u>	<u>1.7</u>

### **Jet Discharge Location**

The Peace River experiences significant ice runs during break-up in the spring of every year. These ice runs frequently result in ice jam events. Concerns about potential ice damage to the jet diffuser structure and the desire to minimize the environmental impact led to the decision to use a mid-stream diffuser (Figure 7.2). The in-river portion of the outfall line was 1050 mm diameter steel pipe which was lined with epoxy enamel and was protected by a "yellow jacket" polyethylene wrap with a gunite coating. The outfall structure was fabricated from steel pipe fittings and was concrete encased once in place (plates 7.1 and 7.2). Both the pipeline and the outfall structure were installed a minimum of 2.0 m below the river bed to protect against scour. The tops of the jet nozzles were located about 1.0 m above the river bed to prevent them from being inundated by moving bottom material.

### Jet Nozzle Size

The first activity in sizing the jet nozzles is to determine the maximum allowable jet discharge velocity. Using equation (7.2) with winter discharge conditions and 1.9 m of water above the nozzle, a maximum allowable velocity of 6.4 m/s can be determined. Based on the methods outlined in A. A. Aquatics (1987), fourteen 150 mm diameter nozzles were selected to discharge the effluent at the ultimate flow rate of 1.16 m<sup>3</sup>/s. This resulted in a jet velocity of 4.68 m/s and a velocity ratio of about 4.3, which meets the criterion of equation (7.4).

This effluent discharge configuration, with  $\alpha d/H = 0.34$ , does not quite meet the criterion outlined in equation (7.3). The water surface is probably a factor and a unimodal jet discharge might not occur. For this discharge, the buoyancy length scale is  $l_b = 0.010$  m and the momentum length scale is  $l_m = 0.56$  m, and the criterion in equation (7.5) is met (i.e. the jet momentum dominates the discharge). The jet never becomes buoyancy dominated since  $l_M = 8.4$  m  $>$   $H = 1.9$  m, satisfying the requirements of equation (7.6).

### Jet Spacing

The jet spacing was selected to be 2.0 m. Equation (5.3) indicates that adjacent jets would begin to overlap and result in lower dilution when  $\frac{x}{\alpha d} > 27.5$  or  $x/d > 117$ . This is equivalent to  $\alpha x/d = 500$  for the 7Q10 flow condition.

### Initial Dilution Assessment

An initial dilution assessment has been carried out for the 7Q10 and the mean annual flow conditions (Figure 7.3). Equation (5.1) indicates that an initial dilution of 35:1 can be achieved during the 7Q10 flow condition. This far exceeds the initial dilution zone requirement of 20:1 for rivers which has been indicated in some water quality guidelines.

The maximum initial dilution potential in the Peace River at this flow condition is 474:1. The maximum dilution potential in the immediate vicinity of the 26 m wide diffuser outfall would be 71:1. Thus, the jet diffuser ensures that about 50% of this potential will occur within 18 m of the outfall structure.

It is interesting to note that the the jet dilution projected by equation (5.1) does not utilize as much of the river when the mean annual flow condition is assessed. The crossflow dominates the jet ( $\alpha = 2.8$ ) for this discharge configuration. For this flow condition, surface effects are not present ( $\alpha d/H = 0.12 < 0.3$ ) and the discharge is unimodal. The jets do not significantly overlap until  $\frac{x}{\alpha d} = 122$  ( $\alpha x/d = 930$ ). The dilution ratio at this point is

about 50:1 or about 30% of the flow in the vicinity of the diffuser. However, greater dilution than 50:1 should be expected as the mixing will be enhanced by vertical mixing due to river turbulence. The data on Figure 5.19 indicate

that the dilution equation makes low predictions for weak jets at large values of  $\alpha x/d$ .

#### **7.4 Conclusions**

a) The Peace River outfall was assessed using the design criteria developed in the earlier sections for jet diffuser design. The analysis indicates that the jet discharges will be unimodal and will be dominated by the momentum of the discharge (i.e. the buoyancy of the 30° C effluent will not be a factor).

b) The jet diffuser structure ensures that a minimum dilution ratio of 35:1 is achieved within 18 m of the outfall. The initial dilution increases significantly when the river discharge increases at this site. River turbulence becomes more of a factor during these flow conditions.



Figure 7.1 Maximum permissible velocities for jet discharges

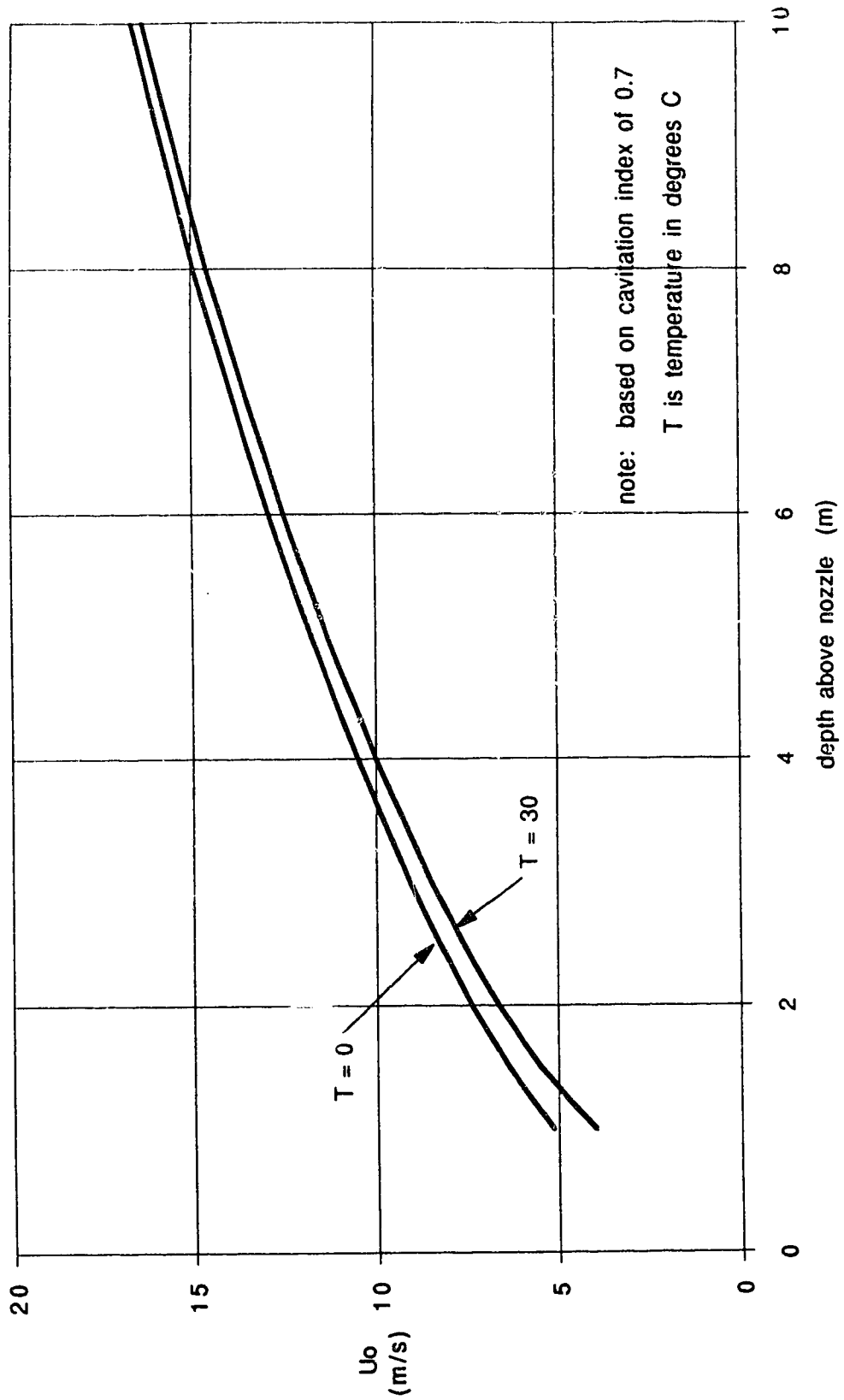


Figure 7.2 River cross-section at Peace River outfall

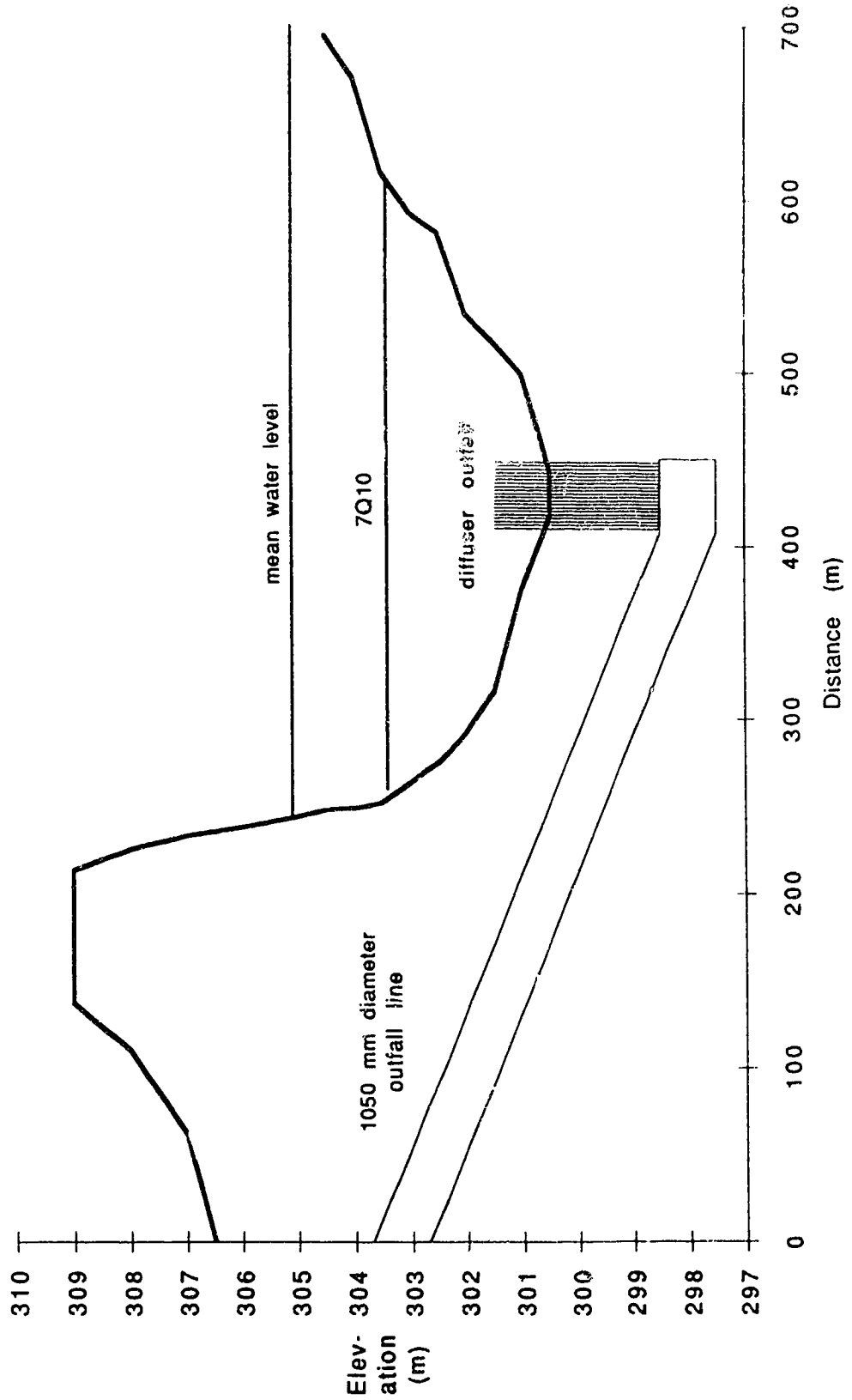
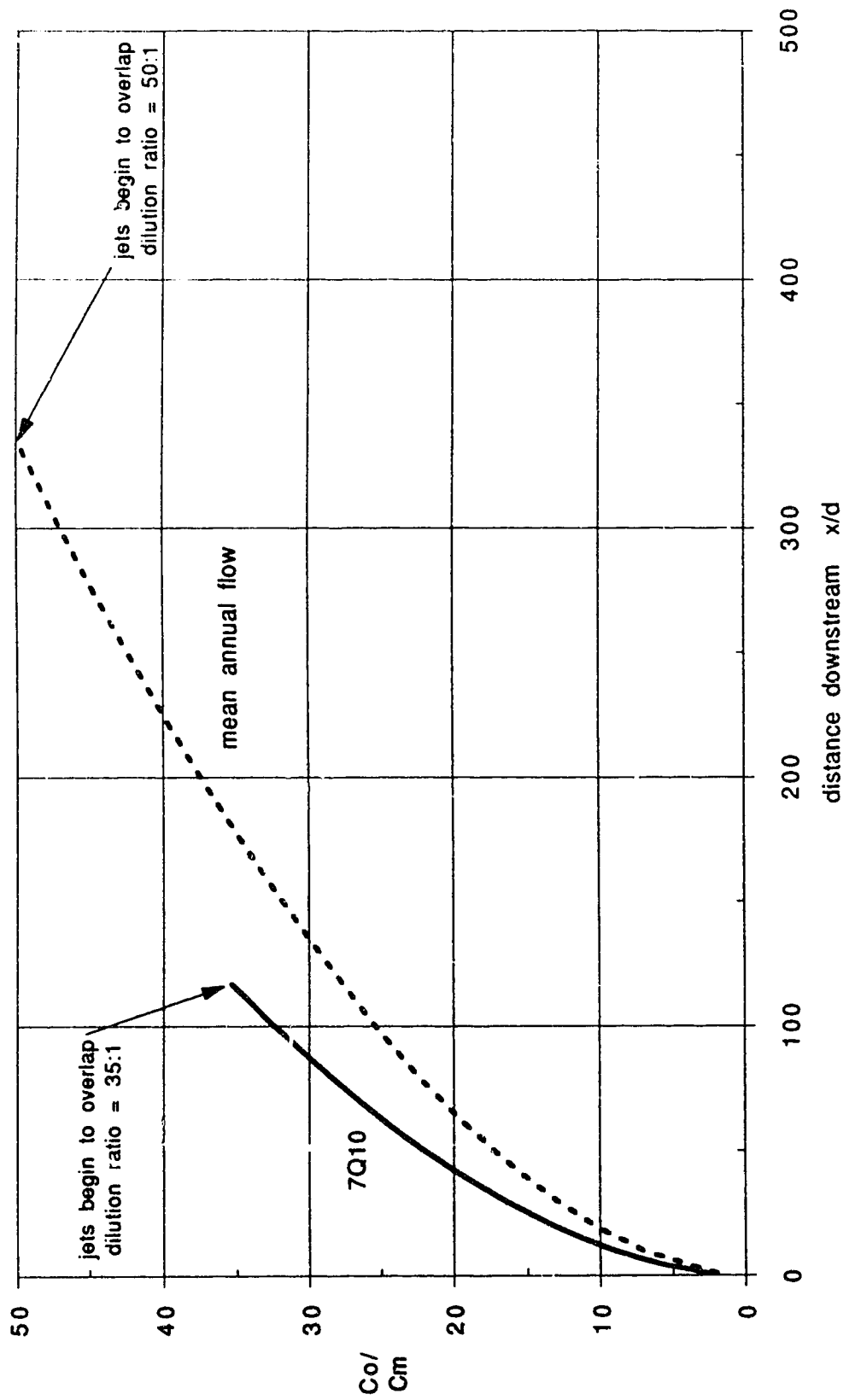


Figure 7.3 Jet dilution for Peace River outfall



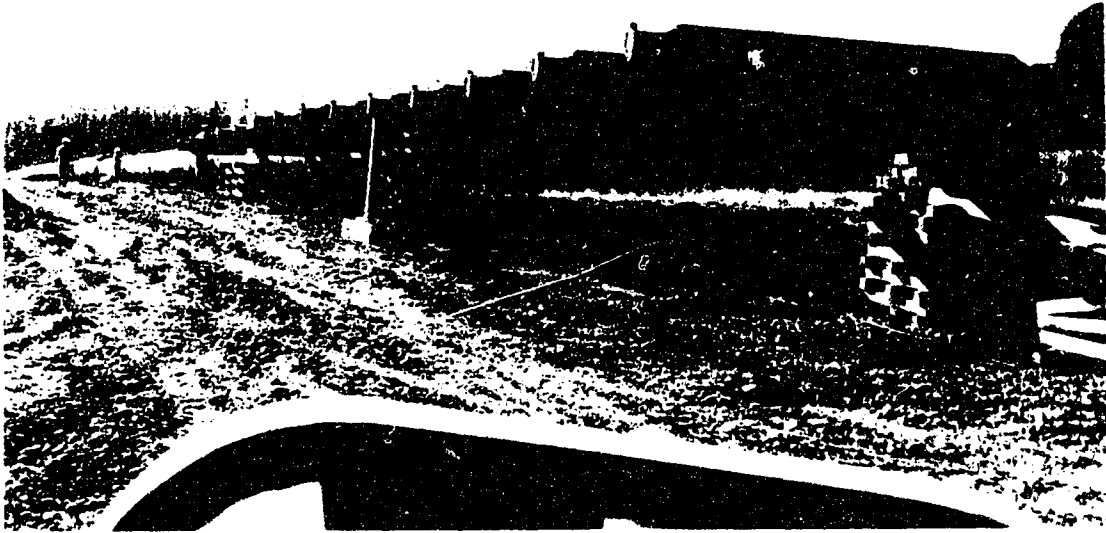


Plate 7.1 Jet diffuser outfall on shore prior to launch.



Plate 7.2 Structure being pulled into place along downstream berm (river flow is right to left beyond berms).

## Chapter 8

### CONCLUSIONS

#### 8.1 General

The previous seven chapters have presented discussions related to numerous aspects of effluent discharges in rivers. In addition, the results of supplemental statistical and mathematical analyses and the data from field and experimental work are presented in the accompanying appendices. As the subject areas of these topics are somewhat diverse, conclusions are made at the end of each chapter where new knowledge has been put forth by the writer.

Effluent discharges in rivers are both a difficult environmental management problem and a complex turbulent flow problem. The former has been discussed in the context of setting a frame of reference for the study of the latter. Although dispersion and dilution are not the primary means for practising environmental management, they are the primary mitigative mechanisms once the discharge of a specific effluent has been committed to. As a result of the analytical, field and laboratory investigations conducted for this dissertation, the design of effluent diffusers for rivers can now be carried out on a rational basis. Assurances of initial dilutions of up to 50:1 are now possible within metres of an effluent discharge.

This chapter summarizes the conclusions of the previous chapters from a more global perspective. The summary will highlight areas where significant contributions have been made. As well, discussion as to where there is a need for further knowledge is presented.

## 8.2 Findings

### Environmental Context

The complete mixing of an effluent discharge in a river is ultimately controlled by the turbulence of the river. However, the mixing in the immediate vicinity of an outfall (the **near field**) can be controlled by the design of the discharge structure. If a jet diffuser outfall is used, initial dilutions of up to 50:1 can be accomplished (if there is sufficient river flow) within metres of the structure. The mixing in this **initial dilution zone** is important for receiving stream assessment as the length of the **mixing zone** is about three orders of magnitude greater than the length of the near field.

A jet diffuser outfall can provide a significant degree of near field mixing and will provide more confidence that environmental protection objectives are being served than an outfall which relies solely on river turbulence to accomplish the mixing. Meeting objective concentrations within the initial dilution zone is the level of protection that some of the existing water quality guidelines suggest.

### **Photographic Analysis**

The review of the literature on jet discharges in crossflow indicated that no equations exist to describe the bulk properties of jet discharges in crossflows of finite depth. A quantification of these properties is important for most natural rivers as their depths are relatively small. This work has identified five zones of flow for circular jet discharges into crossflows of finite depth:

- a) the potential core,
- b) the momentum dominated near field (MDNF),
- c) the momentum dominated far field (MDF),
- d) the surface dominated field (SDF), and
- e) the terminal level region.

Equations describing the centreline location of jet discharges have been developed in a laboratory investigation and have been described in Section 3. Several points are worth noting:

- a) the MDNF and MDF regions were both observed with the latter being the more significant,
- b) the boundary and centreline equations presented by Pratte and Baines (1967) tend to predict higher values than were observed,
- c) the centreline relations developed in this work predict values which are higher than what would be predicted by Wright (1977a); this may be due to the presence of the

boundary layer in this work and the absence of one in Wright's work,

d) the **relative jet strength parameter**  $\alpha d/D$  is preferable for describing the jet centreline location; the relative jet strength parameter  $\alpha^2 d/D$  is preferable for describing the jet width.

### **Field and Laboratory Dilution Studies**

A power law dilution equation can be fitted to jet discharges in the **jet entrainment zone**:

$$C_o / C_m = a \left( \frac{\xi}{d} \right)^b \quad (4.14)$$

Values for the coefficient  $a$  and the exponent  $b$  can be found for any individual jet discharge. These dilution equation parameters can be correlated to the inverse of velocity ratio ( $p = 1/\alpha$ ) for jet strengths ranging from  $p = 0$  (simple jets) to  $p = 0.3$  (weak jets in strong crossflows). The parameters also appear to be sensitive to the relative jet strength  $\alpha d/D$ .

Vortices form in the jet discharge at low values for the velocity ratio ( $\alpha$ ) but do not separate. The concentration distributions for these jet discharge conditions are **unimodal**. When the vortices partially separate, the concentration distributions become **bimodal**. When the jet strength is even greater, the vortices will completely separate and the jet is called **bifurcated**. In the



experiments carried out for this work, the occurrence of the bimodal condition appeared to be more dependent on the relative jet strength than on the velocity ratio. The bimodal jets began to occur when  $\alpha d/D > 0.3$ .

Jet dilution was found to be a function of the distance parameter  $\alpha x/d$ . This work is the first investigation to suggest this parameter as a means to describe jet dilution. This distance parameter allows the jet dilution to be quantified relative to the more appropriate direction (i.e.  $x$ ) for river systems:

$$C_o / C_m = 1.09 \left( \frac{\alpha x}{d} \right)^{0.56} \quad (5.1)$$

Equation 5.1 quantifies the jet dilution in both the jet entrainment and vortex entrainment zones. The equation was verified by the laboratory experiments for a range of  $\alpha x/d$  covering three orders of magnitude. The relation was also verified to some extent by the laboratory work of others (Ramsey and Goldstein, 1971; Wright, 1977a; Andreopoulos, 1983).

Field investigations of jet dilution are more difficult to carry out than laboratory work. However, it is possible to carry out such scientific investigations in natural rivers. The field study carried out for this work supported the dilution relations as well as the location, width and thickness relations determined from the laboratory studies. From these field and laboratory studies, it can be concluded

that laboratory work on jet discharges in crossflow represents prototype conditions very well.

### **Far Field Analysis**

Siting an effluent discharge structure at the bank of a river does not provide the best opportunity for the dilution of the discharge. Siting the structure at midstream would result in the shortest mixing zone length, however, a line diffuser outfall should usually be preferred as it will offer the best initial dilution zone characteristics.

Determining the **mixing zone length** is an important beginning for the assessment of an effluent discharge. Theoretical equations to determine the mixing zone length must be used with care as the configuration of natural rivers (e.g. bends, slope changes and islands) can significantly shorten this length. The actual length of the mixing zone is not a precise dimension as it is sensitive to the criterion (i.e. 95% or 98% mixed) used. This is because mixing occurs slowly in the latter part of the mixing zone.

If an effluent discharge does not meet the receiving water guidelines at the downstream end of the initial dilution zone, then the distribution of concentrations within the mixing zone should be evaluated using **limited use zone** concepts. Gowda (1980 and 1984) provided the initial presentation of this method of analysis for point source outfalls. The work in this dissertation extends his work

plus provides further equations for the analysis of line source outfalls.

### **Case History**

A case history was presented to illustrate the application of the design principles developed in this work. The jet diffuser structure, designed for the discharge of a pulp mill effluent into the Peace River, is able to achieve an initial dilution in the order of 35:1 for river flows as low as the 7Q10 flow condition. The jet discharge is sufficiently strong that stratification due to density differences for this 30° C effluent will not be a problem.

### **8.3 Further Investigation**

In conducting an intense examination of a physical phenomena, it is typical that a number of additional areas of work become obvious by the time the research has fulfilled its original objectives. A number of areas that the writer feels further investigation would provide useful knowledge are described below. These investigations would extend the range that one can quantify jet dilution in the near field.

### **Unimodal, Bimodal and Bifurcated Jets**

A better explanation of the various conditions of jet flow in the vortex entrainment zone is desired. A photographic investigation (using long and short time exposures) could provide much insight on how the formation of

unimodal, bimodal and bifurcated conditions depend on the velocity ratio and the relative jet strength of the jet discharge. The experimental work should cover a wide range of parameters:

distance:	$0 < x/d < 200$
velocity ratio:	$2 < \alpha < 12$
relative jet strength:	$0.05 < \alpha d/D < 0.6$

### **Laboratory Dilution Studies**

Two further laboratory dilution studies would help extend the range of applicability for equation 5.1. The first should investigate extending the range of equation 5.1 further downstream for unimodal jet discharges. It should also focus on investigating cross sectional concentration distributions for bimodal jets in order to develop a relation for the bimodal ratio. This would allow better predictions for the dilution of bimodal jet discharges.

The second laboratory investigation should be conducted to verify the analytical work, presented in Appendix E, on Reichardt's hypothesis. The work should first be carried out on multiple jet discharges in a quiescent ambient to verify the equations established in the appendix. Then, further laboratory investigation should be carried out in a crossflow to determine if the interaction of multiple jets is as expected. This work would require the measurement of both velocity and concentration fields.

**Foaming of Jet Discharges**

In presenting the criteria for determining the maximum jet discharge velocity, the objective used was the prevention of jet nozzle cavitation noise. This criteria may not be sufficiently conservative to prevent adverse environmental consequences in the case of effluents which have a propensity to foam. An investigation should be carried out to determine the relation between the onset of foaming and jet discharge conditions such as the cavitation index, the effluent's dissolved air content, the effluent's temperature and other parameters. Actual treated effluents from municipal and industrial (e.g. pulp mill) wastewater treatment facilities should be used as well as various concentrations of known surfactants.

**BIBLIOGRAPHY**

- A. A. Aquatics Research Limited, 1987. Initial dilution zone and limited use zone concepts for receiving streams. Prepared for Alberta Environment, Standards and Approvals Division, Water Quality Branch. Edmonton, Alberta.
- Abdel-Gawad, S. T. and J. A. McCorquodale, 1985. Initial mixing of cross-flowing jets in trapezoidal channels. Proceedings of the XXI IAHR Congress. Melbourne, Australia. pp 140-145.
- Abdelwahed, M. S. T. and V. H. Chu, 1978. Bifurcation of buoyant jets in cross flow. Technical Report No. 78-1. Department of Civil Engineering and Applied Mechanics. McGill University. Montreal, Quebec.
- Abraham, G., 1960. Jet diffusion in liquid of greater density. ASCE Journal of the Hydraulics Division, Vol. 86, No. HY6, pp 1-13.
- Abramovich, G. N., 1963. The theory of turbulent jets. English translation published by M. I. T. Press. Cambridge, Massachusetts.
- Adler, D. and A. Baron, 1979. Prediction of a three-dimensional circular turbulent jet in a crossflow. AIAA Journal, Vol. 17, No. 2, pp 168-174.
- Alberta Environment, 1977. Surface water quality objectives. Water Quality Branch, Standards and Approvals Division. Edmonton, Alberta.
- Alberta-Pacific Environmental Impact Assessment Review Board, 1990. The proposed Alberta-Pacific Pulp Mills: Report of the EIA Review Board. Edmonton, Alberta.
- Albertson, M. L., Y. B. Dai, R. A. Jensen and H. Rouse, 1950. Diffusion of submerged jets. Transactions, ASCE, Vol. 115, pp 639-697.
- Andreopoulos, J., 1983. Heat transfer measurements in a heated jet-pipe flow issuing into a cold cross stream. Physics of Fluids, Vol. 26, No. 11, pp 3201-3210.
- Andreopoulos, J. and W. Rodi, 1984. Experimental investigations of jets in a crossflow. Journal of Fluid Mechanics, Vol. 138, pp 93-127.
- Antonia, R. A., A. Prabhu and S. E. Stephenson, 1975. Conditionally sampled measurements in a heated turbulent jet. Journal of Fluid Mechanics, Vol. 72, part 3, pp 455-480.

Becker, H. A., H. C. Hottel and G. C. Williams, 1967. The nozzle-fluid concentration field of the round turbulent, free jet. *Journal of Fluid Mechanics*, Vol. 30, Part 2, pp 285-303.

Beltaos, S., 1975. Evaluation of transverse mixing coefficients from slug tests. *Journal of Hydraulic Research*, Vol. 13, No. 3, pp 351-360.

Beltaos, S., 1978a. Transverse mixing in natural streams. Report No. SWE-78/01. Alberta Research Council. Edmonton, Alberta.

Beltaos, S., 1978b. Mixing processes in natural streams. Proceedings of the Transport Processes and River Modelling Workshop. National Water Research Institute. Burlington, Ontario.

Beltaos, S., 1979. Transverse mixing in natural streams. *Canadian Journal of Civil Engineering*, Vol. 6, No. 4, pp 575-591.

Beltaos, S., 1980. Transverse mixing tests in natural streams. *ASCE Journal of the Hydraulics Division*, Vol. 106, No. HY10, pp 1607-1625.

Birch, A. D., D. R. Brown, M. G. Dodson and J. R. Thomas, 1978. The turbulent concentration field of a methane jet. *Journal of Fluid Mechanics*, Vol. 88, pp 431-449.

Calaghan, E. E. and R. S. Ruggeri, 1951. A general correlation of temperature profiles of a heated air jet directed perpendicularly to an air stream. NACA Technical Note 2466.

Campbell, J. F. and J. A. Schetz, 1973. Flow properties of submerged heated effluents in a waterway. *AIAA Journal*, Vol. 11, No. 2, pp 223-230.

CCREM, 1987. Canadian water quality guidelines. Prepared by the Task Force on Water Quality Guidelines of the Canadian Council of Resource and Environment Ministers. Ottawa, Ontario.

Chan, D. T. L., J. T. Lin and J. F. Kennedy, 1976. Entrainment and drag forces of deflected jets. *ASCE Journal of the Hydraulics Division*, Vol. 102, No. HY5, pp 615-635.

Chassaing, P., J. George, A. Claria and F. Sananes, 1974. Physical characteristics of subsonic jets in a cross-stream. *Journal of Fluid Mechanics*, Vol. 62, Part 1, pp 41-64.

- Chevray, R. and N. K. Tutu, 1978. Intermittency and preferential transport in a round jet. *Journal of Fluid Mechanics*, Vol. 88, part 1, pp 133-160.
- Chevrier, J. (editor), 1979. MTS/Minitab supplement. Computing Services, University of Alberta. Edmonton, Alberta.
- Chien, J. C. and J. A. Schetz, 1975. Numerical solution of the three-dimensional Navier-Stokes equations with applications to channel flows and a buoyant jet in a cross flow. *ASME Journal of Applied Mechanics*, pp 575-579.
- Chu, V. H., 1979. L. N. Fan's data on buoyant jets in crossflow. Technical Note. *ASCE Journal of the Hydraulics Division*, Vol. 105, No. HY5, pp 612-617.
- Chu, V. H., 1985. Oblique turbulent jets in a crossflow. *ASCE Journal of Engineering Mechanics*, Vol. 111, No. 11, pp 1343-1360.
- Chu, V. H. and M.B. Goldberg, 1974. Buoyant forced-plumes in cross flow. *ASCE Journal of Hydraulics Division*, Vol. 100, No. HY9, pp 1203-1213.
- Crabb, D., D. F. G. Durao and J. H. Whitelaw, 1981. A round jet normal to a crossflow. *ASME Journal of Fluids Engineering*, Vol. 103, pp 142-153.
- Crank, J., 1956. *The mathematics of diffusion*. Oxford University Press. London, England.
- Crank, J., N. R. McFarlane, J. C. Newby, G. D. Paterson and J. B. Pedley, 1981. *Diffusion processes in environmental systems*. McMillan Press Ltd. London, England.
- Crowe, C. T. and H. Riesebieter, 1967. *An analytical and experimental study of jet deflection in a cross-flow*. Vereinigte Flugtechnische Werke. Bremen, Germany.
- Csanady, G. T., 1973. *Turbulent diffusion in the environment*. D. Reidel Publishing Company. Boston, Massachusetts.
- Davis, L. R., M. A. Shirazi and D. L. Siegel, 1978. Measurement of buoyant jet entrainment from single and multiple sources. *ASME Journal of Heat Transfer*, Vol. 100, pp 442-447.
- Demissie, M. and W. H. C. Maxwell, 1982. Three-dimensional slot jets. *ASCE Journal of the Hydraulics Division*, Vol. 108, No. HY2, pp 247-251.



- Elhady, N., A. Harrington, I. Hill, Y. L. Lau and B. G. Krishnappan, 1984. River mixing--a state-of-the-art report. Canadian Journal of Civil Engineering, Vol. 11, No. 3, pp 585-609.
- Engmann, J. E. O. and R. Kellerhals, 1974. Transverse mixing in an ice-covered river. Water Resources Research, Vol. 10, No. 4, pp 775-784.
- Environment Canada, 1988a. Citizen's guide to the Canadian Environmental Protection Act. Ottawa, Ontario.
- Environment Canada, 1988b. Canadian Environmental Protection Act - enforcement and compliance policy. Ottawa, Ontario.
- Fan, L. N., 1967. Turbulent buoyant jets into stratified or flowing ambient fluids. Report No. KH-R-15, W. M. Keck Laboratory of Hydraulics and Water Resources, California Institute of Technology. Pasadena, California.
- Fearn, R. L. and R. P. Weston, 1974. Vorticity associated with a jet in a cross flow. AIAA Journal, Vol. 12, No. 12, pp 1666-1671.
- Fearn, R. L. and R. P. Weston, 1979. Velocity field of a round jet in a cross flow for various injection angles and velocity ratios. NASA Technical Paper 1506.
- Fischer, H. B., 1967. Transverse mixing in a sand bed channel. U. S. Geological Survey Prof. Paper 575-D.
- Fischer, H. B., 1969. The effect of bends on dispersion in streams. Water Resources Research, Vol. 5, No. 2, pp 496-506.
- Fischer, H. B., E. J. List, R. C. Y. Koh, J. Imberger and N. H. Brooks, 1979. Mixing in inland and coastal waters. Academic Press. New York, New York.
- Forstall, W. and E. W. Gaylord, 1955. Momentum and mass transfer in a submerged water jet. ASME Journal of Applied Mechanics, Vol. 22, No. 2, pp 161-164.
- Gallier, R. L., 1959. Studies on fluid jets discharging normally into moving liquid. St. Anthony Falls Hydraulic Laboratory, University of Minnesota, Technical Paper 28, Series B.
- Gowda, T. P. H., 1980. Stream tube model for water quality prediction in mixing zones of shallow rivers. Water Resources Paper No. 14. Water Resources Branch, Ontario Ministry of Environment. Toronto, Ontario.

- Gowda, T. P. H., 1984. Critical point methods for mixing zones in rivers. ASCE Journal of Environmental Engineering, Vol. 110, No. 1, pp 244-262.
- Hewett, T. A., J. A. Fay and D. P. Hoult, 1971. Laboratory experiments of smokestack plumes in a stable atmosphere. Atmospheric Environment. Vol. 5, pp 767-789.
- Kinze, J. O. and B. G. van der Hegge Zijnen, 1949. Transfer of heat and matter in the turbulent mixing zone of an axially symmetrical jet. Applied Scientific Research, Vol. A1, pp 435-461.
- Hirst, E., 1972. Zone of flow establishment for round buoyant jets. Water Resources Research, Vol. 8, No. 5, pp 1234-1246.
- Hodgson, J. E., 1981. Transverse mixing of neutral substances in natural streams (unpublished). University of Alberta. Edmonton, Alberta.
- Hodgson, J. E., 1986. A review of analytical equations for two dimensional dispersion (unpublished). University of Alberta. Edmonton, Alberta.
- Hodgson, J., 1989. Limited Use Zone concepts for line source outfalls. Proceedings of the XXIII IAHR Congress. Ottawa, Ontario. Vol. S, pp 107-114.
- Hodgson, J. E. and N. Rajaratnam, 1988a. The location of circular jet discharges in crossflows of finite depth. Technical Report WRE 88-5. Department of Civil Engineering, University of Alberta. Edmonton, Alberta.
- Hodgson, J. E. and N. Rajaratnam, 1988b. The dilution of circular discharges in crossflows. Technical Report WRE 88-8. Department of Civil Engineering, University of Alberta. Edmonton, Alberta.
- Hodgson, J. and N. Rajaratnam, 1989. Field measurements of the dilution of jets in rivers. Proceedings of the XXIII IAHR Congress. Ottawa, Ontario. Vol. D, pp 1-7.
- Holley, E. R., J. Siemons and G. Abraham, 1972. Some aspects of analyzing transverse diffusion in rivers. Journal of Hydraulic Research, Vol. 10, No. 1, pp 27-57.
- Holley, F. M. Jr. and G. Nerat, 1983. Field calibration of stream-tube dispersion model. ASCE Journal of Hydraulic Engineering, Vol. 109, No. 11, pp 1455-1470.

Hossain, M. S. and W. Rodi, 1982. A turbulence model for buoyant flows and its application to vertical buoyant jets. In: *"Turbulent Buoyant Jets and Plumes"*, W. Rodi (editor), Pergamon Press, pp 121-178.

IJC, 1981. Report to the aquatic ecosystem objectives committee. Presented to the Science Advisory Board of the International Joint Commission.

Jobson, H. E., 1987. Estimation of dispersion and first-order rate coefficient by numerical routing. *Water Resources Research*, Vol. 23, No. 1, pp 169-180.

Jobson, H. E. and W. W. Sayre, 1970. Vertical transfer in open channel flow. *ASCE Journal of the Hydraulics Division*, Vol. 96, No. HY3, pp 703-724.

Jordinson, R., 1956. Flow in a jet directed normal to the wind. Imperial College Aeronautics Department Paper No. 35 (British Aeronautical Research Council, Reports and Memoranda No. 3074).

Kamotani, Y. and I. Greber, 1972a. Experiments on a turbulent jet in a cross flow. *AIAA Journal*, Vol. 10, No. 11, pp 1425-1429.

Kamotani, Y. and I. Greber, 1972b. Experiments on a turbulent jet in a cross flow. AIAA 10th Aerospace Sciences Meeting. San Diego, California. Paper No. 72-149.

Keffer, J. F. and W. D. Baines, 1963. The round jet in a cross-wind. *Journal of Fluid Mechanics*, Vol. 15, pp 481-496.

Kellerhals, R., C. R. Neill and D. I. Bray, 1972. Hydraulic and geomorphic characteristics of rivers in Alberta. River Engineering and Surface Hydrology Report 72-1. Alberta Research Council. Edmonton, Alberta.

Knystautas, R., 1964. The turbulent jet from a series of holes in a line. *The Aeronautical Quarterly*, Vol. XV, February, 1964, pp 1-28.

Kotsovinos, N. E., 1975. A study of the entrainment and turbulence in a plane buoyant jet. Report No. KH-R-32. W. M. Keck Laboratory of Hydraulics and Water Resources. California Institute of Technology. Pasadena, California.

Kotsovinos, N. E., 1978. Dilution in a vertical round buoyant jet. *ASCE Journal of the Hydraulics Division*, Vol. 104, No. HY5, pp 795-798.

Krausche, D., R. L. Fearn and R. P. Weston, 1978. Round jet in a cross flow: influence of injection angle on vortex properties. *AIAA Journal*, Vol. 16, No. 6, pp 636-637.

- Krenkel, P. A. and V. Novotny, 1980. Water quality management. Academic Press Inc. Orlando, Florida.
- Kristmanson, D. and P. V. Dankwerts, 1961. Studies in turbulent mixing - I: dilution of a jet. Chemical Engineering Science, Vol. 16, pp 267-277.
- Lau, Y. L., 1985. Mixing coefficient for ice-covered and free-surface flows. Canadian Journal of Civil Engineering, Vol. 12, No. 3, pp 521-526.
- Lau, Y. L. and B. G. Krishnappan, 1977. Transverse dispersion in rectangular channels. ASCE Journal of the Hydraulics Division, Vol. 103, No. HY10, pp 1173-1189.
- Lau, Y. L. and B. G. Krishnappan, 1981. Modeling transverse mixing in natural streams. ASCE Journal of the Hydraulics Division, Vol. 107, No. HY2, pp 209-226.
- Leimkuhler, W., J. Connor, J. Wang, G. Christodoulou and S. Jundgren, 1975. Two-dimensional finite element dispersion model. ASCE Symposium on Modelling Techniques. San Francisco, California. pp 1467-1486.
- List, E. J., 1982. Mechanics of turbulent buoyant jets and plumes. In: *"Turbulent Buoyant Jets and Plumes"*, W. Rodi (editor), Pergamon Press, pp 1-68.
- McMahon, H. M. and D. K. Mosher, 1969. Experimental investigation of pressures induced on a flat plate by a jet issuing into a subsonic crosswind. Proceedings: Analysis of a jet in a subsonic crosswind. NASA SP-218, pp 49-62.
- Margason, F. J., 1968. The path of a jet directed at large angles to a subsonic free stream. NASA Technical Note D-4919.
- Morton, B. R., G. I. Taylor and J. S. Turner, 1956. Turbulent gravitational convection from maintained and instantaneous sources. Proceedings, Royal Society of London, A234, pp 1-23.
- Moussa, Z. M., J. W. Trischka and S. Eskinazi, 1977. The near field in the mixing of a round jet with a cross-stream. Journal of Fluid Mechanics, Vol. 80, Part 1, pp 49-81.
- Nemerow, N. L., 1974. Scientific stream pollution analysis. Scripta Book Company. Washington, D. C.
- Northwest Territories Waterboard, 1981. Guidelines for municipal type wastewater discharges in the Northwest Territories. Yellowknife, Northwest Territories.

- Ooi, K. K., 1985. Scale effects on cavitation inception in submerged water jets: a new look. *Journal of Fluid Mechanics*, Vol. 151, pp 367-390.
- Pani, B. and R. Dash, 1983a. Three-dimensional single and multiple free jets. *ASCE Journal of Hydraulic Engineering*, Vol. 109, No. 2, pp 254-269.
- Pani, B. S. and R. N. Dash, 1983b. Three-dimensional wall jets from multiple outlets. Technical Note 376, Proceedings of the Institution of Civil Engineers, Vol. 75, Part 2, pp 735-749.
- Papanicolaou, P. N. and E. J. List, 1988. Investigations of round vertical turbulent buoyant jets. *Journal of Fluid Mechanics*, Vol. 195, pp 341-391.
- Papantoniou, D. and E. J. List, 1989. Large-scale structure in the far field of buoyant jets. *Journal of Fluid Mechanics*, Vol. 209, pp 151-190.
- Patrick, M. A., 1967. Experimental investigation of the mixing and penetration of a round turbulent jet injected perpendicularly into a transverse stream. *Transactions, Institute of Chemical Engineers*, Vol. 45, pp T16-T31.
- Platten, J. L. and J. F. Keffer, 1968. Entrainment in deflected axisymmetric jets at various angles to the stream. Technical Report 6808, Department of Mechanical Engineering, University of Toronto. Toronto, Ontario.
- Platten, J. L. and J. F. Keffer, 1971. Deflected turbulent jet flows. *ASME Journal of Applied Mechanics*, pp 756-758.
- Pollution Control Board, 1977. Pollution control objectives for the forestry products industry of British Columbia. British Columbia Ministry of the Environment. Victoria, British Columbia.
- Pratte, B. D. and W. D. Baines, 1967. Profiles of round turbulent jet in a cross flow. *ASCE Journal of the Hydraulics Division*, Vol. 92, No. HY6, pp 53-64. plus: "corrections", Vol. 93. No. HY3, pp 815-816.
- Rahmeyer, W. J., 1986. Test procedures for determining cavitation limits in control valves. *AWWA Journal*, pp 55-58, November, 1986.
- Rajaratnam, N., 1976. *Turbulent jets*. Elsevier Scientific Publishing Company. Amsterdam, Netherlands.
- Rajaratnam, N., 1979. Reichardt's hypothesis for plane jets. Lecture notes, University of Alberta. Edmonton, Alberta.

- Rajaratnam, N., 1983. Theory of turbulent jets. in: *Handbook of Fluids in Motion*, N. P. Chermisinoff and R. Gupta (editors), Ann Arbor Science, pp 251-278.
- Rajartnam, N., 1985. Reichardt's hypothesis for circular jets. Lecture notes, University of Alberta. Edmonton, Alberta.
- Rajaratnam, N. and L. Flint-Peterson, 1987. Low Reynolds number circular turbulent jets. Technical Report WRE 87-3. Department of Civil Engineering, University of Alberta. Edmonton, Alberta.
- Rajaratnam, N. and T. Gangadhariah, 1980. Circular jets in cross-flow. Technical Report, Department of Civil Engineering, University of Alberta. Edmonton, Alberta.
- Rajaratnam, N. and T. Gangadhariah, 1981a. Axis of a circular jet in cross-flow. *Water, Air and Soil Pollution*, Vol. 15, pp 317-321.
- Rajaratnam, N. and T. Gangadhariah, 1981b. Scales for circular jets in cross-flow. Technical Note. *ASCE Journal of the Hydraulics Division*, Vol. 107, No. HY4, pp 497-500.
- Rajaratnam, N. and T. Gangadhariah, 1982. Entrainment by circular jets in cross-flow. *Journal of Wind Engineering and Industrial Aerodynamics*, Vol. 9, pp 251-255.
- Rajaratnam, N. and T. Gangadhariah, 1983. Vortex structure of circular jets in crossflow. *Journal of Wind Engineering and Industrial Aerodynamics*, Vol. 12, pp 155-164.
- Ramsey, J. W. and R. J. Goldstein, 1971. Interactions of a heated jet with a deflecting stream. *ASME Journal of Heat Transfer*, Vol. 94, pp 365-372.
- Reichardt, H., 1943. On a new theory of free turbulence. *Journal of the Royal Aeronautical Society*, Vol. 47, pp 167-176.
- Ricou, F. P. and D. B. Spalding, 1961. Measurements of entrainment by axisymmetrical turbulent jets. *Journal of Fluid Mechanics*, Vol. 11, Part 1, pp 21-32.
- Rodi, W., 1980. Turbulence models and their application in hydraulics. IAHR, State-of-the-Art Paper. Delft, The Netherlands.
- Rodi, W. and S. K. Srivatsa, 1979. A locally elliptic calculation procedure for three-dimensional flows and its application to a jet in a cross-flow. Sonderforschungsbereich 80. University of Karlsruhe.

- Rouse, H., 1953. Cavitation in the mixing zone of a submerged jet. *LaHouille Blanche*, Vol. 8, No. 1, pp 236-242.
- Rouse, H., 1966. Jet diffusion and cavitation. *Journal of the Boston Society of Civil Engineers*, Vol. 53, No. 3, pp 529-544.
- Ruggeri, R. S., 1952. General correlation of temperature profiles of a heated jet directed at various angles to an air stream. *NACA Technical Note 2855*. December, 1952.
- Ruggeri, R. S., E. E. Callaghan and D. T. Bowden, 1949. Penetration of air jets issuing from circular, square and elliptical orifices directed perpendicularly to an air stream. *NACA Technical Note 2019*.
- Sami, S., T. Carmody and H. Rouse, 1967. Jet diffusion in the region of flow establishment. *Journal of Fluid Mechanics*, Vol. 27, No. 2, pp 231-252.
- Saskatchewan Environment and Public Safety, 1988. Surface water quality objectives. Water Quality Branch. Regina, Saskatchewan.
- Schlichting, H., 1979. *Boundary-layer theory*. McGraw-Hill Book Company. New York, New York.
- Shandorov, G. S., 1966. Calculation of the axis of a jet in a cross flow. *Soviet Aeronautics*, pp 60-62.
- Shaughnessy, E. J. and J. B. Morton, 1977. Laser light-scattering measurements of particle concentration in a turbulent jet. *Journal of Fluid Mechanics*, Vol. 80, part 1, pp 129-148.
- Sherif, S. A. and R. H. Pletcher, 1989. Measurements of the flow and turbulence characteristics of round jets in cross flow. *Journal of Fluids Engineering*, Vol. 111, pp 165-171.
- Solanki, S., 1988. Finite element solutions of the pollutant conservation equation and its application to river plumes. M. Sc. Thesis. University of Alberta. Edmonton, Alberta.
- Steffler, P. M., 1980. Deflection of jets by weak cross flows. M. Sc. Thesis. University of Alberta. Edmonton, Alberta.
- Steffler, P. M. and N. Rajaratnam, 1983. Deflection of jets by weak crossflows. *ASCE Journal of Engineering Mechanics*, Vol. 109, No. 5, pp 1303-1307.
- Steffler, P. M. and N. Rajaratnam, 1985. Deflection of a circular jet by a weak cross-flow. *International Journal of Heat and Mass Transfer*, Vol. 28, No. 7, pp 714-717.

- Stoy, R. L. and Y. Ben-Haim, 1973. Turbulent jets in a confined crossflow. ASME Journal of Fluids Engineering, pp 551-556, December, 1973.
- Strachan, W. M. J., 1986. Research and other needs in support of national water quality guidelines (draft). National Water Research Institute, Canada Centre for Inland Waters. Burlington, Ontario.
- Sucec, J. and W. W. Bowley, 1976. Prediction of the trajectory of a turbulent jet injected into a crossflowing stream. ASME Journal of Fluids Engineering, pp 667-673.
- Tullis, J. P. and B. W. Marschner, 1968. Review of cavitation research on valves. ASCE Journal of the Hydraulics Division, Vol. 94, No. HY1, pp 1-16.
- Vizel, Y. M. and I. L. Mostinskii, 1965. Deflection of a jet injected into a stream. Faraday Press translation of the Journal of Engineering Physics, pp 160-163.
- Webel, G. and M. Schatzmann, 1984. Transverse mixing in open channel flow. ASCE Journal of Hydraulic Engineering, Vol. 110, No. 4, pp 423-435.
- Wyganski, I. and H. Fielder, 1969. Some measurements in the self-preserving jet. Journal of Fluid Mechanics, Vol. 38, part 3, pp 577-612.
- Wright, S. J., 1977a. Effects of ambient crossflows and density stratification on the characteristic behaviour of round turbulent buoyant jets. Report No. KH-R-36. W. M. Keck Laboratory of Hydraulics and Water Resources, California Institute of Technology. Pasadena, California.
- Wright, S. J., 1977b. Mean behaviour of buoyant jets in a crossflow. ASCE Journal of the Hydraulics Division, Vol. 103, No. HY5, pp 499-513.
- Yotsukura, N. and E. D. Cobb, 1972. Transverse diffusion of solutes in natural streams. U. S. Geological Survey Prof. Paper 582-C.
- Yotsukura, N. and M. B. Fiering, 1964. Numerical solution to a dispersion equation. ASCE Journal of the Hydraulics Division, Vol. 90, No. HY5, pp 83-104.
- Yotsukura, N. and W. W. Sayre, 1976. Transverse mixing in natural channels. Water Resources Research, Vol. 12, No. 4, pp 695-704.



Young, T. 1800. Outlines of experiments and inquiries respecting sound and light. Proceedings, Physics Society, Vol. 90, pp 604-626.

Ziegler, H. and P. T. Wooler, 1971. Multiple jets exhausting into a crossflow. Journal of Aircraft, Vol. 8, pp 414-420.

**APPENDIX A**  
**DATA SUMMARY FOR PHOTOGRAPHIC STUDY**

The following pages present the partially reduced data for the side view and plan view measurements of the jet profiles and jet widths examined in this dissertation. For the jet profiles, the data comprise the station ( $x$ ), the computed axis location ( $E_x$ ) for the jet centreline, the six-photo average for the inner ( $y_i$ ) and outer ( $y_o$ ) jet boundary locations, the computed jet centreline ( $y_c$ ) location and the computed jet thickness ( $W_y$ ). All measurements are in mm. A number of other computed parameters describing the jet profile and other aspects of each run are also presented.

For the jet widths, the data comprise the station ( $x$ ), the computed axis location ( $E_{x'}$ ), the corrected station ( $x'$ ) and the six-photo average for the total jet width ( $W_z$ ). A number of other computed parameters describing the jet width and other aspects of each run are also presented.

CIRCULAR JETS DISCHARGING INTO CROSSFLOWS OF FINITE DEPTH  
 PROFILE DATA EXTRACTED FROM RAW DATA FILES

FILE: PROF

MEASUREMENTS BY:

JOHN HODGSON

LAST CHANGED (mm/dd/yy):

11/13/90

TIME: 17:48

PROFILE DATA 6 PHOTO AVERAGES						COMPUTED VALUES					RUN	
x	Ex	yi	yo	yc	Wy	x/R*d	Ex/R*d	yi/R*d	yo/R*d	yc/R*d	Wy/R*d	DESCRIPTION
								1235	1236	1236	1236	
0	12	0	24	12	24	3.39E-06	0.413	3E-06	0.225	0.413	0.8255	HODGSON DATA
17	34	9	43	26	34	0.59	1.15	0.29	1.45	0.68	1.16	
34	54	15	58	36	43	1.15	1.83	0.51	1.98	1.23	1.45	RUN 1236
52	72	17	59	38	42	1.73	2.44	0.57	1.99	1.28	1.42	d 12.7
77	97	15	68	42	53	2.61	3.30	0.51	2.31	1.41	1.80	D 300
102	123	16	79	47	63	3.46	4.17	0.54	2.67	1.61	2.13	Uo 0.526
127	148	17	83	50	66	4.31	5.02	0.57	2.82	1.69	2.25	U 0.226
152	174	20	90	55	70	5.16	5.89	0.67	3.05	1.86	2.39	R 2.32
177	199	21	87	54	66	6.00	6.74	0.70	2.94	1.82	2.24	Rd/D 0.098
202	224	20	90	55	70	6.85	7.59	0.68	3.06	1.87	2.39	RRd/D 0.228
227	249	17	92	55	75	7.70	8.44	0.59	3.12	1.85	2.53	Yot 114
252	274	13	91	52	78	8.55	9.29	0.45	3.09	1.77	2.63	Yct 67
277	299	11	93	52	83	9.40	10.14	0.36	3.17	1.76	2.80	Yit 20
302	324	11	103	57	92	10.24	11.00	0.38	3.51	1.94	3.12	Xot
327	349	16	100	58	84	11.09	11.85	0.55	3.40	1.98	2.85	Xc. 500
352	374	15	104	60	88	11.94	12.70	0.52	3.52	2.02	3.00	Xit
377	399	14	109	61	95	12.79	13.55	0.47	3.69	2.08	3.21	Yc/D 2.23
402	425	17	112	65	96	13.64	14.41	0.57	3.81	2.19	3.25	Yc/(R*d) 2.27
427	450	18	110	64	92	14.49	15.25	0.60	3.73	2.17	3.13	Xct/(R*d) 16.96
452	476	24	118	71	94	15.33	16.14	0.83	4.01	2.42	3.19	
								1231	1231	1231	1231	
0	19	0	37	19	37	0.00	0.63	0.00	0.97	0.49	0.97	HODGSON DATA
17	39	13	47	30	34	0.45	1.03	0.33	1.24	0.79	0.90	
34	61	17	70	43	53	0.90	1.60	0.45	1.83	1.14	1.39	RUN 1231
52	79	18	74	46	56	1.37	2.08	0.48	1.96	1.22	1.47	d 12.7
77	104	21	82	52	61	2.03	2.75	0.55	2.16	1.36	1.61	D 298
102	130	23	92	58	68	2.89	3.43	0.61	2.41	1.51	1.80	Uo 0.658
127	155	24	99	61	75	3.34	4.09	0.62	2.61	1.62	1.98	U 0.220
152	180	25	100	63	75	4.00	4.75	0.67	2.63	1.65	1.97	R 2.99
177	205	21	104	63	83	4.86	5.41	0.56	2.75	1.65	2.19	Rd/D 0.127
202	230	20	104	62	84	5.32	6.07	0.53	2.74	1.63	2.21	RRd/D 0.381
227	256	25	111	68	87	5.98	6.75	0.65	2.93	1.79	2.28	Yot 155
252	281	29	112	70	83	6.64	7.41	0.75	2.95	1.85	2.19	Yct 90
277	307	26	122	74	95	7.29	8.07	0.69	3.20	1.95	2.51	Yit 25
302	332	27	124	76	97	7.95	8.73	0.72	3.27	2.00	2.55	Xot
327	357	24	124	74	100	8.61	9.39	0.63	3.27	1.95	2.63	Xct 535
352	383	25	138	81	113	9.27	10.08	0.66	3.63	2.14	2.97	Xit
377	408	27	140	84	113	9.93	10.74	0.71	3.69	2.20	2.98	Yc/D 0.302
402	433	20	141	81	120	10.59	11.40	0.54	3.70	2.12	3.17	Yc/(R*d) 2.37
427	459	22	157	89	135	11.24	12.10	0.57	4.13	2.35	3.56	Xct/(R*d) 14.09
452	484	21	159	90	138	11.90	12.76	0.55	4.18	2.37	3.63	
								1232	1232	1232	1232	
0	27	0	54	27	54	0.00	0.72	0.00	1.04	0.52	1.04	HODGSON DATA
17	52	23	67	45	44	0.32	0.99	0.44	1.27	0.85	0.83	
34	76	36	90	63	54	0.65	1.45	0.68	1.71	1.19	1.03	RUN 1232
52	96	40	102	71	62	0.99	1.83	0.76	1.95	1.36	1.19	d 12.7
77	123	45	115	80	70	1.47	2.34	0.86	2.20	1.53	1.33	D 298
102	148	47	122	85	75	1.94	2.83	0.90	2.33	1.61	1.42	Uo 0.908
127	175	51	137	94	86	2.42	3.33	0.97	2.61	1.79	1.64	U 0.220
152	200	56	136	96	80	2.90	3.81	1.07	2.60	1.83	1.53	R 4.13
177	227	58	154	106	96	3.37	4.32	1.11	2.93	2.02	1.82	Rd/D 0.176

202	252	59	151	105	92	3.85	4.80	1.12	2.88	2.00	1.76 RRd/D	0.727
227	277	63	157	110	94	4.33	5.29	1.21	3.00	2.10	1.79 Yot	190
252	303	64	167	115	103	4.80	5.77	1.21	3.18	2.20	1.97 Yct	131
277	328	65	170	118	105	5.28	6.25	1.24	3.24	2.24	2.00 Yit	72
302	354	71	176	123	105	5.76	6.74	1.35	3.35	2.35	2.00 Xot	
327	379	70	178	124	108	6.23	7.22	1.34	3.40	2.37	2.06 Xct	414
352	404	70	182	126	112	6.71	7.69	1.33	3.46	2.40	2.13 Xit	
377	429	69	179	124	110	7.19	8.17	1.31	3.41	2.36	2.10 Yc/D	0.440
402	454	73	181	127	108	7.66	8.65	1.39	3.45	2.42	2.06 Yc/(R*d)	2.50
427	479	72	189	131	117	8.14	9.13	1.37	3.61	2.49	2.24 Xct/(R*d)	7.89
452	504	70	191	131	121	8.62	9.61	1.33	3.65	2.49	2.31 -----	
								2111	2111	2111	2111	
0	14	0	28	14	28	0.00	0.26	0.00	0.67	0.34	0.67 HODGSON DATA	
17	40	15	53	34	39	0.41	0.98	0.36	1.30	0.83	0.94 -----	
34	60	19	68	43	49	0.83	1.45	0.46	1.65	1.06	1.19 RUN	2111
52	78	21	75	48	54	1.27	1.90	0.51	1.83	1.17	1.32 d	11.0
77	104	25	81	53	56	1.88	2.53	0.61	1.97	1.29	1.36 D	174
102	129	26	88	57	63	2.48	3.14	0.63	2.15	1.39	1.53 Uo	0.877
127	154	27	89	58	61	3.09	3.75	0.67	2.16	1.41	1.49 U	0.235
152	179	30	94	62	64	3.70	4.37	0.74	2.30	1.52	1.56 R	3.73
177	205	32	101	66	69	4.31	4.99	0.77	2.46	1.62	1.69 Rd/D	0.236
202	230	33	103	68	70	4.92	5.60	0.81	2.51	1.66	1.70 RRd/D	0.880
227	255	32	107	69	75	5.53	6.21	0.77	2.61	1.69	1.84 Yot	125
252	280	33	108	70	75	6.14	6.82	0.80	2.62	1.71	1.83 Yct	79
277	305	34	104	69	70	6.75	7.43	0.82	2.53	1.68	1.71 Yit	33
302	330	32	110	71	78	7.36	8.04	0.79	2.68	1.73	1.89 Xot	
327	355	29	116	72	87	7.97	8.65	0.70	2.83	1.78	2.13 Xct	468
352	380	28	115	71	87	8.57	9.26	0.67	2.79	1.73	2.12 Xit	
377	405	29	119	74	89	9.19	9.87	0.71	2.89	1.80	2.18 Yc/D	0.454
402	430	31	119	75	89	9.79	10.48	0.75	2.91	1.83	2.16 Yc/(R*d)	1.92
427	455	31	123	77	92	10.40	11.09	0.76	3.00	1.88	2.23 Xct/(R*d)	11.40
452	480	34	126	80	91	11.01	11.70	0.84	3.06	1.95	2.22 -----	
								1233	1233	1233	1233	
0	35	0	69	35	69	0.00	0.84	0.00	1.04	0.52	1.04 HODGSON DATA	
17	70	34	96	65	62	0.25	1.04	0.51	1.44	0.98	0.93 -----	
34	93	45	116	81	70	0.51	1.38	0.68	1.73	1.20	1.05 RUN	1233
52	113	52	128	90	77	0.78	1.69	0.77	1.92	1.34	1.15 d	12.7
77	139	59	136	98	77	1.15	2.08	0.88	2.04	1.46	1.16 D	298
102	164	61	144	102	83	1.52	2.46	0.91	2.15	1.53	1.24 Uo	1.58
127	191	66	154	110	88	1.90	2.85	0.98	2.30	1.64	1.32 U	0.220
152	216	65	154	110	89	2.27	3.22	0.98	2.30	1.64	1.32 R	5.27
177	241	68	161	114	93	2.64	3.60	1.01	2.41	1.71	1.39 Rd/D	0.225
202	266	65	167	116	102	3.02	3.97	0.98	2.49	1.74	1.52 RRd/D	1.184
227	292	71	172	122	101	3.39	4.36	1.07	2.57	1.82	1.51 Yot	225
252	317	73	179	126	106	3.76	4.74	1.10	2.67	1.88	1.58 Yct	152
277	342	73	184	129	110	4.14	5.11	1.10	2.74	1.92	1.65 Yit	79
302	368	75	195	135	120	4.51	5.50	1.13	2.91	2.02	1.79 Xot	
327	393	73	200	137	127	4.89	5.87	1.09	2.99	2.04	1.90 Xct	505
352	418	70	205	137	136	5.26	6.25	1.04	3.06	2.05	2.02 Xit	
377	443	70	211	141	141	5.63	6.62	1.05	3.15	2.10	2.11 Yc/D	0.510
402	469	75	217	146	142	6.01	7.00	1.13	3.24	2.18	2.12 Yc/(R*d)	2.27
427	494	80	220	150	141	6.38	7.38	1.19	3.29	2.24	2.10 Xct/(R*d)	7.54
452	519	79	225	152	146	6.75	7.76	1.19	3.37	2.28	2.18 -----	
								2112	2112	2112	2112	
0	29	0	58	29	58	0.00	0.44	0.00	1.02	0.51	1.02 HODGSON DATA	
17	61	30	82	56	52	0.30	1.07	0.53	1.43	0.98	0.91 -----	
34	82	39	99	69	61	0.59	1.43	0.67	1.73	1.20	1.06 RUN	2112
52	101	45	106	75	61	0.91	1.77	0.78	1.84	1.31	1.06 d	11.0
77	128	50	119	85	69	1.34	2.23	0.87	2.07	1.47	1.20 D	174
102	153	50	126	88	76	1.78	2.67	0.87	2.20	1.54	1.33 Uo	1.227
127	179	55	133	94	78	2.21	3.12	0.96	2.31	1.63	1.35 U	0.235
152	204	56	135	95	79	2.65	3.55	0.97	2.35	1.66	1.38 R	5.22
177	230	59	141	100	82	3.08	4.00	1.03	2.46	1.75	1.43 Rd/D	0.330
202	255	60	144	102	84	3.52	4.43	1.04	2.51	1.77	1.47 RRd/D	1.723

227	280	56	144	100	88	3.95	4.87	0.98	2.50	1.74	1.53	Yot	172
252	305	57	153	105	96	4.39	5.31	0.99	2.66	1.83	1.67	Yct	121
277	330	58	157	108	99	4.82	5.75	1.02	2.73	1.87	1.72	Yit	70
302	356	59	164	112	105	5.26	6.19	1.03	2.86	1.94	1.83	Xot	
327	381	61	165	113	104	5.69	6.63	1.06	2.88	1.97	1.82	Xct	465
352	406	61	170	115	109	6.13	7.07	1.06	2.95	2.01	1.90	Xit	
377	431	66	171	119	105	6.56	7.50	1.15	2.98	2.07	1.83	Yc/D	0.695
402	456	64	169	117	105	7.00	7.94	1.11	2.94	2.03	1.83	Yc/(R*d)	2.11
427	481	66	171	118	105	7.43	8.38	1.14	2.98	2.06	1.83	Xct/(R*d)	8.10
452	506	70	172	121	102	7.87	8.82	1.22	3.00	2.11	1.78	-----	
									1234	1234	1234	1234	
0	44	0	87	44	87	0.00	0.76	0.00	1.02	0.51	1.02	HODGSON DATA	
17	78	35	112	74	78	0.20	0.91	0.41	1.32	0.86	0.91	-----	
34	108	55	140	98	85	0.40	1.26	0.65	1.65	1.15	1.00	RUN	1234
52	129	68	152	110	83	0.61	1.52	0.80	1.78	1.29	0.98	d	12.7
77	161	85	174	130	89	0.90	1.89	1.00	2.05	1.52	1.05	D	298
102	188	90	187	138	97	1.20	2.20	1.06	2.19	1.62	1.13	Ub	1.474
127	214	90	202	146	112	1.49	2.51	1.05	2.37	1.71	1.31	U	0.220
152	239	91	212	152	122	1.78	2.81	1.06	2.49	1.78	1.43	R	6.71
177	264	91	215	153	124	2.08	3.10	1.07	2.52	1.79	1.45	Rd/D	0.286
202	290	91	222	156	131	2.37	3.40	1.08	2.60	1.83	1.54	RRd/D	1.919
227	315	88	229	158	141	2.66	3.69	1.03	2.69	1.86	1.66	Yot	264
252	340	92	233	163	141	2.96	3.99	1.08	2.74	1.91	1.65	Yct	185
277	365	96	231	164	135	3.25	4.28	1.13	2.71	1.92	1.59	Yit	106
302	390	98	237	168	139	3.54	4.58	1.15	2.78	1.97	1.63	Xot	
327	418	105	254	179	149	3.84	4.90	1.23	2.98	2.10	1.75	Xct	402
352	443	106	261	183	155	4.13	5.20	1.24	3.06	2.15	1.82	Xit	
377	468	104	262	183	158	4.42	5.49	1.22	3.07	2.15	1.85	Yc/D	0.621
402	493	106	264	185	158	4.72	5.79	1.24	3.10	2.17	1.86	Yc/(R*d)	2.17
427	519	115	266	190	151	5.01	6.09	1.35	3.12	2.23	1.77	Xct/(R*d)	4.72
452	545	110	258	184	148	5.30	6.39	1.29	3.03	2.16	1.74	-----	
									1235	1235	1235	1235	
0	56	0	112	56	112	0.00	0.66	0.00	1.11	0.56	1.11	HODGSON DATA	
17	91	41	133	87	92	0.17	0.91	0.40	1.32	0.86	0.92	-----	
34	121	58	165	112	107	0.34	1.21	0.58	1.64	1.11	1.06	RUN	1235
52	146	76	181	129	105	0.52	1.45	0.76	1.81	1.28	1.05	d	12.7
77	173	81	198	139	117	0.77	1.72	0.80	1.97	1.39	1.16	D	298
102	200	91	209	150	118	1.02	1.99	0.90	2.08	1.49	1.18	Ub	1.737
127	227	99	219	159	120	1.26	2.26	0.98	2.18	1.58	1.20	U	0.220
152	253	100	229	165	129	1.51	2.51	1.00	2.28	1.64	1.28	R	7.91
177	278	100	236	168	136	1.76	2.77	0.99	2.35	1.67	1.35	Rd/D	0.337
202	303	105	236	171	130	2.01	3.02	1.05	2.35	1.70	1.30	RRd/D	2.666
227	329	105	253	179	149	2.26	3.28	1.04	2.52	1.78	1.48	Yot	289
252	355	108	264	186	156	2.51	3.54	1.08	2.63	1.85	1.55	Yct	201
277	380	112	264	188	152	2.76	3.79	1.12	2.63	1.87	1.51	Yit	113
302	405	106	265	186	158	3.01	4.04	1.06	2.63	1.85	1.58	Xot	
327	431	98	277	188	179	3.26	4.29	0.98	2.76	1.87	1.78	Xct	397
352	456	103	283	193	179	3.50	4.54	1.03	2.81	1.92	1.79	Xit	
377	482	113	289	201	176	3.75	4.80	1.12	2.87	2.00	1.75	Yc/D	0.674
402	507	114	294	204	180	4.00	5.05	1.13	2.92	2.03	1.79	Yc/(R*d)	2.00
427	533	113	289	201	175	4.25	5.30	1.13	2.87	2.00	1.75	Xct/(R*d)	3.95
452	558	106	288	197	182	4.50	5.55	1.06	2.87	1.96	1.82	-----	
									2113	2113	2113	2113	
0	35	0	70	35	70	0.00	0.35	0.00	0.95	0.48	0.95	HODGSON DATA	
17	73	40	99	69	59	0.23	0.99	0.54	1.34	0.94	0.79	-----	
34	97	52	118	85	66	0.46	1.31	0.70	1.60	1.15	0.90	RUN	2113
52	116	59	128	93	69	0.70	1.58	0.79	1.73	1.26	0.94	d	11.0
77	144	65	145	105	79	1.04	1.95	0.89	1.96	1.42	1.07	D	174
102	170	70	155	112	85	1.38	2.30	0.94	2.10	1.52	1.16	Ub	1.578
127	195	74	159	117	84	1.72	2.65	1.01	2.15	1.58	1.14	U	0.235
152	221	75	166	121	91	2.06	2.99	1.02	2.25	1.63	1.23	R	6.71
177	246	75	172	124	98	2.40	3.33	1.01	2.33	1.67	1.32	Rd/D	0.424
202	271	75	173	124	97	2.74	3.67	1.02	2.34	1.68	1.32	RRd/D	2.846
227	296	76	174	125	98	3.08	4.01	1.03	2.36	1.70	1.32	Yot	174

252	321	81	174	128	93	3.41	4.35	1.10	2.36	1.75	1.26	Yct	129
277	346	84	174	129	90	3.75	4.69	1.13	2.36	1.75	1.22	Yit	84
302	371	85	174	130	89	4.09	5.03	1.16	2.36	1.76	1.20	Xot	
327	396	84	174	129	90	4.43	5.37	1.14	2.36	1.75	1.21	Xct	264
352	421	84	174	129	90	4.77	5.70	1.13	2.36	1.75	1.22	Xit	
377	446	84	174	129	90	5.11	6.04	1.14	2.36	1.75	1.21	Yc/D	0.741
402	471	84	174	129	90	5.45	6.38	1.14	2.36	1.75	1.22	Yc/(R*d)	1.75
427	496	83	174	128	91	5.79	6.72	1.12	2.36	1.74	1.24	Xct/(R*d)	3.58
452	521	80	174	127	94	6.12	7.06	1.09	2.36	1.72	1.27	-----	
								2114	2114	2114	2114	-----	
0	46	0	93	46	93	0.00	0.63	0.00	1.03	0.51	1.03	HODGSON DATA	
17	88	47	122	85	75	0.19	0.98	0.52	1.35	0.94	0.83	-----	
34	114	62	147	105	85	0.38	1.27	0.69	1.63	1.16	0.94	RUN	2114
52	137	72	166	119	94	0.58	1.52	0.79	1.84	1.32	1.05	d	11.0
77	163	79	172	126	92	0.85	1.81	0.88	1.90	1.39	1.02	D	174
102	189	87	174	131	87	1.13	2.09	0.96	1.93	1.45	0.96	Ub	1.929
127	214	91	174	133	83	1.41	2.37	1.01	1.93	1.47	0.92	U	0.235
152	239	94	174	134	80	1.69	2.65	1.04	1.93	1.48	0.89	R	8.20
177	264	93	174	134	81	1.98	2.93	1.03	1.93	1.48	0.89	Rd/D	0.518
202	289	90	174	132	84	2.24	3.20	1.00	1.93	1.47	0.93	RRd/D	4.251
227	314	93	174	133	81	2.52	3.48	1.03	1.93	1.48	0.90	Yot	174
252	339	92	174	133	82	2.79	3.76	1.02	1.93	1.47	0.91	Yct	134
277	364	92	174	133	82	3.07	4.03	1.02	1.93	1.47	0.91	Yit	93
302	389	91	174	132	83	3.35	4.31	1.01	1.93	1.47	0.92	Xot	
327	414	88	174	131	86	3.63	4.59	0.97	1.93	1.45	0.96	Xct	137
352	439	89	174	132	85	3.90	4.87	0.99	1.93	1.46	0.94	Xit	
377	464	93	174	133	81	4.18	5.14	1.03	1.93	1.48	0.90	Yc/D	0.767
402	489	95	174	135	79	4.46	5.42	1.05	1.93	1.49	0.88	Yc/(R*d)	1.48
427	514	99	174	136	75	4.73	5.70	1.09	1.93	1.51	0.84	Xct/(R*d)	1.52
452	539	100	174	137	74	5.01	5.98	1.10	1.93	1.52	0.82	-----	
								1136	1136	1136	1136	-----	
0	75	0	149	75	149	0.00	0.83	0.00	1.09	0.54	1.09	HODGSON DATA	
17	121	50	187	118	137	0.12	0.88	0.36	1.36	0.86	1.30	-----	
34	161	88	220	154	131	0.25	1.17	0.64	1.60	1.12	0.96	RUN	1136
52	184	104	232	168	128	0.38	1.34	0.76	1.69	1.22	0.93	d	12.7
77	222	123	271	197	148	0.56	1.62	0.90	1.98	1.44	1.08	D	298
102	250	128	290	209	161	0.74	1.82	0.93	2.11	1.52	1.18	Ub	1.395
127	276	138	296	217	158	0.93	2.01	1.01	2.16	1.58	1.15	U	0.129
152	302	148	298	223	150	1.11	2.20	1.08	2.17	1.62	1.10	R	10.81
177	327	148	298	223	150	1.29	2.38	1.08	2.17	1.62	1.09	Rd/D	0.461
202	352	153	298	223	145	1.47	2.56	1.11	2.17	1.64	1.06	RRd/D	4.980
227	377	156	298	227	142	1.65	2.75	1.14	2.17	1.65	1.03	Yot	298
252	402	159	298	229	139	1.84	2.93	1.16	2.17	1.66	1.01	Yct	235
277	427	158	298	228	140	2.02	3.11	1.15	2.17	1.66	1.02	Yit	172
302	452	160	298	229	138	2.20	3.29	1.17	2.17	1.67	1.01	Xot	
327	477	166	298	232	132	2.38	3.48	1.21	2.17	1.69	0.96	Xct	354
352	502	169	298	233	129	2.56	3.66	1.23	2.17	1.70	0.94	Xit	
377	527	171	298	235	127	2.75	3.84	1.25	2.17	1.71	0.93	Yc/D	0.789
402	552	170	298	234	128	2.93	4.02	1.24	2.17	1.70	0.93	Yc/(R*d)	1.71
427	577	173	298	235	125	3.11	4.21	1.26	2.17	1.71	0.91	Xct/(R*d)	2.58
452	603	177	298	238	121	3.29	4.39	1.29	2.17	1.73	0.88	-----	
								2115	2115	2115	2115	-----	
0	58	0	115	58	115	0.00	0.42	0.00	1.08	0.54	1.08	HODGSON DATA	
17	102	49	149	99	100	0.16	0.96	0.46	1.40	0.93	0.94	-----	
34	128	69	167	118	98	0.32	1.20	0.64	1.57	1.10	0.92	RUN	2115
52	148	78	174	126	96	0.49	1.38	0.73	1.63	1.18	0.90	d	11.0
77	173	87	174	131	87	0.72	1.62	0.82	1.63	1.22	0.82	D	174
102	198	96	174	135	78	0.96	1.86	0.90	1.63	1.27	0.73	Ub	2.260
127	223	99	174	136	75	1.19	2.09	0.92	1.63	1.28	0.71	U	0.235
152	248	101	174	138	73	1.42	2.33	0.95	1.63	1.29	0.68	R	9.70
177	273	106	174	140	68	1.66	2.56	0.99	1.63	1.31	0.64	Rd/D	0.613
202	298	105	174	140	69	1.89	2.80	0.98	1.63	1.31	0.65	RRd/D	5.948
227	323	104	174	139	70	2.13	3.03	0.98	1.63	1.30	0.65	Yot	174
252	348	102	174	138	72	2.36	3.27	0.96	1.63	1.29	0.67	Yct	138

277	374	100	174	137	74	2.60	3.50	0.93	1.63	1.28	0.70	Yit	102
302	399	98	174	136	76	2.83	3.74	0.92	1.63	1.27	0.72	Xot	
327	424	102	174	138	72	3.06	3.97	0.95	1.63	1.29	0.68	Xct	147
352	449	99	174	137	75	3.30	4.20	0.93	1.63	1.28	0.70	Xit	
377	474	100	174	137	74	3.53	4.44	0.93	1.63	1.28	0.70	Yc/D	0.793
402	499	97	174	136	77	3.77	4.67	0.91	1.63	1.27	0.72	Yc/(R*d)	1.29
427	524	98	174	136	76	4.00	4.91	0.92	1.63	1.27	0.72	Xct/(R*d)	1.38
452	549	95	174	135	79	4.24	5.14	0.89	1.63	1.26	0.74	-----	-----
								1135	1135	1135	1135		
0	92	0	184	92	184	0.00	0.86	0.00	1.11	0.56	1.11	HODGSON DATA	
17	138	49	221	135	172	0.10	0.83	0.30	1.33	0.81	1.04	-----	-----
34	188	96	267	181	171	0.21	1.13	0.58	1.61	1.09	1.03	RLN	1135
52	215	114	290	202	175	0.31	1.30	0.69	1.75	1.22	1.06	d	12.7
77	245	137	298	218	161	0.46	1.48	0.83	1.80	1.31	0.97	D	298
102	272	160	298	229	138	0.62	1.64	0.97	1.80	1.38	0.83	Uo	1.684
127	297	168	298	233	130	0.77	1.79	1.02	1.80	1.41	0.78	U	0.129
152	322	170	298	234	128	0.92	1.94	1.02	1.80	1.41	0.77	R	13.05
177	348	178	298	238	120	1.07	2.10	1.07	1.80	1.44	0.72	Rd/D	0.556
202	373	183	298	240	115	1.22	2.25	1.10	1.80	1.45	0.70	RRd/D	7.258
227	398	184	298	241	114	1.37	2.40	1.11	1.80	1.45	0.69	Yot	298
252	423	186	298	242	112	1.52	2.55	1.12	1.80	1.46	0.68	Yct	242
277	448	185	298	241	113	1.67	2.70	1.11	1.80	1.46	0.68	Yit	185
302	473	186	298	242	112	1.82	2.85	1.12	1.80	1.46	0.68	Xot	
327	498	187	298	243	111	1.97	3.00	1.13	1.80	1.46	0.67	Xct	235
352	523	186	298	242	112	2.12	3.15	1.12	1.80	1.46	0.68	Xit	
377	548	186	298	242	112	2.27	3.31	1.12	1.80	1.46	0.68	Yc/D	0.812
402	573	186	298	242	112	2.43	3.46	1.12	1.80	1.46	0.68	Yc/(R*d)	1.46
427	598	184	298	241	114	2.58	3.61	1.11	1.80	1.46	0.69	Xct/(R*d)	1.42
452	623	184	298	241	114	2.73	3.76	1.11	1.80	1.46	0.69	-----	-----
MAX	623	187	298	243	184	15.33	16.14				2115.00		
MIN	12	0	24	12	24	0.00	0.28	0.00	0.67	0.34	0.64		
x	Ex	yi	yo	yc	Wy	x/R*d	Ex/R*d	yi/R*d	yo/R*d	yc/R*d	Wy/R*d		

NOTES: x IS DISTANCE DOWNSTREAM FROM CENTRE OF THE JET NOZZLE.  
 Ex IS DISTANCE ALONG AXIS FOR THE SIDE VIEW MEASUREMENTS.  
 yi IS DISTANCE FROM FLUME BED TO LOWER JET BOUNDARY.  
 yo IS DISTANCE FROM FLUME BED TO UPPER JET BOUNDARY.  
 yc IS DISTANCE FROM FLUME BED TO JET CENTRELINE (COMPUTED).  
 Wy IS SIDE VIEW JET WIDTH (COMPUTED JET THICKNESS).  
 d IS JET NOZZLE DIAMETER (CONVERGING NOZZLE DESIGN).  
 D IS FLUME DEPTH.  
 Uo IS JET NOZZLE VELOCITY.  
 U IS FLUME VELOCITY.  
 R IS VELOCITY RATIO (Uo/U).  
 Yot IS OUTER BOUNDARY TERMINAL LEVEL.  
 Yct IS CENTRELINE TERMINAL LEVEL.  
 Yit IS INNER BOUNDARY TERMINAL LEVEL.  
 Xct IS DISTANCE TO CENTRELINE TERMINAL LEVEL.  
 ALL DISTANCES ARE IN mm; ALL VELOCITIES ARE IN m/s.

CIRCULAR JETS DISCHARGING INTO CROSSFLOWS OF FINITE DEPTH  
WIDTH DATA EXTRACTED FROM RAW DATA FILES

FILE: WID

MEASUREMENTS BY: JOHN HODGSON

LAST CHANGED:

11/13/90

TIME: 17:53

WIDTH DATA 6 PHOTO AVERAGES				COMPUTED VALUES				RUN DESCRIPTION
x	Ex'	x'	Wz	x / R*d	Ex' / R*d	x' / R*d	Wz /R*d	
0	13.69	1.2	28.2	0.00	0.46432	0.04071	0.9559	HODGSON DATA
17	37	19	42	0.58	1.24	0.65	1.43	-----
34	57	37	51	1.15	1.93	1.25	1.74	RUN 1236
52	75	55	56	1.76	2.53	1.85	1.90	d 12.7
77	100	79	56	2.61	3.38	2.69	1.90	D 300
102	125	104	62	3.46	4.25	3.53	2.10	Uo 0.526
127	150	129	71	4.31	5.08	4.65	2.42	U 0.226
152	175	153	74	5.16	5.93	5.59	2.52	R 2.32
177	199	178	72	6.00	6.76	6.02	2.45	Rd/D 0.098
202	224	202	83	6.85	7.59	6.84	2.80	RRd/D 0.228
227	248	226	87	7.70	8.41	7.67	2.96	-----
252	273	251	96	8.55	9.25	8.50	3.24	
277	297	275	97	9.40	10.08	9.32	3.29	
302	322	299	107	10.24	10.91	10.14	3.62	
327	346	324	109	11.09	11.74	10.97	3.71	
352	370	348	116	11.94	12.57	11.79	3.95	
377	395	372	105	12.79	13.39	12.61	3.56	
402	419	396	114	13.64	14.21	13.42	3.86	
427	443	421	111	14.49	15.03	14.26	3.78	
452	468	444	110	15.33	15.86	15.05	3.72	
-----								
0	21	2	32	0.00	0.54	0.05	0.84	HODGSON DATA
17	42	20	44	0.45	1.12	0.52	1.16	-----
34	64	37	55	0.90	1.69	0.98	1.45	RUN 1231
52	82	55	67	1.37	2.16	1.45	1.75	d 12.7
77	107	80	73	2.03	2.83	2.10	1.93	D 298
102	133	105	81	2.69	3.50	2.75	2.12	Uo 0.658
127	157	129	86	3.34	4.15	3.39	2.27	U 0.220
152	182	153	91	4.00	4.79	4.03	2.40	R 2.99
177	206	178	90	4.66	5.43	4.67	2.37	Rd/D 0.127
202	230	202	92	5.32	6.07	5.31	2.41	RRd/D 0.381
227	255	226	95	5.98	6.73	5.95	2.51	-----
252	280	250	98	6.64	7.37	6.58	2.59	
277	304	274	111	7.29	8.01	7.22	2.92	
302	328	299	105	7.95	8.64	7.86	2.76	
327	353	323	107	8.61	9.28	8.49	2.81	
352	377	347	115	9.27	9.93	9.12	3.03	
377	401	370	125	9.93	10.57	9.74	3.29	
402	426	395	122	10.59	11.21	10.39	3.21	



427	450	418	135	11.24	11.86	11.00	3.55	
452	474	442	148	11.90	12.49	11.63	3.89	
-----								
0	31	3	39	0.00	0.59	0.05	0.75	HODGSON DATA
17	58	21	48	0.32	1.10	0.40	0.91	-----
34	82	39	57	0.65	1.56	0.74	1.09	RUN 1232
52	101	57	65	0.99	1.93	1.08	1.24	d 12.7
77	127	82	77	1.47	2.43	1.55	1.46	D 298
102	152	106	87	1.94	2.90	2.02	1.67	Uo 0.908
127	178	130	93	2.42	3.39	2.48	1.76	U 0.220
152	202	154	99	2.90	3.86	2.94	1.88	R 4.13
177	228	178	109	3.37	4.34	3.40	2.08	Rd/D 0.176
202	252	202	111	3.85	4.80	3.85	2.12	RRd/D 0.727
227	276	226	112	4.33	5.26	4.30	2.13	-----
252	300	249	129	4.80	5.72	4.75	2.47	
277	324	273	130	5.28	6.17	5.20	2.49	
302	348	296	129	5.76	6.63	5.65	2.46	
327	372	320	140	6.23	7.08	6.10	2.67	
352	395	344	135	6.71	7.53	6.55	2.57	
377	419	367	131	7.19	7.98	7.00	2.50	
402	443	391	135	7.66	8.44	7.44	2.57	
427	466	414	141	8.14	8.88	7.89	2.70	
452	489	437	160	8.62	9.33	8.33	3.04	
-----								
0	16	1	27	0.00	0.39	0.03	0.65	HODGSON DATA
17	44	20	42	0.41	1.06	0.49	1.03	-----
34	63	37	51	0.83	1.53	0.91	1.24	RUN 2111
52	82	55	56	1.27	1.99	1.35	1.36	d 11.0
77	107	80	67	1.88	2.60	1.95	1.63	D 174
102	132	105	72	2.48	3.20	2.55	1.75	Uo 0.877
127	156	129	83	3.09	3.80	3.14	2.03	U 0.235
152	181	153	80	3.70	4.40	3.74	1.95	R 3.73
177	205	178	89	4.31	5.00	4.33	2.16	Rd/D 0.236
202	230	202	88	4.92	5.60	4.92	2.14	RRd/D 0.880
227	254	226	85	5.53	6.19	5.52	2.06	-----
252	278	250	99	6.14	6.78	6.10	2.40	
277	303	275	97	6.75	7.37	6.70	2.35	
302	327	299	101	7.36	7.96	7.29	2.45	
327	351	323	111	7.97	8.55	7.87	2.70	
352	375	347	123	8.57	9.14	8.46	2.99	
377	399	371	118	9.18	9.73	9.03	2.88	
402	424	395	119	9.79	10.32	9.63	2.91	
427	448	419	113	10.40	10.90	10.22	2.74	
452	472	443	127	11.01	11.49	10.80	3.09	
-----								
0	42	4	50	0.00	0.63	0.06	0.74	HODGSON DATA
17	78	23	61	0.25	1.16	0.34	0.91	-----
34	100	40	73	0.51	1.49	0.60	1.09	RUN 1233
52	119	58	87	0.78	1.78	0.87	1.31	d 12.7
77	145	83	98	1.15	2.16	1.23	1.47	D 298
102	169	107	107	1.52	2.53	1.59	1.61	Uo 1.158
127	194	131	123	1.90	2.90	1.95	1.84	U 0.220

152	218	154	124	2.27	3.26	2.31	1.86 R	5.27
177	242	178	127	2.64	3.62	2.66	1.89 Rd/D	0.225
202	266	202	139	3.02	3.97	3.02	2.07 RRd/D	1.184
227	290	226	146	3.39	4.34	3.37	2.18 -----	
252	314	249	149	3.76	4.69	3.72	2.23	
277	338	273	143	4.14	5.05	4.07	2.14	
302	362	296	146	4.51	5.40	4.42	2.18	
327	385	319	152	4.89	5.76	4.77	2.28	
352	409	343	161	5.26	6.11	5.12	2.40	
377	432	366	177	5.63	6.46	5.47	2.64	
402	456	389	169	6.01	6.81	5.81	2.52	
427	479	412	170	6.38	7.16	6.16	2.54	
452	502	435	191	6.75	7.50	6.50	2.85	
0	35	3	37	0.00	0.61	0.05	0.64 HODGSON DATA	
17	67	22	51	0.30	1.17	0.38	0.89 -----	
34	88	39	66	0.59	1.53	0.68	1.14 RUN	2112
52	107	57	77	0.91	1.86	0.99	1.34 d	11.0
77	133	82	77	1.34	2.31	1.42	1.35 D	174
102	157	106	89	1.78	2.74	1.84	1.55 Uo	1.227
127	182	130	98	2.21	3.17	2.27	1.70 U	0.235
152	206	154	107	2.65	3.59	2.68	1.87 R	5.22
177	231	178	107	3.08	4.02	3.10	1.87 Rd/D	0.330
202	255	202	114	3.52	4.43	3.52	1.99 RRd/D	1.723
227	279	226	116	3.95	4.85	3.93	2.02 -----	
252	303	250	113	4.39	5.27	4.35	1.98	
277	327	273	116	4.82	5.69	4.76	2.02	
302	351	297	129	5.26	6.11	5.17	2.25	
327	374	321	134	5.69	6.52	5.59	2.33	
352	398	344	137	6.13	6.93	6.00	2.38	
377	422	368	136	6.56	7.35	6.41	2.37	
402	446	392	137	7.00	7.76	6.82	2.39	
427	469	415	143	7.43	8.17	7.23	2.49	
452	493	439	141	7.87	8.58	7.64	2.45	
0	53	5	60	0.00	0.62	0.06	0.70 HODGSON DATA	
17	90	24	72	0.20	1.06	0.28	0.84 -----	
34	117	42	84	0.40	1.37	0.49	0.98 RUN	1234
52	139	60	98	0.61	1.63	0.70	1.15 d	12.7
77	169	84	114	0.90	1.98	0.99	1.33 D	298
102	194	108	120	1.20	2.28	1.27	1.41 Uo	1.474
127	219	132	126	1.49	2.57	1.55	1.48 U	0.220
152	243	155	134	1.78	2.85	1.82	1.57 R	6.71
177	266	179	148	2.08	3.12	2.10	1.73 Rd/D	0.286
202	290	202	157	2.37	3.40	2.37	1.84 RRd/D	1.919
227	313	225	168	2.66	3.67	2.64	1.97 -----	
252	336	248	175	2.96	3.95	2.91	2.05	
277	360	271	174	3.25	4.22	3.18	2.05	
302	383	295	184	3.54	4.49	3.46	2.16	
327	407	317	189	3.84	4.78	3.72	2.21	
352	431	340	196	4.13	5.06	3.99	2.30	
377	454	363	211	4.42	5.32	4.26	2.48	

402	477	385	203	4.72	5.59	4.52	2.38	
427	500	408	192	5.01	5.86	4.79	2.26	
452	523	431	187	5.30	6.13	5.06	2.20	
-----								
0	68	6	68	0.00	0.68	0.06	0.68	HODGSON DATA
17	106	25	83	0.17	1.05	0.25	0.83	-----
34	134	43	101	0.34	1.33	0.43	1.01	RUN 1235
52	156	61	111	0.52	1.55	0.61	1.10	d 12.7
77	182	85	129	0.77	1.81	0.85	1.28	D 298
102	208	109	127	1.02	2.07	1.08	1.26	Ub 1.737
127	232	132	141	1.26	2.31	1.32	1.41	U 0.220
152	256	156	147	1.51	2.55	1.55	1.46	R 7.91
177	280	179	160	1.76	2.78	1.78	1.59	Rd/D 0.337
202	303	202	175	2.01	3.02	2.01	1.75	RRd/D 2.666
227	327	225	173	2.26	3.26	2.24	1.72	-----
252	351	248	184	2.51	3.49	2.47	1.83	
277	374	271	204	2.76	3.72	2.70	2.03	
302	397	294	211	3.01	3.95	2.92	2.10	
327	420	316	198	3.26	4.18	3.15	1.97	
352	443	339	211	3.50	4.41	3.38	2.10	
377	466	362	214	3.75	4.64	3.60	2.13	
402	489	384	206	4.00	4.87	3.82	2.05	
427	512	406	237	4.25	5.10	4.05	2.36	
452	535	429	230	4.50	5.33	4.27	2.29	
-----								
0	44	4	44	0.00	0.59	0.05	0.60	HODGSON DATA
17	82	23	57	0.23	1.11	0.31	0.77	-----
34	104	41	73	0.46	1.41	0.55	0.99	RUN 2113
52	123	58	86	0.70	1.67	0.79	1.17	d 11.0
77	150	83	93	1.04	2.03	1.12	1.26	D 174
102	175	107	105	1.38	2.37	1.45	1.43	Ub 1.578
127	199	131	113	1.72	2.70	1.77	1.53	U 0.235
152	223	155	120	2.06	3.03	2.09	1.63	R 6.71
177	247	178	123	2.40	3.35	2.42	1.67	Rd/D 0.424
202	271	202	127	2.74	3.67	2.74	1.72	RRd/D 2.846
227	294	226	134	3.08	3.99	3.06	1.82	-----
252	318	249	139	3.41	4.31	3.37	1.89	
277	342	273	154	3.75	4.63	3.69	2.09	
302	365	296	155	4.09	4.95	4.01	2.10	
327	389	320	157	4.43	5.27	4.33	2.13	
352	412	343	171	4.77	5.59	4.65	2.31	
377	436	367	192	5.11	5.91	4.97	2.60	
402	460	391	216	5.45	6.23	5.29	2.92	
427	483	414	218	5.79	6.55	5.61	2.95	
452	507	438	223	6.12	6.87	5.93	3.03	
-----								
0	59	5	47	0.00	0.66	0.06	0.52	HODGSON DATA
17	100	25	59	0.19	1.11	0.27	0.65	-----
34	125	42	75	0.38	1.39	0.47	0.83	RUN 2114
52	146	60	89	0.58	1.62	0.67	0.98	d 11.0
77	170	84	97	0.85	1.89	0.93	1.08	D 174
102	195	108	119	1.13	2.16	1.19	1.32	Ub 1.929

127	218	131	137	1.41	2.42	1.46	1.52 U	0.235
152	242	155	152	1.69	2.68	1.72	1.69 R	8.20
177	265	178	162	1.96	2.94	1.98	1.80 Rd/D	0.518
202	289	202	179	2.24	3.20	2.24	1.98 RRd/D	4.251
227	312	226	197	2.52	3.46	2.50	2.18 -----	
252	336	249	219	2.79	3.73	2.76	2.43	
277	360	273	229	3.07	3.99	3.02	2.54	
302	383	296	246	3.35	4.25	3.28	2.73	
327	407	320	250	3.63	4.51	3.54	2.77	
352	430	343	256	3.90	4.77	3.80	2.84	
377	454	367	263	4.18	5.03	4.06	2.91	
402	477	390	286	4.46	5.29	4.32	3.17	
427	501	414	296	4.73	5.55	4.58	3.28	
452	524	437	297	5.01	5.81	4.84	3.30	
-----								
0	99	9	74	0.00	0.72	0.06	0.54 HODGSON DATA	
17	149	29	89	0.12	1.08	0.21	0.65 -----	
34	177	46	106	0.25	1.29	0.34	0.77 RUN	1136
52	203	64	118	0.38	1.48	0.47	0.86 d	12.7
77	235	88	138	0.56	1.71	0.64	1.00 D	298
102	260	111	154	0.74	1.89	0.81	1.12 Uo	1.395
127	284	134	167	0.93	2.07	0.98	1.22 U	0.129
152	307	157	179	1.11	2.23	1.14	1.30 R	10.81
177	329	179	179	1.29	2.40	1.31	1.30 Rd/D	0.461
202	352	202	225	1.47	2.56	1.47	1.64 RRd/D	4.980
227	375	224	235	1.65	2.73	1.63	1.71 -----	
252	397	247	261	1.84	2.89	1.80	1.90	
277	420	269	279	2.02	3.06	1.96	2.04	
302	442	292	312	2.20	3.22	2.13	2.27	
327	464	314	322	2.38	3.38	2.29	2.35	
352	487	337	341	2.56	3.55	2.45	2.48	
377	509	359	368	2.75	3.71	2.61	2.68	
402	532	381	385	2.93	3.87	2.78	2.80	
427	554	404	404	3.11	4.04	2.94	2.94	
452	576	426	419	3.29	4.20	3.10	3.06	
-----								
0	75	7	59	0.00	0.70	0.06	0.56 HODGSON DATA	
17	116	26	73	0.16	1.08	0.24	0.69 -----	
34	138	43	83	0.32	1.29	0.40	0.78 RUN	2115
52	156	61	93	0.49	1.46	0.57	0.87 d	11.0
77	180	84	118	0.72	1.69	0.79	1.11 D	174
102	204	108	158	0.96	1.91	1.01	1.48 Uo	2.280
127	228	132	183	1.19	2.14	1.23	1.71 U	0.235
152	251	155	200	1.42	2.36	1.45	1.87 R	9.70
177	275	179	214	1.66	2.58	1.67	2.00 Rd/D	0.613
202	298	202	244	1.89	2.80	1.89	2.28 RRd/D	5.948
227	322	225	268	2.13	3.02	2.11	2.52 -----	
252	345	249	292	2.36	3.24	2.33	2.73	
277	369	272	307	2.60	3.46	2.55	2.87	
302	393	296	321	2.83	3.68	2.78	3.01	
327	416	319	338	3.06	3.90	2.99	3.17	
352	440	343	355	3.30	4.12	3.22	3.33	

377	463	366	364	3.53	4.34	3.43	3.42	
402	487	390	381	3.77	4.56	3.66	3.57	
427	510	413	388	4.00	4.78	3.87	3.64	
452	534	437	399	4.24	5.00	4.10	3.74	
-----								
0	121	11	100	0.00	0.73	0.06	0.60	HODGSON DATA
17	180	31	116	0.10	1.08	0.19	0.70	-----
34	210	49	142	0.21	1.27	0.29	0.86	FLUN 1135
52	232	66	166	0.31	1.40	0.40	1.00	d 12.7
77	258	89	210	0.46	1.56	0.54	1.27	D 298
102	282	112	272	0.62	1.70	0.68	1.64	Uo 1.684
127	305	135	303	0.77	1.84	0.81	1.83	U 0.129
152	328	157	355	0.92	1.98	0.95	2.14	R 13.05
177	350	180	385	1.07	2.11	1.08	2.33	Rd/D 0.556
202	373	202	412	1.22	2.25	1.22	2.49	RRd/D 7.258
227	395	224	430	1.37	2.38	1.35	2.59	-----
252	417	247	467	1.52	2.52	1.49	2.82	
277	440	269	493	1.67	2.65	1.62	2.97	
302	462	291	525	1.82	2.79	1.76	3.17	
327	484	314	553	1.97	2.92	1.89	3.33	
352	507	336	583	2.12	3.06	2.03	3.52	
377	529	358	577	2.27	3.19	2.16	3.48	
402	551	381	607	2.43	3.33	2.30	3.66	
427	574	403	621	2.58	3.46	2.43	3.74	
452	596	425	637	2.73	3.60	2.57	3.84	
-----								
MAX	596	444	637	15.33	15.86	15.05	3.95	
MIN	14	1	27	0.00	0.39	0.03	0.52	
-----								
x	Ex'	x'	Wz	x / R*d	Ex' / R*d	x' / R*d	Wz /R*d	
-----								

NOTES: x IS DISTANCE DOWNSTREAM FROM CENTRE OF JET NOZZLE.  
 Ex' IS DISTANCE ALONG AXIS FOR SIDE VIEW MEASUREMENTS.  
 x' IS DISTANCE FROM NOZZLE CORRECTED FOR PARALAX.  
 Wz IS PLAN VIEW JET WIDTH (CORRECTED VALUE).  
 d IS JET NOZZLE DIAMETER (CONVERGING NOZZLE DESIGN).  
 D IS FLUME DEPTH.  
 Uo IS JET NOZZLE VELOCITY.  
 U IS FLUME VELOCITY.  
 R IS VELOCITY RATIO (Uo/U).  
 ALL DISTANCES ARE IN mm; ALL VELOCITIES ARE IN m/s.

**APPENDIX B**  
**SUMMARY OF REGRESSION ANALYSES**

The equation coefficients developed in the text were determined by regression analysis using the statistical package MINITAB. The package was originally developed at Pennsylvania University and the University of Wisconsin. The program was applied on the University of Alberta's computer system. MINITAB presents sufficient information to conduct ANOVA (ANalysis Of VARIance) testing on the regressions to determine their validity. The following tables present the results of the various regression analyses carried out. Information presented includes:

- the equations and equation numbers,
- the coefficient of determination ( $r^2$ ),
- the number of pieces of data used in the regression ( $n$ ),
- the number of parameters estimated ( $m$ ),
- the F ratio ( $F_r$  - which is the average mean squared deviation explained by the regression parameter divided by the mean squared error), and
- the F statistic for the 99.5% confidence interval.

If the value of the F statistic is flagged by a single asterisk (\*), then the F statistic is for the 99% confidence interval; if it is flagged by a double asterisk (\*\*), then the F statistic is for the 95% confidence interval. To be statistically significant, the  $F_r$  value must be greater than the F statistic for a reasonable level of confidence (i.e. the

95% level or greater). All of the following regressions satisfy the 95% criterion; most satisfy even the 99.5% criterion.

Table B.1 Regression analysis results for equations in Section 3

Equation	$r^2$	n	m	$F_r$	$F_{0.995, m, n-m-1}$
(3.26) $Y_p/D = 0.53 \alpha d/D$	0.993	13	1	1668	12.3
(3.28) $C1 = 0.72 \alpha^{0.52}$	0.947	13	1	217	12.3
(3.29) $C2 = 1.01 \alpha^{0.22}$	0.919	10	1	104	14.7
$C3 = 1.44 \pm 6\%$		7			95% t test
(3.30) $C3 = 0.86 \alpha^{0.28}$	0.700	8	1	17.3	13.7*
(3.31) $m = 0.34 (1 - 1.2 \alpha d/D)$	0.852	10	1	52.8	14.7
(3.32) $m = 0.29 - (\alpha^2 d/D)/27$	0.588	10	1	13.8	11.3*
(3.33) $m = 0.03 (\alpha d/D)^{-1.8}$	0.862	7	1	38.6	22.8
(3.34) $m = 0.51 (\alpha^2 d/D)^{-1.0}$	0.878	6	1	37.1	31.3
(3.35) $Y_i/D = 1.55 (\alpha d/D)^{1.30}$	0.916	11	1	111	13.6
(3.36) $Y_c/D = 1.66 (\alpha d/D)^{0.83}$	0.960	9	1	191	16.2
(3.37) $Y_o/D = 2.18 (\alpha d/D)^{0.73}$	0.978	8	1	319	18.6



Table B.1 (continued) Regression analysis results for equations in Section 3

Equation	$r^2$	n	m	$F_r$	$F_{0.995, m, n-m-1}$
(3.38) $Y_i/D = 0.22 (\alpha^2 d/D)^{0.74}$	0.928	10	1	116	14.7
(3.39) $Y_c/D = 0.47 (\alpha^2 d/D)^{0.46}$	0.965	9	1	222	16.2
(3.40) $Y_o/D = 0.71 (\alpha^2 d/D)^{0.37}$	0.956	9	1	175	16.2
(3.41) $X_c/(\alpha d) = 0.85 (\alpha d/D)^{-1.41}$	0.850	13	1	69	12.3
(3.42) $X_c/(\alpha d) = 7.38 (\alpha^2 d/D)^{-0.77}$	0.890	13	1	98	12.3
(3.49) $C4 = C5 = 1.1 - \alpha^2 d/(8D)$	0.904	9	1	82	16.2
(3.51) $n = \alpha^2 d/(4D)$	0.968	8	1	211	18.6
(3.52) $\xi/(\alpha d) = 22 D/(\alpha^2 d)$	0.971	4	1	102	98.5*

Table B.2 Regression analysis results for dilution equations in Section 4

Data Source	$\alpha$	p	a	b	r <sup>2</sup>	n	m	F <sub>r</sub>	F <sub>0.995,m,n-m-1</sub>
This work: Run 1	3.68	0.272	1.759	0.729	0.994	3	1	327	161**
This work: Run 2	6.99	0.143	2.567	0.631	0.995	3	1	367	161**
This work: Run 3	5.11	0.196	1.148	0.819	0.998	3	1	872	161**
This work: Run 4	6.74	0.148	0.408	1.086	0.987	4	1	234	98.5*
Wright: 107/114	20.6	0.049	0.101	1.443	0.890	8	1	58	18.6
Wright: 119/122	30.0	0.033	0.241	1.122	0.984	4	1	190	98.5*
Wright: 123/126	36.2	0.028	0.118	1.309	0.953	4	1	63	18.6**
Becker et al	$\infty$	0	0.154	1.025	0.998	21	1	9434	10.1
Patrick	$\infty$	0	0.118	1.137	0.999	9	1	9453	16.2
Patrick	45.0	0.022	0.194	1.076	0.995	8	1	1403	18.6
Patrick	41.3	0.024	0.116	1.222	0.997	9	1	2729	16.2
Patrick	40.3	0.025	0.136	1.192	0.997	6	1	1629	31.3
Patrick	20.9	0.048	0.144	1.249	0.998	7	1	3792	22.8
Patrick	20.2	0.050	0.174	1.183	1	9	1	18149	16.2
Patrick	19.9	0.050	0.188	1.245	0.999	7	1	4638	22.8
Patrick	16.1	0.062	0.192	1.183	0.998	8	1	4047	18.6
Patrick	13.9	0.072	0.172	1.334	0.996	6	1	1412	31.3
Patrick	11.9	0.084	0.248	1.178	0.990	8	1	710	18.6
Patrick	9.43	0.106	0.263	1.253	0.998	7	1	3215	22.8
Patrick	7.76	0.129	0.359	1.180	0.998	7	1	3129	22.8
Patrick	6.56	0.152	0.393	1.189	0.996	7	1	1436	22.8
Kamotani and Greber	$\infty$	0	0.366	0.975	0.999	15	1	21245	11.5
Kamotani and Greber	7.72	0.130	0.568	1.129	0.954	15	1	293	11.5
Kamotani and Greber	3.91	0.256	1.097	0.840	0.993	17	1	2403	10.8
Hinze and Zijnen: gas	$\infty$	0	0.197	1.020	0.993	19	1	2590	10.5
Hinze and Zijnen: temp	$\infty$	0	0.149	1.158	0.991	19	1	1939	10.5
Forstall and Gaylord	$\infty$	0	0.247	0.924	0.979	21	1	926	10.1
Birch et al	$\infty$	0	0.145	1.171	0.999	49	1	45157	8.8

Table B.3 Regression analysis results for equations in Section 4

Equation	$r^2$	n	m	$F_r$	$F_{0.995, m, n-m-1}$
(4.7) $C_o/C_m = 0.210 (x/d)^{0.966}$	0.969	72	1	2192	8.4
(4.8) $C_o/C_m = 0.194 x/d$	0.989	72	1	6364	8.4

Table B.4 Regression analysis results for equations in Section 5

Equation	$r^2$	n	m	$F_r$	$F_{0.995, m, n-m-1}$
(5.1) $C_o/C_m = 1.09 (\alpha x/d)^{0.56}$	0.973	86	1	3053	8.4
(5.2) $\frac{y_c}{\alpha d} = 1.46 \left( \frac{x}{\alpha d} \right)^{0.26}$	0.899	86	1	761	8.4
(5.3) $\frac{w_z}{\alpha d} = 1.20 \left( \frac{x}{\alpha d} \right)^{0.29}$	0.957	18	1	375	10.6
(5.4) $\frac{w_z}{\alpha d} = 0.98 \left( \frac{\xi}{\alpha d} \right)^{0.36}$	0.937	18	1	255	10.6
(5.5) $\frac{w_y}{\alpha d} = 0.78 \left( \frac{x}{\alpha d} \right)^{0.52}$	0.901	25	1	221	9.6
(5.6) $\frac{w_y}{\alpha d} = 0.78 \left( \frac{x}{\alpha d} \right)^{0.37}$	0.920	44	1	492	8.9
(5.7) $\frac{w_y}{\alpha d} = 0.36 \left( \frac{\xi}{\alpha d} \right)^{1.28}$	0.834	27	1	132	9.4
(5.8) $\frac{w_y}{\alpha d} = 0.60 \left( \frac{\xi}{\alpha d} \right)^{0.46}$	0.894	42	1	346	8.9

**APPENDIX C**  
**SUMMARY OF CONCENTRATION MEASUREMENTS**  
**LESSER SLAVE RIVER FIELD TRIP**

This appendix presents the partially reduced data from the three bottom jet discharge conditions and the one side jet discharge condition examined during the Lesser Slave River field program of June 1988. General information on the jet conditions are first presented followed by a tabulation of the concentration measurements. The data comprises:

- the section number,
- the profile or transect identification,
- the distance downstream of the jet nozzle (x),
- the distance across from the nozzle (z),
- the height above the nozzle (y),
- the reading number, and
- the concentration readings (adjusted to eliminate background fluorescence).

Three columns of concentration values are presented:

- the first contains all readings,
- the second has the duplicated readings averaged and/or eliminated, and
- the third indicates the maximum concentration ( $C_m$ ) for the cross section that can be determined from the data.

## LESSER SLAVE RIVER FIELD TRIP CONCENTRATION DATA

## BOTTOM JET DISCHARGE -- JET 1

FILE: BOTM-01

DATE: 12-Nov 90

## JET CONDITIONS:

-----

d =	50.4 mm	Uo =	3.255 m/s
D =	889 mm	R =	3.682
D/d =	17.6	Rd/D =	0.209
Qp =	386.8 L/m	RRd/D	0.769
Qi =	2.9 L/m		
Qo =	389.7 L/m		
U =	0.884 m/s		
T =	15.5 deg C		
Co =	74.4 ppb		
full scale	77.5 ppb		

SEC #	V/H	x mm	z mm	y mm	FDG #	ADJ FDG ppb	ADJ FDG ppb	Cm
1	v1	305	0	89	13	0.08	0.1	
1	v1	305	0	139	8	0.40	0.4	
1	v1	305	0	189	7	2.94	2.9	
1	v1	305	0	239	6	6.97	7.0	
1	v1	305	0	289	5	9.18		9.18
1	v1	305	0	339	2	7.71	7.7	
1	v1	305	0	389	4	5.73	5.7	
1	v1	305	0	439	3	2.01	2.0	
1	v1	305	0	489	12	0.62	0.6	
1	v2	305	89	139	25	0.23	0.2	
1	v2	305	89	239	24	5.42	5.4	
1	v2	305	89	289	19	7.46		
1	v2	305	89	339	20	8.44	8.4	
1	v2	305	89	389	21	6.97	7.0	
1	v2	305	89	489	22	4.33	4.3	
1	v2	305	89	539	23	0.25	0.3	
1	v3	305	191	189	26	2.70	2.7	
1	v3	305	191	239	27	4.33	4.3	
1	v3	305	191	339	28	4.80	4.8	

1	v3	305	191	439	29	2.01	2.0	
1	v3	305	191	539	30	0.01	0.0	
1	h	305	-165	289	18	0.06	0.1	
1	h	305	-63	289	17	5.11	5.1	
1	h	305	0	289	5	9.18	9.2	
1	h	305	89	289	19	7.46	7.5	
1	h	305	140	289	14	5.75	5.7	
1	h	305	191	289	---	3.52	3.5	
1	h	305	242	289	15	0.89	0.9	
1	h	305	343	289	16	0.18	0.2	
2	v1	914	-153	89	47	0.01	0.0	
2	v1	914	-153	189	46	0.99	1.0	
2	v1	914	-153	289	48	1.23	1.2	
2	v1	914	-153	389	49	1.54		
2	v1	914	-153	389	38	2.23		
2	v1	914	-153	489	50	1.48	1.5	
2	v2	914	0	189	42	0.70	0.7	
2	v2	914	0	289	43	4.48	4.5	4.48
2	v2	914	0	389	37	4.33		
2	v2	914	0	489	44	2.93	2.9	
2	v2	914	0	589	45	0.45	0.5	
2	v3	914	152	89	31	0.06	0.1	
2	v3	914	152	189	32	0.84	0.8	
2	v3	914	152	289	33	2.08	2.1	
2	v3	914	152	389	34	3.24		
2	v3	914	152	489	35	2.62	2.6	
2	v3	914	152	589	36	0.04	0.0	
2	h	914	-305	389	39	0.04	0.0	
2	h	914	-153	389	38	2.23		
2	h	914	-153	389	49	1.54	1.9	
2	h	914	0	389	37	4.33	4.3	
2	h	914	152	389	34	3.24	3.2	
2	h	914	304	389	40	0.89	0.9	
2	h	914	457	389	41	0.04	0.0	
3	v1	2013	-153	-11	73	0.08	0.1	
3	v1	2013	-153	139	68	0.57	0.6	
3	v1	2013	-153	289	69	1.35	1.4	
3	v1	2013	-153	439	70	1.15		
3	v1	2013	-153	439	58	1.74		
3	v1	2013	-153	439	59	1.61		
3	v1	2013	-153	589	71	0.66	0.7	

3	v1	2013	-153	739	72	0.02	0.0	
3	v2	2013	0	-11	51	0.19	0.2	
3	v2	2013	0	139	52	0.85	0.8	
3	v2	2013	0	289	53	2.15	2.2	
3	v2	2013	0	439	54	2.69		
3	v2	2013	0	589	55	1.38	1.4	
3	v2	2013	0	689	56	0.85	0.8	
3	v2	2013	0	789	57	0.19	0.2	
3	v3	2013	152	139	64	0.44	0.4	
3	v3	2013	152	289	65	1.56	1.6	
3	v3	2013	152	439	61	2.42		
3	v3	2013	152	589	66	1.25	1.3	
3	v3	2013	152	739	67	0.27	0.3	
3	h	2013	-305	439	60	0.17	0.2	
3	h	2013	-153	439	58	1.69		
3	h	2013	-153	439	59	1.56	1.5	
3	h	2013	-153	439	70	1.10		
3	h	2013	0	439	54	2.80	2.8	2.80
3	h	2013	152	439	61	2.42	2.4	
3	h	2013	304	439	62	1.30	1.3	
3	h	2013	457	439	63	0.56	0.6	

---

## LESSER SLAVE RIVER FIELD TRIP CONCENTRATION DATA

## BOTTOM JET DISCHARGE -- JET 2

FILE: BOTM-02

DATE: 12-Nov 90

## JET CONDITIONS:

-----

d =	34.5 mm	Uo =	5.73 m/s
D =	762 mm	R =	6.987
D/d=	22.1	Rd/D=	0.316
Qp=	318.5 L/m	RRd/D	2.21
Qi =	2.9 L/m		
Qo =	321.4 L/m		
U =	0.82 m/s		
T =	15.5 deg C		
Co =	180.5 ppb		
full scale	77.5 ppb		

SEC #	V/H	x mm	z mm	y mm	FDG #	ADJ CONC ppb	ADJ CONC ppb	Cm
1	v1	305	-152	172	22	0.01	0.0	
1	v1	305	-152	272	24	4.24	4.2	
1	v1	305	-152	322	25	5.17	5.2	
1	v1	305	-152	372	19	10.53		
1	v1	305	-152	422	26	5.14	5.1	
1	v1	305	-152	522	27	0.28	0.3	
1	v1	305	-152	622	28	0.03	0.0	
1	v2	305	0	72	4	0.03	0.0	
1	v2	305	0	172	5	1.56	1.6	
1	v2	305	0	272	6	7.05	7.1	
1	v2	305	0	372	7	12.32		
1	v2	305	0	372	15	13.99		
1	v2	305	0	472	8	8.60	8.6	
1	v2	305	0	572	9	2.71	2.7	
1	v2	305	0	672	10	2.24	2.2	
1	v3	305	153	172	30	0.45	0.5	
1	v3	305	153	222	32	2.00	2.0	
1	v3	305	153	272	31	7.03	7.0	
1	v3	305	153	322	33	10.95	11.0	



1	v3	305	153	372	34	10.46	
1	v3	305	153	372	16	11.93	
1	v3	305	153	472	35	7.52	7.5
1	v3	305	153	572	36	0.45	0.4
1	v3	305	153	672	37	-0.04	0.0
1	h	305	-610	372	13	0.32	0.3
1	h	305	-457	372	12	0.32	0.3
1	h	305	-305	372	11	1.91	1.9
1	h	305	-152	372	19	10.06	10.3
1	h	305	0	372	15	13.99	
1	h	305	0	372	7	12.32	13.2 13.15
1	h	305	153	372	16	11.53	
1	h	305	153	372	34	10.06	11.0
1	h	305	305	372	17	3.77	3.8
1	h	305	457	372	18	0.69	0.7
2	v1	914	-152	187	67	0.24	0.2
2	v1	914	-152	287	68	2.49	2.5
2	v1	914	-152	387	69	4.66	4.7
2	v1	914	-152	437	51	4.89	
2	v1	914	-152	487	70	5.28	5.3
2	v1	914	-152	587	71	2.33	2.3
2	v1	914	-152	687	72	0.09	0.1
2	v2	914	0	87	40	0.01	0.0
2	v2	914	0	187	41	0.38	0.4
2	v2	914	0	287	42	1.89	1.9
2	v2	914	0	387	43	8.08	8.1
2	v2	914	0	437	52	8.08	
2	v2	914	0	487	44	7.59	7.6
2	v2	914	0	587	45	4.60	4.6
2	v2	914	0	687	47	1.21	1.2
2	v2	914	0	737	48	0.18	0.2
2	v3	914	153	187	57	0.33	0.3
2	v3	914	153	287	58	1.88	1.9
2	v3	914	153	387	59	6.02	6.0
2	v3	914	153	437	53	7.00	
2	v3	914	153	487	60	6.51	6.5
2	v3	914	153	587	61	3.28	3.3
2	v3	914	153	687	62	0.64	
2	v3	914	153	687	63	1.12	0.9
2	v3	914	153	737	64	0.18	0.2
2	h	914	-305	437	50	0.18	0.2
2	h	914	-152	437	51	5.01	5.0

2	h	914	0	437	52	8.18	8.2	8.18
2	h	914	153	437	53	6.95	7.0	
2	h	914	305	437	54	2.45	2.5	
2	h	914	457	437	55	0.11	0.1	
3	v1	2013	-152	152	102	0.47	0.5	
3	v1	2013	-152	252	103	1.01	1.0	
3	v1	2013	-152	352	104	1.92	1.9	
3	v1	2013	-152	452	105	3.31	3.3	
3	v1	2013	-152	552	106	3.78		
3	v1	2013	-152	552	86	3.47		
3	v1	2013	-152	652	107	2.23	2.2	
3	v1	2013	-152	732	108	1.45	1.5	
3	v2	2013	0	52	75	0.18	0.2	
3	v2	2013	0	152	76	0.26	0.3	
3	v2	2013	0	252	77	1.31	1.3	
3	v2	2013	0	352	78	2.97	3.0	
3	v2	2013	0	452	79	4.21	4.2	
3	v2	2013	0	552	80	5.29		
3	v2	2013	0	552	87	4.44		
3	v2	2013	0	652	81	3.90	3.9	
3	v2	2013	0	742	82	3.43	3.4	
3	v3	2013	153	52	93	0.04	0.0	
3	v3	2013	153	152	94	0.23	0.2	
3	v3	2013	153	252	95	0.60	0.6	
3	v3	2013	153	352	96	1.63	1.6	
3	v3	2013	153	452	97	3.52	3.5	
3	v3	2013	153	552	98	4.30		
3	v3	2013	153	552	88	4.07		
3	v3	2013	153	652	99	3.99	4.0	
3	v3	2013	153	737	100	2.98	3.0	
3	h	2013	-457	552	84	0.11	0.1	
3	h	2013	-305	552	85	1.09	1.1	
3	h	2013	-152	552	86	3.45		
3	h	2013	-152	552	106	3.76	3.6	
3	h	2013	0	552	87	4.61		
3	h	2013	0	552	80	5.46	5.0	5.03
3	h	2013	153	552	88	4.07		
3	h	2013	153	552	98	4.30	4.2	
3	h	2013	305	552	89	2.36	2.4	
3	h	2013	457	552	90	0.35	0.4	
3	h	2013	610	552	91	0.01	0.0	

---

## LESSER SLAVE RIVER FIELD TRIP CONCENTRATION DATA

## BOTTOM JET DISCHARGE -- JET 3

FILE: BOTM-03

DATE: 12-Nov 90

## JET CONDITIONS:

-----

d =	34.5 mm	Uo =	4.189 m/s
D =	762 mm	R =	5.108
D/d=	22.1	Rd/D=	0.231
Qp=	232.1 L/m	RRd/D	1.181
Qi =	2.9 L/m		
Qo =	235 L/m		
U =	0.82 m/s		
T =	15.5 deg C		
Co =	246.9 ppb		
full scale	77.5 ppb		

SEC #	V/H	x mm	z mm	y mm	FDG #	ADJ CONC ppb	ADJ CONC ppb	Cm
1	v1	305	-76	167	202	0.30	0.3	
1	v1	305	-76	217	203	3.95	3.9	
1	v1	305	-76	267	204	19.38		
1	v1	305	-76	267	185	20.36		
1	v1	305	-76	317	205	21.46	21.5	
1	v1	305	-76	367	206	16.44	16.4	
1	v1	305	-76	417	207	2.55	2.6	
1	v1	305	-76	467	208	0.64	0.6	
1	v2	305	0	67	---	0.26	0.3	
1	v2	305	0	117	174	1.31	1.3	
1	v2	305	0	167	175	8.10	8.1	
1	v2	305	0	217	176	29.21	29.2	
1	v2	305	0	267	177	29.21		
1	v2	305	0	267	186	27.66		
1	v2	305	0	317	178	25.34	25.3	
1	v2	305	0	367	179	12.51	12.5	
1	v2	305	0	417	180	3.79	3.8	
1	v2	305	0	467	181	0.45	0.4	
1	v3	305	76	117	191	0.74	0.7	
1	v3	305	76	167	192	3.48	3.5	

1	v3	305	76	217	193	12.27	12.3	
1	v3	305	76	267	194	19.87		
1	v3	305	76	267	187	20.12		
1	v3	305	76	317	195	19.14	19.1	
1	v3	305	76	367	196	11.04	11.0	
1	v3	305	76	417	197	4.41	4.4	
1	v3	305	76	467	198	2.24	2.2	
1	v3	305	76	517	199	0.61	0.6	
1	v3	305	76	567	200	0.15	0.2	
1	h	305	-305	267	183	0.04	0.0	
1	h	305	-152	267	184	1.02	1.0	
1	h	305	-76	267	185	20.22		
1	h	305	-76	267	204	19.24	19.7	
1	h	305	0	267	186	27.52		
1	h	305	0	267	177	29.07	28.3	28.30
1	h	305	76	267	187	19.98		
1	h	305	76	267	194	19.73	19.9	
1	h	305	153	267	188	12.37	12.4	
1	h	305	229	267	189	2.10	2.1	
2	v1	914	-76	62	167	0.23	0.2	
2	v1	914	-76	162	168	3.71	3.7	
2	v1	914	-76	262	169	9.82	9.8	
2	v1	914	-76	362	170	11.29	11.3	
2	v1	914	-76	462	171	3.24	3.2	
2	v1	914	-76	562	172	0.04	0.0	
2	v2	914	0	62	145	0.35	0.4	
2	v2	914	0	162	146	5.00	5.0	
2	v2	914	0	262	147	11.83	11.8	
2	v2	914	0	312	149	13.55		
2	v2	914	0	312	156	14.29		
2	v2	914	0	362	148	11.34	11.3	
2	v2	914	0	462	150	5.46	5.5	
2	v2	914	0	562	151	0.60	0.6	
2	v3	914	153	62	160	0.40	0.4	
2	v3	914	153	162	161	1.83	1.8	
2	v3	914	153	212	163	3.76	3.8	
2	v3	914	153	262	162	6.19	6.2	
2	v3	914	153	312	157	7.91		
2	v3	914	153	362	164	8.40	8.4	
2	v3	914	153	462	165	3.29	3.3	
2	v3	914	153	562	166	0.50	0.5	
2	h	914	-305	312	153	0.01		
2	h	914	-305	312	155	0.08	0.0	

2	h	914	-152	312	154	5.74	5.7	
2	h	914	-76	312	---	10.58	10.6	
2	h	914	0	312	156	14.26		
2	h	914	0	312	149	13.52	13.9	13.89
2	h	914	153	312	157	7.88	7.9	
2	h	914	305	312	158	0.30	0.3	
3	v1	2013	-152	72	134	0.50	0.5	
3	v1	2013	-152	172	135	1.69	1.7	
3	v1	2013	-152	272	136	2.93	2.9	
3	v1	2013	-152	372	139	3.09		
3	v1	2013	-152	372	121	3.40		
3	v1	2013	-152	472	140	2.00	2.0	
3	v1	2013	-152	572	141	0.60	0.6	
3	v1	2013	-152	672	142	0.30	0.3	
3	v2	2013	0	72	110	1.19	1.2	
3	v2	2013	0	172	111	3.21	3.2	
3	v2	2013	0	272	112	4.84	4.8	
3	v2	2013	0	372	113	7.17		
3	v2	2013	0	372	122	7.17		
3	v2	2013	0	472	114	4.38	4.4	
3	v2	2013	0	572	115	2.05	2.1	
3	v2	2013	0	672	116	0.11	0.1	
3	v2	2013	0	722	117	0.11	0.1	
3	v3	2013	153	72	127	1.44	1.4	
3	v3	2013	153	172	126	2.07	2.1	
3	v3	2013	153	272	128	4.32	4.3	
3	v3	2013	153	372	129	5.87		
3	v3	2013	153	372	123	5.72		
3	v3	2013	153	472	130	3.39	3.4	
3	v3	2013	153	572	131	1.07	1.1	
3	v3	2013	153	672	132	0.45	0.5	
3	h	2013	-305	372	120	0.31	0.3	
3	h	2013	-152	372	121	3.55		
3	h	2013	-152	372	139	3.09	3.3	
3	h	2013	0	372	122	7.27		
3	h	2013	0	372	113	7.27	7.3	7.27
3	h	2013	153	372	123	5.72		
3	h	2013	153	372	129	5.87	5.8	
3	h	2013	305	372	124	1.48	1.5	
3	h	2013	457	372	125	0.23	0.2	

---

## LESSER SLAVE RIVER FIELD TRIP CONCENTRATION DATA

## SIDE JET DISCHARGE -- JET 4

FILE: SIDE-01

DATE: 12-Nov 90

## JET CONDITIONS:

-----

d = 34.5 mm                      U<sub>o</sub> = 5.325 m/s  
 D = 914 mm                        R = 6.740  
 y<sub>n</sub> = 457 mm  
 Q<sub>p</sub> = 295.8 L/m  
 Q<sub>i</sub> = 2.9 L/m  
 Q<sub>o</sub> = 298.7 L/m  
 U = 0.79 m/s  
 T = 15.5 deg C  
 Co = 194.2 ppb  
 full scale            77.5 ppb

SEC #	V/H	x mm	z mm	y mm	FDG #	ADJ FDG ppb	ADJ FDG ppb	Cm
4	h	378	131	439	67	0.10	0.1	
4	h	272	241	439	62	2.57	2.6	
4	h	220	296	439	64	14.22	14.2	
4	h	167	351	439	63	32.68	32.7	33.37
4	h	114	406	439	65	12.21	12.2	
4	h	62	461	439	66	0.27	0.3	
4	v	167	351	189	68	0.12	0.1	
4	v	167	351	289	69	0.12	0.1	
4	v	167	351	339	70	3.38	3.4	
4	v	167	351	389	71	22.52	22.5	
4	v	167	351	439	72	34.07	34.1	
4	v	167	351	489	73	30.29	30.3	
4	v	167	351	539	74	23.75	23.7	
4	v	167	351	589	75	12.75	12.8	
4	v	167	351	639	76	0.47	0.5	
4	v	167	351	689	77	0.00	0.0	

3	h	873	81	414	43	0.02	0.0	
3	h	815	222	414	44	0.17	0.2	
3	h	756	363	414	45	2.46	2.5	
3	h	727	433	414	46	6.26	6.3	
3	h	698	503	414	46	10.92	10.9	
3	h	668	574	414	49	9.14	9.1	
3	h	639	644	414	47	6.50	6.5	
3	h	581	785	414	50	0.38	0.4	
3	h	522	926	414	51	0.08	0.1	
3	v	698	503	64	53	0.57	0.6	
3	v	698	503	164	54	2.81	2.8	
3	v	698	503	264	55	9.16	9.2	
3	v	698	503	364	56	13.12	13.1	13.12
3	v	698	503	414	46	10.94	10.9	
3	v	698	503	464	57	8.00	8.0	
3	v	698	503	564	58	6.76	6.8	
3	v	698	503	664	59	2.47	2.5	
3	v	698	503	764	60	0.08	0.1	
2	h	1432	97	464	25	0.00	0.0	
2	h	1366	395	464	26	1.88	1.9	
2	h	1349	469	464	32	3.58	3.6	
2	h	1332	544	464	27	5.60	5.6	
2	h	1316	618	464	31	5.29	5.3	
2	h	1299	692	464	28	4.05	4.0	
2	h	1266	841	464	29	0.64	0.6	
2	h	1233	990	464	30	0.07	0.1	
2	v	1316	618	64	33	3.43	3.4	
2	v	1316	618	214	34	6.53	6.5	
2	v	1316	618	314	35	8.31	8.3	8.31
2	v	1316	618	414	36	6.30	6.3	
2	h	1316	618	464	31	5.29	5.3	
2	v	1316	618	514	37	5.75	5.8	
2	v	1316	618	614	38	3.58	3.6	
2	v	1316	618	714	39	1.37	1.4	
2	v	1316	618	814	40	0.15	0.1	
1	h	2064	-48	464	12	0.12	0.1	
1	h	2064	105	464	11	0.47	0.5	
1	h	2064	257	464	10	1.18	1.2	
1	h	2064	410	464	7	2.75	2.8	
1	h	2064	486	464	8	3.06	3.1	

1	h	2064	562	464	6	3.68	3.7	
1	h	2064	638	464	9	2.91	2.9	
1	h	2064	714	464	5	2.60	2.6	
1	h	2064	867	464	4	0.50	0.5	
1	h	2064	1019	464	3	0.05	0.1	
1	h	2064	1324	464	2	0.00	0.0	
1	v	2064	525	14	14	2.85	2.9	
1	v	2064	525	114	15	4.40	4.4	
1	v	2064	525	214	16	4.56	4.6	4.56
1	v	2064	525	314	17	4.09	4.1	
1	v	2064	525	414	18	3.86	3.9	
1	v	2064	525	514	19	3.47	3.5	
1	v	2064	525	614	20	2.77	2.8	
1	v	2064	525	714	21	1.12	1.1	
1	v	2064	525	814	22	0.41	0.4	
1	v	2064	525	904	23	0.00	0.0	

---



**APPENDIX D**  
**DATA SUMMARY FOR LABORATORY DILUTION STUDY**

This appendix presents the partially reduced data from the laboratory dilution study conducted during August, September and October of 1990. General data for each run are first presented. These include:

- the run number,
- the jet exit velocity ( $U_0$ ),
- the crossflow velocity ( $U$ ),
- the jet nozzle diameter ( $d$ ), and
- the depth of the crossflow ( $D$ ).

The dilution measurements are then presented. These data include:

- the reading number,
- the horizontal distance downstream from the jet nozzle centreline ( $x$ ),
- the vertical distance above the bed ( $y$ ),
- the transverse distance from the jet nozzle centreline ( $z$ ); here, 0 is at the nozzle, negative values are to the left (looking downstream) and positive values are to the right, and
- the jet dilution ( $C/C_m$ ) in percent; these have been corrected to eliminate background fluorescence.

DATA SUMMARY FOR LABORATORY DILUTION STUDY

DISK: HOGY08  
FILE: APPD.100

RUN: 101  
Uo = 0.500  
U = 0.171  
d = 10.7  
D = 168

RUN: 102  
Uo = 0.751  
U = 0.171  
d = 10.7  
D = 168

RUN: 103  
Uo = 0.980  
U = 0.171  
d = 10.7  
D = 168

RUN: 104  
Uo = 1.170  
U = 0.171  
d = 10.7  
D = 168

READING #	x mm	y mm	z mm	C/Cm %	READING #	x mm	y mm	z mm	C/Cm %	READING #	x mm	y mm	z mm	C/Cm %
section 1														
472	1012.8	102.0	-59.7	41.4	343	535.0	41.4	0.0	7.1	366	535.0	71.4	0.0	12.7
471	1012.8	102.0	-44.5	68.3	344	535.0	61.4	0.0	26.9	367	535.0	91.4	0.0	29.6
484	1012.8	22.0	-29.3	30.5	345	535.0	81.4	0.0	56.1	368	535.0	111.4	0.0	53.6
483	1012.8	42.0	-29.3	60.4	346	535.0	101.4	0.0	90.1	369	535.0	131.4	0.0	79.3
482	1012.8	62.0	-29.3	87.3	351	535.0	111.4	0.0	98.3	370	535.0	141.4	0.0	87.6
481	1012.8	82.0	-29.3	93.7	352	535.0	116.4	0.0	100.0	371	535.0	151.4	0.0	94.8
470	1012.8	102.0	-29.3	86.2	347	535.0	121.4	0.0	97.9	374	535.0	156.4	0.0	97.3
485	1012.8	122.0	-29.3	55.7	350	535.0	131.4	0.0	92.0	372	535.0	161.4	0.0	100.0
486	1012.8	142.0	-29.3	23.8	348	535.0	141.4	0.0	78.8	373	535.0	165.9	0.0	101.3
469	1012.8	102.0	-14.0	96.3	349	535.0	161.4	0.0	29.9	section 2: transsects and search for Cm				
473	1012.8	102.0	-6.4	98.6	section 2: search for max					380	529.6	161.4	-62.5	95.1
462	1012.8	22.0	0.0	31.4	383	535.0	116.4	-62.5	38.3	379	529.6	161.4	-47.2	102.7
463	1012.8	42.0	0.0	51.6	357	535.0	116.4	-47.2	75.0	378	529.6	161.4	-35.1	107.8
464	1012.8	62.0	0.0	75.9	356	535.0	116.4	-35.1	96.2	377	529.6	161.4	-25.9	106.6
465	1012.8	82.0	0.0	94.5	355	535.0	116.4	-25.9	101.7	376	529.6	161.4	-16.8	104.7
480	1012.8	92.0	0.0	97.4	354	535.0	116.4	-16.8	106.8	375	529.6	161.4	-7.6	103.3
466	1012.8	102.0	0.0	96.2	353	535.0	116.4	-7.6	99.3	381	529.6	161.4	0.0	100.0
474	1012.8	102.0	0.0	100.0	358	535.0	116.4	0.0	100.6	382	529.6	161.4	13.7	100.0
467	1012.8	102.0	0.0	83.5	359	535.0	116.4	10.7	96.7	383	529.6	161.4	29.0	99.8
492	1012.8	112.0	0.0	87.6	360	535.0	116.4	22.9	96.0	384	529.6	161.4	44.2	101.0
479	1012.8	122.0	0.0	72.6	381	535.0	116.4	38.1	79.8	385	529.6	161.4	68.6	86.7
468	1012.8	142.0	0.0	33.6	382	535.0	116.4	53.3	56.5	386	529.6	161.4	96.0	26.2
475	1012.8	102.0	13.4	98.3						396	529.6	161.4	0.0	100.0
487	1012.8	42.0	28.7	35.2	415	535.0	116.4	-25.9	104.4	389	529.6	131.4	-32.0	127.5
488	1012.8	62.0	28.7	59.5	414	535.0	116.4	-16.8	114.4	388	529.6	151.4	-32.0	110.9
489	1012.8	82.0	28.7	78.0	413	535.0	116.4	-7.6	106.9	387	529.6	161.4	-32.0	104.6
476	1012.8	102.0	28.7	86.1	412	535.0	116.4	0.0	100.4					
490	1012.8	122.0	28.7	61.5						396	529.6	161.4	0.0	100.0
491	1012.8	132.0	28.7	41.8	416	535.0	101.4	-16.8	105.8					
477	1012.8	102.0	46.9	67.6	417	535.0	111.4	-15.8	110.7	401	529.6	81.4	-32.0	52.1
478	1012.8	102.0	62.2	41.1	418	535.0	121.4	-16.8	109.2	400	529.6	101.4	-32.0	90.2
section 2: cross section														
508	1012.8	88.9	-26.2	93.4	745	534.4	73.8	-57.0	39.3	399	529.6	121.4	-32.0	121.6
515	1012.8	78.9	-17.1	95.9	746	534.4	93.8	-57.0	61.3	404	529.6	128.4	-32.0	127.2
507	1012.8	88.9	-17.1	97.3	747	534.4	106.3	-57.0	62.9	403	529.6	131.4	-32.0	124.2
514	1012.8	98.9	-17.1	95.9	708	534.4	116.8	-57.0	61.4	398	529.6	141.4	-32.0	117.2
506	1012.8	88.9	-7.9	98.8	748	534.4	133.8	-57.0	37.4	397	529.6	161.4	-32.0	108.9
504	1012.8	73.9	0.0	90.3	744	534.4	53.8	-41.8	26.9					



277	316.9	71.2	-9.1	101.1	283	316.9	101.2	0.0	99.2	576	316.9	116.4	0.0	87.0	775	107.4	100.8	-22.6	167.8
276	316.9	71.2	0.0	100.0	286	316.9	108.2	0.0	100.0	528	316.9	126.4	0.0	95.7	774	107.4	120.8	-22.6	110.2
279	316.9	71.2	9.1	88.3	287	316.9	108.7	0.0	98.3	531	316.9	136.4	0.0	100.0	773	136.4	135.8	-22.6	86.0
section 4					285	316.9	111.2	0.0	99.4	529	316.9	146.4	0.0	94.1	772	107.4	150.8	-22.6	18.8
201	161.3	21.0	0.0	7.8	284	316.9	121.2	0.0	83.4	530	316.9	161.4	0.0	64.8	760	107.4	90.8	-18.0	178.0
202	161.3	36.0	0.0	46.3	288	316.9	141.2	0.0	31.4	545	316.9	86.4	15.5	42.1	764	107.4	120.8	-18.0	115.2
203	161.3	51.0	0.0	88.5	section 3: transect at y=56.5					544	316.9	106.4	15.5	87.8	784	107.4	90.8	-8.8	125.8
207	161.3	61.0	0.0	99.1	292	316.9	108.2	-33.5	78.1	546	316.9	116.4	15.5	100.5	763	107.4	120.8	-8.8	106.9
208	161.3	63.5	0.0	98.5	291	316.9	108.2	-21.3	100.2	543	316.9	126.4	15.5	102.2	757	107.4	70.8	0.0	14.5
204	161.3	66.0	0.0	100.0	290	316.9	106.2	-9.1	102.7	547	316.9	136.4	15.5	90.4	758	107.4	90.8	0.0	50.5
206	161.3	71.0	0.0	92.0	289	316.9	108.2	0.0	100.7	542	316.9	146.4	15.5	85.2	759	107.4	110.8	0.0	93.4
205	161.3	81.0	0.0	59.7	293	316.9	108.2	9.1	95.8	541	316.9	161.4	15.5	58.6	762	107.4	120.8	0.0	98.8
209	161.3	98.0	0.0	6.4	294	316.9	106.2	27.4	90.3	573	316.9	106.4	24.7	108.9	767	107.4	120.8	0.0	101.5
section 5					295	316.9	108.2	42.7	84.6	572	316.9	126.4	24.7	106.9	760	107.4	130.8	0.0	93.4
152	107.4	20.8	0.0	9.8	section 4					561	316.9	116.4	27.7	109.9	761	107.4	150.8	0.0	28.3
153	107.4	35.8	0.0	66.7	210	161.3	41.0	0.0	8.1	562	316.9	116.4	36.9	97.5	785	107.4	90.8	9.4	84.1
154	107.4	50.8	0.0	95.3	211	161.3	58.0	0.0	41.9	571	316.9	66.4	39.9	11.9	768	107.4	120.8	9.4	102.0
158	107.4	55.8	0.0	98.7	212	161.3	71.0	0.0	93.2	570	316.9	86.4	39.9	51.8	786	107.4	90.8	18.6	123.7
159	107.4	57.8	0.0	100.0	216	161.3	81.0	0.0	96.3	569	316.9	106.4	39.9	87.2	769	107.4	120.8	18.6	99.1
157	107.4	60.8	0.0	98.7	217	161.3	83.5	0.0	98.9	568	316.9	126.4	39.9	85.6	793	107.4	80.8	23.2	23.4
155	107.4	65.8	0.0	95.0	213	161.3	88.0	0.0	99.8	567	316.9	146.4	39.9	84.3	794	107.4	70.8	23.2	63.4
156	107.4	80.8	0.0	18.6	218	161.3	89.5	0.0	100.0	566	316.9	161.4	39.9	34.1	792	107.4	80.8	23.2	115.3
section 6					214	161.3	96.0	0.0	96.3	563	316.9	116.4	49.1	72.8	790	107.4	90.8	23.2	130.4
104	64.5	10.8	0.0	2.7	215	161.3	106.0	0.0	74.2	564	316.9	116.4	64.3	30.7	791	107.4	100.8	23.2	122.6
105	64.5	20.8	0.0	16.3	219	161.3	111.0	0.0	57.6	565	316.9	116.4	79.6	6.0	795	107.4	130.8	23.2	74.4
106	64.5	30.8	0.0	49.4	220	161.3	121.0	0.0	22.8	section 4									
107	64.5	40.8	0.0	78.7	section 5					229	158.2	52.0	0.0	2.2	787	107.4	90.8	27.7	125.8
112	64.5	45.8	0.0	90.8	160	107.4	40.8	0.0	12.6	230	158.2	67.0	0.0	15.7	770	107.4	120.8	27.7	88.5
108	64.5	50.8	0.0	100.0	161	107.4	55.8	0.0	64.4	231	158.2	82.0	0.0	52.4	788	107.4	90.8	36.9	98.2
113	64.5	52.8	0.0	98.7	162	107.4	70.8	0.0	96.3	232	158.2	97.0	0.0	91.3	771	107.4	120.8	36.9	63.9
111	64.5	55.8	0.0	95.8	167	107.4	75.8	0.0	99.4	233	158.2	112.0	0.0	100.0	789	107.4	90.8	46.0	54.7
108	64.5	60.8	0.0	76.7	166	107.4	80.8	0.0	100.0	237	158.2	115.0	0.0	95.0	section 6				
109	64.5	70.8	0.0	13.3	168	107.4	82.8	0.0	99.9	235	158.2	117.0	0.0	97.8	134	64.5	50.8	0.0	2.4
110	64.5	80.8	0.0	1.0	163	107.4	85.8	0.0	98.8	238	158.2	119.0	0.0	94.7	135	64.5	65.8	0.0	14.6
section 7					165	107.4	90.8	0.0	89.9	236	158.2	122.0	0.0	91.2	136	64.5	80.8	0.0	46.1
56	33.3	11.8	0.0	2.2	164	107.4	100.8	0.0	53.1	234	158.2	127.0	0.0	82.3	137	64.5	95.8	0.0	79.9
57	33.3	21.8	0.0	23.8	169	107.4	110.8	0.0	15.0	239	158.2	137.0	0.0	58.3	141	64.5	105.8	0.0	95.8
58	33.3	31.8	0.0	55.0	section 6					240	158.2	147.0	0.0	25.4	138	64.5	110.8	0.0	100.0
59	33.3	41.8	0.0	90.3	114	64.5	40.8	0.0	20.1	section 4: transects and search for Cm									
63	33.3	44.8	0.0	100.0	115	64.5	50.8	0.0	52.9	432	158.2	115.2	-26.2	97.0	142	64.5	112.8	0.0	100.0
62	33.3	46.8	0.0	98.9	116	64.5	60.8	0.0	84.8	438	158.2	90.2	-23.2	139.5	139	64.5	115.8	0.0	96.8
60	33.3	51.8	0.0	79.9	122	64.5	65.8	0.0	89.9	437	158.2	80.2	-17.1	132.5	143	64.5	125.8	0.0	66.6
61	33.3	61.8	0.0	9.0	117	64.5	70.8	0.0	97.0	436	158.2	90.2	-17.1	147.8	section 6: search for maximums				
section 8					123	64.5	73.3	0.0	100.0	435	158.2	100.2	-17.1	144.6	828	64.5	84.5	-39.3	52.6
6	14.3	12.9	0.0	15.0	121	64.5	75.8	0.0	98.3	434	158.2	110.2	-17.1	121.6	816	64.5	109.5	-39.3	39.5
5	14.3	22.9	0.0	36.4	118	64.5	80.8	0.0	92.0	431	158.2	115.2	-17.1	107.9	829	64.5	109.5	-30.2	111.0
11	14.3	26.9	0.0	58.6	119	64.5	90.8	0.0	52.9	433	158.2	120.2	-17.1	97.0	815	64.5	109.5	-30.2	85.2
12	14.3	29.9	0.0	84.6	120	64.5	100.8	0.0	7.6	439	158.2	90.2	-11.0	137.1	846	64.5	64.5	-27.1	34.1
7	14.3	32.9	0.0	95.7	section 7					430	158.2	115.2	-7.9	105.3	845	64.5	74.5	-27.1	98.5
14	14.3	34.4	0.0	100.0	64	33.3	31.8	0.0	11.4	427	158.2	110.2	0.0	96.5	844	64.5	119.5	-27.1	49.9
13	14.3	35.9	0.0	96.9	65	33.3	41.8	0.0	50.2	429	158.2	115.2	0.0	98.6	830	64.5	84.5	-21.0	144.3
10	14.3	38.9	0.0	75.9	66	33.3	51.8	0.0	74.4	428	158.2	120.2	0.0	94.6	814	64.5	109.5	-21.0	105.9

8	14.3	42.9	0.0	50.5	67	33.3	61.8	0.0	97.2	440	158.2	115.2	10.4	91.7	826	64.5	64.5	-14.9	59.2
9	14.3	52.9	0.0	3.0	72	33.3	64.3	0.0	100.0	447	158.2	90.2	13.4	91.5	824	64.5	74.5	-14.9	121.7
					71	33.3	66.8	0.0	99.5	446	158.2	80.2	19.5	96.1	823	64.5	84.5	-14.9	149.4
					68	33.3	71.8	0.0	82.2	445	158.2	90.2	19.5	108.2	825	64.5	87.5	-14.9	140.3
					69	33.3	81.8	0.0	26.8	444	158.2	100.2	19.5	103.4	822	64.5	94.5	-14.9	128.2
					70	33.3	91.8	0.0	0.8	443	158.2	115.2	19.5	91.5	813	64.5	109.5	-14.9	108.2
					section 8														
					15	14.3	22.9	0.0	11.6	452	158.2	70.2	22.6	62.4	821	64.5	119.5	-14.9	79.8
					16	14.3	32.9	0.0	36.2	450	158.2	85.2	22.6	105.7	827	64.5	129.5	-14.9	38.3
					17	14.3	42.9	0.0	70.7	453	158.2	100.2	22.6	108.2	812	64.5	84.5	-8.8	121.4
					22	14.3	47.9	0.0	93.9	448	158.2	90.2	25.6	110.8	805	64.5	109.5	-8.8	105.0
					23	14.3	50.4	0.0	100.0	442	158.2	115.2	28.7	81.2	806	64.5	94.5	0.0	74.6
					24	14.3	51.6	0.0	99.3	449	158.2	90.2	31.7	103.7	810	64.5	104.5	0.0	93.7
					18	14.3	52.9	0.0	95.8	443	158.2	115.2	43.9	44.9	811	64.5	109.5	0.0	100.0
					21	14.3	57.9	0.0	77.1	section 5					807	64.5	114.5	0.0	93.7
					19	14.3	62.9	0.0	41.0	172	107.4	50.8	0.0	3.1	809	64.5	124.5	0.0	74.6
					20	14.3	72.9	0.0	4.1	173	107.4	65.8	0.0	24.5	808	64.5	134.5	0.0	31.6
										174	107.4	80.8	0.0	73.6	832	64.5	84.5	9.4	84.1
										175	107.4	95.8	0.0	97.2	817	64.5	109.5	9.4	93.4
										178	107.4	100.8	0.0	100.0	833	64.5	84.5	15.5	101.5
										179	107.4	103.3	0.0	97.5	818	64.5	109.5	15.5	91.1
										177	107.4	105.8	0.0	96.5	841	64.5	59.5	18.6	37.9
										176	107.4	110.8	0.0	95.6	840	64.5	64.5	18.6	60.4
										180	107.4	125.8	0.0	55.2	839	64.5	74.5	18.6	99.7
										181	107.4	135.8	0.0	18.6	837	64.5	84.5	18.6	104.7
										section 5									
										600	102.6	98.9	-54.3	13.0	842	64.5	104.5	18.6	88.1
										599	102.6	98.9	-39.0	78.3	843	64.5	119.5	18.6	54.6
										628	102.6	53.9	-28.8	23.1	834	64.5	84.5	21.6	104.8
										629	102.6	73.9	-26.8	132.9	819	64.5	109.5	21.6	78.5
										598	102.6	98.9	-26.8	118.6	835	64.5	84.5	30.8	79.1
										630	102.6	113.9	-26.8	73.6	820	64.5	109.5	30.8	48.7
										631	102.6	123.9	-26.8	28.1	836	64.5	84.5	36.9	42.7
										616	102.6	53.9	-17.7	16.8	section 7				
										617	102.6	63.9	-17.7	84.8	85	33.3	51.8	0.0	12.6
										615	102.6	73.9	-17.7	147.5	86	33.3	61.8	0.0	37.2
										613	102.6	63.9	-17.7	160.4	87	33.3	71.8	0.0	60.5
										614	102.6	93.9	-17.7	144.8	88	33.3	81.8	0.0	80.4
										597	102.6	98.9	-17.7	129.8	94	33.3	86.8	0.0	90.4
										618	102.6	113.9	-17.7	67.6	89	33.3	91.8	0.0	100.0
										619	102.6	123.9	-17.7	54.2	95	33.3	93.8	0.0	95.4
										820	102.6	133.9	-17.7	16.4	93	33.3	96.8	0.0	97.6
										622	102.6	73.9	-8.5	94.8	90	33.3	101.8	0.0	86.9
										596	102.6	98.9	-8.5	115.9	91	33.3	111.8	0.0	43.7
										621	102.6	113.9	-8.5	94.8	92	33.3	121.8	0.0	8.8
										585	102.6	63.9	0.0	16.8	section 8				
										586	102.6	83.9	0.0	73.0	38	14.3	32.9	0.0	10.9
										591	102.6	93.9	0.0	92.9	37	14.3	42.9	0.0	40.2
										595	102.6	98.9	0.0	100.0	39	14.3	52.9	0.0	49.1
										587	102.6	103.9	0.0	99.9	40	14.3	62.9	0.0	77.8
										594	102.6	103.9	0.0	99.4	46	14.3	67.9	0.0	93.0
										592	102.6	108.9	0.0	95.8	47	14.3	70.9	0.0	99.0

590	102.6	113.9	0.0	94.6	41	14.3	72.9	0.0	100.0
593	102.6	113.9	0.0	93.4	45	14.3	77.9	0.0	95.7
586	102.6	123.9	0.0	66.9	42	14.3	82.9	0.0	82.5
589	102.6	143.9	0.0	5.9	43	14.3	92.9	0.0	46.6
623	102.6	73.9	9.8	82.6	44	14.3	102.9	0.0	10.2
601	102.6	98.9	9.8	98.2					
624	102.6	113.9	9.8	82.6					
609	102.6	53.9	18.9	29.2					
608	102.6	73.9	18.9	112.0					
612	102.6	83.9	18.9	116.6					
607	102.6	93.9	18.9	106.8					
602	102.6	98.9	18.9	99.5					
606	102.6	103.9	18.9	93.4					
611	102.6	113.9	18.9	68.8					
610	102.6	123.9	18.9	38.0					
627	102.6	53.9	28.0	22.5					
626	102.6	73.9	28.0	91.9					
603	102.6	98.9	28.0	84.3					
625	102.6	113.9	28.0	45.3					
604	102.6	98.9	37.2	50.1					
605	102.6	98.9	43.3	15.9					
section 6									
124	64.5	50.8	0.0	9.1					
125	64.5	65.8	0.0	45.4					
126	64.5	75.8	0.0	77.3					
127	64.5	85.8	0.0	98.0					
130	64.5	90.8	0.0	99.9					
128	64.5	95.8	0.0	100.0					
129	64.5	105.8	0.0	81.0					
131	64.5	115.8	0.0	36.9					
section 7									
75	33.3	41.8	0.0	8.2					
76	33.3	51.8	0.0	37.8					
77	33.3	61.8	0.0	71.3					
78	33.3	71.8	0.0	85.6					
83	33.3	76.8	0.0	97.0					
84	33.3	79.8	0.0	100.0					
79	33.3	81.9	0.0	98.9					
82	33.3	86.8	0.0	94.6					
80	33.3	81.8	0.0	74.8					
81	33.3	101.8	0.0	24.3					
section 8									
25	14.3	32.9	0.0	22.7					
26	14.3	42.9	0.0	43.2					
27	14.3	52.9	0.0	63.8					
33	14.3	57.9	0.0	88.0					
28	14.3	62.9	0.0	99.7					
34	14.3	64.9	0.9	100.0					
32	14.3	67.9	0.0	94.3					
29	14.3	72.9	0.0	81.3					
30	14.3	82.9	0.0	28.8					
31	14.3	92.9	0.0	3.7					

DISK: HOGY09 DATA SUMMARY FOR LABORATORY DATA STUDY  
 FILE: APPD.200

RUN: 201  
 Uo = 0.175 m/s  
 U = 0.120 m/s  
 d = 19.0 mm  
 D = 442 mm

RUN: 202  
 Uo = 0.356 m/s  
 U = 0.120 m/s  
 d = 19.0 mm  
 D = 442 mm

READING #	x mm	y mm	z mm	C/Cm %	READING #	x mm	y mm	z mm	C/Cm %
section 5					section 5				
1137	58.8	41.5	-32.0	28.9	1155	58.8	76.5	-44.2	30.7
1136	58.8	41.5	-25.9	70.5	1154	58.8	76.5	-38.1	59.7
1135	58.8	41.5	-13.7	108.6	1153	58.8	76.5	-29.0	94.2
1141	58.8	41.5	-7.6	105.6	1152	58.8	76.5	-19.8	108.8
1142	58.8	46.5	-7.6	106.2	1164	58.8	46.5	-16.8	95.3
1143	58.8	56.5	-7.6	50.3	1163	58.8	56.5	-16.8	112.2
1134	58.8	16.5	0.0	47.2	1161	58.8	66.5	-16.8	108.6
1127	58.8	26.5	0.0	71.7	1162	58.8	76.5	-16.8	106.9
1131	58.8	31.5	0.0	82.8	1160	58.8	86.5	-16.8	82.6
1128	58.8	36.5	0.0	93.8	1151	58.8	76.5	-13.7	109.4
1132	58.8	41.5	0.0	100.0	1150	58.8	76.5	-7.6	104.1
1133	58.8	44.0	0.0	99.4	1144	58.8	26.5	0.0	13.4
1129	58.8	46.5	0.0	93.5	1145	58.8	46.5	0.0	63.3
1130	58.8	56.5	0.0	42.9	1146	58.8	66.5	0.0	92.1
1138	58.8	41.5	7.6	86.9	1148	58.8	76.5	0.0	100.0
1139	58.8	41.5	16.8	69.4	1147	58.8	86.5	0.0	87.9
1140	58.8	41.5	21.3	44.8	1149	58.8	106.5	0.0	18.2
section 4					section 4				
1184	38.1	39.3	-24.4	54.1	1156	58.8	76.5	7.6	92.6
1183	38.1	39.3	-18.3	92.2	1157	58.8	76.5	16.8	89.8
1189	38.1	21.8	-12.2	97.5	1158	58.8	76.5	25.9	71.4
1188	38.1	31.8	-12.2	111.9	1159	58.8	76.5	32.0	38.1
1190	38.1	34.8	-12.2	114.3	section 4				
1182	38.1	39.3	-12.2	106.7	1202	38.1	71.8	-33.5	38.7
1181	38.1	39.3	-6.1	104.3	1201	38.1	71.8	-27.4	74.5
1173	38.1	16.8	0.0	43.5	1200	38.1	71.8	-18.3	104.8
1174	38.1	26.8	0.0	66.4	1211	38.1	41.8	-12.2	103.3
1178	38.1	31.8	0.0	84.5	1210	38.1	51.8	-12.2	108.0
1175	38.1	36.8	0.0	98.5	1208	38.1	61.8	-12.2	108.0
1179	38.1	39.3	0.0	100.0	1209	38.1	66.8	-12.2	106.6
1177	38.1	41.8	0.0	95.2	1207	38.1	71.8	-12.2	108.0
1176	38.1	46.8	0.0	70.7	1199	38.1	71.8	-9.1	108.3
1180	38.1	56.8	0.0	8.9	1191	38.1	26.8	0.0	14.8
1185	38.1	39.3	9.1	84.5	1192	38.1	46.8	0.0	66.3
1186	38.1	39.3	18.3	62.8	1197	38.1	56.8	0.0	82.9
1187	38.1	39.3	24.4	22.8	1193	38.1	66.8	0.0	99.6
section 3					section 3				
1228	28.6	34.8	-18.3	80.6	1194	38.1	66.8	0.0	99.9
1229	28.6	26.8	-12.2	101.1	1198	38.1	71.8	0.0	100.0
1231	28.6	31.8	-12.2	107.5	1196	38.1	76.8	0.0	94.1
1227	28.6	34.8	-12.2	102.6	1195	38.1	86.8	0.0	58.1
1230	28.6	41.8	-12.2	66.4	1203	38.1	71.8	9.1	96.0
1232	28.6	31.8	-6.1	93.3	1204	38.1	71.8	18.3	83.6
1226	28.6	34.8	-6.1	103.7	1205	38.1	71.8	27.4	61.5
1220	28.6	26.8	0.0	69.4	1206	38.1	71.8	33.5	30.4
1224	28.6	31.8	0.0	92.2	section 3				
					1242	28.6	66.8	-18.3	83.2
					1246	28.6	46.8	-12.2	107.0

1225	28.6	34.8	0.0	98.1	1245	28.6	51.8	-12.2	110.6
1221	28.6	36.8	0.0	100.0	1244	28.6	56.8	-12.2	108.8
1223	28.6	41.8	0.0	79.1	1243	28.6	61.8	-12.2	107.0
1222	28.6	46.8	0.0	37.1	1241	28.6	66.8	-12.2	102.3
section 2					1240	28.6	66.8	-6.1	98.2
1261	19.1	31.9	-14.0	90.6	1233	28.6	46.8	0.0	64.3
1262	19.1	26.9	-7.9	97.0	1234	28.6	56.8	0.0	91.7
1260	19.1	31.9	-7.9	102.1	1238	28.6	61.8	0.0	88.1
1263	19.1	34.9	-7.9	88.9	1235	28.6	66.8	0.0	100.0
1255	19.1	16.9	0.0	38.5	1239	28.6	68.8	0.0	95.2
1256	19.1	26.9	0.0	88.5	1237	28.6	71.8	0.0	95.2
1259	19.1	29.9	0.0	97.9	1236	28.6	76.8	0.0	83.3
1258	19.1	31.9	0.0	100.0	section 2				
1257	19.1	36.9	0.0	66.3	1271	19.1	56.9	-17.1	89.0
section 1					1273	19.1	51.9	-7.9	96.2
1287	14.3	27.2	-12.8	88.2	1270	19.1	56.9	-7.9	97.6
1286	14.3	27.2	-6.7	98.1	1275	19.1	56.9	-7.9	96.2
1280	14.3	17.2	0.0	36.0	1274	19.1	60.9	-7.9	92.3
1284	14.3	22.2	0.0	70.8	1272	19.1	56.9	-4.9	92.3
1281	14.3	27.2	0.0	98.1	1264	19.1	36.9	0.0	42.7
1290	14.3	28.2	0.0	100.0	1265	19.1	46.9	0.0	69.8
1285	14.3	29.2	0.0	100.0	1269	19.1	52.9	0.0	92.6
1283	14.3	32.2	0.0	90.2	1266	19.1	56.9	0.0	100.0
1282	14.3	37.2	0.0	43.8	1268	19.1	60.9	0.0	94.5
1288	14.3	27.2	5.5	100.0	1267	19.1	66.9	0.0	76.0
1289	14.3	27.2	11.6	88.2	section 1				
					1300	14.3	53.2	-12.8	87.4
					1299	14.3	53.2	-6.7	101.1
					1291	14.3	37.2	0.0	46.1
					1292	14.3	47.2	0.0	90.3
					1293	14.3	47.2	0.0	80.1
					1297	14.3	53.2	0.0	100.0
					1298	14.3	55.2	0.0	100.0
					1302	14.3	55.2	0.0	99.9
					1294	14.3	57.2	0.0	91.5
					1296	14.3	61.2	0.0	75.5
					1295	14.3	67.2	0.0	55.0
					1301	14.3	53.2	5.5	99.9





861	1004.3	166.6	0.0	95.0	957	1015.4	225.4	-7.6	100.2	1019	1020.2	276.9	9.1	97.8	1071	1004.3	342.8	-22.9	106.6
860	1004.3	176.6	0.0	93.6	946	1015.4	95.4	0.0	16.9	1047	1020.2	186.9	24.4	40.7	1064	1004.3	277.8	0.0	60.3
865	1004.3	176.6	0.0	91.2	947	1015.4	125.4	0.0	39.9	1046	1020.2	216.9	24.4	57.1	1069	1004.3	302.8	0.0	81.4
862	1004.3	186.6	0.0	96.9	948	1015.4	145.4	0.0	47.2	1045	1020.2	246.9	24.4	86.0	1065	1004.3	327.8	0.0	97.4
859	1004.3	186.6	0.0	86.9	949	1015.4	165.4	0.0	75.6	1020	1020.2	276.9	24.4	90.1	1062	1004.3	341.2	0.0	100.0
863	1004.3	216.6	0.0	65.4	950	1015.4	185.4	0.0	83.7	1044	1020.2	306.9	24.4	71.1	1070	1004.3	342.8	0.0	99.3
864	1004.3	236.6	0.0	47.1	951	1015.4	205.4	0.0	99.5	1043	1020.2	336.9	24.4	37.1	1068	1004.3	352.8	0.0	95.8
871	1004.3	166.6	9.4	80.9	954	1015.4	215.4	0.0	93.5	1021	1020.2	276.9	45.7	74.8	1066	1004.3	377.8	0.0	86.8
898	1004.3	106.6	15.5	47.7	952	1015.4	225.4	0.0	100.0	1052	1020.2	186.9	48.8	31.8	1067	1004.3	427.8	0.0	46.6
896	1004.3	126.6	15.5	73.1	973	1015.4	225.4	0.0	100.1	1048	1020.2	216.9	48.8	61.0	1076	1004.3	342.8	20.3	93.2
897	1004.3	146.6	15.5	75.4	953	1015.4	245.4	0.0	78.7	1050	1020.2	246.9	48.8	68.2	1103	1004.3	246.2	40.6	49.9
898	1004.3	186.6	15.5	88.5	955	1015.4	275.4	0.0	64.8	1049	1020.2	306.9	48.8	55.5	1102	1004.3	286.2	40.6	88.8
900	1004.3	206.6	15.5	64.4	956	1015.4	305.4	0.0	28.7	1051	1020.2	336.9	48.8	32.8	1101	1004.3	316.2	40.6	94.8
901	1004.3	226.6	15.5	49.1	965	1015.4	225.4	7.6	86.1	1022	1020.2	276.9	73.2	45.4	1099	1004.3	341.2	40.6	95.4
872	1004.3	166.6	16.6	77.5	992	1015.4	165.4	13.7	50.3	1023	1020.2	276.9	94.5	30.0	1077	1004.3	342.8	40.6	99.2
873	1004.3	166.6	27.7	63.4	991	1015.4	195.4	13.7	79.1	section 2					1100	1004.3	366.2	40.6	94.4
54	520.7	44.7	0.0	5.5	990	1015.4	255.4	13.7	77.5	5	530.2	82.8	0.0	4.0	1104	1004.3	396.2	40.6	70.8
55	520.7	74.7	0.0	28.8	968	1015.4	225.4	16.8	95.1	6	530.2	112.8	0.0	27.7	1105	1004.3	431.2	40.6	30.5
56	520.7	104.7	0.0	84.0	967	1015.4	225.4	29.0	82.8	7	530.2	142.8	0.0	57.7	1078	1004.3	342.8	61.0	96.7
63	520.7	114.7	0.0	86.7	994	1015.4	165.4	38.1	42.3	8	530.2	172.8	0.0	84.3	1118	1004.3	236.2	78.7	31.9
57	520.7	124.7	0.0	100.0	993	1015.4	195.4	38.1	69.2	14	530.2	187.8	0.0	100.0	1117	1004.3	286.2	78.7	72.2
64	520.7	129.7	0.0	97.0	995	1015.4	255.4	38.1	52.4	15	530.2	195.3	0.0	100.0	1115	1004.3	341.2	78.7	79.2
62	520.7	134.7	0.0	94.1	968	1015.4	225.4	44.2	71.4	9	530.2	202.8	0.0	98.3	1116	1004.3	398.2	78.7	50.0
58	520.7	144.7	0.0	90.9	969	1015.4	225.4	59.4	50.2	13	530.2	217.8	0.0	93.2	1079	1004.3	342.8	81.3	94.8
61	520.7	154.7	0.0	64.7	section 2					11	530.2	262.8	0.0	37.4	1080	1004.3	342.8	101.6	61.5
59	520.7	164.7	0.0	61.5	32	508.0	82.1	0.0	36.0	12	530.2	282.8	0.0	8.3	section 2			121.9	44.1
60	520.7	184.7	0.0	37.4	33	508.0	102.1	0.0	63.9	section 3					53	522.3	187.8	0.0	29.8
927	489.9	129.3	-88.6	72.5	31	508.0	122.1	0.0	95.8	16	327.0	89.3	0.0	8.5	54	522.3	227.8	0.0	64.3
926	489.9	129.3	-59.4	91.4	35	508.0	132.1	0.0	90.5	17	327.0	113.3	0.0	43.5	60	522.3	247.8	0.0	84.6
925	489.9	129.3	-50.3	102.9	34	508.0	142.1	0.0	97.8	18	327.0	143.3	0.0	83.0	55	522.3	267.8	0.0	96.1
924	489.9	129.3	-41.1	102.0	36	508.0	152.1	0.0	100.0	24	327.0	158.3	0.0	98.3	61	522.3	277.8	0.0	100.0
923	489.9	129.3	-32.0	102.5	30	508.0	162.1	0.0	91.0	25	327.0	165.8	0.0	99.9	59	522.3	287.8	0.0	96.1
922	489.9	129.3	-22.9	105.7	29	508.0	202.1	0.0	23.9	19	327.0	173.3	0.0	100.0	58	522.3	307.8	0.0	85.2
921	489.9	129.3	-13.7	108.9	section 3				-0.8	20	327.0	188.3	0.0	87.8	57	522.3	347.8	0.0	42.6
932	489.9	129.3	-13.7	104.9	14	325.4	44.6	0.0	1.1	22	327.0	233.3	0.0	14.6	section 5			0.0	12.3
934	489.9	139.3	-13.7	102.4	5	325.4	84.6	0.0	34.4	section 4					6	319.1	122.8	0.0	3.8
935	489.9	139.3	-13.7	105.2	9	325.4	104.6	0.0	62.9	4	161.9	58.8	0.0	1.1	7	319.1	152.8	0.0	16.8
936	489.9	149.3	-13.7	101.8	12	325.4	124.6	0.0	85.2	6	161.9	88.8	0.0	28.2	8	319.1	182.8	0.0	47.2
937	489.9	159.3	-13.7	78.5	6	325.4	144.6	0.0	97.6	7	161.9	118.8	0.0	92.9	14	319.1	212.8	0.0	76.3
920	489.9	129.3	-4.6	103.0	11	325.4	164.6	0.0	100.0	11	161.9	128.8	0.0	94.5	15	319.1	235.3	0.0	98.0
910	489.9	69.3	0.0	24.3	10	325.4	144.6	0.0	97.0	12	161.9	138.8	0.0	100.0	9	319.1	242.8	0.0	99.9
911	489.9	89.3	0.0	65.3	13	325.4	154.6	0.0	85.0	8	161.9	148.8	0.0	96.9	13	319.1	257.8	0.0	95.4
912	489.9	109.3	0.0	93.1	7	325.4	164.6	0.0	68.2	14	161.9	153.8	0.0	91.1	10	319.1	272.8	0.0	83.7
916	489.9	119.3	0.0	97.2	8	325.4	204.6	0.0	4.2	13	161.9	168.8	0.0	89.1	11	319.1	302.8	0.0	47.9
917	489.9	124.3	0.0	96.0	section 4					15	161.9	168.8	0.0	71.5	12	319.1	332.8	0.0	11.8
913	489.9	129.3	0.0	100.0	3	160.3	55.1	0.0	20.6	9	161.9	178.8	0.0	50.9	section 4			0.0	8.8
915	489.9	139.3	0.0	93.6	8	160.3	75.1	0.0	64.9	10	161.9	208.8	0.0	0.6	16	166.7	112.5	0.0	8.8
914	489.9	149.3	0.0	84.0	11	160.3	85.1	0.0	68.3	section 5					17	166.7	142.5	0.0	30.0
918	489.9	169.3	0.0	62.2	4	160.3	95.1	0.0	99.4	16	108.0	68.9	0.0	10.7	18	166.7	172.5	0.0	63.2
919	489.9	189.3	0.0	23.1	108	9	105.1	0.0	100.0	17	108.0	98.9	0.0	61.3	24	166.7	187.5	0.0	81.5
928	489.9	129.3	4.6	92.0	7	160.3	115.1	0.0	95.2	23	108.0	118.9	0.0	94.0	19	166.7	202.5	0.0	97.5
929	489.9	129.3	13.7	87.3	10	160.3	125.1	0.0	73.5	18	108.0	128.9	0.0	100.0	25	166.7	210.0	0.0	99.9
930	489.9	129.3	22.9	69.4	5	160.3	135.1	0.0	42.6	22	108.0	138.9	0.0	99.8	23	166.7	217.5	0.0	100.0
931	489.9	129.3	32.0	54.8	6	160.3	155.1	0.0	5.2	21	108.0	138.9	0.0	98.7	26	166.7	225.0	0.0	57.7

section 2: search for Cm

section 3	65	317.5	35.0	0.0	4.3	section 5	9	106.4	47.1	0.0	3.2	24	108.0	146.9	0.0	84.5	20	166.7	232.5	0.0	93.2
66	317.5	65.0	0.0	0.0	31.9	10	106.4	77.1	0.0	0.0	61.5	19	108.0	158.9	0.0	56.7	21	166.7	262.5	0.0	36.0
67	317.5	95.0	0.0	0.0	88.0	17	106.4	87.1	0.0	0.0	81.6	20	108.0	178.9	0.0	7.5	22	166.7	282.5	0.0	8.4
72	317.5	105.0	0.0	0.0	97.9	16	106.4	97.1	0.0	0.0	99.4	25	66.7	68.7	0.0	22.0	27	109.5	112.5	0.0	17.6
73	317.5	110.0	0.0	0.0	100.0	18	106.4	102.1	0.0	0.0	99.2	28	66.7	88.7	0.0	61.8	28	109.5	142.5	0.0	41.4
68	317.5	115.0	0.0	0.0	97.1	11	106.4	107.1	0.0	0.0	100.0	31	66.7	98.7	0.0	80.8	29	109.5	162.5	0.0	70.1
71	317.5	125.0	0.0	0.0	77.5	19	106.4	112.1	0.0	0.0	90.3	27	66.7	168	0.0	93.5	30	109.5	182.5	0.0	93.1
69	317.5	135.0	0.0	0.0	70.0	15	106.4	117.1	0.0	0.0	78.8	32	66.7	113	0.0	100.0	36	109.5	187.5	0.0	98.0
section 4	70	317.5	155.0	0.0	20.4	14	106.4	127.1	0.0	0.0	56.5	30	66.7	137	0.0	96.5	34	109.5	192.5	0.0	100.0
74	165.1	35.0	0.0	0.0	2.1	12	106.4	137.1	0.0	0.0	27.2	28	66.7	137	0.0	84.7	35	109.5	197.5	0.0	98.0
75	165.1	65.0	0.0	0.0	60.4	13	106.4	167.1	0.0	0.0	0.5	29	66.7	143.7	0.0	15.1	31	109.5	202.5	0.0	96.0
76	165.1	85.0	0.0	0.0	93.1	3	65.1	47.1	0.0	0.0	10.0	33	34.9	56.7	0.0	32.6	32	109.5	222.5	0.0	57.4
82	165.1	90.0	0.0	0.0	100.0	4	65.1	77.1	0.0	0.0	84.3	34	34.9	78.7	0.0	73.3	33	109.5	242.5	0.0	16.9
84	165.1	92.5	0.0	0.0	100.0	10	65.1	82.1	0.0	0.0	88.9	39	34.9	88.7	0.0	65.4	section 5	66.7	94.2	0.0	16.0
81	165.1	95.0	0.0	0.0	99.9	7	65.1	87.1	0.0	0.0	87.8	41	34.9	93.7	0.0	94.2	6	66.7	114.2	0.0	34.9
83	165.1	100.0	0.0	0.0	98.6	9	65.1	92.1	0.0	0.0	100.0	35	34.9	98.7	0.0	100.0	7	66.7	134.2	0.0	62.8
77	165.1	105.0	0.0	0.0	83.2	6	65.1	97.1	0.0	0.0	97.8	40	34.9	103.7	0.0	98.8	8	66.7	154.2	0.0	91.6
80	165.1	115.0	0.0	0.0	87.0	5	65.1	107.1	0.0	0.0	74.9	38	34.9	108.7	0.0	89.1	13	66.7	159.2	0.0	100.0
78	165.1	125.0	0.0	0.0	30.0	6	65.1	137.1	0.0	0.0	3.2	36	34.9	118.7	0.0	46.9	12	66.7	164.2	0.0	96.3
79	165.1	135.0	0.0	0.0	8.7	11	33.3	46.8	0.0	0.0	29.4	37	34.9	128.7	0.0	17.8	9	66.7	174.2	0.0	86.7
section 5	37	108.0	44.7	0.0	28.0	12	33.3	66.6	0.0	0.0	83.6	42	15.9	38.4	0.0	9.2	11	66.7	194.2	0.0	43.6
45	108.0	54.7	0.0	0.0	60.9	16	33.3	71.8	0.0	0.0	86.9	43	15.9	58.4	0.0	52.9	section 7	34.9	83.9	0.0	34.0
38	108.0	64.7	0.0	0.0	93.7	15	33.3	76.8	0.0	0.0	98.4	46	15.9	68.4	0.0	79.7	14	34.9	103.9	0.0	60.9
44	108.0	74.7	0.0	0.0	99.3	17	33.3	81.8	0.0	0.0	100.0	49	15.9	73.4	0.0	99.4	15	34.9	123.9	0.0	94.1
46	108.0	79.7	0.0	0.0	96.8	13	33.3	86.8	0.0	0.0	93.4	44	15.9	78.4	0.0	100.0	16	34.9	128.9	0.0	100.3
47	108.0	82.2	0.0	0.0	99.1	18	33.3	91.8	0.0	0.0	67.2	50	15.9	83.4	0.0	98.7	21	34.9	133.9	0.0	99.8
39	108.0	84.7	0.0	0.0	100.0	14	33.3	106.8	0.0	0.0	10.3	45	15.9	88.4	0.0	84.7	20	34.9	138.9	0.0	94.5
43	108.0	94.7	0.0	0.0	87.8	19	17.5	38.4	0.0	0.0	13.8	46	15.9	98.4	0.0	46.0	22	34.9	143.9	0.0	87.3
40	108.0	104.7	0.0	0.0	52.1	20	17.5	56.4	0.0	0.0	72.2	45	15.9	118.4	0.0	2.4	17	34.9	143.9	0.0	43.4
42	108.0	114.7	0.0	0.0	25.2	26	17.5	61.4	0.0	0.0	89.1	46	15.9	118.4	0.0	9.2	18	34.9	163.9	0.0	19.4
41	108.0	124.7	0.0	0.0	1.2	24	17.5	66.4	0.0	0.0	96.5	45	15.9	118.4	0.0	2.4	19	34.9	173.9	0.0	0.0
section 6	5	63.5	34.6	0.0	7.5	27	17.5	68.9	0.0	0.0	100.0	46	15.9	118.4	0.0	9.2	section 8	14.3	64.4	0.0	42.5
6	63.5	54.6	0.0	0.0	67.8	25	17.5	71.4	0.0	0.0	95.1	45	15.9	118.4	0.0	9.2	29	14.3	64.4	0.0	85.8
11	63.5	64.6	0.0	0.0	90.7	21	17.5	76.4	0.0	0.0	80.6	44	15.9	118.4	0.0	9.2	30	14.3	64.4	0.0	98.2
12	63.5	69.6	0.0	0.0	98.2	23	17.5	86.4	0.0	0.0	32.0	43	15.9	118.4	0.0	9.2	31	14.3	99.4	0.0	100.0
14	63.5	71.0	0.0	0.0	100.0	22	17.5	96.4	0.0	0.0	2.8	42	15.9	118.4	0.0	9.2	32	14.3	104.4	0.0	98.4
13	63.5	72.1	0.0	0.0	97.1	22	17.5	96.4	0.0	0.0	2.8	41	15.9	118.4	0.0	9.2	33	14.3	114.4	0.0	87.8
7	63.5	74.6	0.0	0.0	95.0	29	15.9	54.3	0.0	0.0	95.0	41	15.9	118.4	0.0	9.2	34	14.3	124.4	0.0	63.2
10	63.5	84.6	0.0	0.0	81.5	32	15.9	59.3	0.0	0.0	78.3	40	15.9	118.4	0.0	9.2	35	14.3	144.4	0.0	17.9
8	63.5	94.6	0.0	0.0	37.4	30	15.9	64.3	0.0	0.0	48.6	39	15.9	118.4	0.0	9.2	36	14.3	144.4	0.0	0.0
9	63.5	114.6	0.0	0.0	2.2	31	15.9	74.3	0.0	0.0	12.3	38	15.9	118.4	0.0	9.2	37	14.3	144.4	0.0	0.0
section 7	15	31.8	24.6	0.0	1.8	25	15.9	14.3	0.0	0.0	0.3	37	15.9	118.4	0.0	9.2	38	14.3	144.4	0.0	0.0
16	31.8	34.6	0.0	0.0	22.9	26	15.9	24.3	0.0	0.0	9.2	36	15.9	118.4	0.0	9.2	39	14.3	144.4	0.0	0.0
17	31.8	44.6	0.0	0.0	57.9	27	15.9	34.3	0.0	0.0	36.2	35	15.9	118.4	0.0	9.2	40	14.3	144.4	0.0	0.0
18	31.8	54.6	0.0	0.0	83.7	28	15.9	44.3	0.0	0.0	71.6	34	15.9	118.4	0.0	9.2	41	14.3	144.4	0.0	0.0
23	31.8	59.6	0.0	0.0	98.8	33	15.9	49.3	0.0	0.0	96.6	33	15.9	118.4	0.0	9.2	42	14.3	144.4	0.0	0.0
24	31.8	62.1	0.0	0.0	100.0	34	15.9	51.8	0.0	0.0	100.0	32	15.9	118.4	0.0	9.2	43	14.3	144.4	0.0	0.0
19	31.8	64.6	0.0	0.0	96.8	29	15.9	54.3	0.0	0.0	95.0	31	15.9	118.4	0.0	9.2	44	14.3	144.4	0.0	0.0
22	31.8	69.6	0.0	0.0	83.8	32	15.9	59.3	0.0	0.0	78.3	30	15.9	118.4	0.0	9.2	45	14.3	144.4	0.0	0.0
20	31.8	74.6	0.0	0.0	59.8	30	15.9	64.3	0.0	0.0	48.6	29	15.9	118.4	0.0	9.2	46	14.3	144.4	0.0	0.0
21	31.8	84.6	0.0	0.0	17.1	31	15.9	74.3	0.0	0.0	12.3	28	15.9	118.4	0.0	9.2	47	14.3	144.4	0.0	0.0

## APPENDIX E

Application of Reichardt's Hypothesis  
to the Concentration Field of Multiple Jet Discharges  
in a Quiescent Ambient

Contents

Introduction

Governing Equations for Circular Jet Discharges

Results of Integral Analysis of a Circular Jet

Results of Applying Reichardt's Hypothesis to the Velocity  
Field of Multiple Circular Jets

Application of Reichardt's Hypothesis to the Concentration  
Field of Multiple Circular Jets

Extension of the Analyses to Multiple Plane Jets

Examination of the Velocity and Concentration Fields for  
Multiple Circular Jet Discharges

Conclusions

### **Introduction**

The equations describing the dispersion of passive plume discharges in rivers are linear equations. One of the desirable properties of linear equations is that solutions to multiple concurrent conditions are independent of each other. For multiple effluent discharges to a river, this means that the concentrations determined for each discharge can be added to determine their combined effect. This greatly facilitates the far field analysis of multiple effluent discharges in a river system.

The equations describing the dilution of jet discharges in a quiescent ambient, however, are not linear. When several jets are located adjacent to each other, the velocity and concentration fields of nearby jets will interact. Their interaction does not result in the net concentration being determined simply by adding the contributions of each jet.

Reichardt's (1943) turbulent transfer theory has been described by Abramovich (1963). Reichardt assumed that the lateral transport of momentum is proportional to the transverse gradient of the longitudinal component of momentum:

$$\overline{uv} = - \Lambda(x) \frac{\partial}{\partial y} \overline{u^2} \quad (\text{E.1})$$

where:  $u$  is the instantaneous longitudinal velocity,

$\overline{u^2}$  is the time-averaged value of the square of the longitudinal velocity,

$v$  is the instantaneous transverse velocity,

$\bar{uv}$  is the time-averaged value of the product of the longitudinal and transverse velocities,  $y$  is the transverse distance from the jet axis, and  $\Lambda$  is a function which is only dependent on the distance along the jet axis ( $x$ ).

Reichardt's hypothesis has previously been applied to determine the velocity fields of multiple circular jet discharges (Knystautas, 1964; Pani and Dash, 1983a; Rajaratnam, 1985), multiple unbounded plane jet discharges (Rajaratnam, 1979) and multiple unbounded slot jet discharges (Demissie and Maxwell, 1982; Pani and Dash, 1983a). It has also been used to assess circular and rectangular wall jets (Pani and Dash, 1983b).

In this appendix, Reichardt's hypothesis is used to determine the concentration fields of multiple jet discharges in a quiescent ambient. The analysis is first carried out in detail for circular jets. The analysis is then extended to consider multiple plane jets.

The combined effects of multiple jet discharges is important in the design of a diffuser outfall. Jet discharge ports can be spaced along the diffuser so that the edges of the concentration fields overlap, however, the jets should not be spaced so closely that they interfere with the dilution that a single jet can achieve along its centreline. Considering these needs, the velocity and concentration fields of multiple circular jet discharges are examined to provide a basis for the selection of the jet spacing.

### **Governing Equations for Circular Jet Discharges**

For circular turbulent non-buoyant jets, the governing equations for momentum, continuity and pollutant flux can be written (Figure 2.1):

$$\text{momentum:} \quad \frac{\partial}{\partial x} r \cdot u^2 + \frac{\partial}{\partial r} r u v = 0 \quad (\text{E.2})$$

$$\text{continuity:} \quad \frac{\partial}{\partial x} r u + \frac{\partial}{\partial r} r v = 0 \quad (\text{E.3})$$

$$\text{pollutant flux:} \quad \frac{\partial}{\partial x} r u c + \frac{\partial}{\partial r} r v c = 0 \quad (\text{E.4})$$

where:  $x$  is the distance along the jet centreline axis,

$r$  is the radial distance away from the  $x$  axis,

$u$  is the instantaneous axial velocity (in the  $x$  direction),

$v$  is the instantaneous radial velocity (in the  $r$  direction), and

$c$  is the instantaneous concentration at a point.

In equation (E.2), laminar stresses have been assumed to be relatively small and, hence, are neglected.

### **Results of Integral Analysis of a Circular Jet**

Equations (E.2), (E.3) and (E.4) can be solved for a single circular jet discharge using integral analysis procedures coupled with certain experimental observations. The solutions to these equations result in a number of simple

expressions for the time-averaged characteristics of the jet discharge (Rajaratnam, 1983):

a) velocity along the x axis:

$$\frac{u_m}{U_o} = k_1 / x = 6.13 d / x \quad (\text{E.5})$$

b) half width of jet (at  $u/u_m = 0.5$ ):

$$b = k_2 x = 0.096 x \quad (\text{E.6})$$

c) concentration along the x axis:

$$\frac{c_m}{C_o} = k_3 / x = 5.34 d / x \quad (\text{E.7})$$

d) velocity distribution at a section:

$$\frac{u}{u_m} = f\left(\frac{r}{b}\right) = f(\eta) = \exp\{-\ln 2 \eta^2\} = \exp\{-0.693 \eta^2\} \quad (\text{E.8})$$

e) concentration distribution at a section:

$$\frac{c}{c_m} = h\left(\frac{r}{b}\right) = h(\eta) = \exp\left\{\frac{-\ln 2 \eta^2}{k^2}\right\} = \exp\{-0.506 \eta^2\} \quad (\text{E.9})$$

where:  $u$  is the axial velocity at a point in a section of the jet,

$u_m$  is the maximum velocity in the section,



$U_0$  is the velocity at the jet nozzle,  
 $d$  is the jet nozzle diameter,  
 $b$  is the jet half-width (the distance from the jet  
 centreline to the point where  $u/u_m = 0.5$ ),  
 $c$  is the concentration at a point in a section of  
 the jet,  
 $c_m$  is the maximum concentration in the section,  
 $C_0$  is the concentration at the jet nozzle,  
 $\eta$  is the dimensionless radial distance ( $\eta = r/b$ ),  
 $f$  is a function describing the self-similar velocity  
 distribution,  
 $h$  is a function describing the self-similar  
 concentration distribution,  
 $k$  is the ratio of concentration and momentum  
 diffusion coefficients ( $k = b_c/b = 1.17$ ),  
 $b_c$  is the concentration half-width, and  
 $k_1$ ,  $k_2$  and  $k_3$  are constants.

Equations (E.5) to (E.9) are applicable in the zone of  
 established flow of a single jet discharge (i.e.  $x > 6d$ ).  
 These equations can be used to provide a complete description  
 of the axial velocity and concentration distributions  
 throughout the field of the jet.

### **Results of Applying Reichardt's Hypothesis to the Velocity Field of Multiple Circular Jets**

Reichardt's hypothesis has been applied to equations  
 (E.1) and (E.2) previously (Knystautas, 1964; Pani and Dash,

1983a; Rajaratnam, 1985). The results of these analyses indicate that the square of the time-averaged axial velocity is a linear equation. Rajaratnam's work indicates:

$$\frac{u^2}{u_m^2} = \exp\left\{-2 \ln 2 \left(\frac{r}{b}\right)^2\right\} = \exp\{-1.386 \eta^2\} \quad (\text{E.10})$$

Thus, the squares of the axial velocities (i.e. the axial momentum) of adjacent jet discharges are additive.

If a series of  $2m + 1$  identical jets are spaced a distance of  $\lambda$  apart, the velocity in the plane of the diffuser jets can be determined from (Figure E.1):

$$u^2 = \sum_{n=-m}^{n=+m} u_n^2 = \frac{37.6 U_o^2 d^2}{x^2} \sum_{n=-m}^{n=+m} \exp\left\{-1.386 \left(\frac{y-n\lambda}{b}\right)^2\right\} \quad (\text{E.11})$$

where:  $u_n^2$  is the momentum contribution of the  $n^{\text{th}}$  jet, and

$y$  is the distance from the central jet axis in the plane of the diffuser jets.

Examination of equation (E.11) for  $n = 0$  results in equation (E.5) for a single jet discharge.

Equation (E.11) can be expanded to consider any point about the central jet (Figure E.2):

$$\begin{aligned} u^2 &= \frac{37.6 U_o^2 d^2}{x^2} \sum_{n=-m}^{n=+m} \exp\left\{-1.386 \left(\frac{r_n}{b}\right)^2\right\} \\ &= \frac{37.6 U_o^2 d^2}{x^2} \sum_{n=-m}^{n=+m} \exp\left\{-150 \left(\frac{r_n}{x}\right)^2\right\} \end{aligned} \quad (\text{E.12})$$

where the square of the axial distance ( $r_n^2$ ) from the  $n^{\text{th}}$  jet is determined from:

$$r_n^2 = (n\lambda - y)^2 + z^2 = n^2\lambda^2 - 2n\lambda y + y^2 + z^2 \quad (\text{E.13})$$

where  $z$  is the distance from the plane of the jet discharges.

**Application of Reichardt's Hypothesis to the  
Concentration Field of Multiple Circular Jets**

The continuity and pollutant flux equations for a circular turbulent jet have been given earlier:

$$\text{continuity:} \quad \frac{\partial}{\partial x} r u + \frac{\partial}{\partial r} r v = 0 \quad (\text{E.3})$$

$$\text{pollutant flux:} \quad \frac{\partial}{\partial x} r u c + \frac{\partial}{\partial r} r v c = 0 \quad (\text{E.4})$$

From calculus, it can be shown that:

$$\frac{\partial}{\partial x} r u c = r \frac{\partial}{\partial x} u c + u c \frac{\partial}{\partial x} r = r \frac{\partial}{\partial x} u c \quad (\text{E.14})$$

Using equation (E.14) in equation (E.4) gives:

$$r \frac{\partial}{\partial x} u c = - \frac{\partial}{\partial r} r v c \quad (\text{E.15})$$

$$\frac{\partial}{\partial x} u c = \frac{-1}{r} \frac{\partial}{\partial r} r v c \quad (\text{E.16})$$

Time averaging equation (E.16), using  $u = \bar{u} + u'$  and  $c = \bar{c} + c'$ , then assuming  $u \gg u'$  and  $c \gg c'$  (to allow the smaller terms to be discarded) gives:

$$\frac{\partial}{\partial x} \bar{u} \bar{c} = -\frac{1}{r} \frac{\partial}{\partial r} r \bar{v} \bar{c} \quad (\text{E.17})$$

Similar to Reichardt's hypothesis, it would be convenient to assume:

$$\bar{v} \bar{c} = -H \frac{\partial}{\partial r} \bar{u} \bar{c} \quad (\text{E.18})$$

The assumption is that the radial transport of a tracer is proportional to the radial gradient of the axial transport of the tracer and, that the constant of proportionality is a function of the distance downstream only.

Substituting equation (E.18) into equation (E.17) gives:

$$\frac{\partial}{\partial x} \bar{u} \bar{c} = \frac{1}{r} \frac{\partial}{\partial r} r H \frac{\partial}{\partial r} \bar{u} \bar{c} = \frac{H}{r} \frac{\partial}{\partial r} r \frac{\partial}{\partial r} \bar{u} \bar{c} \quad (\text{E.19})$$

Equation (E.19) is a linear second order partial differential equation. The linearity provides promise that a useful solution (which would allow concentrations to be determined for multiple jets by superposition) can be found.

Let the function H be of the form:

$$H = k_4 x^t \quad (\text{E.20})$$

Dropping the overbars (which so far have been used to denote time-averaged values) equation (E.19) becomes:

$$\frac{\partial}{\partial x} u c = \frac{k_4 x^t}{r} \left[ \frac{\partial}{\partial r} r \frac{\partial}{\partial r} u c \right] \quad (\text{E.21})$$

This equation form will be used later in determining the final solution.

Examining equation (E.19) using equations (E.8) and (E.9) results in:

$$\frac{\partial}{\partial x} f(\eta) h(\eta) u_m c_m = \frac{H}{r} \frac{\partial}{\partial r} r \frac{\partial}{\partial r} f(\eta) h(\eta) u_m c_m \quad (\text{E.22})$$

Using equations (E.5) and (E.7) (and by noting that  $r = \eta b$ ;  $\frac{\partial \eta}{\partial r} = 1/b$ ; and  $\partial r = b \partial \eta$ ), equation (E.22) becomes:

$$\begin{aligned} \frac{\partial}{\partial x} \frac{f(\eta) h(\eta) k_1 k_3 U_o C_o}{x^2} \\ = \frac{H}{\eta b^2} \frac{\partial}{\partial \eta} \eta \frac{\partial}{\partial \eta} \frac{f(\eta) h(\eta) k_1 k_3 U_o C_o}{x^2} \end{aligned} \quad (\text{E.23})$$

Using equation (E.6) for the jet half width (b) gives:

$$\begin{aligned} \frac{\partial}{\partial x} \frac{k_1 k_3 U_o C_o f(\eta) h(\eta)}{x^2} &= \frac{-2 k_1 k_3 U_o C_o f(\eta) h(\eta)}{x^3} \\ &= H \frac{k_1 k_3 U_o C_o}{k_2^2 x^4} \frac{1}{\eta} \frac{\partial}{\partial \eta} \eta \frac{\partial}{\partial \eta} f(\eta) h(\eta) \end{aligned} \quad (\text{E.24})$$

Thus:

$$H = \frac{-2 k_2^2 x \eta f(\eta) h(\eta)}{\frac{\partial}{\partial \eta} \eta \frac{\partial}{\partial \eta} f(\eta) h(\eta)} \quad (\text{E.25})$$

Inspection of equation (E.25) indicates that H is a linear function of x (i.e.  $t = 1$  in equation E.20). Thus:

$$\frac{\partial}{\partial x} u c = \frac{k_4 x}{r} \left[ \frac{\partial}{\partial r} r \frac{\partial}{\partial r} u c \right] \quad (\text{E.26})$$

The solution to equation (E.26) is of the form (Knystautas, 1964):

$$u c = \frac{A}{x^2} \exp\left\{\frac{-r^2}{\bar{k} x^2}\right\} \quad (\text{E.27})$$

where  $\bar{k} = 2 k_4$ .

The constant A can be found by examining the conditions at  $r = 0$ :

$$u c = u_m c_m = \frac{A}{x^2} \exp(-0) \quad (\text{E.28})$$

This gives:

$$A = x^2 u_m c_m = \frac{6.13 U_0 5.34 C_0 d^2}{x^2} \quad (\text{E.29})$$

Thus:

$$\begin{aligned} u c &= u_m c_m \exp\left\{\frac{-r^2}{\bar{k} x^2}\right\} \\ &= \frac{32.73 U_0 C_0 d^2}{x^2} \exp\left\{\frac{-r^2}{\bar{k} x^2}\right\} \end{aligned} \quad (\text{E.30})$$

The constant  $\bar{k}$  can be found by examining the condition when  $r = b$  (i.e.  $\eta = 1$  and  $u c = 0.30 u_m c_m$ ) and using equations (E.8), (E.9) and (E.30):

$$\begin{aligned} u c &= \exp(-0.693) u_m \exp(-0.506) c_m \\ &= u_m c_m \exp\left\{\frac{-r^2}{\bar{k} (b/0.096)^2}\right\} \end{aligned} \quad (\text{E.31})$$

which gives:

$$1.199 = \frac{r^2}{108.5 \bar{k} b^2} = \frac{1}{108.5 \bar{k}} \quad (\text{E.32})$$

and, therefore:

$$\bar{k} = \frac{1}{130} \quad (\text{E.33})$$

Equation (E.30) now can be used to describe the concentration field of multiple jet discharges:

$$\begin{aligned}
 u c &= \frac{32.73 U_0 C_0 d^2}{x^2} \exp\left\{\frac{-1.199 r^2}{b^2}\right\} \\
 &= \frac{32.73 U_0 C_0 d^2}{x^2} \exp\left\{\frac{-130 r^2}{x^2}\right\} \quad (E.34)
 \end{aligned}$$

The contributions of  $u c$  for  $2m + 1$  identical jets located a distance  $\lambda$  apart can be summed. The following equation can be used to determine the value of  $u c$  at a point relative to the central jet in the plane of the jets (i.e.  $r = y$ ):

$$\begin{aligned}
 u c &= \sum_{n=-m}^{n=+m} u_n c_n = \frac{32.73 U_0 C_0 d^2}{x^2} \sum_{n=-m}^{n=+m} \exp\left\{-1.199 \left(\frac{y-n\lambda}{b}\right)^2\right\} \\
 &= \frac{32.73 U_0 C_0 d^2}{x^2} \sum_{n=-m}^{n=+m} \exp\left\{-130 \left(\frac{y-n\lambda}{x}\right)^2\right\} \quad (E.35)
 \end{aligned}$$

The procedure for application would be to determine  $u$ , by using equation (E.11), then the product  $u c$  can be determined from equation (E.35). The concentration at the point can then be found from:

$$c = u c / u \quad (E.36)$$

The generality of equation (E.35) can be extended to anywhere in the jet flow field (relative to the central jet) by using the form:

$$u c = \sum_{n=-m}^{n=+m} u_n c_n = \frac{32.73 U_0 C_0 d^2}{x^2} \sum_{n=-m}^{n=+m} \exp\left\{-1.199 \left(\frac{r_n}{b}\right)^2\right\}$$

$$= \frac{32.73 U_0 C_0 d^2}{x^2} \sum_{n=-m}^{n=+m} \exp\left\{-130\left(\frac{r_n}{x}\right)^2\right\} \quad (\text{E.37})$$

where  $r_n$  is determined using equation (E.13). Equations (E.12), (E.13), (E.36) and (E.37) can be used together to determine the axial velocity and concentration anywhere in the flow field.

### **Extension of the Analyses to Multiple Plane Jets**

The analysis carried out in the previous section can also be applied to multiple plane jets. As this analysis involves a similar procedure for a simpler case, only the major steps are presented.

For plane turbulent non-buoyant jets the governing equations are:

$$\text{momentum:} \quad u \frac{\partial}{\partial x} u + v \frac{\partial}{\partial y} u = 0 \quad (\text{E.38})$$

$$\text{continuity:} \quad \frac{\partial}{\partial x} u + \frac{\partial}{\partial y} v = 0 \quad (\text{E.39})$$

$$\text{pollutant flux:} \quad u \frac{\partial}{\partial x} c + v \frac{\partial}{\partial y} c = 0 \quad (\text{E.40})$$

where  $y$  is the distance from the jet centreline.

Integral analysis of a single plane jet discharge results in the following time-averaged characteristics (Rajaratnam, 1983):



a) velocity along the x axis:

$$\frac{u_m}{U_0} = k_1 / \sqrt{x} = 3.70 \sqrt{b_0} / \sqrt{x} \quad (\text{E.41})$$

b) half-width of jet (at  $u/u_m = 0.5$ ):

$$b = k_2 x = 0.097 x \quad (\text{E.42})$$

c) concentration along the x axis:

$$\frac{c_m}{C_0} = k_3 / \sqrt{x} = 3.44 \sqrt{b_0} / \sqrt{x} \quad (\text{E.43})$$

d) velocity distribution at a section:

$$\frac{u}{u_m} = f\left(\frac{y}{b}\right) = f(\eta) = \exp\{-\ln 2 \eta^2\} = \exp\{-0.693 \eta^2\} \quad (\text{E.44})$$

e) concentration distribution at a section:

$$\frac{c}{c_m} = h\left(\frac{y}{b}\right) = h(\eta) = \exp\left\{-\frac{\ln 2 \eta^2}{k^2}\right\} = \exp\{-0.506 \eta^2\} \quad (\text{E.45})$$

where  $b_0$  is the slot half width, and  $k = 1.27$ .

Reichardt's hypothesis has been applied to equations (E.38) and (E.39) previously (Rajaratnam, 1979). The results of the analysis indicate that the time-averaged axial velocity for a series of  $2m + 1$  identical jets can be determined from:

$$\begin{aligned}
u^2 &= \sum_{n=-m}^{n=+m} u_n^2 = \frac{13.7 U_o^2 b_o}{x} \sum_{n=-m}^{n=+m} \exp\left\{-2 \ln 2 \left(\frac{y-n\lambda}{b}\right)^2\right\} \\
&= \frac{13.7 U_o^2 b_o}{x} \sum_{n=-m}^{n=+m} \exp\left\{-1.386 \left(\frac{y-n\lambda}{b}\right)^2\right\} \\
&= \frac{13.7 U_o^2 b_o}{x} \sum_{n=-m}^{n=+m} \exp\left\{-1.47 \left(\frac{y-n\lambda}{x}\right)^2\right\} \quad (E.46)
\end{aligned}$$

The concentration field can be considered by manipulating equations (E.39) and (E.40), using calculus and then time-averaging the results, to give (overbars deleted):

$$\frac{\partial}{\partial x} u c = - \frac{\partial}{\partial x} v c \quad (E.47)$$

Similar to Reichardt's hypothesis it is assumed:

$$v c = - H_p \frac{\partial}{\partial y} u c \quad (E.48)$$

Thus, a linear second order partial differential equation can be developed:

$$\frac{\partial}{\partial x} u c = H_p \frac{\partial^2}{\partial y^2} u c \quad (E.49)$$

Examination of equation (E.49), using equations (E.41) through (E.45), indicates that the form of the function  $H_p$  is linear ( $H_p = k_5 x$ ).

Using the function:

$$\xi = x^2 \quad (E.50)$$

gives: 
$$\frac{\partial}{\partial x} = \frac{\partial}{\partial \xi} \frac{\partial \xi}{\partial x} = 2 x \frac{\partial}{\partial \xi} \quad (\text{E.51})$$

Equation (E.49) can then be rewritten as:

$$\frac{\partial}{\partial \xi} u c = \bar{k} \frac{\partial^2}{\partial y^2} u c \quad (\text{E.52})$$

The solution to equation (E.52) is:

$$u c = \frac{A}{\sqrt{\xi}} \exp\left\{\frac{-y^2}{4 \bar{k} \xi}\right\} \quad (\text{E.53})$$

Evaluation of equation (E.53) for the conditions at  $y = 0$  (i.e.  $u c = u_m c_m$ ) and  $y = b$  (i.e.  $u c = 0.10 u_m c_m$ ) gives:

$$\begin{aligned} u c &= \frac{11.73 U_0 C_0 b_0}{x} \exp\left\{-1.199 \left(\frac{y}{b}\right)^2\right\} \\ &= \frac{11.73 U_0 C_0 b_0}{x} \exp\left\{-127 \left(\frac{y}{x}\right)^2\right\} \end{aligned} \quad (\text{E.54})$$

For  $2m + 1$  jets located a distance  $\lambda$  apart, the contributions of  $u c$  can be summed:

$$\begin{aligned} u c &= \sum_{n=-m}^{n=+m} u_n c_n = \frac{11.73 U_0 C_0 b_0}{x} \sum_{n=-m}^{n=+m} \exp\left\{-1.199 \left(\frac{y-n\lambda}{b}\right)^2\right\} \\ &= \frac{11.73 U_0 C_0 b_0}{x} \sum_{n=-m}^{n=+m} \exp\left\{-127 \left(\frac{y-n\lambda}{x}\right)^2\right\} \end{aligned} \quad (\text{E.55})$$

The procedure for application is to first determine  $u$ , by using equation (E.46). Then the value of  $u c$  is determined from equation (E.55) and  $c$  is subsequently found from  $c = u c / u$  (equation E.36).

**Examination of the Velocity and Concentration Fields  
for Multiple Circular Jet Discharges**

Equations (E.12) and (E.37) have been examined to provide some insight on the characteristics of the velocity and concentration fields for multiple circular jet discharges.

a) velocities and concentrations along the central jet axis:

Velocities and concentrations along the central jet axis (i.e.  $y = z = 0$ ) were computed for a number of jet spacing intervals (figures E.3 and E.4). The velocities and concentrations for a single circular jet discharge is represented on these figures by an infinite spacing (i.e.  $\lambda/d = \infty$ ). For this condition, the velocities and concentrations along the central jet axis decreases in a linear fashion as described in equations (E.5) and (E.7).

A series of circular jets can be spaced close enough together to have the characteristics of a plane jet. Pani and Dash (1983a) indicated that the equivalent slot width for a plane jet could be determined based on the port areas. This results in:

$$\frac{\pi d^2}{4} = 2 b_o \lambda \quad (E.56)$$

Equation (E.56) gives a value of  $\lambda = 0.785 d$  for a theoretical plane jet with a slot half width of  $b_o = d/2$ . Examination of equations (E.12) and (E.37) for multiple circular jets with a theoretical spacing of  $\lambda/d = 0.785$  gives

the same results as equations (E.41) and (E.43) for plane jets (figures E.3 and E.4).

In practical terms, the minimum jet spacing would be  $\lambda/d = 1$  for a series of thin walled tubes but, for welded steel outfall diffusers, the minimum value would more likely be  $\lambda/d = 2$ .

The axial velocity and concentration distributions for jet spacings of  $\lambda/d = 2, 5$  and  $10$  have also been shown on figures E.3 and E.4. The distributions indicate that the flows are like circular jets (i.e. vary with the inverse of  $x/d$ ) for some distance, then eventually become like plane jets (i.e. vary with the inverse of  $\sqrt{x/d}$ ). The distance to the point at which the velocity stops behaving like a circular jet is about  $6 \lambda$  (the concentration reaches this point a bit sooner). Knystautas (1964) indicated that the point at which the circular jets behave like a plane jet was a distance of  $12 \lambda$  from the outlets. Although the plane jet behaviour is approached asymptotically, the  $12 \lambda$  distance is supported by this work.

One common mistake often made in assessing multiple jet discharges is to use the principle of superposition to determine the velocity and concentration fields. This can result in significant overestimations (figures E.5, E.6, E.7, and E.8). The significance of the error increases with the distance from the nozzles, being in the order of 2 to 4 times the correct values at  $x/d = 100$ .

b) Velocities and concentrations in the plane of diffuser:

Velocities and concentrations in the plane of the diffuser have been examined in figures E.9 and E.10 for a jet spacing of  $\lambda/d = 5$ . Near the outlets, at  $x = 10 d$ , the velocities and concentrations are independent of the adjacent jets. At  $x = 20 d$  they interact (note the overestimation by the method of superposition). At  $x = 50 d$  (i.e.  $x = 10 \lambda$ ) the jets appear like a plane jet with a slot half width of:

$$b_0 = \frac{\pi d^2}{8 \lambda} \quad (\text{E.57})$$

c) Velocities and concentrations normal to diffuser plane:

Velocities and concentrations normal to the diffuser plane have been examined in figures E.11, E.12, E.13, E.14, E.15 and E.16. Near the nozzle, the jets behave like a single jet until the spacing is very close. At some significant distance from the nozzle, each jet discharge configuration behaves like a plane jet. When  $\lambda/d = 0.785$  the jet diffuser behaves exactly like a plane jet.

### **Conclusions**

a) Reichardt's hypothesis has been successfully applied by others to determine the velocity fields of multiple jet discharges. Reichardt's hypothesis can also be adapted to develop equations for the concentration fields of multiple jet discharges. This work has done so for multiple circular jet discharges and multiple plane jet discharges.

b) Equation (E.56) can be used to determine the equivalent slot half width ( $b_0$ ) for a series of circular jets spaced at a distance of  $\lambda$  apart. The use of the multiple circular jet discharge equations (E.12) and (E.37) with a theoretical jet spacing of  $\lambda/d = 0.785$  gives the same velocity and concentration distributions as the plane jet equations (E.41) and (E.43).

c) Multiple circular jet discharges behave like independent circular jets (i.e. the velocity and concentration vary inversely with the distance  $x/d$ ) for a distance of  $6\lambda$  from the nozzle. Beyond this distance, adjacent jets begin to affect the velocity and concentration conditions of their neighbours and, the mixing is not as efficient as that for a lone jet.

d) As the discharges from multiple circular jets progress downstream, their behaviour becomes increasingly similar to that of a plane jet. This work confirms the work of Knystautas (1964) which indicates that multiple circular jets behave like a plane jet (i.e. where the velocity and concentration vary inversely with  $\sqrt{x/d}$ ) after a distance of  $12\lambda$  from the nozzles. The equivalent slot half-width ( $b_0$ ) can be determined from the jet diameter ( $d$ ) and the jet spacing ( $\lambda$ ) using equation (E.57).

e) A common mistake often made in assessing multiple jet discharges is to use the principle of superposition to determine the velocity and concentration fields. The superposition procedure results in a significant overestimation of the magnitude of the velocities and concentrations.



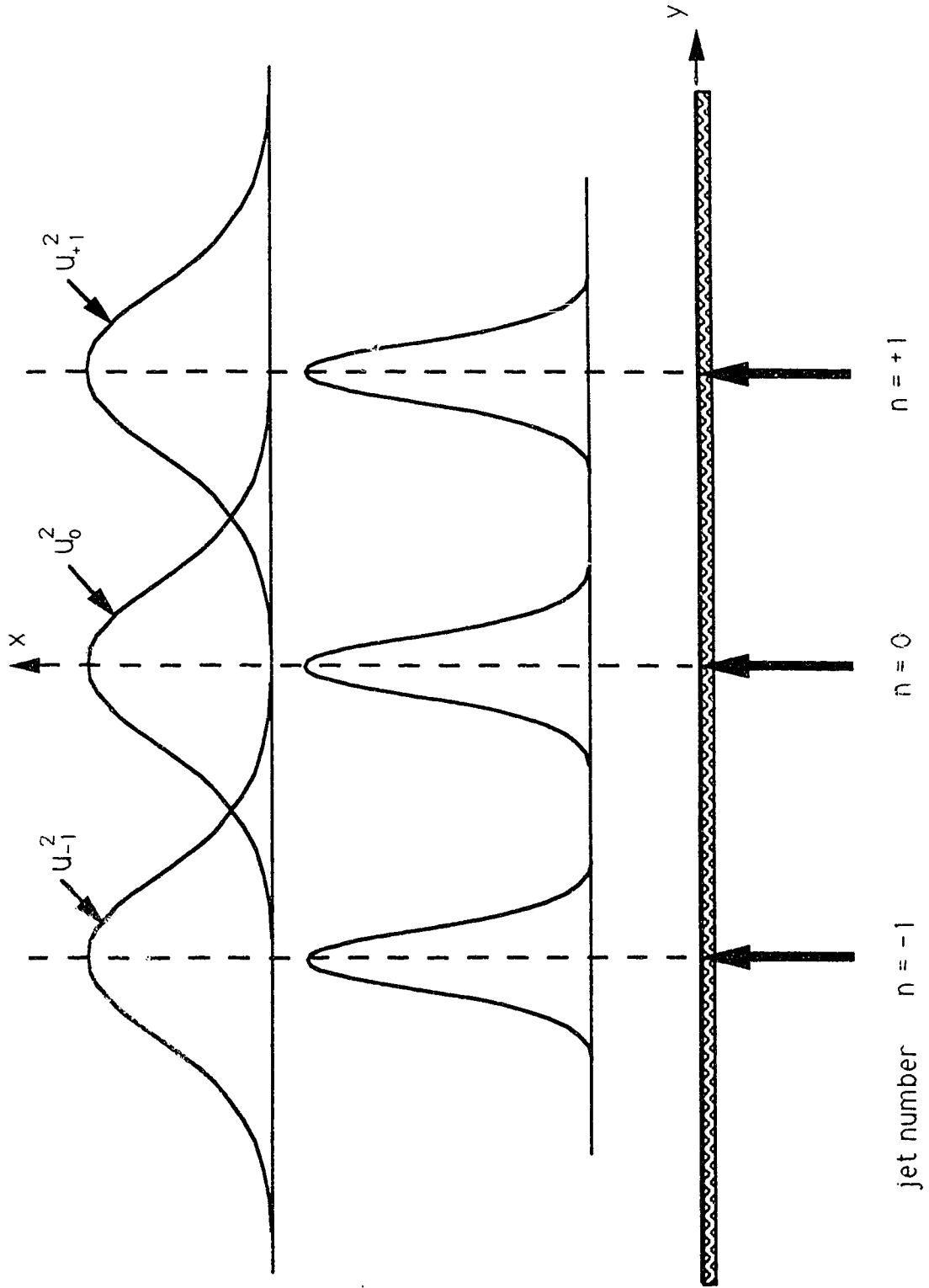


Figure E.1 Velocity distribution within jet plane

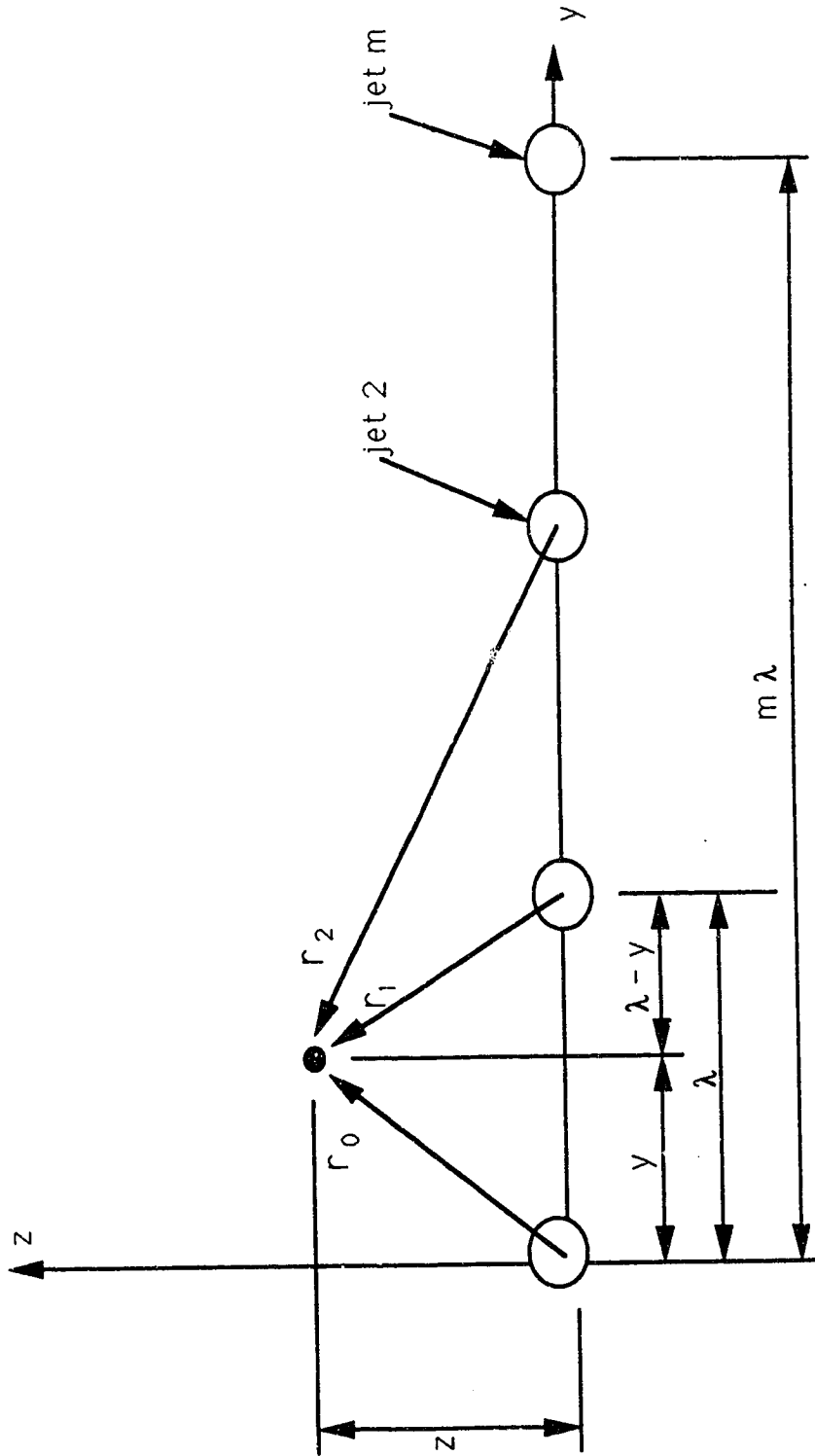


Figure E.2 Distances within plane normal to jets

Figure E.3 Velocities along central jet axis

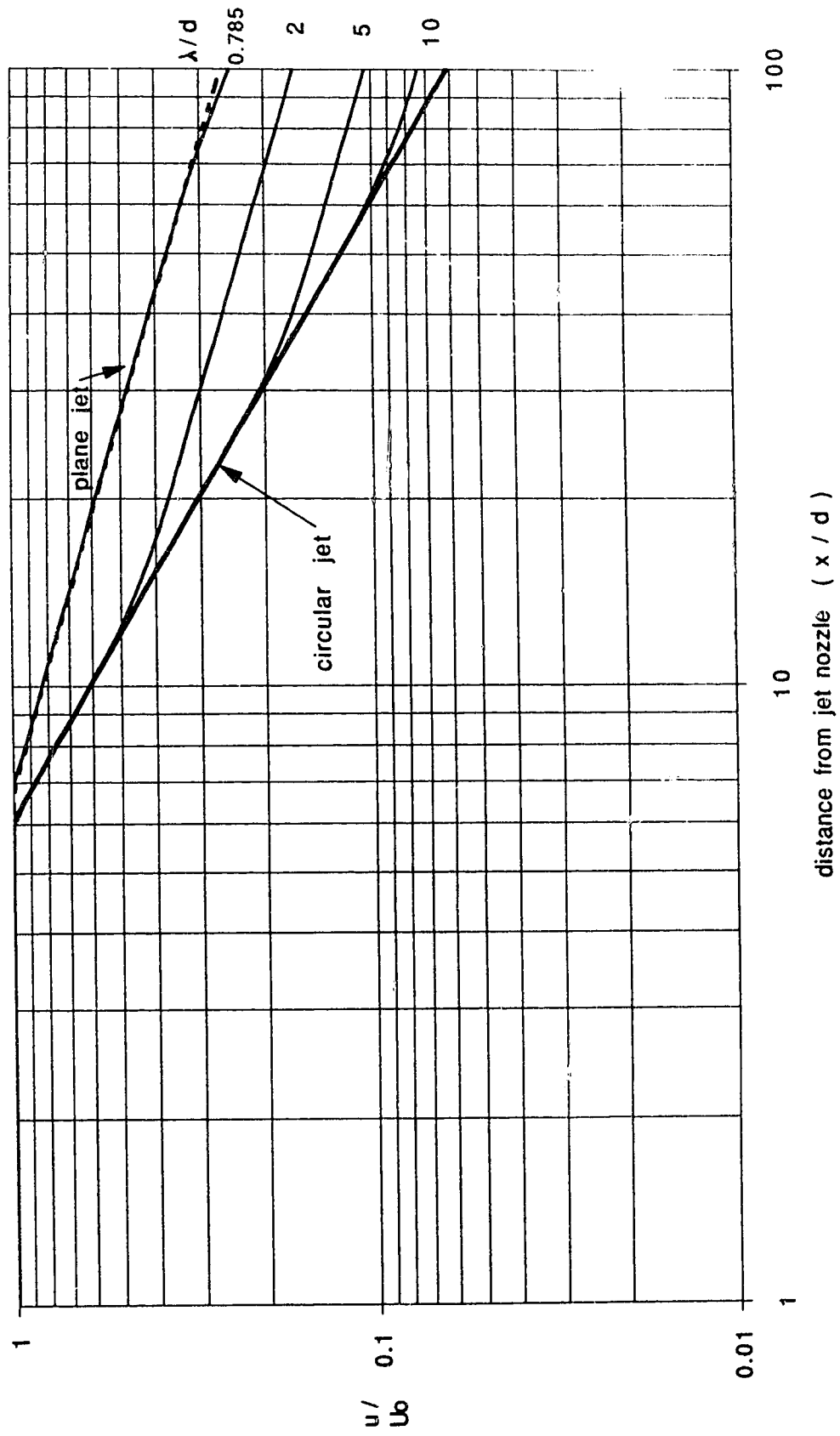


Figure E.4 Concentrations along central jet axis

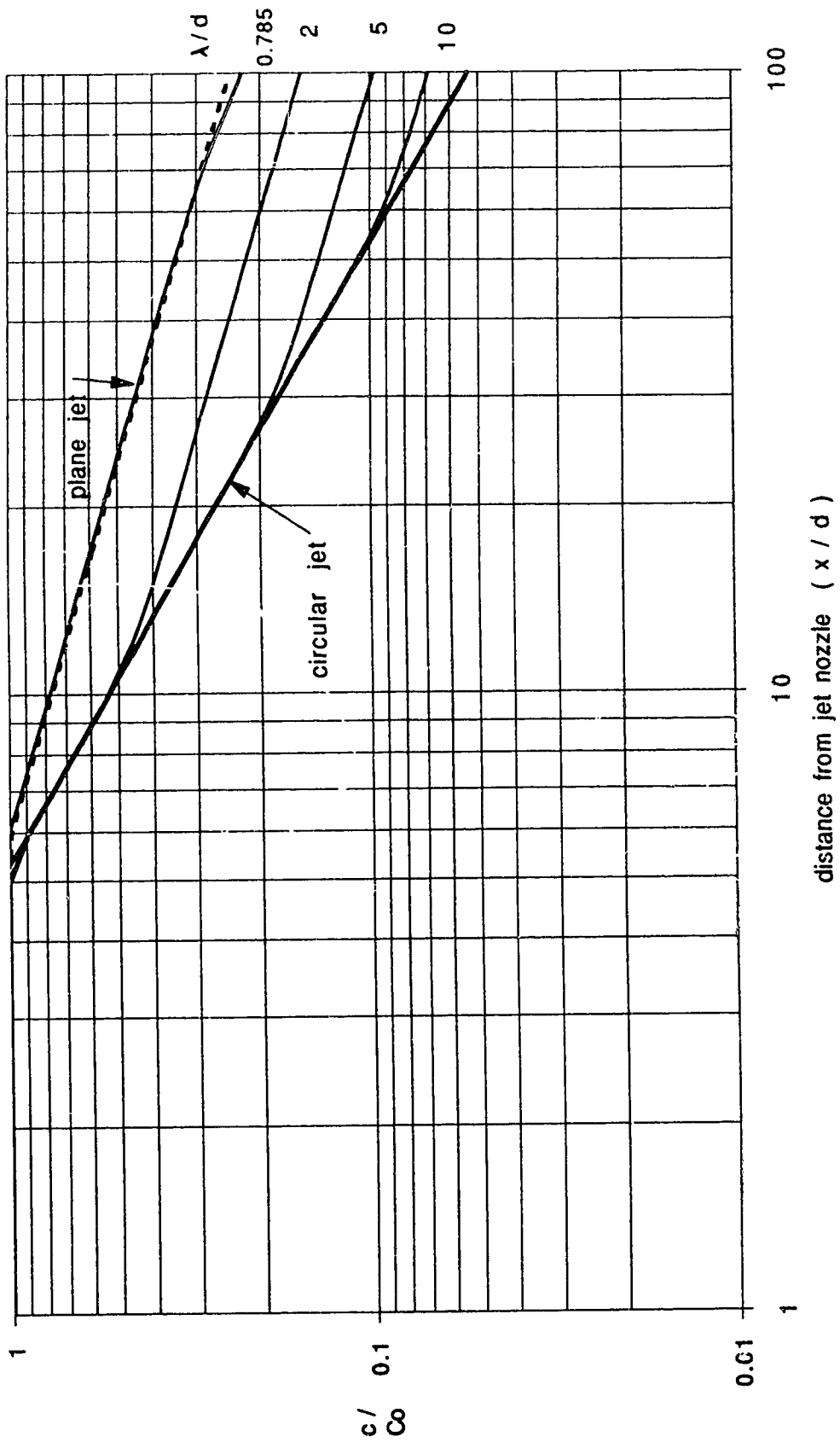


Figure E.5 Comparison of velocity estimates along central jet axis ( $\lambda = 2 d$ )

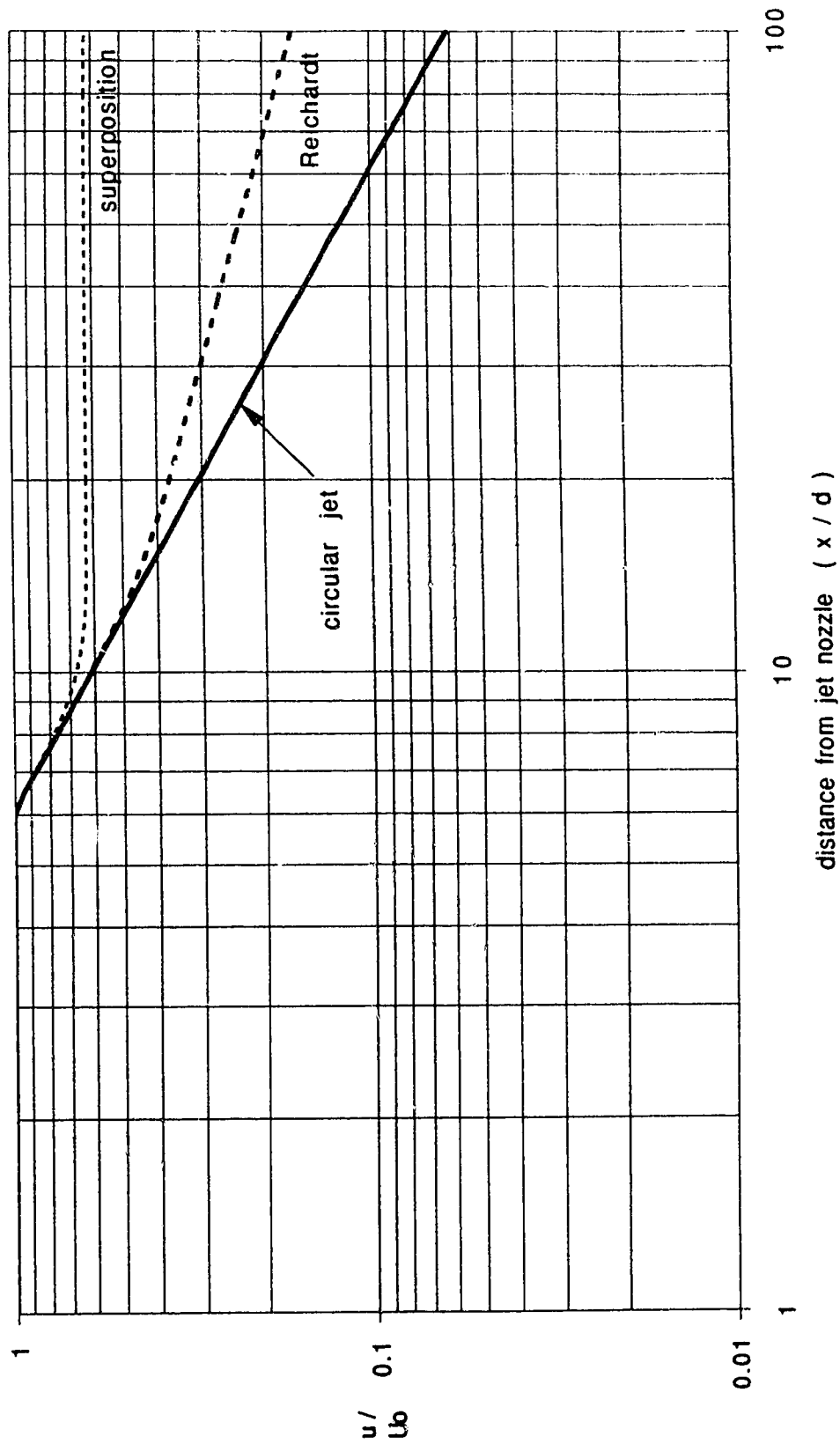


Figure E.6 Comparison of velocity estimates along central jet axis ( $\lambda = 5 d$ )

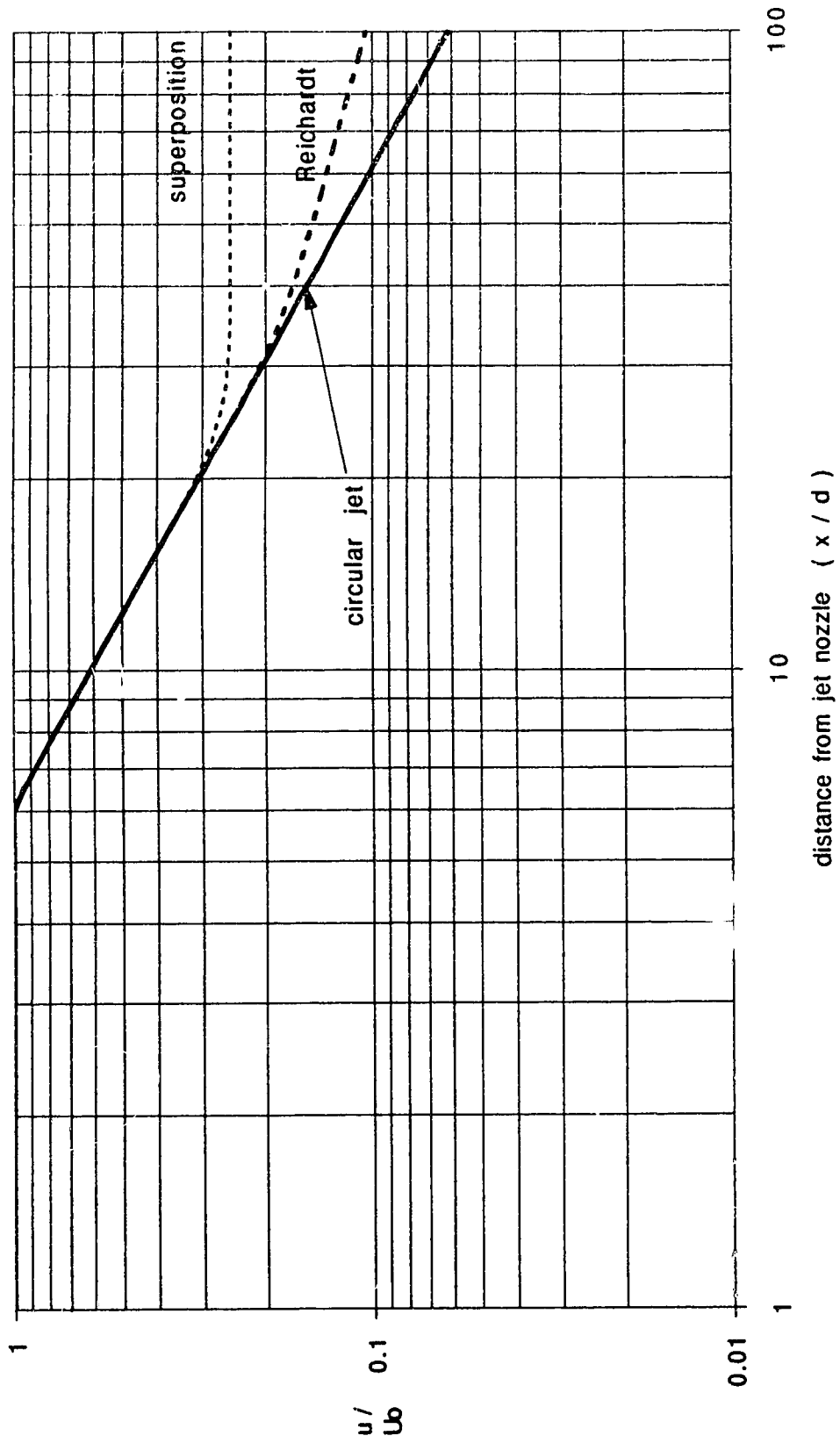


Figure E.7 Comparison of concentration estimates along central jet axis ( $\lambda = 2 d$ )

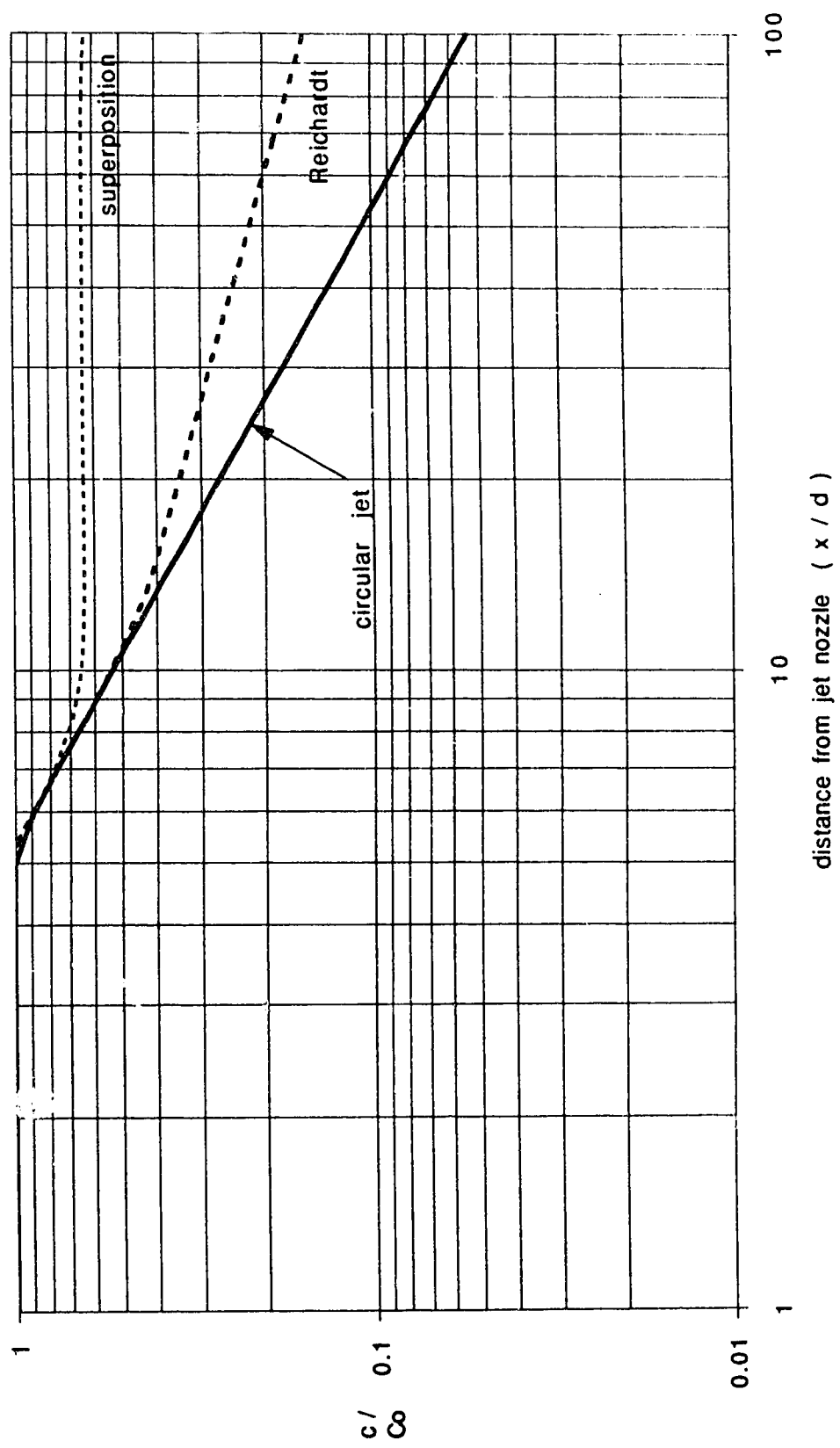


Figure E.8 Comparison of concentration estimates along central jet axis ( $\lambda = 5 d$ )

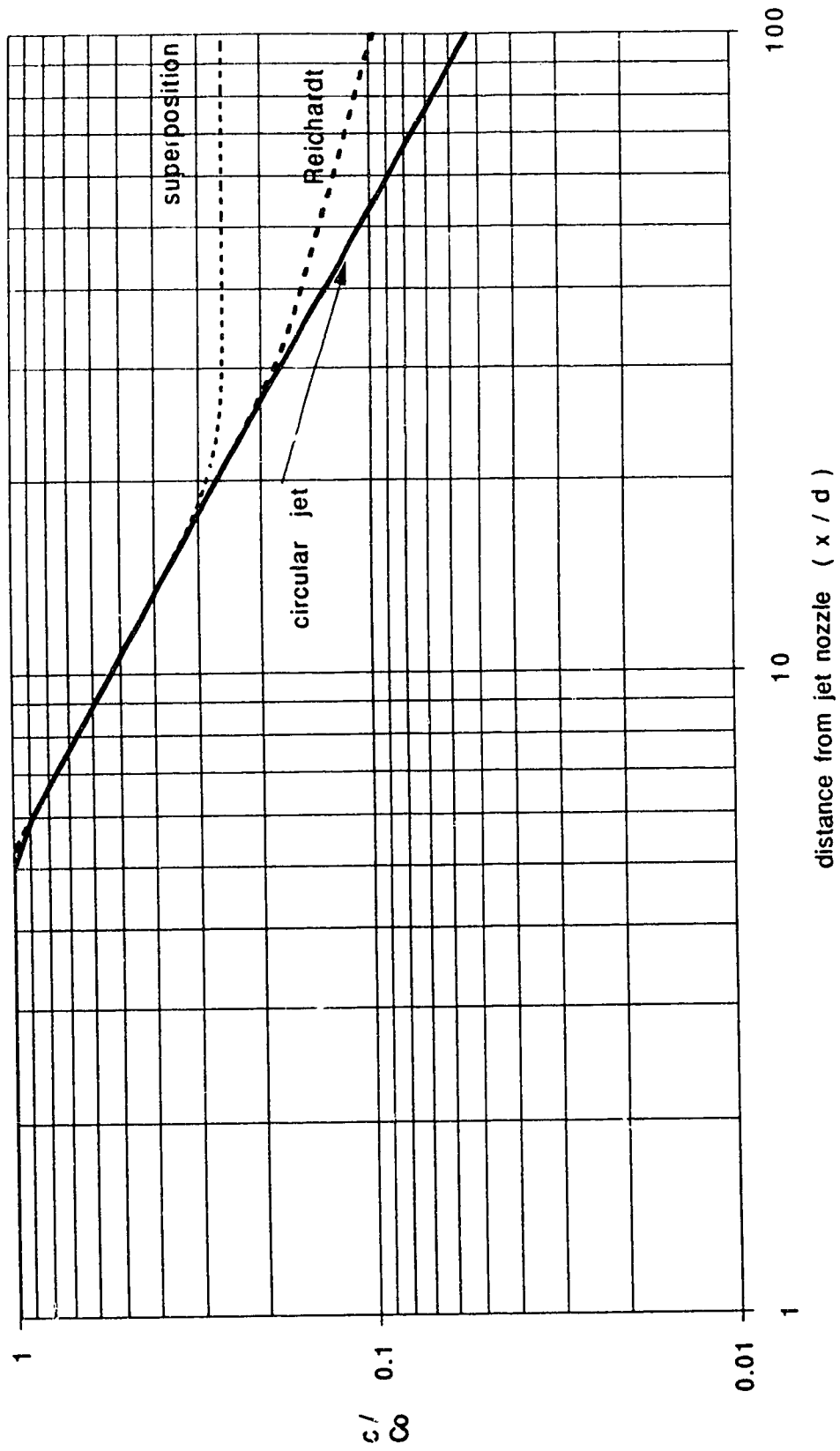




Figure E.9 Velocity distribution in plane of diffuser  
( $\lambda = 5 d$ )

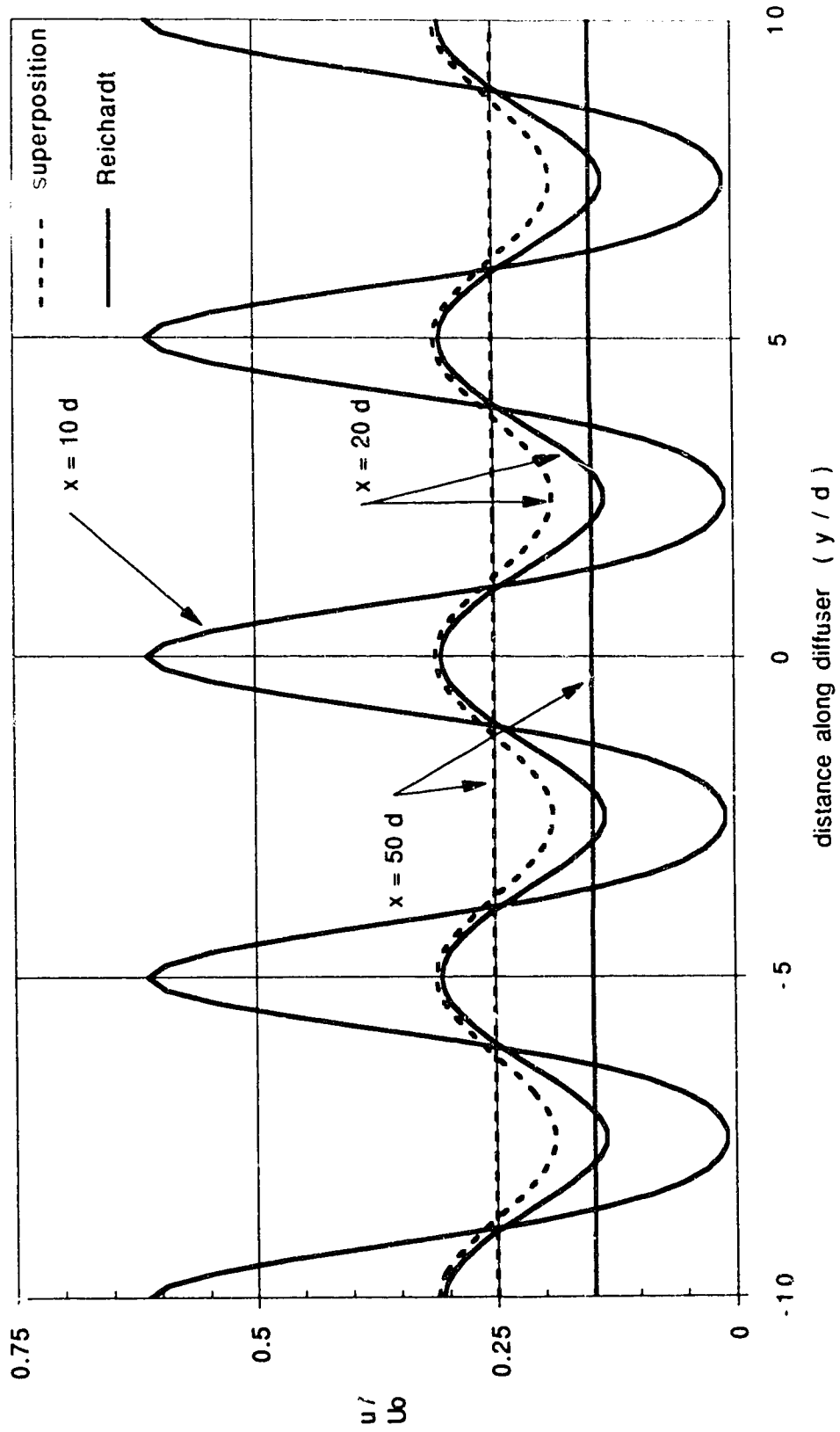


Figure E.10 Concentration distribution in plane of diffuser  
( $\lambda = 5 d$ )

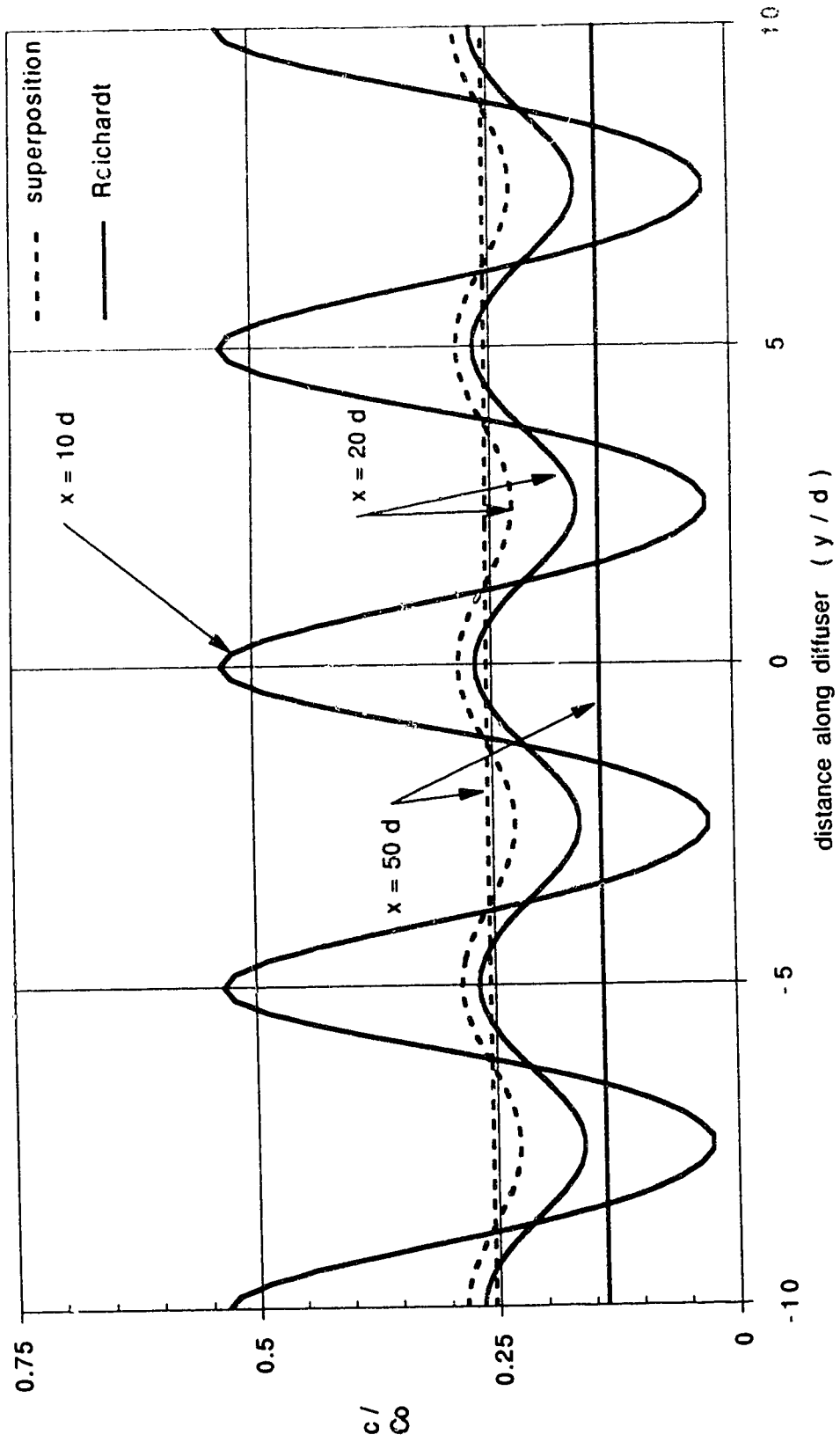


Figure E.11 Velocity distribution normal to diffuser plane through central jet (  $x = 10 d$  )

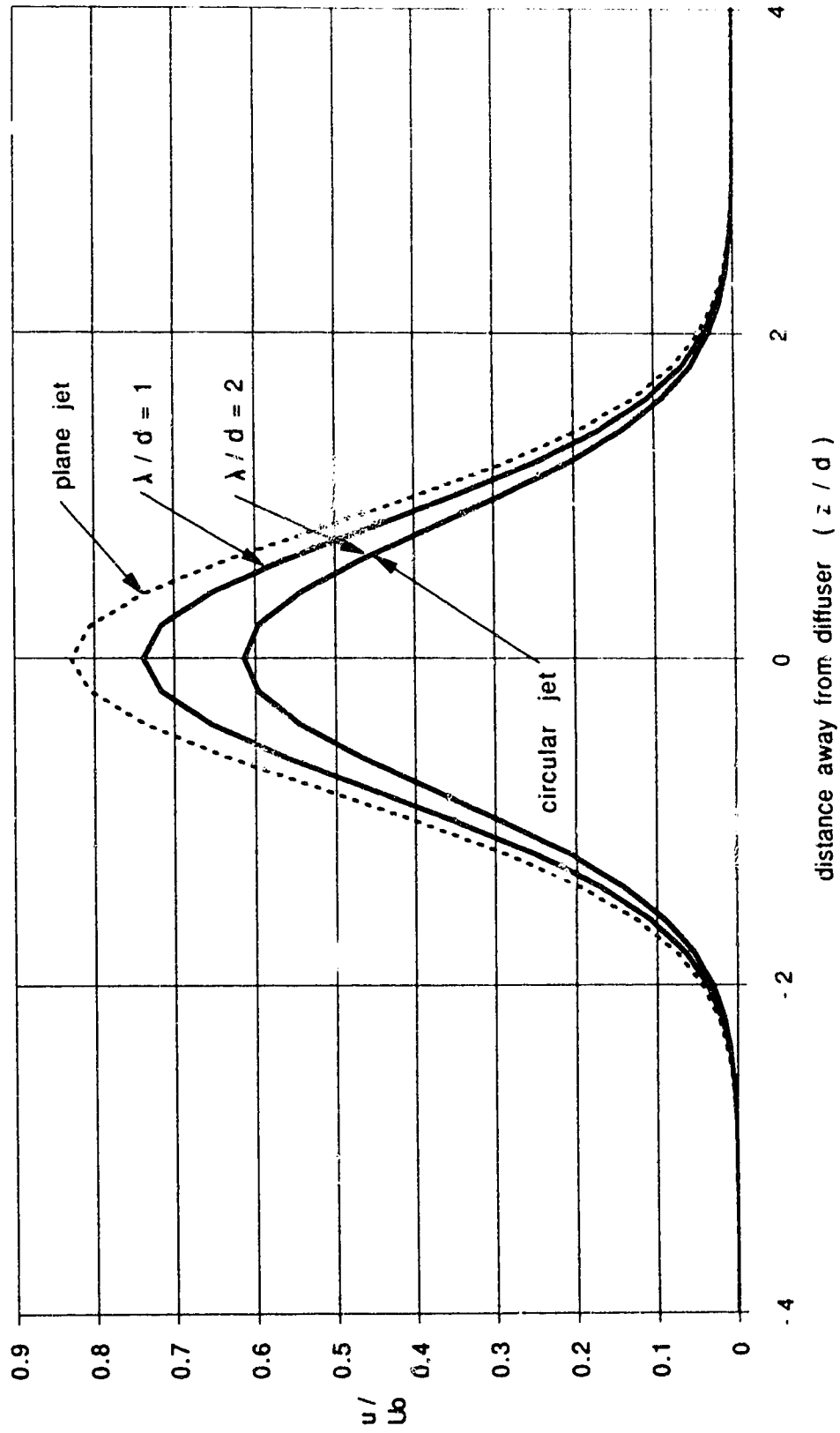


Figure E.12 Velocity distribution normal to diffuser plane through central jet (  $x = 20 d$  )

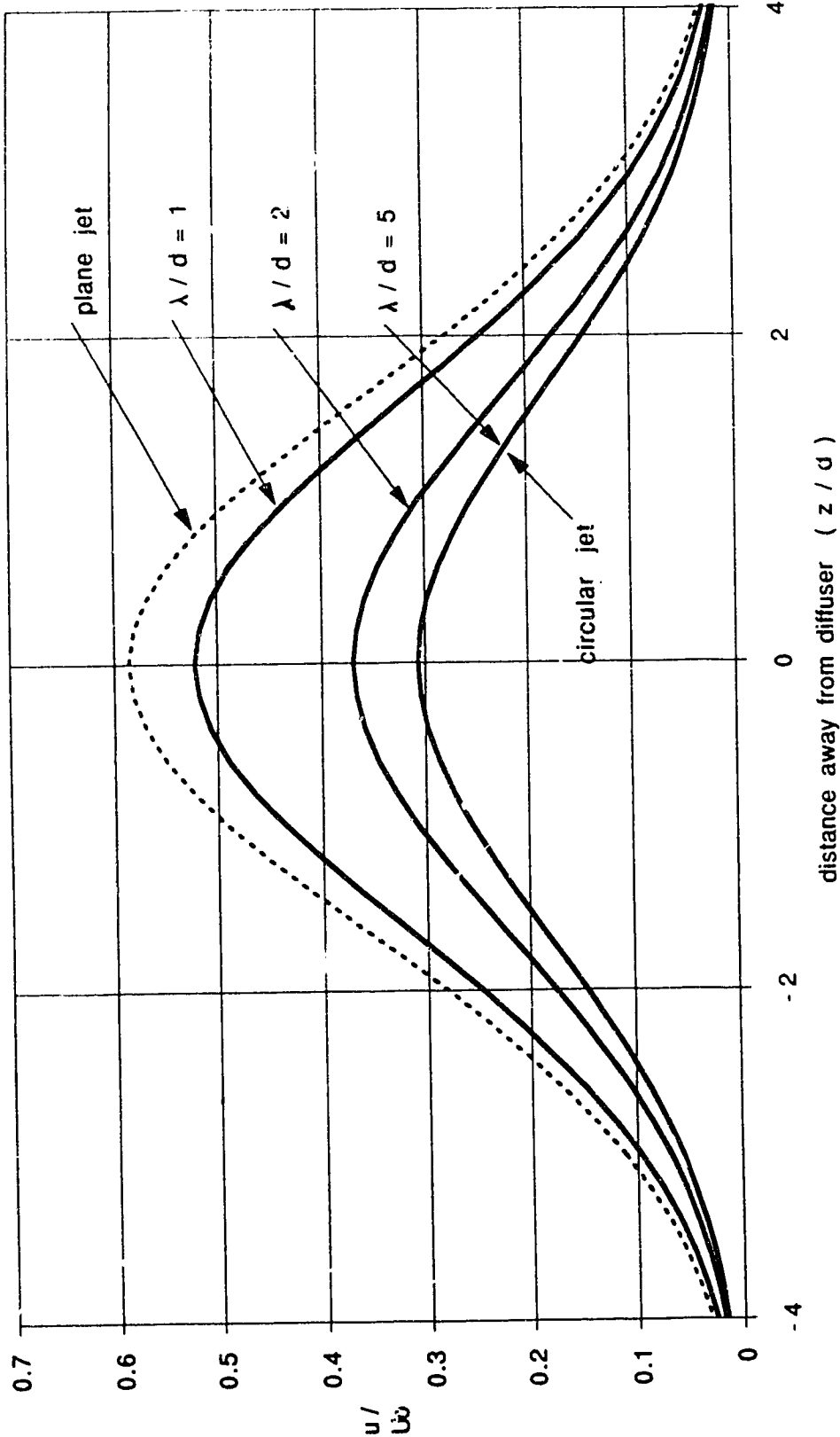


Figure E.13 Velocity distribution normal to diffuser plane through central jet (  $x = 50 d$  )

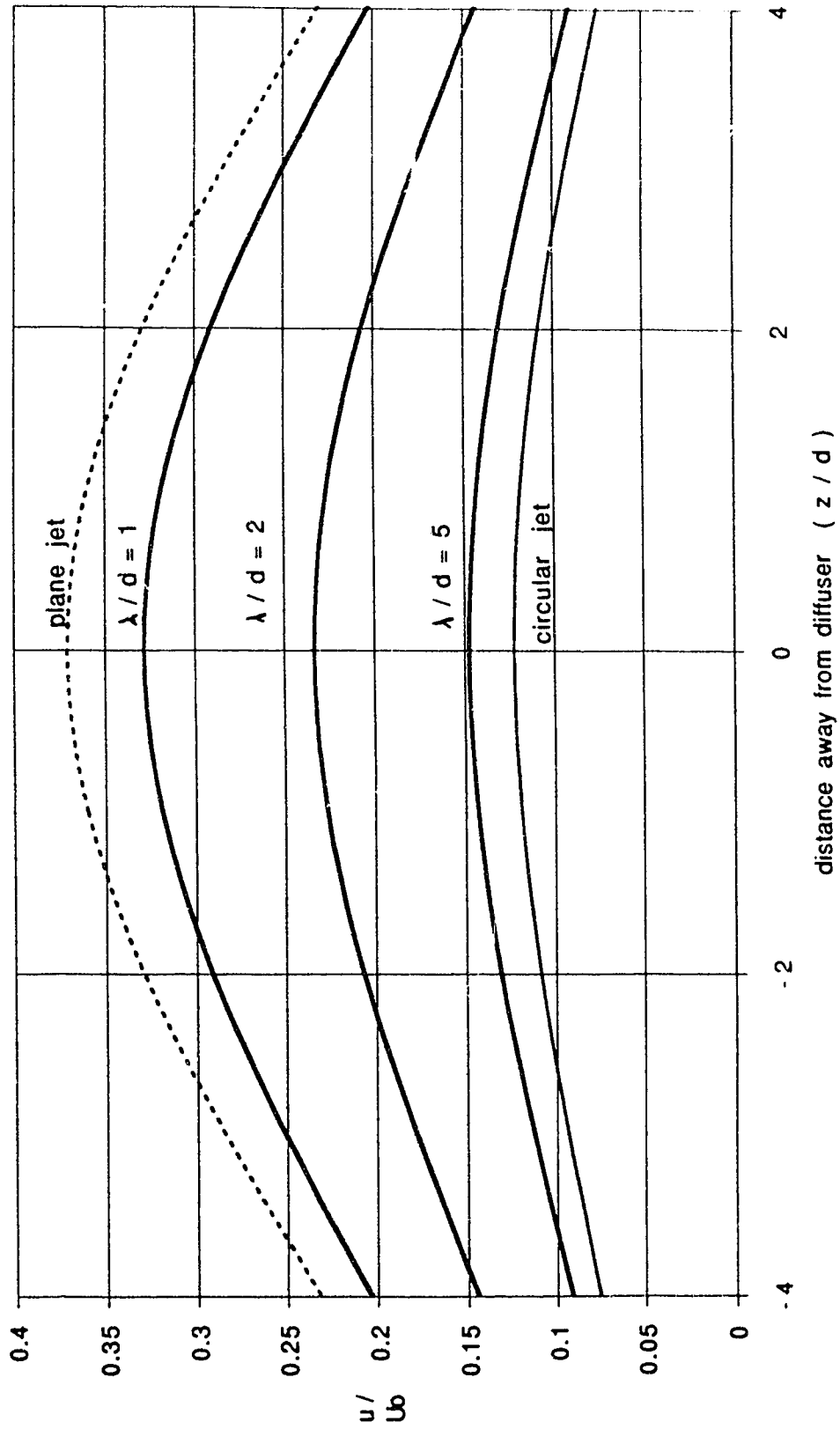


Figure E.14 Concentration distribution normal to diffuser plane through central jet (  $x = 10 d$  )

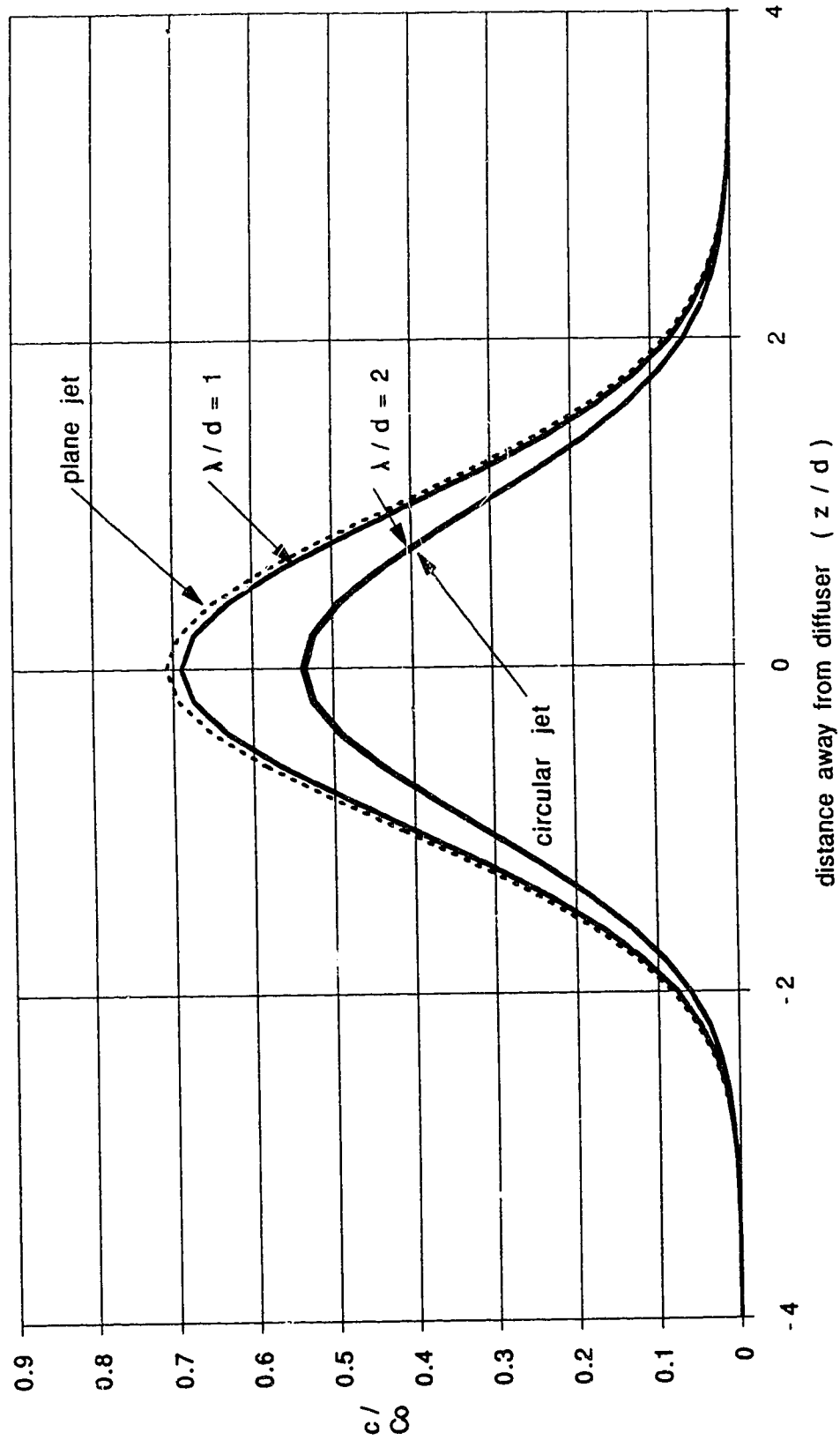


Figure E.15 Concentration distribution normal to diffuser plane through central jet (  $x = 20 d$  )

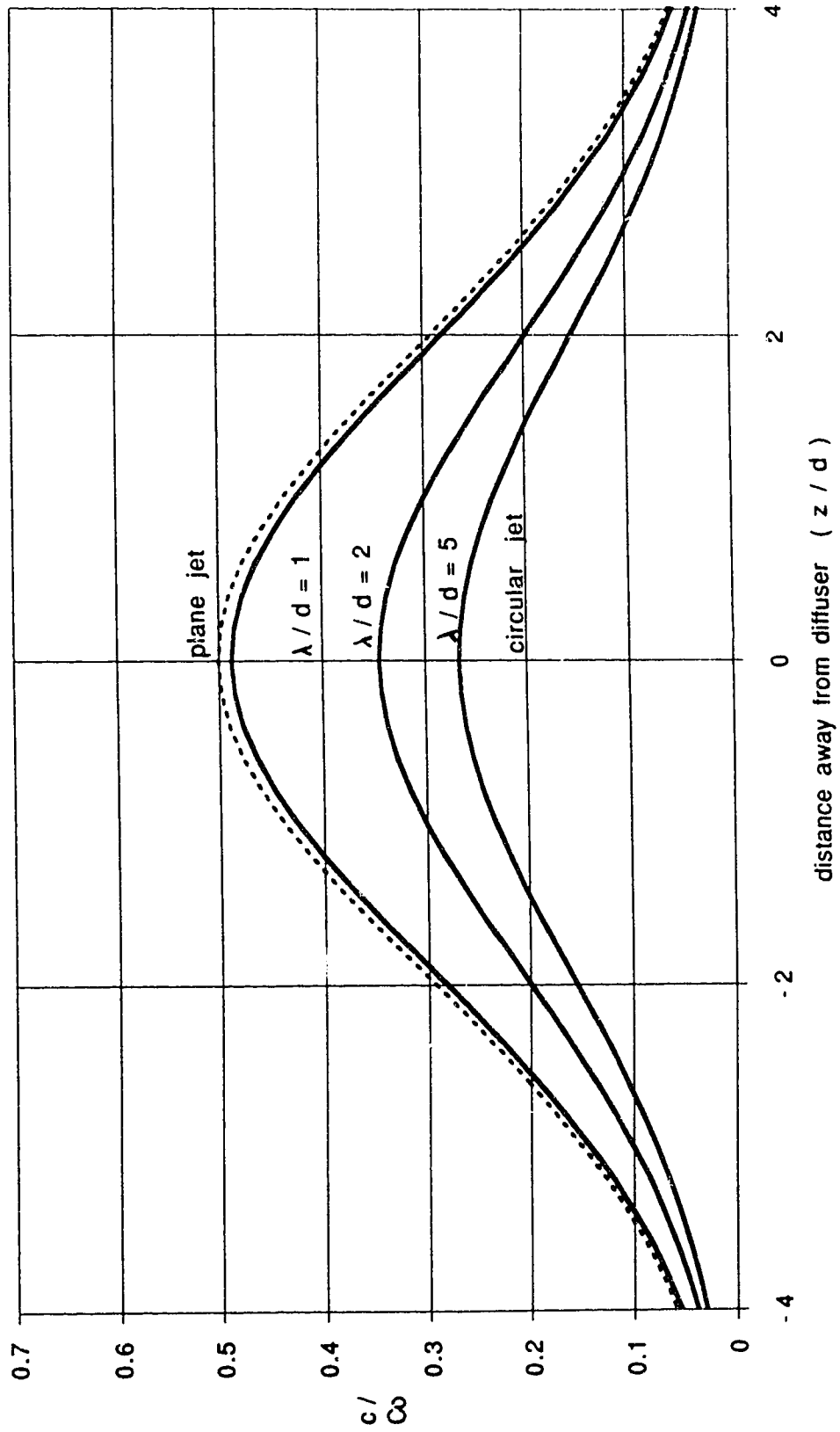
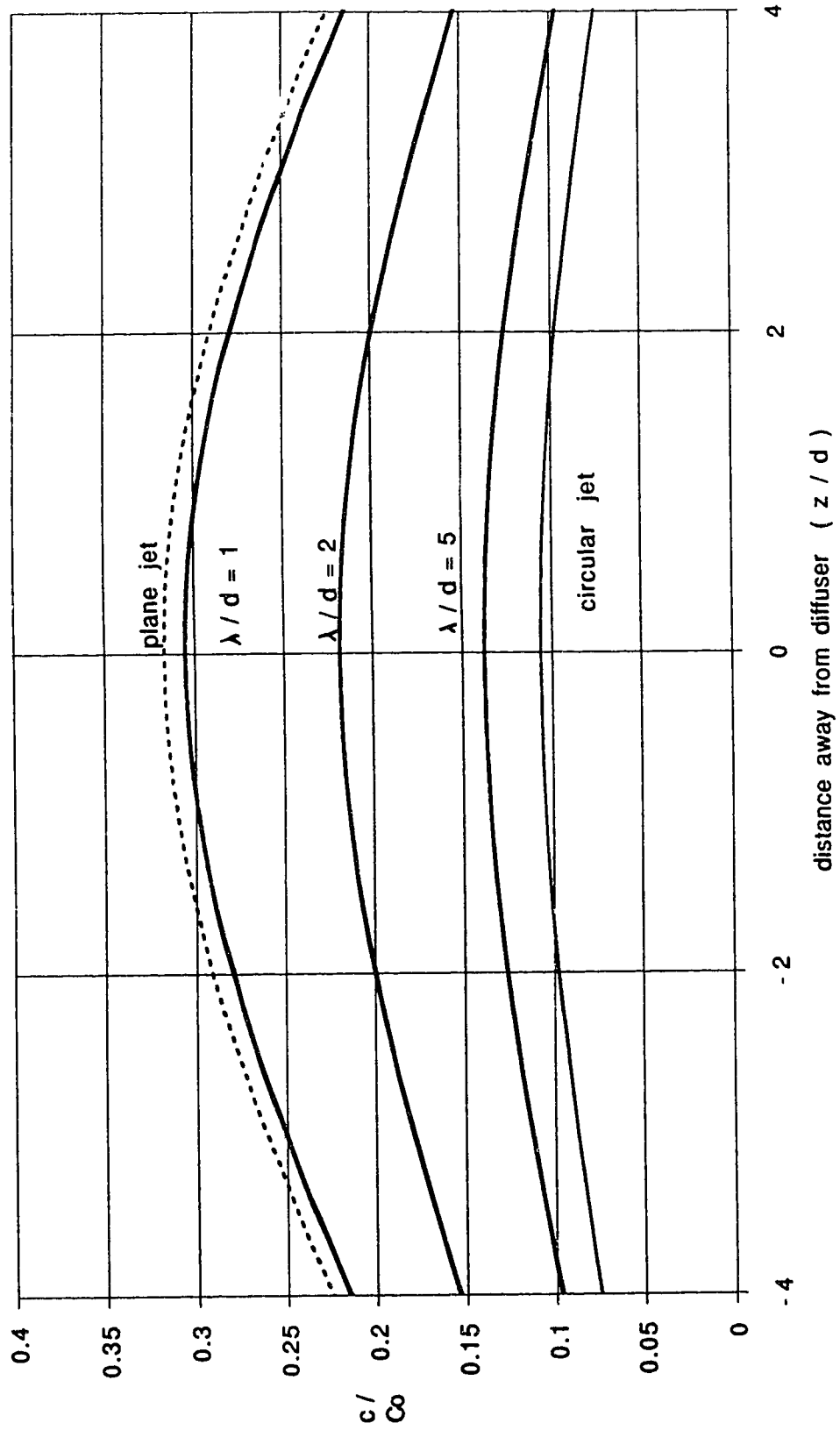


Figure E.16 Concentration distribution normal to diffuser plane through central jet (  $x = 50 d$  )





## APPENDIX F

## GLOSSARY

**advection:** the transport of an effluent by the current.

**Best Available Technology:** the most sophisticated and effective in-plant environmental protection and waste treatment technologies.

**Best Practical Technology:** the most commonly used and economical in-plant environmental control practices and waste treatment technologies.

**bifurcation:** the splitting of a jet discharge into two distinctly separated vortices.

**bimodal jet:** a jet discharge which develops concentration distributions having two maximums located equidistant from the jet centreline.

**bimodal ratio:** the average of the two bimodal peak concentrations divided by the maximum concentration for a vertical profile through the section's centreline.

**cavitation:** the local vaporization (i.e. boiling) of a flowing fluid resulting from low local pressures as the flow encounters a discontinuity.

**criteria:** scientific data evaluated to derive the recommended limits for water uses.

**critical concentration ( $C_1$ ):** the maximum concentration along the LUZ (limited use zone) boundary.

**critical length ( $X_1$ ):** the distance from the outfall downstream to the point of maximum concentration along the LUZ (limited use zone) boundary.

**critical point:** the point along the LUZ (limited use zone) boundary where the concentration profile reaches a maximum value.

**crossing length:** the distance from the outfall downstream to the point where a noticeable (e.g. 2% to 5%) in the concentration of effluent parameters occurs in the river near the opposite shoreline.

**deep water jets:** jet discharges which are in crossflows sufficiently deep to exclude surface effects.

**differential advection:** the spreading of an effluent due to the uneven advection resulting from the non-uniform velocity distributions in rivers; the velocity distributions can occur due to the vertical velocity gradient (due to the stream bed alone or in conjunction with an ice cover) and the transverse velocity gradient which would occur due to the varying depths across the river's cross-section.

**dilution ratio:** the ratio of the concentration of the jet discharge to the maximum concentration at a section.

**far field mixing zone:** the reach of a river, downstream of an effluent discharge, from the section where vertical mixing has been achieved to the section where the effluent is completely mixed across the river.

**initial dilution zone:** the region in the immediate vicinity of an effluent discharge structure where a specified minimum degree of dilution is expected to occur.

**jet centreline penetration distance ( $Y_p$ ):** one half the distance from the nozzle to the outer visual boundary of the jet at  $x = 0$ .

**jet entrainment zone:** the region of a jet discharge (nearest the nozzle) where the growth and dilution of the discharge is dominated by jet entrainment.

**jet half-width:** the distance from the centreline to the point where the velocity is one half the maximum for the section.

**limited use zone (LUZ):** the portion of the width of a river where pollutant concentrations may exceed receiving stream guidelines.

**limited use zone length ( $X_s$ ):** the distance from the outfall to the point where the shoreline concentration reaches the receiving stream guideline.

**maximum permissible LUZ length ( $X_p$ ):** a prescribed constraint on the LUZ length based on existing and future water users.

**maximum terminal levels:** for jet discharges into a crossflow of finite depth, the maximum elevation a jet boundary profile can achieve regardless of the relative jet strength.

**mixing length ( $X_m$ ):** the distance from an outfall to the river section downstream where the effluent has become completely (e.g. 95% or 98%) mixed.

**mixing zone:** the reach of river where vertical and transverse mixing of an effluent is taking place.

**molecular diffusion:** the movement of matter on a molecular scale; these random motions move an effluent from areas of high concentration to areas of low concentration.

**momentum dominated far field (MDFF):** the region of flow, for a jet discharging into a crossflow, where the centreline profile  $(\frac{y_c}{\alpha d})$  varies with the cube root of the distance downstream  $(\frac{x}{\alpha d})$ ; jet momentum dominates the flow in this region.

**momentum dominated near field (MDNF):** the region of flow, for a jet discharging into a crossflow, where the centreline profile  $(\frac{y_c}{\alpha d})$  varies with the square root of the distance downstream  $(\frac{x}{\alpha d})$ ; jet momentum dominates the flow in this region.

**near field mixing zone:** the region downstream of an effluent discharge structure where complete vertical mixing is achieved.

**passive plume:** an effluent discharge which has no momentum flux of buoyancy flux.

**potential core:** the region of flow development in a jet discharge where the velocities change from being uniform with

low turbulence (potential flow) to turbulent flow; just beyond the potential core, the centreline velocities begin to decrease from that at the nozzle (also called the zone of flow establishment).

**relative jet strength:** a dimensionless ratio to quantify the strength of the jet discharge relative to the strength of the crossflow; two measures of this have been identified in this dissertation:  $\frac{\alpha d}{D}$  and  $\frac{\alpha^2 d}{D}$ .

**secondary currents:** lateral circulation of the flow, as a river progresses downstream, induced by the shape of the cross-section or the curvature of the channel's alignment.

**shallow water jets:** jet discharges in crossflows which are affected by the depth of flow.

**subsequent dilution zone:** the river reach, downstream of the mixing zone, where tributary inflow and diffuse lateral inflow reduce parameter concentrations further.

**surface dominated field (SDF):** the region of the flow, for a jet discharging into a crossflow of finite depth, where the water surface slows the upward progression of the jet.

**terminal level region:** the region of flow, for a jet discharging into a crossflow of finite depth, where the jet maintains a relatively stable position.

**transition zone jets:** jet discharges which are only partially affected by the finite depth of flow.

**turbulent diffusion:** the movement of material due to the random fluctuations of a fluid in turbulent flow; these

motions also move material from areas of high concentration to areas of low concentration; in rivers, the dispersive effect of turbulent diffusion is far more significant than molecular diffusion.

**unimodal jet:** a jet discharge which develops concentration distributions having only one maximum located on or near the jet centreline.

**visual jet centreline:** the midpoint line between the inner and outer jet boundaries (determined photographically).

**vortex entrainment zone:** the region of a jet discharge (downstream of the jet entrainment zone) where the jet velocities approach that of the free stream and the motion and dilution of the flow is dominated by the jet vortices.

**water quality guideline:** numerical concentration or narrative statement recommended to support and maintain a designated water use.

**water quality objective:** numerical concentration or narrative statement which has been established to support and protect the designated uses of water at a specified site.

**water quality standard:** an objective that is recognized in enforceable environmental control laws of a level of government.

**zone of established flow (ZEF):** the region in a jet discharge, beyond the potential core, where the flow is fully developed and the velocity distributions are self-similar.

**zone of flow establishment (ZFE):** see potential core.

**zone of passage:** the portion of the width of the river where pollutant concentrations must be within the limits set out in receiving stream guidelines.

